UNIVERSITY OF
LIVERPOOL

The Phase Transition of

Poly(*N*-isopropylacrylamide)

Thesis submitted in accordance with the requirements of the University of Liverpool for the degree of Doctor of Philosophy

by

Christopher David Bentley

November 2010

ABSTRACT

Poly(*N*-isopropylacrylamide) (pNIPAM) is a thermoresponsive polymer that undergoes a phase transition when heated over a lower critical solution temperature (LCST). Due to the potential uses of this polymer in biomedical applications as well as its purely theoretical significance as a model polymer for the coil-globule transition, it has received much interest. The aim of this PhD project is to investigate the phase transition of pNIPAM and other acrylamide based thermoresponsive polymers using FTIR spectroscopy and rapid temperature jump techniques, to improve our knowledge of the solvation changes during the coil-globule transition and the phase transition dynamics

The various temperature jump set-ups used to carry out the experiments presented in this PhD thesis are described in detail in chapter 2, with special emphasis on the technical aspects involved in the implementation of the pump-probe laser systems used in the pursuit of observing pNIPAM dynamics. A detailed description of the method used for data analysis is also given.

Chapter 3 presents a detailed FTIR investigation on the effect of the phase transition on the hydration structure of pNIPAM. This is work was undertaken by utilising band extraction techniques to study the detailed composition of the amide I' band (which largely consists of a carbonyl vibration, sensitive to hydrogen bonding changes). The effects of chain length, concentration and copolymerisation on the hydrogen bonding structure were examined by FTIR measurements at incremental temperatures around the LCST. The amide I' band of each polymer was then analysed using a global pseudo-Voigt fitting algorithm that resolves the amide I' into component sub-bands, each one referring to a different H-bonding environment.

Despite the large variation in polymer samples, 3 bands are required to fit each sample's amide I' band. A new interpretation for these sub-bands was developed that takes into account the new results herein; below the LCST, the polymer exists in a random coil, with the majority of carbonyls being fully solvated (amide I' sub-band is seen at 1625 cm^{-1}). The population of normally solvated carbonyls (1625 cm^{-1}) decreases as temperature increases. A corresponding increase is observed in the number of single/intramolecular (1650 cm^{-1}) H-bonds and carbonyls that are H-bonded to "trapped" water molecules (1610 cm^{-1}) found in collapsed polymer sections as temperature increases and globules are formed.

The observed amide I' band behaviour is used in conjunction with current literature to develop a coherent picture for the hydrogen bonding and solution changes that pNIPAM undergoes during phase transition, consistent with the "pearl-necklace" model, in which the polymer forms small collapsed sections that increase in proportion as the temperature is increased prior to the LCST, after which the entire chain collapses.

In chapter 4, the dynamics of the single chain pNIPAM coil-globule transition was investigated, using a variety of laser induced temperature jump methods with IR spectroscopy. Here, the transition was examined over a large range of time windows from the extremely rapid (<50 ns) to the slow (4 hours). Fast (ns) experiments utilised an Nd-YAG laser to induce a temperature jump in a D_2O polymer solution. Structural dynamics were then detected by probing the sample with an infrared laser tuned to the amide I' band frequency in the heated volume, with a time resolution of 10 ns. These

measurements showed an initial fast (<2 ns) change in structure related to a local change in conformation that was too fast to resolve. The remainder (i.e. the coil-globule portion) of the transition was seen to occur on the 10-100 s timescale, separated in time by many orders of magnitude. This timescale is inaccessible to Nd-YAG induced Tjump experiments, so modified pump techniques (a c/w laser and waterbath heating) were utilised. Finally, aggregation was seen to occur on the 200 s-20 hour timescale. Ar laser pumped measurements at higher concentrations show that the overlapping of chains in solution has a major effect on the dynamics due to the cooperative nature of the transition.

In chapter 5, the phase transition dynamics of nanoparticles of cross-linked pNIPAM gel was studied, using fast (10 ns) laser induced temperature jumps probed by IR spectroscopy. Here, we see that such cross-linked pNIPAM gels react much more rapidly than single diluted chains, further supporting the hypothesis that chain length and local concentration have a major effect of the speed of the transition due to cooperative collapse. It was also shown that starting the temperature jump in a state of partial collapse slows the transition in gels. Higher states of initial collapse show slower dynamics that deviate further from monoexponential behaviour, due to the collapse of the outer shell in preference to core chains. This can dramatically slow the ejection of water due to mechanical constraints caused by the shell forming a hydrophobic barrier to the ejection of water from the core.

ACKNOWLEDGEMENTS

First and foremost, I would like to acknowledge the contributions of my supervisor, Martin Volk. It is impossible to state how important an influence he has been during these past 4 years. I could always count on his advice, encouragements, patience, enthusiasm, expertise and, most importantly, sense of humour to see us through difficulties. I would never have completed this PhD without his help.

I would also like to thank my family, in particular my parents, without whose constant, unconditional support and encouragement, I would never have made it to University in the first place, much less finished a PhD. In particular I'd like to thank them for their unwavering support (financial and otherwise!) during the writing up process.

Thanks to Renee and Teresa for helpful discussions and excellent teamwork throughout, and especially for sitting through my interminable presentations about polymer physics.

Thanks to all the wonderful friends I've made in the last four years, especially Matt, Phil, Adolfo, Jonas, Natalia and Alex for making life in the SSRC a little less grim! Thanks to Minos and Paul for the heated political discussions over lunch. Thanks to Ralph, Gareth, Tim and my brother Paul for being there when pints were in order. Thanks to Mark, Matt, Hannah, Paul and the guys at Next Gen for "character building" and for being a font of advice on and off the mat. A special thanks to Nooshin for being a constant source of encouragement and inspiration during the last 6 months.

I would also like to thank Dr Alexander and Professor Asher for fruitful collaborations, the CLFLP for the loan of the Ar laser, Sam Haq for putting his precious turbopump in jeopardy every month, Ralph for help with NMR assignments, Dr Costick for the use of lab-space and the EPSRC for financial support.

TABLE OF CONTENTS

CHAPTER 1: INTRODUCTION

1.1 Poly(*N*-Isopropylacrylamide and its Applications

Poly(*N*-isopropylacrylamide) (pNIPAM, figure 1.1A) is perhaps the best known thermoresponsive polymer outside of biology. It is of great interest because it undergoes a dramatic change in solute properties when heated over a lower critical solution temperature (LCST). This results[1] in a phase transition is a with a structural change from a hydrated coil at room temperature solutions, to a partially dehydrated globular structure[2-4], which then aggregate due to hydrophobic interactions between desolvated alkyl groups and an increase in the number of intermolecular hydrogen bonds between pNIPAM chains.[3] The LCST is commonly reported as 32-33°C (defined as the first onset of turbidity observed when pNIPAM begins to aggregate). This temperature is very close to body temperature, and can be easily modified by the inclusion of comonomers, further improving its applicability to *in vivo* biomedical applications.

Cross-linking polymers during synthesis creates gels which transform this nanomolecular transition into a macroscopic effect. Gels collapse at the same temperature as the single chain, and the dehydration during phase transition in a gel results in the ejection of internal water molecules, as well as any other internally contained small molecules as the 80% reduction in volume squeezes out molecules in the core[5]. The coil-to-globule (C-G) transition, therefore, is particularly attractive to researchers[6] as it acts in the manner of a "biomechanical transistor". Typically, devices make use of the C-G transition in the controlled release of drugs and therapeutic agents[7,8]. Thus, preloading the polymer with therapeutic agents prior to implantation *in vivo* allows the switching on of drug release when the gel is heated over a certain temperature. Recently, there has been a surge in the number of reports of innovative biomedical applications that make use of the potential for controlled drug release provided by pNIPAM[8], particularly those utilising superparamagnetic materials as a thermal switch to enable remote switching *in vivo*. For example, Purushotham *et al*[9] have reported pNIPAM capped iron oxide nanoparticles that display bifunctional therapeutic effects when used in the treatment of tumors (preloading the pNIPAM

shell with doxorubicin before using a rapidly switching magnetic field to heat the core nanoparticles resulted in a simultaneous attack on tumor cells by release of the toxic agent, and hyperthermia caused by the nanoparticle). Hoare *et al*[10] report a similar approach to controlled release in a nanocomposite membrane based on thermosensitive pNIPAM nanogels and magnetite nanoparticles. However, in this case the pNIPAM gels are used as gateways which block the outward flow of therapeutic agents from an internal pocket in the device. Remote heating causes the pNIPAM gels to collapse, which releases the materials. Both approaches show promising results in *in vivo* testing.

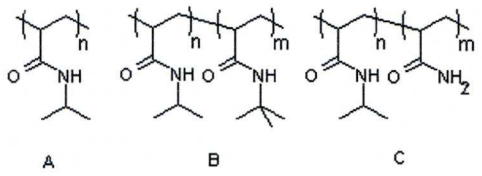

Figure 1.1 A) poly(*N*-isopropylacrylamide) (pNIPAM) and co-polymers B) pNIPAM-co-poly(*N*-tertiarybutylacrylamide) C) pNIPAM-co-poly(*N*-acrylamide)

Due to the potential uses of this polymer in biomedical applications[11,12], as well as its purely theoretical significance as a model polymer for the coil-globule transition[13], availability and ease of handling, there has been an extraordinary increase in research attempting to elucidate this transition that has continued unabated since it was first described[14].

As a result of this interest, pNIPAM has become the "Drosophila" of polymer physics, and the mechanism behind the transition has been probed from a large variety of exploratory angles. Previous investigations include those exploiting light scattering[15-17], NMR[18-20], Microcalorimetry[2,21], fluorescence[15,22,23] and vibrational[3,24-40] spectroscopic techniques.

pNIPAM Synthesis

pNIPAM has been synthesised by a variety of methods. Free radical initiation of organic solutions and redox initiation in aqueous media have been the most widely used techniques[3,11,15,20,21,24-26,41-47], but others have been employed. By using carefully selected comonomers, the LCST can be tailored to different temperatures and by using

difunctional comonomers crosslinking leads to macroscopic gelation. This section will summarise various routes to synthesising pNIPAM single chains[44].

Free Radical synthesis:

Free radical polymerisation of N-isopropylacrylamide is perhaps the "standard" method of producing pNIPAM (indeed, the pNIPAM samples provided by our collaborator (Prof. Cameron Alexander, University of Nottingham) have all been produced using this method), and various initiators and solvents have been used, resulting in diverse molecular weights, as expected. The reactions are typical free radical polymerisations, and azobisisobutylonitrile [AIBN, **(2)**] is the most popular free radical initiator:

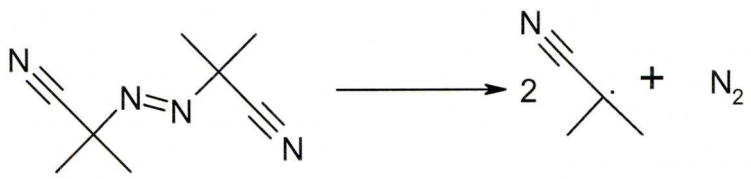

2. AIBN

Figure 1.2 The formation of an AIBN free radical.

As in other polymers, the chain length can affect the physical properties of the polymers, so there have been some attempts to minimise the variation in chain length and to characterise the effect of initiator and monomer concentrations[48]. In particular, it has been noted that variations in LCST behaviour, as measured by differential scanning calorimetry, has been observed at high polydispersity, which may have a significant effect on results [23,49-52]. Copolymerisation is an important method of functionalising pNIPAM for biomedical purposes. In its simplest form, copolymerisation with arcylamide monomers with different alkyl groups allows the modification of the LCST by increasing or decreasing the hydrophobic effect[53]. However, complex multifunctional devices have been produced by copolymerising with other functional polymers[54]. Copolymerisation with crosslinking monomers such as *N,N'*-methylenebisacrylamide, allow the formation of gels, which are of primary interest in biomedical functionalisation.[55] Recently, this method has been adapted to produce gel nanoparticles via dispersion polymerization.[56]

Less common are the synthetic routes which use redox initiators such as ammonium persulfate or potassium persulfate as the initiator and either sodium metabisulfite or N,N,N',N' –tetramethyl ethylenediamine (TEMED) as accelerators. Crucially, this method allows the synthesis to occur in aqueous solution in contrast to normal free radical polymerisation which can only take place in organic solvents. The solutions have to be buffered, however, as in the absence of buffer a much greater polydispersity is found[57]. Whether or not pNIPAM is synthesised in aqueous or organic solution can have significant effects on polymer properties, particularly with regard to macroscopic gel synthesis[2].

Ionic polymerisation:

Ionic initiators provide a further synthetic route but produce a pNIPAM polymer with surprisingly different properties. The use of metal alkyl/transition metal halide catalysts such as Ziegler-Natta catalysts give a highly crystalline form of pNIPAM that is completely insoluble in aqueous and polar solvents, unlike the usual behaviour of the amorphous polymer. The crystalline variety possesses a higher density, as expected, and the fact that X-ray crystallography gives any results at all further demonstrates its higher crystallinity. There has been very little work done on this polymer since its discovery by Shields and Coover[58], probably owing to its comparative uselessness for any kind of biological functionality. Shields suggests a 1,4- polymerisation through the nitrogen group by Michael addition, thus forcing the monomer to give up its nitrogen bonded hydrogen. This prevents hydrogen bonding to the solvent and probably unbalances the hydrophilic/ hydrophobic character in favour of insolubility.

1.2 The Phase Transition

The propensity of pNIPAM to exhibit a coil-globule structural change in aqueous solution when heated above the LCST is well established. pNIPAM solutions phase separate above the LCST while gels collapse. The potential of this polymer for stimuli responsive devices has inspired extensive research on pNIPAM solutions and gels in order to elucidate the molecular mechanism responsible for this fascinating behaviour. The mechanism behind the LCST phenomenon has been studied in detail

using a broad selection of techniques e.g., Light scattering[17,59], NMR[18,20,60], Microcalorimetry[2,21], infrared[3,24-26] and fluorescence spectrometry[15,22,51,61].

1.2.1 Light Scattering

The first observations of the coil-globule (C-G) transition were made by Scarpa *et al* in 1967[62]. These measurements relied upon a simple visual observation of macroscopic phase separation, and thus yielded only the onset of aggregation (or "cloud-point"). This method has been somewhat improved by the use of a standard UV-vis spectrometer and attempts to standardise the wavelength at which the cloud-point is observed, usually in the range of 500-800 nm[44]. It is still used today as a simple method of characterising the C-G transition, but more precise dynamic light-scattering experiments have taken place which discern important details about the C-G mechanism. Initially, application of this method to pNIPAM was pioneered by Heskins and Guillet[63], but the use of an unfractionated sample and a massive variance of molecular weights within samples gave ambiguous results[17,44].

Kubota *et al*[64] initially used fractionated samples in dynamic light scattering experiments to characterise the solution behaviour of pNIPAM in terms of the "static" (radius of gyration, R_G) and "dynamic" (hydrodynamic radius, R_H) radius below the LCST. In a subsequent and much more detailed study, Kubota *et al* [17] performed a further dynamic light scattering investigation on the temperature dependence of the R_H and R_G of chains fractionated using a molecular sieve, and their response to increasing the temperature above the LCST. According to polymer "blob" theory, a fully globulated polymer should have a ratio of R_G: R_H $\approx$0.7, indicating a fully compact sphere. In fact the ratio drops from 1.3 to 0.775 when increasing the temperature above the LCST. This suggests that, the polymer chain does not collapse fully, but consists of several globular regions that are linked by "strings" of uncollapsed polymer, or that the collapsed globule has a somewhat "looser" structure. However, it should be noted that this value is still very close to that of a hard sphere. The conclusion of a somewhat "looser" structure appears to agree with Maeda[3] and Percot[24] who interpret their FTIR-results as showing that the amide bond is still mostly solvated even in the globule state (see below), and Ahmed *et al*[56], who show that a collapsed gel is still permeable to water, as the gel experiences complete H-D exchange within 5 minutes of exposure to D_2O as a solvent. Fujishige, Kubota, *et al*

also investigated the effect of concentration on the phase transition temperature, indicating that there is an LCST dependence upon concentration[43].

In respect to light scattering measurements, the intramolecular coil-globule mechanism is indistinguishable from intermolecular aggregation. Indeed, the aggregation cloud point can be measured down to extremely small concentrations of 10 μg/l which makes analysing the intermolecular C-G mechanism separately in any more detail rather difficult. To combat this, Ricka *et al* performed a study on the effect of surfactant on the C-G transition[59]. The use of a small amount of surfactant sodium dodecyl sulphate was shown to induce "intermolecular solubilisation", breaking apart aggregates and allowing the phase transition of isolated coils to be measured. Furthermore, an analysis of the hydrodynamic radius (R_H) with respect to temperature at different surfactant concentrations reveals that the LCST is merely shifted to slightly higher temperatures. All other factors, including the extent of change of R_H, steepness of the transition and increase in scattering intensity upon collapse are unaffected by surfactant concentration. This indicates that events on the molecular level are not strongly affected.

1.2.2 Nuclear Magnetic Resonance Spectroscopy

Tokuhiro *et al*[20] were the first to perform an NMR study on the phase transition of pNIPAM solutions and gels related to the LCST phenomenon. In both, the NMR spectra of the single strand and crosslinked gel pNIPAM, there are 4 distinct proton peaks below the LCST. Unfortunately, due to the vast amount of conformations available to solvated pNIPAM chains any structural information is lost because of the large line widths. Also, the N-H proton (the proton we are most interested in) is lost due to H-D exchange with the solvent; however, a lot of information can still be gleaned from the spectrum.

At temperatures above the LCST, a new broad peak is observed at 8.0 ppm, and its growth with temperature along with a corresponding loss in the integral area of the other peaks is significant. NMR spectra of solid dried samples have an identical peak, so it can be inferred from comparison of these spectra that a dynamic equilibrium of two phases exists: Polymer regions that are fully solvated and chains in the form of solid-like aggregates coexist at higher temperatures. The study also confirms that the processes occurring at the LCST show different dynamics information in gels and dissolved polymers; the processes undertaken by gels are on a

much slower timescale. The spin-lattice relaxation effect (T_1, the time constant for spins to relax into an orientation in which the spins align with the external magnetic field when perturbed by a 180° pulse) show that below the LCST, the side chain groups are more mobile than the backbone. Furthermore, thermodynamic equilibrium is recovered "rapidly" (i.e. within the time resolution of the NMR measurements) when the temperature of the sample is disturbed for solution based samples.

Yushmanov *et al*[18] investigate the dynamics of pNIPAM on the 0-100 second timescale. They performed a detailed study on the C-G kinetics of these polymers by exploiting ^{1}H NMR, measuring both the transverse and longitudinal relaxation times of pNIPAM solutions in NMR pulse experiments and performing the first temperature jump measurements (with ~1s time resolution) known. The relaxation due to spin exchange with the solvent or other protons was observed giving information on the molecular dynamics. The changes in longitudinal relaxation time (T_1, by inversion recovery) were measured, along with the transverse relaxation time (T_2, using 90° - t - 180°-2t pulse methods) and self diffusion-coefficient (D), each relaxation giving information about a different scale of behaviour within the pNIPAM chains. Almost no change in T_1 with temperature is reported at and above the LCST. The transverse relaxation time (T_2), on the other hand, gives information about the dynamics of the solution. Yushmanov's steady state NMR measurements show an increase of T_2 above the LCST which represents an acceleration of dynamics in the parts of the chain that are not in the globule state; the solid like nature of these globules eliminates their contribution to the NMR signal at higher temperatures. Alternatively, this could just be a result of the faster tumbling of all molecules in the sample (including aggregates). This outcome matches Tokuhiro's results[20], whose spectra show a gradual narrowing of peaks, indicating more vigorous molecular motion of the remaining non-globular chain sections, at higher temperatures. Yushmanov's temperature jumps show that the polymer collapses within a few seconds, but fail to provide any accurate information below 1s due to experimental constraints. The vast majority of structural changes happens within the time resolution of the ^{1}H NMR experiment, highlighting the need for fast temperature jump IR studies on shorter timescale. These results will be discussed in more detail in comparison with temperature jumps performed in the course of this project (chapter 4).

An attempt to investigate the globular regions has been made by Ohta and Ando[60] by means of magic angle ^{13}C NMR, which gives an up-field shift of the ^{13}C

NMR peak of CO groups above the LCST. Usually this represents hydrogen bond breakage in peptide systems. This seems to indicate that there are at least some carbonyl groups that are non-bonded above the LCST. However, the conclusions drawn do not seem to match the spectra shown in the paper, which show a gradual increase with no noticable effect caused by the LCST.

1.2.4 Microcalorimetry

The C-G transition has also been studied using microcalorimetry to derive values for thermodynamic constants and their temperature dependence. Schild and Tirrel[2] found that the transition is an endothermic process and dependent on chain length at lower temperatures. Fujishage and Kubota *et al*[17,43], whose polymers were characterised by large molecular weights of $>5x10^4$, saw no chain length dependence, but also saw that the transition is endothermic.

Tiktopulo *et al*[21] similarly engage microcalorimetry to analyse the thermodynamic nature of the phase transition. Both Schild and Tiktopulo agree that the heating rate effectively changes the cooperativity of the phase transition, or in other words the number of "blocks" (similar to protein domains) in a single chain. These domains respond separately during the C-G transition, as opposed to an "all or nothing process". Both groups effectively eliminate kinetic contributions from their analysis by heating so slowly that the solutions can be considered in equilibrium when measurements are taken.

The size of cooperative groups found by Schild and Tiktopulo are in agreement; values for ΔH^{eff} or the Van't Hoff enthalpy of a single cooperative unit and ΔH^{Cal} of the whole transition are derived from a plot of Δc^{Cal} against temperature. (ΔH^{eff} derived from the peak value of Δc^{Cal}, ΔH^{Cal} from the integral). The number of cooperative units can then be found from the ratio of these two values $\Delta H^{Cal}/\Delta H^{eff}$. Schild and Tirrel[2] come to the conclusion that each cooperative domain contains on the order of 400 repeating units that is, within the variance of M_n, as large as the polymer they use. (M_n approximately 160000). This represents an almost all-or-nothing process for these polymers. Tiktopulo experiments with chains on the order of 100 time larger, and gets a $\Delta H^{Cal}/\Delta H^{eff}$ ratio which corresponds to about 100 cooperative units, each containing $\approx$ 500 monomer units for a M_w average of $7x10^6$. This shows that for chain lengths below a critical size, a single cooperative unit is seen and the process is "all-or-nothing". One other interesting observation is that the

transition enthalpy is consistent with the loss of 1 amide-solution hydrogen bond per monomer unit, and the ΔC_p is -15 cal mol^{-1} $^oC^{-1}$, an observation interpreted as evidence that the number of water-polymer contacts decrease during the phase transition[2,23]. Interestingly, in a comparison of D_2O and H_2O solutions by Kujawa and coworkers[23] using pressure perturbation calorimetry (PPC), the difference in heat capacity before and after the phase transition is revealed to be nearly doubled in D_2O, a fact interpreted to be a consequence of a higher solvent accessible area in D_2O pNIPAM solutions due a more extended chain. This is backed by light scattering studies which show more extended chains in D_2O than H_2O[65]. This means that there may be a higher level of ordering between D_2O and the chains, hence a larger volume of D_2O molecules that directly interact with the chains by means of a solvent bubble. This agrees with the fact that D_2O forms hydrogen bonds approximately 5% stronger than those of water.

1.2.5 Summary

NMR results show that the C-G transition upon heating above the LCST is a two state process from fluid fully solvated coils to much more solid-like globules which appear as a very broad peak in the ^1H NMR spectra[20], mirroring that of solid, dry pNIPAM[18]. Dynamic measurements show very little structural dynamics on the >1 s timescale.

Dynamic light scattering measurements have been employed to study the effect of temperature on the radii of gyration and hydration of pNIPAM chains throughout the C-G transition and show that the polymer collapses to almost solid spherical globules above the LCST, although they are still permeable to solvent[64]. Surfactant has been used to separate the coil-globule transition from further aggregation[64].

Calorimetry has been used to study the thermodynamic properties of pNIPAM, showing that cooperative groups of about 500 monomer units participate as separate domains during the C-G transition[2]. It seems that both hydrophobic groups and the hydrogen bonding network are involved in the transition, during which the entropic gain of ejecting bonded solvent molecules becomes greater than the gain of hydrogen bonding of coil to solvent and the entropic freedom of polymer chains. There is a severe lack of dynamic information about this process, and we intend to elucidate the

dynamics of this process utilising fast temperature jumps measurements using infrared absorption for following the process.

1.3 Vibrational Spectroscopy

Vibrational spectroscopy is a valuable tool in the study of secondary structural change. The poly(*N*-alkylacrylamide) family of polymers are uniquely suitable among synthetic polymers for such analysis, as the amide bonds in the side groups act as a highly sensitive probe of the secondary structure/solvation. Infrared spectroscopy is also useful in terms of probing dynamics, because of the high time resolution measurements that are possible; in fact, the vibrations seen in the infrared spectrum can respond to structural changes in 10 - 100 fs[66]. Accordingly, one would expect vibrational spectroscopy to clarify the mechanism of what is essentially a secondary structural/solvation transition. The published literature in this field is somewhat controversial, however, and no time resolved results have been published so far.

The infrared absorbance spectrum of the pNIPAM amide bond closely mirrors that seen in polypeptides. In peptides, absorbance takes place in nine regions of the IR spectrum, the amide A, B, I---VII bands. Amide bands I, II and III show particular sensitivity to secondary structure and of these, the amide I band is most useful as it is stronger than the amide III absorption and better characterised than the amide II band. The amide I absorption is largely made up of a C=O stretch (80%) and a minor C-N stretching component (10%) and an N-H bend (10%); it occurs in the 1600-1700 cm^{-1} region[67]and is susceptible to changes in vibrational frequency when C=O undergoes hydrogen bonding.

A difference in the hydrogen bond donor results in shifts of the frequency of this band. Secondary structural changes based on perturbations of the C=O hydrogen bonding network due to temperature changes can therefore be followed by observing the shifting populations of the sub-bands.

The position of the amide I band can be assigned to a particular hydration environment depending on the strength (or lack) of hydrogen bonding. When pNIPAM is fully dehydrated, the amide I band is shown to have a frequency of around 1680 cm^{-1} [56], which corresponds to the non-H-bonded carbonyl.

The nature of the carbonyl bond is altered when the polymer is dissolved in water and the solvent has access; there is competition between the N-H group of other amide bonds in the polymer and water as a hydrogen bond donor, thus a number of different frequencies are observed due to varying strengths of hydrogen bonding. Stronger hydrogen bonding, due to either multiple bonds being formed to a single carbonyl or a more stable bond, weakens the carbonyl bond further, causing vibrations at lower frequencies. However, the vibrations due to different hydration states are separated by only 10-20 cm^{-1} and thus the sub-bands overlap, making band assignment difficult, therefore requiring band extraction techniques for examination of the hydration structure.

D_2O is typically used as the aqueous solvent for infrared studies because of the large H_2O absorbance in the amide I region of the spectrum. This causes hydrogen / deuterium (H/D) exchange of solvent accessible amide protons and thereby affects the frequency of the amide I band. The amide I' band ('=H/D exchanged) occurs at lower frequencies than the amide I band. This is due to the larger mass, the deuterium atom causing a decrease in the N-H vibrational frequency, as 10% of the amide I vibration is due to the in-phase N-H bend. However, the repositioning of the large water absorbance away from the amide I' allows much better characterisation.

Percot *et al* [24] initially studied the FTIR spectrum of the amide I vibration in both gels and solution based pNIPAM. The amide I band was then fitted using multiple bands (the band type was not disclosed) to distinguish C=O bonds in different environments and therefore characterise the structural changes during the C-G transition. Percot *et al* assign a single band below the LCST to solvent hydrogen bonded C=O, 20% of which are replaced by a second band representing intramolecularly hydrogen bonded C=O above the LCST. However, they also report a large increase of the integrated absorbance, which seems unlikely. There is a major disadvantage in using the amide I band; as discussed, the large water deformation peak at around the same wavelength (1643.5 cm^{-1}) distorts the amide I band[68]. Percot *et al* used water as the solvent, thus the H_2O peak distorts their results. They attempted to correct for this, but state that they experienced difficulties. Percot *et al* do show however, that the C-G transition can be followed clearly by infrared spectroscopy

Maeda *et al* have analysed many thermally responsive polymers in this manner, including poly-alkyl derivatives of pNIPAM and poly-vinyl caprolactams

and others[3,19,26,29-32,69-78]. The pNIPAM FTIR spectra in D_2O [3,19,26,30,71,73,75-77] show that, unlike in Percot's results[24], the amide I band does not increase in total area above the LCST. A band at 1625 cm^{-1}, assigned to solvent hydrogen bonded C=O, decreases in area with a corresponding increase in a clearly visible higher frequency band (~1650 cm^{-1}) above the LCST, which is interpreted as an increase in amide-amide hydrogen bonding during collapse and subsequent aggregation. Shifting of the C-H vibrations is observed when heating above the LCST, indicating a loss in hydration of alkyl groups when undergoing the phase transition. It is this effect that primarily brings about the phase transition, as the entropic gain to the overall system following the loss of water bound in clathrate cages becomes a stronger factor than the enthalpy gain from polymer-water hydrogen bonds.

In comparison, even in the fully collapsed state, a large proportion of carbonyl bonds remain hydrated. Detailed secondary structural information is unobtainable from the C-H vibrational region of the spectrum. Although they do not report directly on the major causal factor of the transition (the dehydration of the isopropyl groups), the amide bands reaction to changes in hydration give a valuable window into the secondary structural activity of the polymers during transitions.

Approximately 33% of water-hydrogen bonded carbonyl groups are lost upon the coil-globule transition in Maeda's interpretation; however, there is compelling evidence within the results presented that indicates that a 2-band fit is insufficient to fully describe the transition, notably the fact that this assignment no longer fits when applied to other poly-alkylacrylamides. Discussion on this topic can be found in chapter 3.

There has been an attempt by Katsumoto *et al*[25] to use DFT simulations in explaining the structural changes seen in the FTIR spectrum during the transition. Again, the FTIR spectrum is taken of a solution in water, leading to difficulties in baseline removal. However, the correction in this case seems much better and an FTIR spectrum that resembles Maeda's spectra in D_2O is presented. DFT calculations are used to simulate the IR-spectra of pNIPAM in vaccum and in solution, the solution simulations involving the use of the very simple Onsager model as a basis for solvent interactions. Simulated spectra show that the most likely conformations of the side chains involve intramolecular hydrogen bonds between neighbouring amide groups. Somewhat counter-intuitively, a two band model is suggested in which almost all amide hydrogen bonds are intramolecular before the LCST transition. This result

disagrees strongly with the conclusions presented by Maeda and Percot as it leaves solvation to C-H groups which would be clearly unfavourable. After the transition, the C=O bonds are suggested to become non hydrogen bonded as a result of the collapse. The Onsager model is too simple a model to explore the hydration of pNIPAM chains, and Katsumoto *et al* acknowledge that the calculations fail to reproduce all characteristics of the amide I band, and state the need for a more realistic model and more detailed experimental data. It is a much simpler and more intuitive hypothesis that most of the hydrogen bonds are formed with water in the coil state. A later examination by Katsumoto[79] into the solution properties of poly(*N*,*N* diethylacrylamide) in different solvents, reveal a third band at 1610 cm^{-1}. They assign the bands at 1610 cm^{-1} and 1625 cm^{-1} to vibrations related to carbonyls H-bonded to two and one water molecules, respectively. However, the description of the 1650 cm^{-1} band as representing non-bonded carbonyls is questionable, as there is an obvious thermodynamic penalty for having non-hydrogen bonded carbonyls in solution, and the vibration of non-hydrogen bonded carbonyls has been observed in dry polymers [56].

Meersman *et al*[37] in pressure dependent FTIR studies of pNIPAM utilise the assignment (C=O hydrogen bonded to two H_2O) for the 1610 cm^{-1} band that appears when samples of pNIPAM are placed under increasing pressures (thus providing confirmation that a 3-band system is required for a full understanding of pNIPAM's secondary structure. Later studies by Maeda do not recognise the third band[80]

Current interpretation of the FTIR spectra of pNIPAM is therefore somewhat fragmentary.. In our temperature dependent FTIR studies on a variety of pNIPAM based polymers, we aim to clarify this issue and further elucidate the effect of temperature on the hydration structure during the phase transition (Chapter 3).

1.4 Fast Folding Kinetics

Conformational changes that involve a change in the carbonyl hydrogen bonding structure are matched by a change in the IR spectrum. This brings the possibility of using rapid temperature jumps (Tjumps) while measuring the change of absorbance in order to probe the fast folding dynamics of these polymers. This technique has been used previously to study the folding dynamics of proteins and peptides[67,81-84], but very little has been published on the dynamics of synthetic

polymers on a sub-microsecond timescale. Yang *et al*[47] have observed the fast folding dynamics of a phenylacetylene oligomer consisting of 12 monomers. Interestingly, this molecule folds to its helix structure on a sub-microsecond timescale similar to α-helical peptides. By measuring the fluorescence of this molecule in response to a Tjump, Yang *et al*[47] were able to observe the folding kinetics which occurs on the ns/μs timescale, and interpret them as a multistate transition. They conclude the existence of an initial activation barrier to folding representing the nucleation phase and a gradual decrease in free energy with every new coil formed, reflecting stability conferred by π-π stacking. This closely resembles the Zimm-Bragg model for α-helical peptide folding[85].

The pump-probe technique for studying α-helical peptide folding, utilising fast Tjumps in combination with IR detection was pioneered by Woodruff, Dyer and co-workers[83,84,86]. It involves the use of a powerful laser pulse in order to heat a sample on a ps/ns time scale. Many groups have since investigated the speed of peptide and protein dynamics to discover the folding time constants of α-helical peptides in relation to peptide length, composition, stability[87,88] and cold denaturing[89]. As the secondary structure forms on the ns timescale and depends on hydrogen bonding, it is possible to study the structure as it reacts to this temperature jump, measuring the absorbance change with a continuous IR laser. Studies on the phase transition dynamics of pNIPAM have been relatively scarce, on the other hand.

Although the thermodynamic properties of the coil-globule transition have been well studied, there has been a noticable lack of any published data regarding the kinetics of the transition. Tsuboi *et al*[90-92] recently studied the fast (<1 second) kinetics of single chain pNIPAM collapse. Using pump-probe laser techniques with visible laser light as the probe, they measured the light scattered when post-transition globule aggregates form that are large enough to interfere with the probe beam, but under highly undefined conditions[92]. Measurements on the dynamics of the crosslinked gel variants have being performed with visible light scatter[5] and UV resonance Raman pump-probe experiments[56]. These investigations will be discussed in more detail in the relevant chapters (chapter 4 single chain transition dynamics and chapter 5 details the gel phase transition dynamics).

1.5 Outlook on Thesis

The aim of this PhD project is to investigate the phase transition of pNIPAM and other acrylamide based thermoresponsive polymers using FTIR spectroscopy and rapid temperature jump techniques, to improve our knowledge of the solvation changes during the coil-globule transition and the phase transition dynamics

In chapter 2, the various temperature jump set-ups used to carry out the experiments presented in this PhD thesis are described in detail, with special emphasis on the technical aspects involved in the implementation of the various laser systems used in the pursuit of observing pNIPAM dynamics. A detailed description of the method used for data analysis is also given.

Chapter 3 presents a detailed investigation of the hydration structure of pNIPAM around the LCST by utilising band extraction techniques to study the detailed composition of the amide I' band. Comparisons of various factors, such as chain length and copolymerisation, and their effects on the amide I' band are used in conjunction with current literature to develop a coherent detailed picture for the hydrogen bonding and solution changes that pNIPAM undergoes during phase transition.

Chapter 4 investigates the dynamics of the single chain pNIPAM coil-globule transition using a variety of laser induced temperature jump methods with IR spectroscopy. Here, the transition is examined over a large range of time windows from the extremely rapid (<50 ns) to the slow (4 hours). Experiments resolve two distinct phases separated in time by many orders of magnitude, and show that the overlapping of chains in solution has a major effect due to the cooperative nature of the transition.

Chapter 5 studies the phase transition dynamics of nanoparticles of cross-linked pNIPAM gel, using fast laser induced temperature jumps probed by IR spectroscopy. Here, we see that such cross-linked pNIPAM gels react much more rapidly than single diluted chains, further supporting the hypothesis that chain length and local concentration have a major effect of the speed of the transition due to cooperative collapse. In comparison with other investigations[5,56], it is also shown that starting the temperature jump in a state of partial collapse slows the transition in gels, due to the collapse of the outer shell in preference to core chains. This can

dramatically slow the ejection of water due to mechanical constraints caused by the shell forming a hydrophobic barrier to the ejection of water from the core.

CHAPTER 2: EXPERIMENTAL DETAILS

2.1 Introduction

The laser setup used here is in essence the same as that initially used by Dyer[84], combining a pump laser to provide temperature jumps in the sample, and a probe beam to observe secondary structural changes. A variety of laser systems were used in order to access multiple timescales and observe spectroscopic phenomena linked to structural change, but in all cases the basic premise is the same; the pump laser produces light near 520 nm wavelength, which is then absorbed by a heat transducing dye in solution with the sample. The dye relaxes rapidly on the order of a few nanoseconds or faster, transforming the absorbed energy into thermal energy, which then heats the surrounding sample. The resulting changes in secondary structure can be observed directly with cw probe lasers. By using a continuous infrared probe beam tuned to the amide I' band of the polymer we can observe changes in secondary structure, while a HeNe laser beam allows us to observe changes in the light scattering properties of the sample. The various laser systems will be discussed in detail in the following sections.

2.2 Samples

2.2.1 Overview of Samples Used

In this project, the properties of a number of variations of poly(*N*-alkylacrylamide) in solution were studied, including variations in chain length, alkyl side groups, copolymerisation and the crosslinking of the standard polymer into a 3-dimensional network.

The single chain polymers were all synthesised using free radical polymerisation by Dr Cameron Alexander's group at the University of Nottingham, except those which were synthesised in the course of this project at the University of Liverpool in cooperation with Dr Alexander, as described in 2.2.3. Dr Asher,

University of Pittsburgh, kindly provided 145.5 nm diameter nanoparticle samples of cross linked polymer for comparison with single chain samples. Table 2.1 provides details of all samples used.

Polymer code/category	Primary monomer constituent	Comonomer	Made by group	Simple description	Titration M_n	GPC M_n	GPC M_w	GPC pd	LCST(°C)
Chain length Variation									
pNIPAM MCL 1	NIPAM		Alexander	"Standard"		8620	17400	2	35
pNIPAM MCL 2	NIPAM		Alexander	Medium chain length		11500	24600	2.1	35
pNIPAM SCL	NIPAM		Alexander	Short chain standard	2488				35
pNIPAM HCL	NIPAM		Alexander	Long chain standard	66443	28500	48900	1.7	35
Copolymerisation									
pNIPAM-co-tBu	NIPAM	t-Bu acrylamide	Alexander	co-t-Bu	2929	5960	12500	2.1	27.5
pNIPAM-co-Acr	NIPAM	acrylamide	Alexander	co-Acrylamide	10524	11700	23600	2	42
Side Chain Variation									
pNNPAM HCL	NNPAM		Volk	Long chain n-propyl		3640	8270	2.3	23
pNNPAM SCL	NNPAM		Volk	Short chain n-propyl		2650	4990	1.9	27
pNCYPAM HCL	NCYPAM		Volk	Long chain cyclopropyl		12200	32400	2.6	52
Crosslinking									
NANOpNIPAM[56]	NIPAM	AAMPS	Asher	145 nm pNIPAM gel nanoparticles				1.108 (Light scattering)	35

Table 2.1: Polymer component and molecular mass data. NIPAM=N-isopropylacrylamide, NNPAM=N-(n-propyl)acrylamide, NCYPAM=N-cyclopropylacrylamide. tBu= tert-butylamine AAMPS=2-acrylamido-2-methyl-1-propane-sulfonic acid SCL, MCL, HCL refer to short, medium, and high chain-length, respectively. GPC= gel permeation chromatography (see section 2.2.4). LCST= lower critical solution temperature (defined as the midpoint of the transition, as seen in temperature dependent UV-vis absorbance spectra, see section 2.6). M_n=number average molecular weight. M_w=weight averaged molecular weight. Pd= polydispersity.

2.2.2 Synthesis of pNIPAM and Copolymers

Synthesis of single chain pNIPAM

Free radical polymerisation was used for synthesising the polymers investigated here due to its high yield and throughput. It does have some disadvantages, however; due to the limited control over the reaction compared with more modern types of polymer synthesis (e.g. RAFT, or living polymerisation), the products often have a relatively high degree of polydispersity. Although it is impossible to exert complete control over the molecular weight of the products with

this method, polymer size can be adjusted easily by varying the ratio of initiator to monomer, with an increase in the relative initiator concentration resulting in shorter polymers. Adding chain transfer agents, such as 3-mercaptopropanoic acid, to the reaction mixture can further reduce the chain length. Table 2.2 details the reaction conditions for each polymerisation.

Polymer code	M_n(GPC)	M_w(GPC)/ diameter	Primary Monomer	Comonomer	Solvent	Initiator	Chain transfer agent/crosslinker
pNIPAM MCL 1	8620	17400	NIPAM 10 g		2-Propanol (40 mL)	AIBN 0.2 g	2-Aminoethanethiol. HCL 0.2 g
pNIPAM MCL 2	11500	24600	NIPAM 10 g		2-Propanol (40 mL)	AIBN 0.1 g	3-Mercaptopropanoic acid 54 µ l
pNIPAM SCL	2488(by titration)		NIPAM 10 g		2-Propanol (40 mL)	AIBN 0.8 g	3-Mercaptopropanoic acid 54 µ l
pNIPAM HCL	28500	48900	NIPAM 10g		2-Propanol (40 mL)	ACVA 0.05 g	
pNIPAM co-tBu	5960	12500	NIPAM 8.34 g	t-Bu Acrylamide 1.66 g	2-Propanol (40 mL)	AIBN 0.8 g	3-Mercaptopropanoic acid 54 µ l
pNIPAM co-Acr	11700	23600	NIPAM 9 g	Acrylamide 0.63 g	2-Propanol (40 mL)	ACVA 0.3 g	3-Mercaptopropanoic acid 54 µ l
NANOpNIPAM		145nm	pNIPAM 1.4 g	AAMPS	H_2O	$(NH_4)_2S_2O_8$	N-NMBA

Table 2.2: Reaction conditions compared to molecular weight. AIBN=Azobisisobutyronitrile. ACVA=4,4'-Azobis(4-cyanovaleric acid), AAMPS=2-acrylamido-2-methyl-1-propanesulfonic acid, N-NMBA=*N,N'*-methylenebisacrylamide

The lower critical solution temperature (LCST) of pNIPAM is largely unaffected by chain length and concentration[43]; however, it can be tuned by copolymerising pNIPAM with other monomers. To ensure the random dispersal of such comonomers within the chain, a comonomer of similar reactivity to pNIPAM is required, which is why it is desirable to use variants of the NIPAM monomer with alternative alkyl side chains. This ensures a similar reactivity during polymerisation, while the alternative alkyl group influences the LCST by adjusting the hydrophobicity of the polymer. The polymer was then air-dried, and redissolved in D_2O/H_2O for experiments.

Synthesis of pNIPAM nanoparticle gels

Crosslinking of pNIPAM produces a 3-dimensionally structured gel, in which the volume can be thermally controlled in a similar manner to the single chain polymer. It is these bulk gels that provide the most promise as a component of

thermally switchable drug delivery devices, which take advantage of the dramatic changes in volume to block and unblock drug delivery channels or to expel preabsorbed therapeutic agents[93-95]. Asher *et al*[56] synthesised nanoparticle sized pNIPAM gel spheres (NANOpNIPAM) that have an internal gel structure but act as free agents in solution. Professor Asher kindly provided a sample of 145 nm nanoparticles synthesised in an identical fashion to those presented in his paper discussing phase transition dynamics in pNIPAM nanogels, studied by UV-resonance Raman probed Tjump experiments[56] for our investigations (see chapter 5 for a detailed discussion of this work).

The nanoparticles had been synthesised by dispersion polymerisation. 1.4 g of NIPAM monomers were mixed with 0.0242 g of 2-acrylamido-2-methyl-1-propanesulfonic acid (ionic co-monomer), 0.0659 g of *N,N'*-methylenebisacrylamide (cross-linker), 0.036 g of sodium dodecylsulfate (surfactant) and 0.088 g of ammonium persulfate (initiator) in 100 mL of deionized water and reacted at 70°C for 4 hours with stirring. The product was filtered (glass wool) and dialysed against deionized water for 2 weeks using a snakeskin dialysis tube (10'000 MW pore size) to remove impurities and unreacted monomer.

To exchange the solvent for D_2O for IR experiments, 0.5 ml of a 10 mg/ml solution of the nanoparticles (as provided by Asher) was dialysed against 2 successive fractions of 25 ml of D_2O using a Teflon dialyser with the entrance covered with a dialysis membrane (10'000 MW pore size). This was very effective, reducing the HOD content close to that found in the neat D_2O solution purchased from Sigma Aldrich (99-99.9% D_2O), as judged by the HOD band at 1460 cm^{-1}

2.2.3 Synthesis of poly(*N*-Alkylacrylamide) Variations

Polymer code	Mn(GPC)	Mw(GPC)	Primary Monomer	Solvent	Initiator	Chain transfer agent/crosslinker
pNNPAM HCL	3640	8270	NNPAM 2 g	THF (10 mL)	AIBN 0.02 g	
pNNPAM SCL	2650	4990	NNPAM 2 g	THF (10 mL)	AIBN 0.02 g	3-Mercaptopropanoic acid 0.02 g
pCYPAM HCL	12200	32400	NCYPAM 2 g	THF (10 mL)	AIBN 0.02 g	

Table 2.3: Reaction conditions and molecular weight for alkylacrylamide variants. THF = Tetrahydrofuran,

Homopolymers, poly(*N*-cyclopropylamide) (pCYPAM) and poly(*N*-*n*-propylacrylamide) (pNNPAM) were synthesised during the course of this project in

accordance with standard methods of pNIPAM free radical synthesis as performed by Cameron Alexander's group, which are described above (reaction conditions in table 2.3). Briefly, the alkylacrylamide monomers are synthesised, then polymerised using a free radical initiator. A chain transfer reagent is added to the polymerisation reaction mixture to reduce the final chain length.

Initially, the monomers were synthesised at Nottingham University under the supervision of Dr. Cameron Alexander in collaboration with Dr. Wang Wenxin. Polymerisation was initially attempted at Nottingham University. Difficulties with the polymerisation of *N*-cyclopropylamide meant a second attempt at the synthesis of both the monomers and polymers at the University of Liverpool in Dr. Rick Costick's laboratory. The synthesis of each product was confirmed by NMR. The synthesis of the polymers was additionally confirmed by measuring their LCST with UV-vis spectroscopy, and comparing the result with those previously described.[26] (See section 2.6.3 for details). The principle synthetic route is shown in figure 2.1:

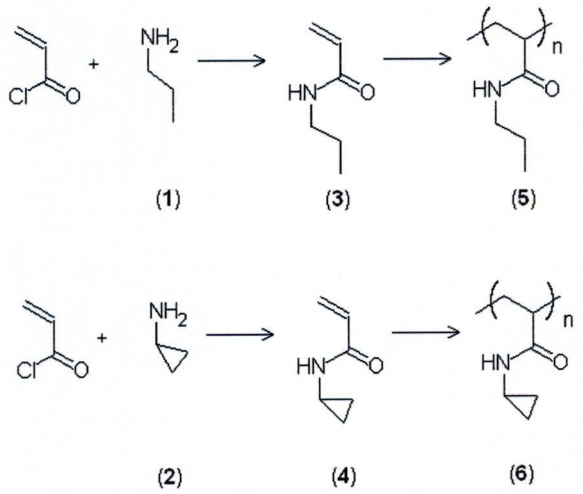

Figure 2.1: (**1**)N-(n-propyl)amine /(**2**) Cyclopropylamine is reacted with acryloyl chloride to produce the monomer (**3**)N-(n-propyl)acrlyamide/(**4**)N-cyclopropylacrylamide. This is then polymerised using AIBN as initiator and mercaptopropanoic acid as chain transfer agent to produce (**5**) poly(N-(n-propyl)acrylamide)/ (**6**)poly(cyclopropylacrylamide).

Synthesis of N-(n-propyl)acrylamide and N-cyclopropylacrylamide

10g (0.11 mol) of acryloyl chloride was added to 150 ml THF under $N_{2(g)}$ and vigorous stirring. To this, 14g of (**1**) cyclopropylamine or (**2**) N-(*n*-propyl)amine was added dropwise over 1 hour (approximately 1 drop per minute) at room temperature

and left over night. TLC showed monomer was formed (RF≈ 0.05 compared with 0.57 for acryloyl chloride and 0.8 for propylamines in 10% diethyl ether in hexane). The crude product was washed with 3 25 ml fractions of diethyl ether, dried with $MgSO_4$, filtered and concentrated *in vacuo*. 1.1 g of a red/yellow residue was produced. Yield is ~10% for both products.

NMR indicates that polymerisation of N-cyclopropylacrylamide occurs even before adding the initiator. Synthesis of poly(N-cyclopropylacrylamide) (**6**) has to be undertaken *immediately* after synthesis of the monomer is complete.

Synthesis of poly(N-(n-propylacrylamide) and poly(N-cyclopropylacrylamide)

10 ml of THF was placed in a sealed 3 neck flask and reflux apparatus and degassed for 10 minutes, the flask then was filled with an inert atmosphere (N_2). 2 g of Alkylacrylamide (**3**)/(**4**) from the previous reaction was dissolved in the THF, followed by 20 mg of AIBN initiator. To synthesise shorter chain-length polymers, an additional 20 mg of 3-mercaptopropanoic acid was added as a chain transfer agent. The reaction mixture was refluxed for 16 hours under nitrogen at 60°C.

For (**5**), after refluxing, the reaction mixture was notably more viscous. The reaction mixture was diluted with THF until it had a viscosity approaching that of water (30 ml THF added). It was then purified using the anti-solvent method, in which the reaction mixture is added dropwise to a beaker containing a large volume of a solvent in which the polymer is insoluble whereas the monomer is soluble (600 ml of Hexane under vigorous stirring). The polymer precipitates, and is allowed to settle before filtering and drying. NMR (in D_2O) showed that the polymer was pure. The product was a white powder, and the yield was 1.1g for pNNPAM-HCL (55%).

For (**6**), problems were encountered due to the unforeseen low solubility of the final product in THF. The polymer precipitated out of solution as it polymerised. This made it extremely difficult to purify, as the resulting polymer melt was too viscous for the antisolvent method to work. H^1 NMR (in D_2O) showed the polymer was correctly synthesised. Doubts about the purity of the polymer remained, however, and measuring the lower critical solution temperature (LCST) via UV-vis light scattering (see section 2.6) showed the transition occurred at a higher temperature than previously reported[26]. Washing the polymer with 10 fractions of toluene (performed

by 3rd year student Josh Musgreave) purified the polymer further, showing an LCST similar to that reported by Maeda *et al*[26].

2.2.4 Polymer Characterisation

Dr Alexander provided number averaged molecular weight (M_n) data determined by titration of acidic endgroups for some of the polymers (table 2.1). This method gives a good indication of the number averaged molecular weight of the polymers (M_n), but no information on the polydispersity or the (more important) weight averaged molecular weight (M_w), and is simply not applicable to polymers without acidic end-groups. To compare experimental observations it is necessary to analyse the M_n/M_w and polydispersity of all polymers in a similar fashion.

pNIPAM and derivatives are renowned for being difficult to analyse by Gel Permeation Chromatography (GPC), which is the standard method for characterising polymer molecular weights. In-house attempts to measure the M_n/M_w by GPC comparison with a number of polystyrene standards in a THF eluent system proved inconclusive due to pNIPAM sticking in the gel, resulting in molecular weights far higher than expected when compared with values obtained by end-group titration. Consequently, samples were sent to the EPSRC Polymer Characterisation Service (University of Swansea, project number AN0195) for comparison against poly(methyl methacrylate) (PMMA) standards in a high temperature (80°C) N,N'-dimethylacetamide eluent system. This gave more sensible results, (unfortunately, for polymer pNIPAM SCL there was not enough sample to analyse by GPC). Comparing the accurate M_n results obtained by titration with the "PMMA equivalent" molecular weights by GPC shows some deviation, meaning the quantitative accuracy of the absolute GPC results cannot be relied upon. Valuable relative information can be derived from the results, however: Firstly, the ratio of M_n to M_w should be accurate and was found to be similar for all polymers, which means that the actual M_w can be approximated from titrated M_n results. Secondly, polymers with the same alkyl-side chain (eg, all homopolymers with an isopropyl group) are expected to follow a similar relationship when comparing the M_n values determined by titration/GPC, so we can investigate the effect of chain length on the phase transition well, as long as the side chain is the same. On the other hand, the ratio of M_n values determined by titration/GPC changes depends on the alkyl side chain of the polymer, probably due to a modified interaction with the GPC column gel. Even a small amount of

copolymerised N-(t-butylamine)-acrylamide is enough to skew the ratio (see table 2.1, pNIPAM-co-t-Bu) vs. pNIPAM which casts doubt on our ability to take into account polymer chain-length effects when comparing the phase transition of samples with diverse side chains. GPC results are included in table 2.1.

Samples were also sent for MALDI-TOF mass spectroscopy at the national EPSRC mass spectrometry institute (Swansea University). The results were universally small masses detected for all polymers, in disagreement with titration and GPC average mass results, indicating severe fragmentation, so were disregarded.

2.2.5 Sample Cell

In all experiments, the sample was held in a homemade temperature controlled cell. A stainless steel and copper cell with the same general design were used. The sample was held between two CaF_2 windows separated by a Teflon spacer, with a thickness usually of the order of 50 μm and temperature controlled by a water jacket connected to a water bath. In cases where the sample required flowing, the spacer was cut to allow fresh sample to be pumped into the cell via luer connectors on either side of the cell jacket.

The extreme sensitivity of pNIPAM to temperature means that the temperature needs to be defined with great accuracy. To control the temperature jump accurately we need to control both the start and target temperature. The start temperature is controlled by flowing water through the jacket of the cell using a temperature controlled water bath (Grant Instruments). Note that the temperature of the cell is lower than the set temperature of the water bath due to heat losses in the intervening tubes. The temperature was calibrated using a Perspex window with an embedded Pt100 resistor. The resistor was calibrated by exposing the window to water at different temperatures (from 0°C to 100°C in 5°C steps) and measuring the resistance. Temperature (ϑ/°C) and resistance (R/Ω) were found to follow a linear relationship described by equation 2.1:

$$R = 0.367 \cdot \vartheta + 101.027 \qquad (2.1)$$

The resistor was then used in the place of a sample in the cell under normal experimental conditions for both cells. The temperature controller was set to a wide range of temperatures and the resistance at each temperature was recorded. The temperature inside the cell was seen to stabilise at temperatures slightly below the set

temperature within ≈ 8 minutes. A linear relationship between the set temperature and the actual sample temperature was established for both the copper and the stainless steel cell, which enabled the start temperature to be set accurately within 0.1 degrees.

2.3 Temperature Jumps on the 20 ns-1 ms Timescale

This setup was initially designed to observe peptide dynamics on the 100-500 ns timescale[81,96,97]. Peptides contain amide bonds, which are primarily responsible for the distinctive secondary structural behaviour as well as a characteristic infrared response to secondary structural changes in the amide I' region of the spectrum. pNIPAM also contains amide bonds which are extremely sensitive to changes in hydrogen bonding, and characteristic changes in hydration structure can be observed by following their resulting effect on the amide I' region. This setup is therefore a perfect candidate for observing the pNIPAM phase transition on a short timescale. Extensive changes have been made to the setup since the work carried out by S. Petty[97]. Although the probe system remains largely unchanged, an entirely new pump laser has been introduced, with corresponding changes in optics. The majority of the technical improvements in this PhD project have therefore been the implementation of this new laser system and solving related issues.

2.3.1 Nd-YAG Laser System and Optics Setup

The Nd-YAG pump laser produces nanosecond pulses of light at 532 nm wavelength to pump the sample. The pump laser used is a Quantel "Brilliant" Nd-YAG laser with a laser gain medium consisting of Nd^{3+} ions doped into yttrium aluminium garnet; a population inversion is induced by pumping the Nd^{3+} ions into an excited state using a flash lamp, which produces intense microsecond flashes of white light. When excited Nd^{3+} ions in this environment relax, 1064 nm light is emitted. To ensure the light is emitted as a strong short pulse rather than a weak CW beam, a Pockels cell Q-switch arrangement is fitted to the laser cavity. The Q-switch blocks transmission of 1064 nm light when no voltage is applied. This prevents lasing and, therefore, allows the build-up of a high population inversion. When the Q-switch is switched to transmission mode, lasing becomes possible and stored energy is converted into a high intensity laser pulse, but with short duration.

Using the internal Q-switch delay, the pulse is emitted from the laser with 100 mJ energy at the fundamental wavelength (measured with a model 17An thermopile, Laser Instrumentation Limited); this value is considerably less than shown in the manufacturer's specifications (360 mJ), and is evidence that the laser has degraded. An external Q-switch delay generator is required to generate the maximum possible pulse energy (120 mJ at 1064 nm), indicating that the population inversion build up is slower. This suggests that something is misaligned or damaged in the laser, slowing/reducing the inversion build up.

A 2^{nd} harmonic generator non-linear crystal is used to convert the fundamental radiation to 532 nm light, the two resulting beams are separated using a dichroic mirror, and the remaining 1064 nm light is dumped into a heat sink. The 532 nm beam then exits the laser and is focussed onto the sample via our optics setup, of which a schematic is shown in Figure 2.2 and details are given in table 2.3.

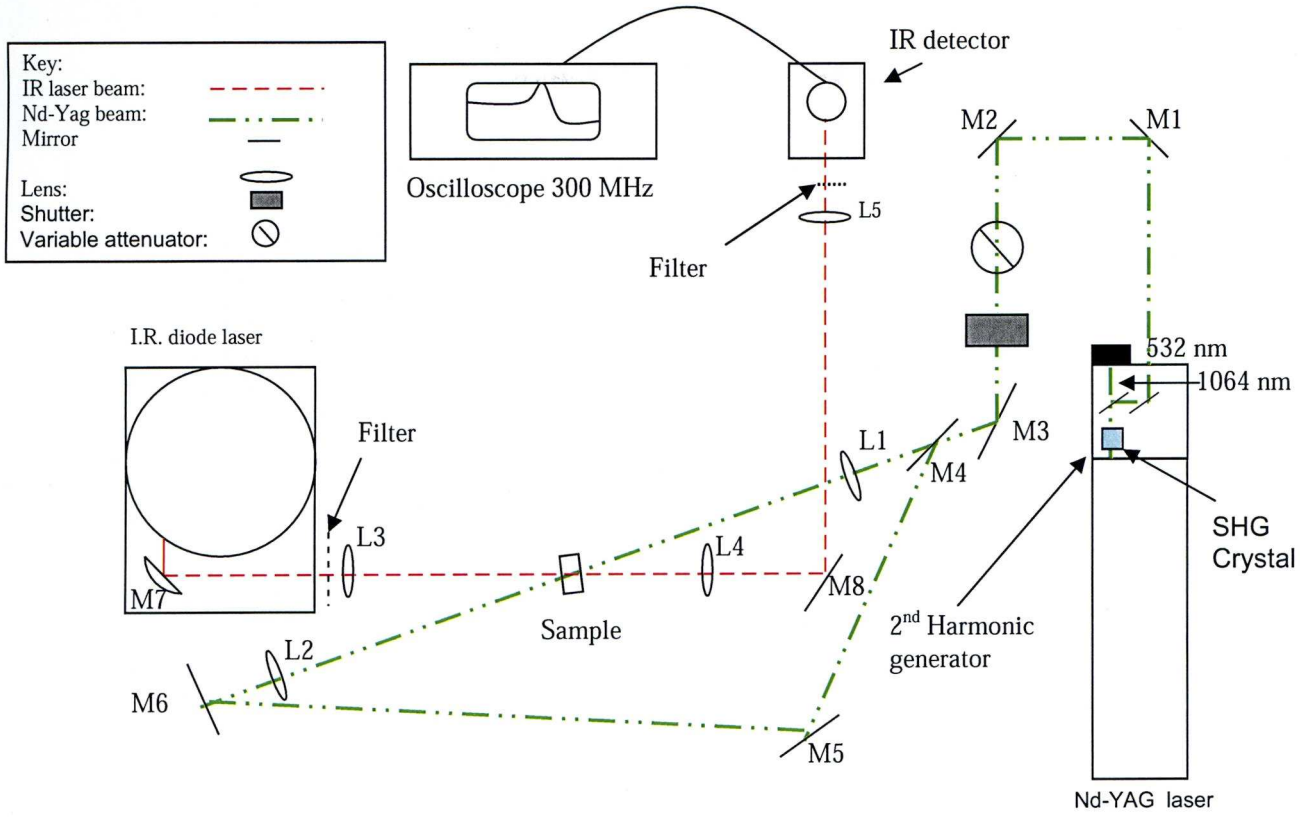

Figure 2.2. Laser setup

Key	Material	Diameter (mm)	Focal Length (mm, lenses)
L1	Quartz	25.4	550
L2	Quartz	25.4	300
L3	Calcium Fluoride	25.3	150
L4	Calcium Fluoride	50.8	150
L5	Calcium Fluoride	50.8	150
M1	UV-mirror (20% reflection @532 nm)	50.8x25.4	
M2	Al	25x20	
M3	Al	25.4	
M4 (beamsplitter)	Broadband femptosecond laser mirror	25.4	-
M5	Al	24.9x21	
M6	Al	24.9x23	
M7	Gold	34x24	Parabolic
M8	Gold	50.8	
Filter	Long –pass interference filters, cut-on 5000 nm	25.4	

Table 2.3: Optics specifications

The second harmonic generator enables us to get 5ns pulses of up to 40 mJ at 532 nm, the wavelength absorbed by the heat transducing dyes. The energy of the

beam is far in excess of what is required for the measurements, so is further reduced by reflection from mirror M_1, which reflects about 20% energy. Additional reflections are blocked by the aperture close to M_3, resulting in a single beam and a mechanical shutter is used to block the beam for temperature jump reference measurements or to preserve the sample during adjustments. An energy of up to 8 mJ is attainable (detected by a Molectron Energy Max 400 Detector) at this point. The pump beam optics and profile are described in section 2.3.4.

2.3.2 IR Probe Beam

The effects of the temperature jump on the sample were probed by measuring the absorbance of a continuous IR beam provided by a single-mode Műtek TLS 150 tunable lead-salt diode laser, which achieves population inversion by applying a voltage to the p-n junction. The laser has a power of ~0.2 mW and can be tuned to wavelengths between 1570 cm^{-1} and 1641 cm^{-1} by small adjustments to the temperature and current. The best available modes were recently calibrated by R. Whynes[98]. The beam produced is collected and collimated by mirror M_7, and focused onto the sample volume affected by the pump beam by lens L_3. Once the beam has passed through the solution, the remaining light is recollimated by L_4, redirected by M_8 and focussed by L_5 into the IR detector. Filters that reject light at 532 nm are placed on lens L3 and in front of the detector in order to prevent scattered light from the pump beam entering the IR laser or detector.

The absorbance after the sample is measured with a Kolmar KMPV50-0.5-J2 fast (50 MHz) infrared detector fitted with an $N_{2(L)}$ cooled Mercury Cadmium-Telluride photodiode. This typically has a rise time of 7.5 ns, but has been modified to eliminate an artefact (signal overshoot) using a 57Ω resistor, which limits the time resolution to 15 ns[97]. The detector signal is read in and digitised by a 300 MHz digital oscilloscope (Tektronic TDS 3032), triggered by the detection of the scattered light produced from the pump laser pulse by a visible light detector. Data collected is then transferred to a computer. The detector response becomes non-linear above 300 mV signal due to saturation effects, i.e. increasing the power incident on the detector does not linearly increase the signal detected. Care was therefore taken to maintain the signal at 300 mV or lower (300 mV is the optimal signal, as a higher signal produces a higher signal-to-noise). Limiting the signal magnitude was achieved by placing CaF_2 windows in front of the detector.

The focus of the IR probe beam was located with a 100 μm circular pinhole, and the position of lens L_3 fine-tuned to optimise the position of the probe focus to obtain a profile with a diameter of <100 μm at the position of the sample. In order to accurately measure the IR beam profile, a razor blade was attached to the same mount as the 100 μm pinhole and the beam profile measured by translating it across the IR beam at exactly the same position, recording the detector signal and differentiating it (Figure 2.3). Because of the change in refractive index of the various optics between the laser and detector when varying wavelength, the position of the beam focus is shifted by a small amount when switching between wavelengths. The position of L_3 in the x, y and z direction are therefore adjusted each time the laser mode is changed to observe a different portion of the amide I' band.

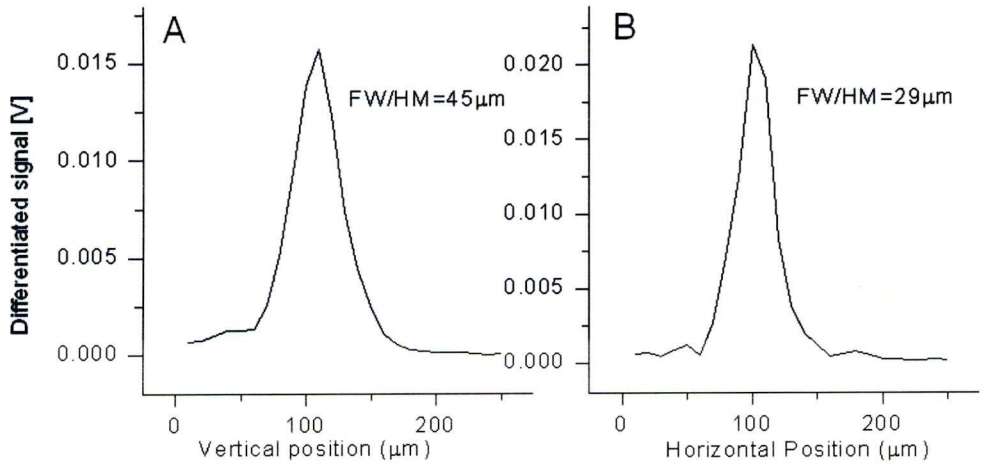

Figure 2.3: IR beam profile at 1583 cm^{-1}. A) Vertical and B) Horizontal.

Typical high signal to noise Tjump measurements involve averaging 25'000 individual measurements probing the polymer dynamics at 1622 cm^{-1} and 15'000 "background" measurements where the IR absorbance response is measured at 1583 cm^{-1}, a wavelength at which the polymer has no absorbance. It is therefore extremely important that the setup is reliably stable for long periods of activity. By making the technical improvements detailed in this chapter and by taking great care during a measurement, the stability of the setup can be maintained for the long periods required for a full experiment.

2.3.3 Indirect Heating Temperature Jumps

2.3.3.1 Heat Transducing Dyes

Our pump lasers emit light at 532 nm. Light at this wavelength does not interact with either the polymers or D_2O solvent, so we require an additional solute that:

- Absorbs strongly at 532 nm;
- transforms absorbed energy into heat faster than our time resolution;
- does not interact with the polymer sample;
- is stable in solution.

Two solutes that fulfil these criteria to varying degrees are basic fuchsin (basic red, BR) and peptide-capped Au nanoparticles (AuNPs).

2.3.3.2 Basic Red Dye

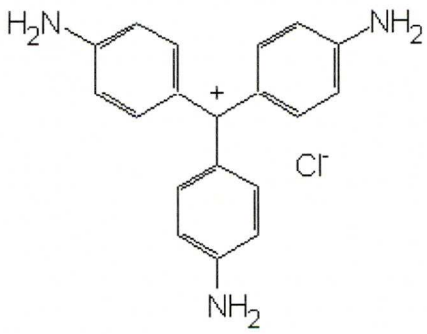

Figure 2.4: Structure of basic red

Initially, only basic red dye was available as a heat transducer. It is more stable to photolysis than similar dyes[97]. Basic Red (BR) is a tri-phenylmethane dye (Figure 2.4) that absorbs light in the 530 nm region near the 2nd harmonic of the Nd:YAG laser (Figure 2.5), promoting it to the S_1 excited state. Rapid relaxation by internal conversion then occurs in which the energy is released into surrounding solution as heat. The relaxation is rapid enough not to affect our time resolution[99]. FTIR measurements comparing the effects of temperature on the amide I' band of PNIPAM with BR dye show that its presence does not change the LCST or otherwise affect the coil-globule transition .

The major drawback of BR is its limited stability. BR is sparingly soluble in D_2O, causing numerous experimental obstacles that must be countered for obtaining consistently stable Tjumps. Bleaching of the dye is a particularly difficult problem, both on the short and long timescale; the dye bleaches visibly when subjected to excitation from 532 nm light at the 10 Hz repetition rate of the Nd:YAG laser. Consequently, the sample must be moved regularly. The first attempt to overcome this problem involved flowing the sample through the cell continuously with a peristaltic pump (Autoclude EV45), but this proved unsuitable, as a number of difficulties then arise. In particular, BR aggregates are pumped through the beam path, which act as an initiator for the occurrence of photoacoustic cavitation events[100] (See section 2.3.3.4). It was also discovered that the dye solution bleaches strongly in the peristaltic pump system, even when not affected by the laser, due to adsorbance of BR onto the walls of the peristaltic pump tubing; and different tubing materials were tried with little success; the only tubing material resistant to BR adsorbance is Teflon, which is too hard to be used with our peristaltic pump. Ultimately, a home-made sample system with a glass reservoir connected via a Teflon tube to the cell and a disposable 1 ml syringe for pumping the solution into and out of the cell proved to be an effective solution. Photobleaching is effectively eliminated by flowing once after every set of 128 laser excitations, and cavitation aggregate-induced cavitation does not occur since the sample is not flowing during the measurements.

Some of the BR molecules are bleached irreversibly during Tjumps, resulting in a gradually declining absorbance and thus temperature jump as the experiment progresses as dye bleaching accumulates. This was counteracted by gradually increasing the power of the pump beam, as described in section 2.3.4.3. Finally, ambient UV light from fluorescent lighting was found to be a further cause of dye bleaching, so all good quality BR-based measurements presented in this thesis were performed in the dark.

Basic red was used as supplied by Sigma-Aldrich. A basic red absorbance of approximately 0.14 was used in Tjump experiments, as this provided a sufficiently large Tjump, while preventing an inhomogeneity of the size of the Tjump along the sample beam path due to absorption of the light as it traverses the sample (see section.2.3.4.1). The BR extinction coefficient at 532 nm was calculated from extremely dilute BR samples to be ~ $M^{-1}45'000\ cm^{-1}$, which indicates a concentration

of 0.62 mM for samples with 0.14 absorbance. With this absorbance, reliable temperature jumps of 6 K where achieved, with relatively few cavitation events.

2.3.3.3 Peptide Capped Gold Nanoparticles

During the course of this PhD, 5 nm diameter gold nanoparticles capped with CALNN peptides (AuNPs)[101] were found to offer an excellent alternative to BR, as they perform effective heat transduction without many of the stability problems associated with BR. Flowing the sample is no longer required, which speeds up the measurement process quite considerably, and removes a possible source of human error. The higher extinction coefficient means that a lower concentration must be used (approximately 4.3×10^{-6} M to give an absorbance of 0.25), which increases the distance between heat transducers in solution, thus slowing temperature equilibration immediately after a temperature jump. However, the equilibration time at this concentration is still ~5 ns, which is faster than our time resolution[98] Gold NPs absorb pump light in the plasmon band, which excites the free electrons of the nanoparticles. The canonical picture of AuNP heat transduction is as follows: The absorbed light is converted to electronic heat, which is rapidly (within ps) coupled to lattice vibration phonons (e-ph coupling), followed by the phonon-phonon equilibration (ph-ph coupling) between the AuNP lattice and surrounding solution.[102] Evidence from pump-probe femtosecond absorption experiments[103] shows that for nanoparticles of 5 nm diameter, the majority of energy is transferred to the solution even before e-ph coupling has reached equilibrium, and transfer to solution occurs on a timescale of 10±5 ps. This energy is then dissipated throughout the solution as heat and reaches a homogenous distribution in the pumped sample volume within 5-10 ns. AuNPs were synthesised by C. Shaw and R. Levy at the University of Liverpool.[101] Figure 2.5 shows a comparison of the UV-vis spectra for BR dye and AuNP. Compared with BR, the absorbance reduces at a far slower rate, allowing many more excitations before moving the sample. Only minor corrections to the pump beam power are required as the experiment progresses to counteract loss of AuNP concentration due to aggregation and binding to the cell windows after laser excitation. This causes peptides capping the nanoparticles to be dissociated off the nanoparticle surface. When the sample is initially irradiated by the pump beam in temperature jump measurements, there is a fast drop in absorbance, which also coincides with a large number of cavitation events. This is possibly linked to an initial deaggregation of any

loosely bound nanoparticles in the pump volume, and the sample quickly stabilises to produce a steady temperature jump with few cavitation. Steady-state FTIR measurements of pNIPAM with dissolved AuNPs around the LCST show no noticeable difference from neat pNIPAm measurements, showing that nanoparticles have no effect on the transition. Solutions of AuNP with concentrations that are usually used in Tjump measurements (~$1x10^{-6}$ mM, in D_2O) have no detectable absorbance contribution in the amide I region, and show no dynamics when Tjumped.

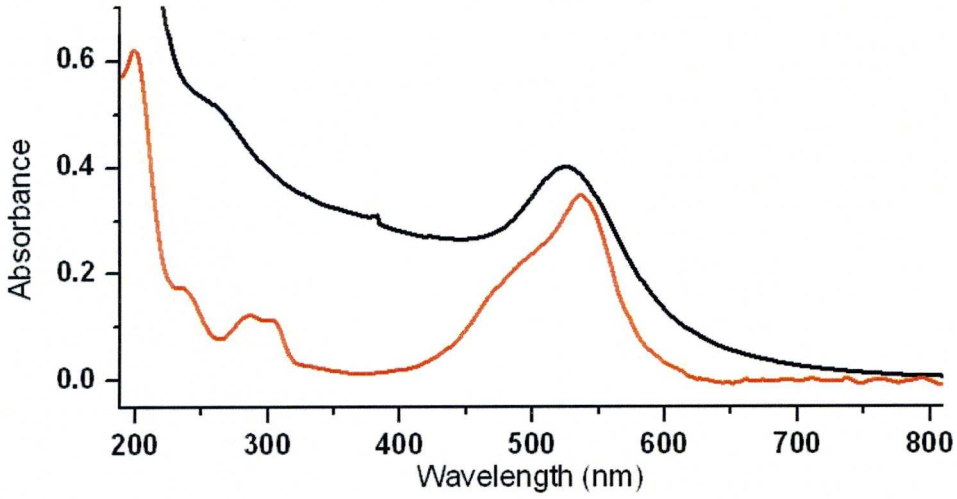

Figure 2.5: The UV-vis absorbance spectra of BR and AuNP dyes in D_2O. AuNP (black line) sample has $8.5x10^{-6}$ M concentration (6.2 mg/ml) BR (red line) sample has 0.6 mM concentration. Both samples are in a cell with a pathlength of 50 μm.

2.3.3.4 Photoacoustic Cavitation

Photoacoustic cavitation is an unwanted side-effect of heating a sample with a laser pulse which has been previously reported[84,100]. It is initiated by the sample being heated by the pulse, which increases the thermal energy of the solvent molecules, thus increasing pressure in the heated volume. The solvent molecules alleviate this pressure by moving outwards from the region of high pressure into the bulk solvent. The molecules, however, do not stop once equilibrium is reached, as inertia carries them past this point. This results in a volume of low pressure that causes a strain on the intermolecular bonds between solvent molecules, potentially exceeding the tensile strength of the solvent. This can create bubbles in the solution precisely where the sample is being heated.

The cavitation occurs rapidly (100 ns), and creates bubbles that distort the IR signal by scattering the probe beam light. The bubbles last long enough to obscure secondary structural changes in the time window from 100 ns~5 μs, and the increase in IR scatter when bubbles are formed is often of a higher magnitude than the IR absorbance change associated with secondary structural modifications. It is therefore necessary to prevent cavitation as far as possible. The effect occurs more frequently when dyes such as basic red are present[97]; dye aggregates seem to act as nucleation sites for cavitation, as stirring the dye sample for longer periods of time before performing Tjumps limits cavitation, whereas leaving the sample to stand has an increasing effect.

Initially, cavitation events could be limited to the rate of about 1 per 30 minutes by filtering the basic red samples with a 0.2 μm pore syringe filter to eliminate aggregates. The cavitation frequency has also been lowered by using a comparatively modest pulse energy (<2.8 mJ between M_2 and M_3) while increasing the concentration of dye, as high energy pulses unload more energy into the same dye aggregate, resulting in higher local pressure on the sample and thus increasing the likelihood of cavitation. Hot spots in the heated fraction due to diffraction patterns in the pump beam tend to increase the amount of cavitation events due to more localised heating. This can be seen from the dramatic increase in the frequency of cavitation events per measurement when early measurements are compared to those later in the project with the same Tjump and dye systems; during the latter, the quality of the Nd:YAG laser beam began to degrade, causing more hot spots in the pump laser profile. Cavitation events were so frequent in the final measurements that Tjumps were limited to 2 K, in comparison to earlier experiments in which 6 K jumps were reliably achieved with both BR dye and AuNPs with very limited cavitation events (often <5 per 25'000 measurements).

2.3.4 Technical Improvements to the Setup

A number of technical improvements to the existing setup[96,104] were required before the Nd-YAG laser was suitable for Tjump measurements. These are described below:

2.3.4.1 Nd-YAG Laser Beam Profile

In order to get high quality results, it is vital that the probed sample volume is heated homogeneously in **all** directions. To ensure equal heating over the cross section of the probe beam, the pump beam is configured to have a beam diameter of 500 μm when heating the sample, approximately 10 times larger than the probe beam, thus ensuring that when the probe is aligned to the centre of the pump beams, a uniformly heated cross section is probed owing to the Gaussian pump beam cross-sections. The lenses and mirrors associated with all 3 beams had to be adjusted carefully to obtain a diameter and profile that would result in high quality temperature jump measurements.

These profiles were measured by translating a 100 μm pinhole orthogonal to the pump beam at the sample position. The pinhole is translated with micrometer screws and the profile was measured by detecting the amount of light scatter produced by the beam on paper behind the pinhole with a visible light detector (Thorlabs, Det210). The maximum intensity of light was found, indicating the centre of the profile; the horizontal and vertical profile were then measured by translating the pinhole across the beam path in steps of 0.05 mm.

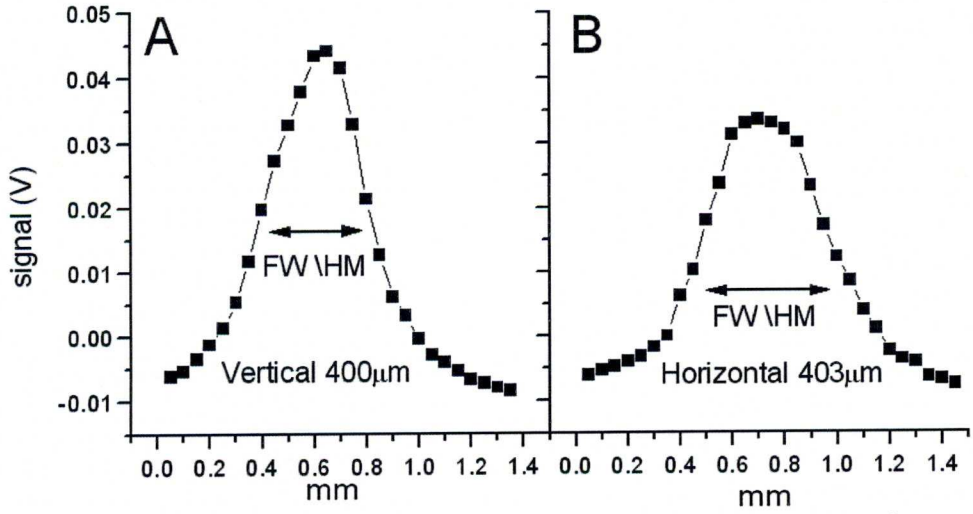

Figure 2.6 A) Vertical and B) Horizontal pump beam profiles at 2.7 mJ pulse energy output (measured after M_2)

A Gaussian profile has been particularly hard to achieve for the pump beam; many variations of lenses have been tested in order to get the desired size and shape, originally settling on the profile pictured in Figure 2.6 by using the optics setup shown in figure 2.3. However, due to the degradation of the Nd-YAG laser, obtaining

Gaussian profiles has been increasingly problematic. A burn spot and interference pattern are now visible on a standard laser paper image in the fundamental beam even before any optics are encountered, giving further proof of damage to the laser cavity. The latest beam profile can be seen in figure 2.7.

The "shoulder" visible in the horizontal profile has developed into a full secondary peak, and a considerable amount of beam energy wasted because of this. There is also an indication that the degrading beamshape has an adverse effect on the amount of cavitation during a temperature jump. (Section 2.3.3.4)

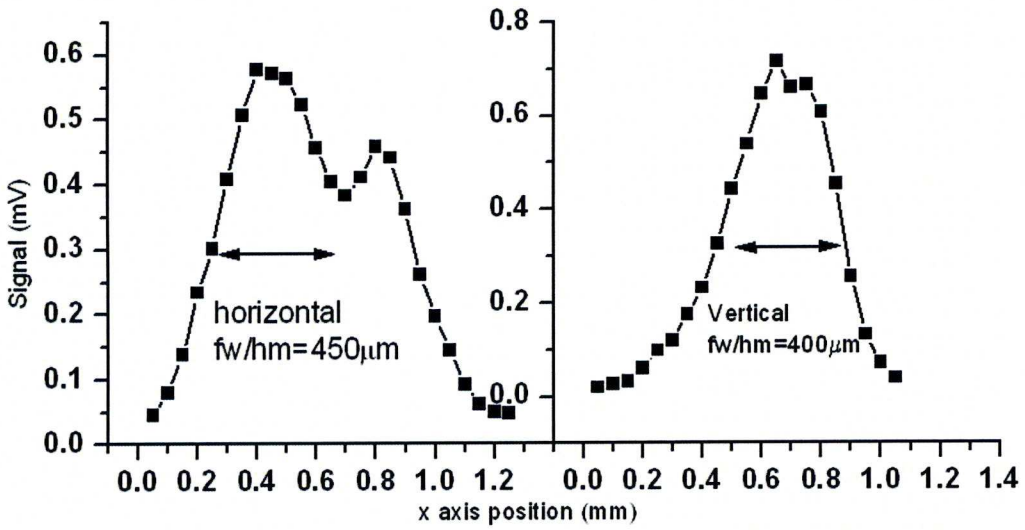

Figure 2.7: Best attainable pump beam profiles towards the end of the project.

2.3.4.2 Homogeneous Heating Along the Beam Path

The pump pulse energy drops as it travels through the cell, leading to a drop in the temperature jump along the beam path. In previous experiments by S. Petty using direct heating of the solvent, a concave mirror at position M_6 was used to reflect and re-focus the pulse back on itself, to provide additional energy and to balance out the non-uniform heating of the sample along the beam path. This setup works for the indirect heating method currently used, but only with low absorbance dye samples (up to approximately 0.15 absorbance). However, above an absorbance of 0.15, too much light is absorbed in the first pass through the sample for the reflected beam to balance the non-uniform heating. Increasing the laser energy is only effective at increasing the Tjump up to a point, because of excitation saturation (i.e. with enough energy, each dye molecule in the pump volume is excited immediately after returning to the ground state, further increases in energy have no additional effect). For larger Tjump

experiments, it was not possible to achieve the required Tjump size, while also attaining a homogeneous heating distribution due to the increasing concentrations of dye required to achieve a satisfactory Tjump, which prompted the implementation of the beam splitting optical setup shown in figure 2.3.

The premise is to ensure an equal amount of laser light is impinging on the sample from both the front and. An ultrafast broadband mirror was used (position M_4 figure 2.3) as a beam splitter. The reflection at 530 nm is highly dependent on the angle of the mirror. Changing the angle by small amounts results in fine tuning of the ratio of the forward and backward beam, enabling us to use a power ratio of 40:60 transmitted/reflected beam power (to account for the reflection losses on the additional mirrors required for retargeting the reflected beam). Calculating the approximate drop in the induced Tjump along the beam path (due to cumulative absorbance) shows that this setup is remarkably successful at heating the sample homogeneously, even for sample with an absorbance of up to 0.40.

2.3.4.3 Nd-YAG Laser Power Adjustment

Local bleaching of the absorbance at 532 nm of the heat transducer occurs in the pump volume as the dye degrades or aggregates, particularly with basic red which bleaches rapidly, lowering the Tjump at a rate of approximately 7% every 150 laser excitations at standard conditions (0.15 OD absorbance, 2.7 mJ laser energy for a 6 K Tjump). Bleaching can be effectively counteracted by moving the cell or flowing the bleached dye solution away from the pump volume in between experimental sets. However, the number of available dye molecules in the entire solution decreases over time, leading to a decrease in the Tjump. The only way to counteract this is by increasing the pump pulse energy.

Increasing the pump pulse energy electronically requires changing the Q-switch delay. However, the built-in Q-switch delay controller is too coarse for the fine adjustments required to correct the gradual decay in temperature jump size during a measurement. Also, changing the delay has an adverse effect on the stability of the laser if adjusted too far from the optimum, and introduces a large variation in the laser power output. Integrating a more sensitive potentiometer into the Q-switch delay controller was a solution good enough to provide a satisfactory Tjump stability, and many of the successful high signal-to-noise pNIPAM dynamics measurements were done with this approach.

The degradation of the Nd:YAG laser performance eventually meant that further changes were necessary to achieve satisfactory Tjumps. The laser output began to fluctuate during experiments and the power output dropped substantially. Ultimately, this problem was rectified by implementation of an external Q-switch trigger and a variable attenuator (actually a high energy femtosecond mirror). Changing the angle of the attenuator/fs-mirror results in a shift of the peak interference wavelength, and a change in the amount of 532 nm light that passes the coating, so the laser pulse energy can be controlled by varying the angle by small amounts. This setup affords complete control over laser power and yields the maximum possible stability. Rotation of the attenuator (with the Q-switch delay set to 85% maximum output, giving a 15% leeway for counteracting the inevitable dye bleach) gives a coarse control over the size of the temperature jump, and fine adjustments can be made by altering the Q-switch delay minimally.

2.3.5 Temperature Jump Measurement and Analysis

2.3.5.1 Sample Characterisation

Before measurements, the samples were characterised by taking an FTIR spectrum to measure the concentration of pNIPAM polymer and a UV-vis spectrum to measure the absorbance of the heat transducing dye/AuNPs. FTIR spectra were taken after each full measurement to ensure that no damage had occurred to the sample by comparing the amide I' band of the spectra before and after the measurement (see section 2.6).

2.3.5.2 Pump-Probe Beam Overlap

Before measurements can be taken, the pump-probe overlap must be optimised to ensure that the volume probed is heated homogenously. The procedure is as follows:

1. The pump beam is blocked using the electronically controlled shutter.
2. The IR laser focus position is marked with a circular 100 μm pinhole. This gives us a reference point for pump/probe overlap.
3. An attenuator is placed behind the shutter so the pump beams do not damage the pinhole. The pump beams are then aligned onto the pinhole, thus ensuring rough overlap on the sample.

4. The pinhole is replaced by the sample in a temperature controlled cell, and the attenuator is removed. By triggering the oscilloscope to record when the scattered light from a pump laser pulse is detected by a fast light detector, the induced Tjump can be detected as a change in the absorbance of the IR probe beam.
5. The beams are not perfectly aligned as the angle of incidence and thus the effect of refraction in the cell windows on the pump and probe beams are different. The overlap is then maximised using a program written for the purpose. The oscilloscope averages four single measurements, and the program downloads this information, takes an average of the signal strength before and after the Tjump and compares the two. Optimisation of the pump-probe overlap is then obtained by readjusting the pump beam positions using L_1 for the "forward" and M_6 for the "backward" pump beams to increase the difference in absorbance as much as possible.

2.3.5.3 Temperature Jump Calibration

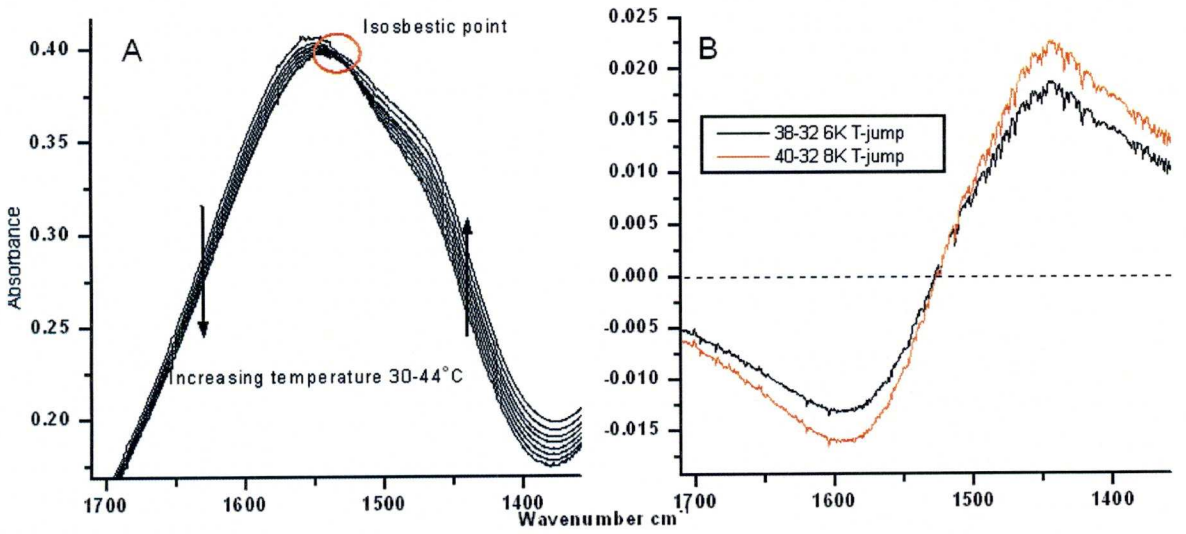

Figure 2.8: A) Temperature dependent absorbance of D_2O in the association band region. **B)** Difference spectrum showing the absorbance changes expected for a 6 and 8 K Tjump at standard temperatures (calculated by subtracting the upper temperature spectrum from the lower).

The temperature jump is calibrated using the association band of D_2O (Figure 2.8 A), which lies in the same spectral region as the amide I' band and responds reproducibly to changes in temperature faster than our time resolution. The association

band therefore makes an ideal "internal thermometer" with which to determine the magnitude of the temperature jump.

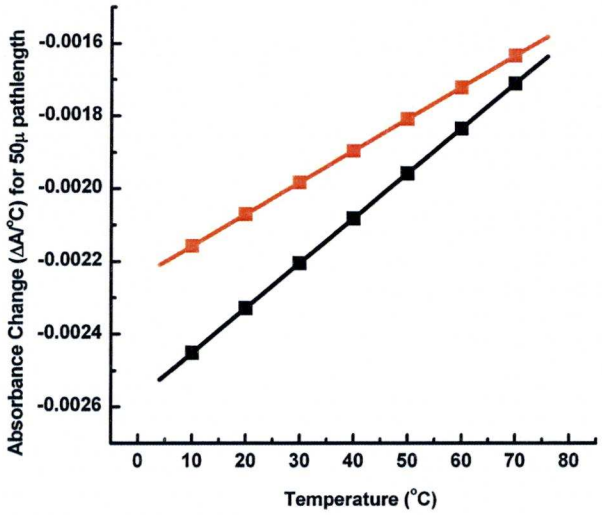

Figure 2.9: The absorbance change of D_2O per degree temperature change at different temperatures measured for 1583 cm^{-1} (black line) and 1632 cm^{-1} (red line) determined by R Whynes[98].

The exact absorbance change per degree was measured first by A. Pozo Ramajo[97] and later corrected by R. Whynes[98] (figure 2.9). Background Tjump measurements are taken at 1583 cm^{-1} at regular intervals during a measurement, as this wavenumber is outside the amide I' band, thus allowing us to measure and adjust the temperature jumps.

2.3.5.4 Measurement Procedure

The pump laser produces radio frequency (RF) electric noise that is picked up in the detector which has been minimised as far as possible by using double wire-mesh sleeves for all cabling, and by shielding all input and output points on the detector with copper tape[97]. Extremely high signal-to-noise measurements (averages of 30'000 single measurements) by A. Pozo Ramajo have shown that this noise is still present, although it is indistinguishable from the noise when averaging over less measurements, (figure 2.10).

The RF noise can be effectively eliminated by subtracting a "background" (BG) measurement in the same time-window, consisting of the same number of trigger events, but with the pump laser blocked, thus removing the reproducible RF noise. A program has been written to do this automatically with the aid of an electric shutter, which blocks the laser for a background measurement immediately after or before a

Tjump measurement (TJ), performed in the alternating order (BG-TJ, TJ-BG) etc (each of these is a BG-TJ "cycle"). This ensures that RF reproducibility is maximised due to the proximity of the measurements and removes the effect of any slow RF drift.

The measurement protocol is slightly different depending on the heat transducer. For BR, each cycle consists of 128 BG and 128 TJ single measurements. To refresh the sample after excitation induced dye bleaching, the sample is flowed with a syringe after each cycle and moved by 1 mm after every set of 5 cycles to avoid build-up of dye on the window. Owing to their higher stability, samples with AuNPs require less care than those with BR to obtain good quality measurements: After subjecting the sample to excitation light for 10 s to "burn off" any unstable nanoparticle aggregates, 5 cycles of 512 averaged individual measurements each are usually undertaken before moving the sample.

The BG and TJ averages for each cycle are imported into a PC as separate signals, and subtracted (the BG signal at times of more than 100 ns before triggering is averaged and used to shift the TJ signal back to its original level). Once the measurements have been imported, the signal is converted into absorbance change (ΔA) with the following equation:

$$\Delta A(t) = -\log\left(\frac{I(t)}{I_0}\right) \qquad 2.2$$

t is the time delay after the temperature jump, I(t) is the time dependent intensity (corrected for RF) and I_0 the intensity at negative times (i.e. before triggering, taken as an average). Note that the detector shows an offset of around -100 mV when the IR beam is blocked; to get the real signal it is necessary to measure this offset at regular intervals throughout the measurement and subtract it from I and I_0. Figure 2.10 shows a comparison of a raw measurement and the same measurement corrected for RF noise and converted into absorbance.

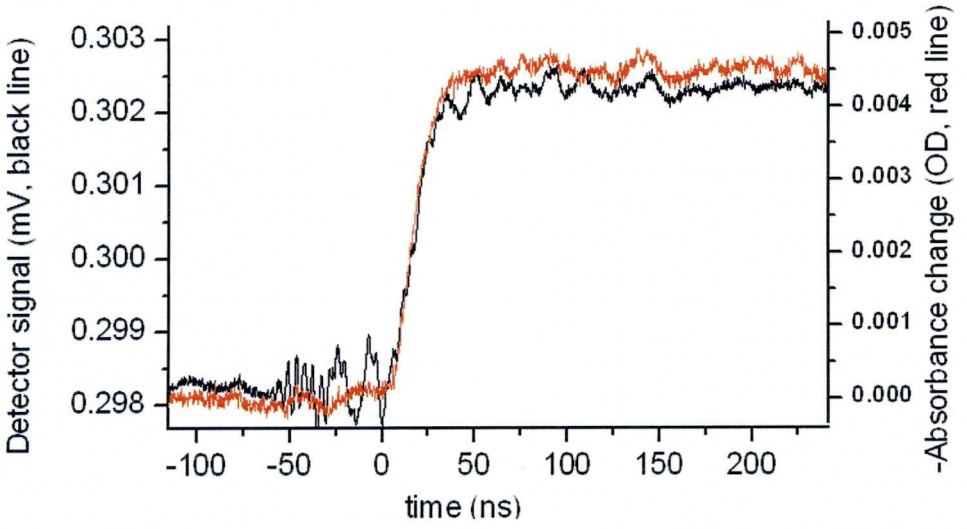

Figure 2.10: Example of a raw Tjump measurement (black line) and the same signal after RF correction by subtracting the corresponding background measurement, and conversion to change in absorbance (red line).

To allow elimination of measurements with cavitation events, a program was used which processes each cycle, allowing analysis of a cycle immediately after it is taken and thus repetition of any measurements which are distorted by cavitation as they happen. After every cycle was analysed in this way and the bad measurements had been removed, all good measurements were averaged to give a single high signal-to-noise curve. This average curve was then logarithmically averaged: After 50 ns, the program averages all values measured at times within 1% of each other, further smoothing the curve.

2.3.6 Measurement Corrections

There are a number of experimental artefacts that affect the absorbance of the sample. These must be corrected for before any pNIPAM dynamics can be accurately analysed. Figure 2.11 shows the reproducible artefacts that need to be corrected in order to isolate any signals from polymer dynamics that may be present. The same artefacts are seen in a neat D_2O sample, confirming that they occur independently of the sample

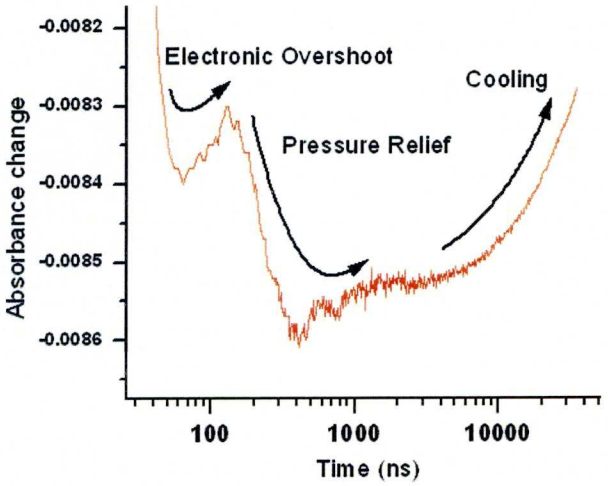

Figure 2.11: An example of a temperature jump measurement (NANOpNIPAM at 1583 cm^{-1}, 4 K Tjump from 34°C, average of 14'592 shots), enlarged so variations of 5% of the total signal change are visible. At this wavelength, the signal mostly arises from D_2O signal changes, and these artefacts are present in neat D_2O samples.

2.3.6.1 Cooling

After a Tjump, the heat contained in the pump volume disperses into the rest of the sample and the cell windows. It takes <10 ns for the temperature equilibrate in the heated volume. Complete cooling, though, is orders of magnitude slower than the initial heating pulse, and complete cooling of the probed sample volume after a temperature jump occurs on the order of milliseconds (figure 2.12); as seen by the recovery of the D_2O absorbance at 1583 cm^{-1}.

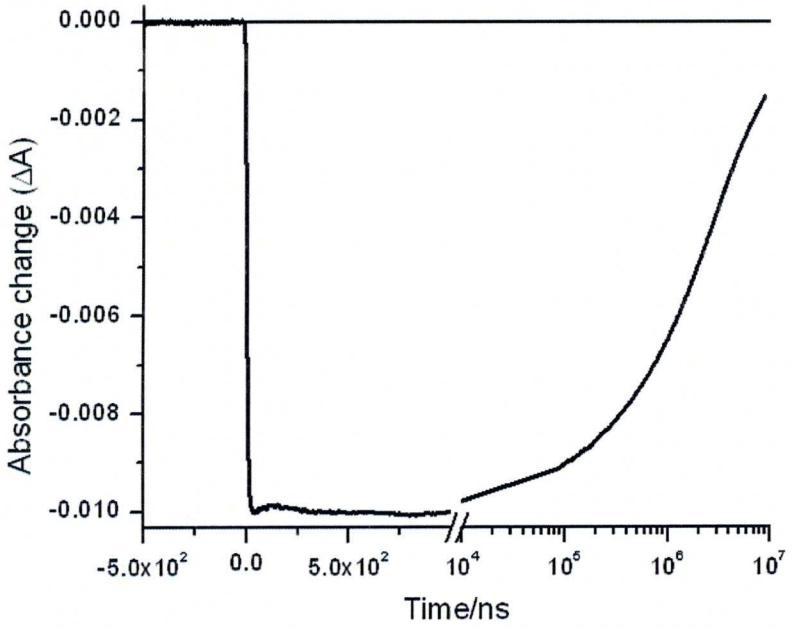

Figure 2.12: Cooling of a D_2O and AuNP sample (essentially, "neat" D_2O) after a 4.6 K Tjump from 32-36.4°C with a 50 μm pathlength. The absorbance changes at 1583 cm^{-1} (black) are shown, which is due a decrease in absorbance in the D_2O association band,. A line is added at ΔA=0 to guide the eye.

After 10 μs, the absorbance bleach at 1583 cm^{-1} has decreased by 1% by 3 μs. The halflife of cooling is about 2.2 ms which sets a limit on the timescale accessible with this setup. If the LCST is the midpoint of the Tjump (ideal, in order to see maximum absorbance change associated with transition dynamics), after the halflife the temperature falls below the LCST, halting the transition. By ~400 μs, the temperature has decreased by 20% in measurements with a 50 μm pathlength, and data after this point are not considered for analysis.

Wray *et al*[100] performed a finite element heat transfer calculation to simulate the cooling on a CaF_2-D_2O system almost identical to ours (with a pump-probe diameter ratio of 300:100 μm), resulting in cooling of about 10% after 50 μs which is in close agreement with our measurements. However, the cooling curve presented[100] shows an odd biphasic relaxation that differs strongly from our observations. The finite element calculation was repeated by M. Volk, who discovered that the reason for the biphasic cooling was simply that Wray had used too few finite element cells. Using the same number of cells replicates the biphasic result, whereas increasing the number of cells (particularly around the CaF_2-D_2O interface) results in a curve that is

in good agreement with our observations. Further, these results show that the majority of the heat transfer occurs at the CaF_2-D_2O interface due to the higher heat conductivity of the windows. Heat therefore escapes the probe volume by flowing into the CaF_2 windows and away from the sample, which has implications for extending the timescale of the measurement (see section 2.4).

There is an instantaneous bleach due to D_2O absorbance changes at 1622 cm^{-1} which is approximately equal to that seen at 1583 cm^{-1} However, this wavelength is inside the amide I' band, so in measurements where transition dynamics are present there will be an additional component due to amide I absorbance. The absorbance change associated with D_2O will follow an identical cooling curve to that seen at 1583 cm^{-1}.

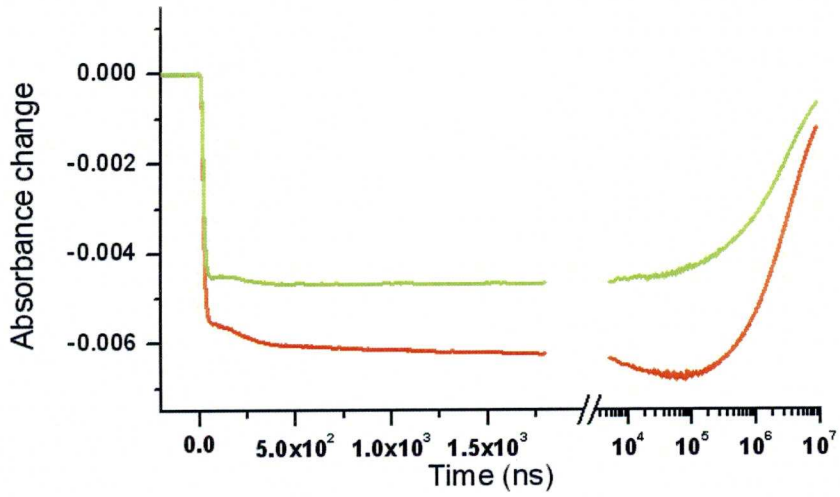

Figure 2.13: Cooling of a 10 mg/ml NanopNIPAM sample after a 1.3 K Tjump from 34-35.3°C. 1583 cm^{-1} D_2O only (green line) is shown alongside 1622 cm^{-1} polymer signal (red line). Each curve is a composite of a 2μs timescale measurement (an average of 20480 shots for 1583 cm^{-1} and 25344 shots for 1622 cm^{-1}) and a 10 ms measurement after the break (an average of 5120 shots each)

Comparing the 1583 cm^{-1} curve with the 1622 cm^{-1} curve (figure 2.13), one can see that there is an additional contribution to the absorbance change over time on the microsecond timescale at 1622 cm^{-1}. This is the polymer signal, containing interesting information about changes in secondary structure. From figure 2.13 we can see clearly that secondary structural changes are still occurring when cooling begins to dominate (around 30 μs); this onset of cooling may distort the dynamic component of any on the

nanosecond timescale, so a correction was also applied to measurements on that timescale.

To correct for the distorting effect of the onset of cooling, we fitted the cooling curve (i.e. absorbance recovery) in neat D_2O with exponential decay functions in the same manner as A. Poz. Ramajo[97], although with different time constants to account for different time windows.

For measurements up to 2 μs the time absorbance recovery due to cooling is described by the following equation (initially found by A. Pozo. Ramajo):

$$(1-c)+c\cdot e^{(-t/\tau_{cool})} \qquad 2.3$$

where c = 0.05 is the initial absorbance recovery due to cooling, t is the time delay (ns) and τ_{cool} = 10000 is the time constant of the initial cooling phase (ns).

For measurements up to 40 μs the absorbance recovery is described by the following equation (fitted by R. Whynes[98]):

$$(1-(a+b))+a\cdot e^{(-t/\tau_{cool1})}+b\cdot e^{(-t/\tau_{cool2})} \qquad 2.4$$

where a = 0.01 is the absorbance recovery due to a fast cooling component (which has a time constant (τ_{cool1}) of 2000 ns) with respect to the initial absorbance change, b = 0.075 is the absorbance recovery due to a slower cooling component (which has a time constant (τ_{cool2}) of 30000 ns) with respect to the initial absorbance change, and t is the time delay (ns).

The absorbance recovery due to cooling was measured on longer time windows and the longer range recovery was similarly cooling corrected using biexponential fits. A neat AuNP in D_2O sample (with AuNP heat transducers) on a timescale of up to 1 s, and then fitted with a biexponential decay on both the 40 μ-2 ms and 2-100 μs timescales to replicate the cooling seen in these timewindows. 2 ms measurements are cooling corrected with a biexponential with the equation 2.4, with a=0.0079 τ_{cool1}=89.3 μs b=0.607 τ_{cool2}=1.74 ms. 100 μs measurements are fitted with a biexponential decay, with a=0.007302 τ_{cool1}=23.1 μs b=0.57 τ_{cool2}=6.08 ms. These fits are shown in figure 2.14. A raw Tjump measurement at 1583 cm^{-1} on neat D_2O (black line) is presented, and simulated curves calculated using the cooling fits are superimposed, showing the accuracy of the cooling correction.

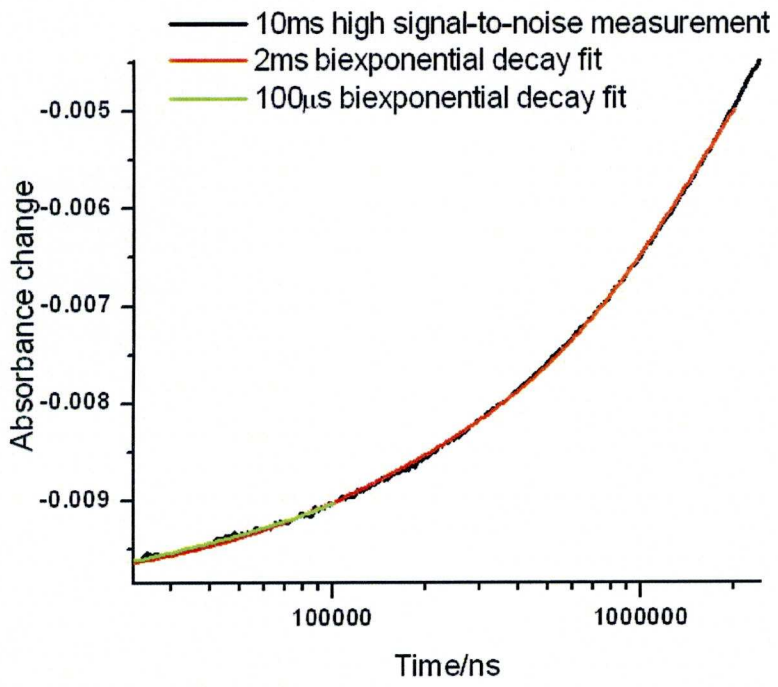

Figure 2.14 D_2O cooling up to 10 ms, an average of 7680 single measurements (experiment performed by R. Whynes), fitted with biexponential decays up to 100 μs and 2 ms. Equation and values are detailed in the text.

The cooling correction is then performed by dividing the raw data by the cooling decay specific to that time window. An example where a cooling correction has been applied is shown in figure 2.15.

Once a measurement has been corrected for the onset of cooling, the fit yields a slightly larger time constant.

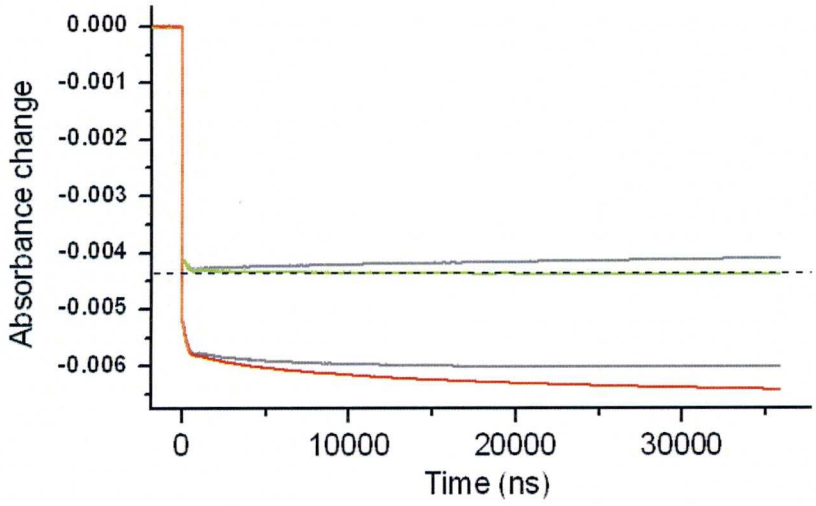

Figure 2.15: Absorbance change for a temperature jump on NANOpNIPAM (10 mg/ml, 2 K Tjump), when before and after correction for cooling. The green and red line represent the cooling corrected signal at 1583 cm^{-1} and 1622 cm^{-1} respectively, and the grey lines show the uncorrected signal for each. The horizontal dotted line has been added to guide the eye.

Although cooling can be well corrected after the 2ms half-life, data after 400 μs is considered questionable, as at this point the sample has already cooled by 20%. In measurements where the polymer dynamics continue after this point, only the data up to 400 μs were considered when analysing the dynamics with fits.

2.3.6.2 Electronic Overshoot

An electronic overshoot artefact was reported previously in high signal to noise Tjump measurements[97] in our setup. Unlike the initial RF noise, this artefact is present only in Tjump measurements, and was present even when the standard sample was replaced by a germanium window (which reacts to excitation by a 1064 nm light pulse by becoming partially opaque to 1601 cm^{-1} probe beam light). This result rules out a D_2O absorbance change response as the cause of the overshoot, indicating a problem intrinsic to the detector/amplifier apparatus. In previous experiments[97] this artefact was disregarded in the analysis due to the small relative amplitude (1% of the overall signal) and rapid decay time relative to peptide relaxation (10s of ns).

2.3.6.3 Pressure Relief

Increasing the temperature of D_2O causes an initial increase of pressure due to the increased thermal motion. This pressure build-up is instantaneous relative to the timescale of our experiments. In the small pump volume with its Gaussian temperature distribution, this pressure is relieved by molecules moving along the pressure gradient towards the surrounding low pressure regions. Unlike the initial increase in pressure,

this relief is limited by the speed at which a pressure wave can travel in D_2O (i.e. the speed of sound, 1428.4 m/s at 309 K[105], the target temperature of the majority of experiments). At the full speed of sound, the pressure wave takes 150 ns to travel 250 μm from the centre of the pump beam to the periphery.

The situation is complicated by the Gaussian shape of the pump laser profile, which results in the pressure distribution around the maximum being fairly even. As our probe beam is $1/10^{th}$ the diameter of the pump beam this maximum is probed almost exclusively. Simulations by M. Volk and Wray *et al*[100] show that the pressure loss in the centre is delayed by the slow formation of a pressure gradient towards the surrounding sample and build up of inertia in the D_2O molecules. Over 100 ns elapse before pressure relief begins in the probe volume, after which there is a gradual increase of the rate of pressure relief. Due to inertia of the D_2O molecules, the pressure decrease continues even after the pressure is equal to that of the bulk sample. If the final pressure is lower than the tensile strength of D_2O, a bubble can form and photoacoustic cavitation occurs (see section 2.3.3.4), otherwise the pressure gradually recovers until it is in equilibrium with the rest of the sample, so a slower recovery is seen from 400 ns-2 μs. The pressure relief and subsequent recovery results in a movement of solvent and dissolved sample out of and into the probed volume, respectively, which corresponds to an initial decrease in infrared absorbance relating to a loss of material in the probe beam, followed by a slight increase in absorbance as solvent and sample move back into the probe volume to reach equilibrium. A representative example of this pressure relief artefact is shown in figure 2.16, in which the 1583 cm^{-1} absorbance change (green/grey lines) shows a clear distortion due to pressure relief (grey line). When corrected for pressure relief (green line), the absorbance remains constant after 50 ns, until absorbance recovery due to cooling. Pressure relief in our setup was first documented by Angela Pozo[97]; however, in her work, the measurements remained uncorrected as the artefact was deemed insignificant; the temperature jump experiments were measured close to the point of maximum density of D_2O (9°C), where the density is only weakly dependent on temperature and the increased pressure induced by temperature jumps only caused a negligible decrease in absorbance. Further analysis of pressure relief at higher temperatures was performed by R. Whynes[98] who measured the temperature dependence of the artefact and produced a correction function for the experimental conditions used in our setup. She observed 2K jumps every 10 degrees from 30-60°C

in D_2O using CT_8 peptide capped gold nanoparticles as a heat transducer and fitted the signal at each temperature with a Gaussian decay function (pressure decrease) followed by a simple exponential recovery (pressure increase) with the following equation:

$$y(t) = \left[A \times e^{\frac{-(t-100)^2}{2w^2}} + A1 \times e^{\frac{-t}{\tau}} - A - A1 \times e^{\frac{-100}{\tau}} \right] * \Delta T * A_{probe} \quad 2.4$$

ΔT is the size of the Tjump (^oC) and A_{probe} is the absorbance of the sample at that wavelength (taken from an FTIR spectrum of the sample). Using Origin 6.0 curve fitting software, the Gaussian centre-point was fixed (at 100 ns) and the (temperature-dependent) variables A, A1, τ and w were allowed to vary freely until a good fit was obtained. Plotting the variables against temperature revealed a linear temperature-dependance for each. The pressure relief correction is perfomed by creating a pressure relief curve using the equation above (2.4) with the parameters relevant to the particular Tjump and probe wavelength, which is then subtracted from the cooling-corrected Tjump absorbance change data after 100 ns. Figure 2.16 shows absorbance changes following a Tjump from 32-34.7^oC both with and without an appropriate pressure relief correction, confirming that the correction works well even with a dissolved 10 mg/ml pNIPAM sample and a different heat transducer (CALNN capped gold nanoparticles).

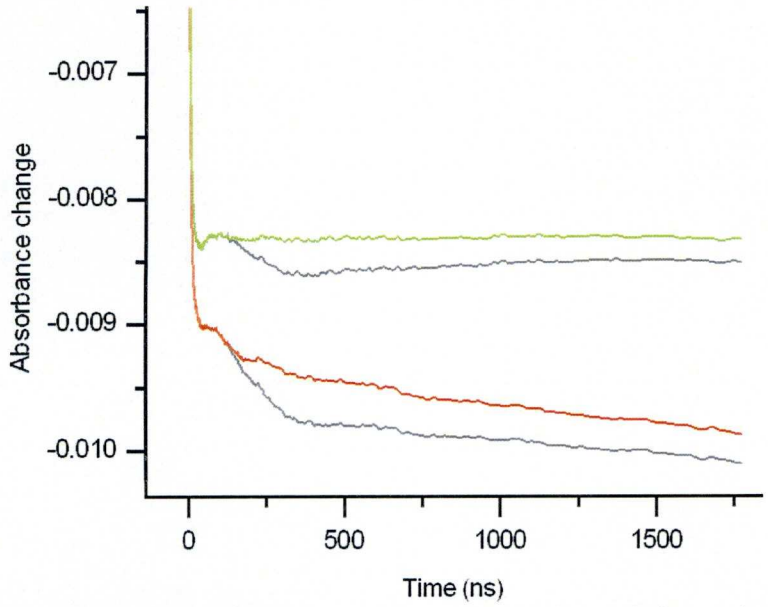

Figure 2.16: Absorbance change in a NANOpNIPAM (10 mg/ml) sample after a 3 K Tjump from 32-5°C, green and red lines show 1583 and 1622 cm^{-1} signal respectively, corrected for cooling as described in section 2.3.6.1, then corrected for pressure relief from 100 ns onwards by subtracting the pressure relief function, equation (2.4). The grey curves the uncorrected curves. The pressure-relief corrected absorbance change at 1583 cm^{-1} (green/grey lines) clearly shows the significance of the correction.

2.4 Temperature Jumps on the 1 ms-50 ms Time Scale

2.4.1 Principle

To view the secondary structural transitions of pNIPAM on longer time scales, we needed to make further adjustments to our setup. The major obstacle to measurements on longer timescales is cooling. Simulations by M. Volk indicate that the major heat loss is primarily due to heat escaping from the solution into the CaF_2 windows, as CaF_2 has a higher heat conductivity than D_2O. This disparity in conductivity manifests itself with the temperature dropping rapidly in the immediate vicinity of the windows, but the rest of the sample maintains its increased temperature until a sufficient temperature gradient is built up.

The key to increasing the time window is therefore to delay the heat loss into the window, and this can be done in two ways:

- Increase the pathlength of the cell, thus increasing the distance required for the heat to diffuse into the CaF_2 window.
- Change the window material to one with a reduced heat conductivity.

Implementing these changes increased the time window quite considerably. Increasing the pathlength of the cell increases the time window by $t \alpha x^2$, where x is the pathlength. Therefore, tripling the pathlength to 150 μm increases the timewindow by a factor of 9. AgCl windows provide another means of slowing the heat transference as the thermal conductivity is much lower than that of CaF_2. As can be seen in figure 2.17, cooling is slowed by approximately a factor of 30. For long timescale infrared measurements, the setup as described in 2.3 was used, however the repetition rate of the laser excitation of the sample was reduced to 0.4 Hz in order to take into account the time required for cooling.

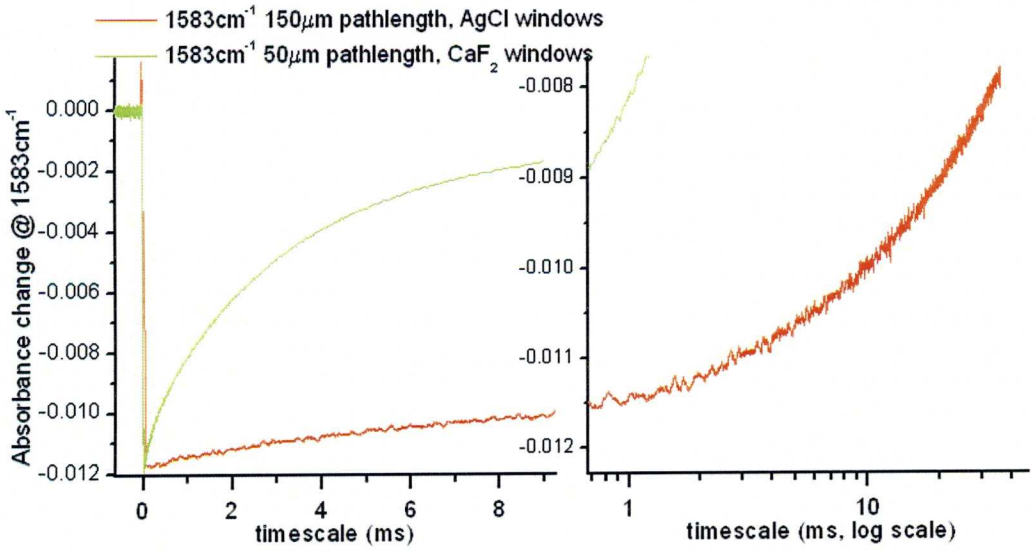

Figure 2.17: Cooling in 150 μm pathlength cell with AgCl windows (red line) compared with standard 50 μm cell with CaF_2 windows (green line) as measured by the absorbance change at 1583 cm^{-1}, shown on a normal (Left) and logarithmic timescale (Right). The standard measurement is an average of single measurements at 10 Hz for a Tjump of 2 K (scaled by a factor 2.7 for comparability). The long pathlength AgCl measurement is an average of 2688 single measurements at 0.4 Hz for a Tjump of 2 K, smoothed by 100 point averaging.

However, these modifications come with severe drawbacks that prevent the adoption of this setup as standard for other temperature jump measurements. Firstly,

increasing the pathlength causes more probe light to be absorbed by the sample, consequently decreasing the signal to noise significantly. The pathlength increase required to extend the timescale to 50 ms is 150 μm, which decreases the signal to noise. Secondly, the heat retention is such that the sample takes longer to completely cool than the time in between laser pulses (100 ms). Therefore, the pumping rate must be reduced, by programming the electronic shutter to block the beam in between measurements. This increases the effect of laser drift and causes measurements to take several days for aquiring a sufficient number of single measurements to give good signal to noise upon averaging, all of which further impacts the signal to noise. Finally, the AgCl windows are extremely fragile, and have a tendency to become unusable after a measurement due to the aggregation of AuNPs to the surface. However, despite these drawbacks, the system was used successfully for experiments described in chapter 4.

2.4.2 HeNe Laser-Detection

Work by Tsuboi *et al*[92] (See introduction, section 1.4) indicates that aggregation, the second phase of the pNIPAM phase transition, begins to occur on the >10 ms timescale. They investigate this effect by observing the increasing visible light scatter caused by interaction with the aggregates as they grow in size. In our experiments we attempted to observe this effect and link it with changes in secondary structure. With this in mind, a HeNe laser was integrated into our setup to probe the pump volume concurrently with the IR probe. Figure 2.18 shows the modified setup and table 2.4 details the additional optics.

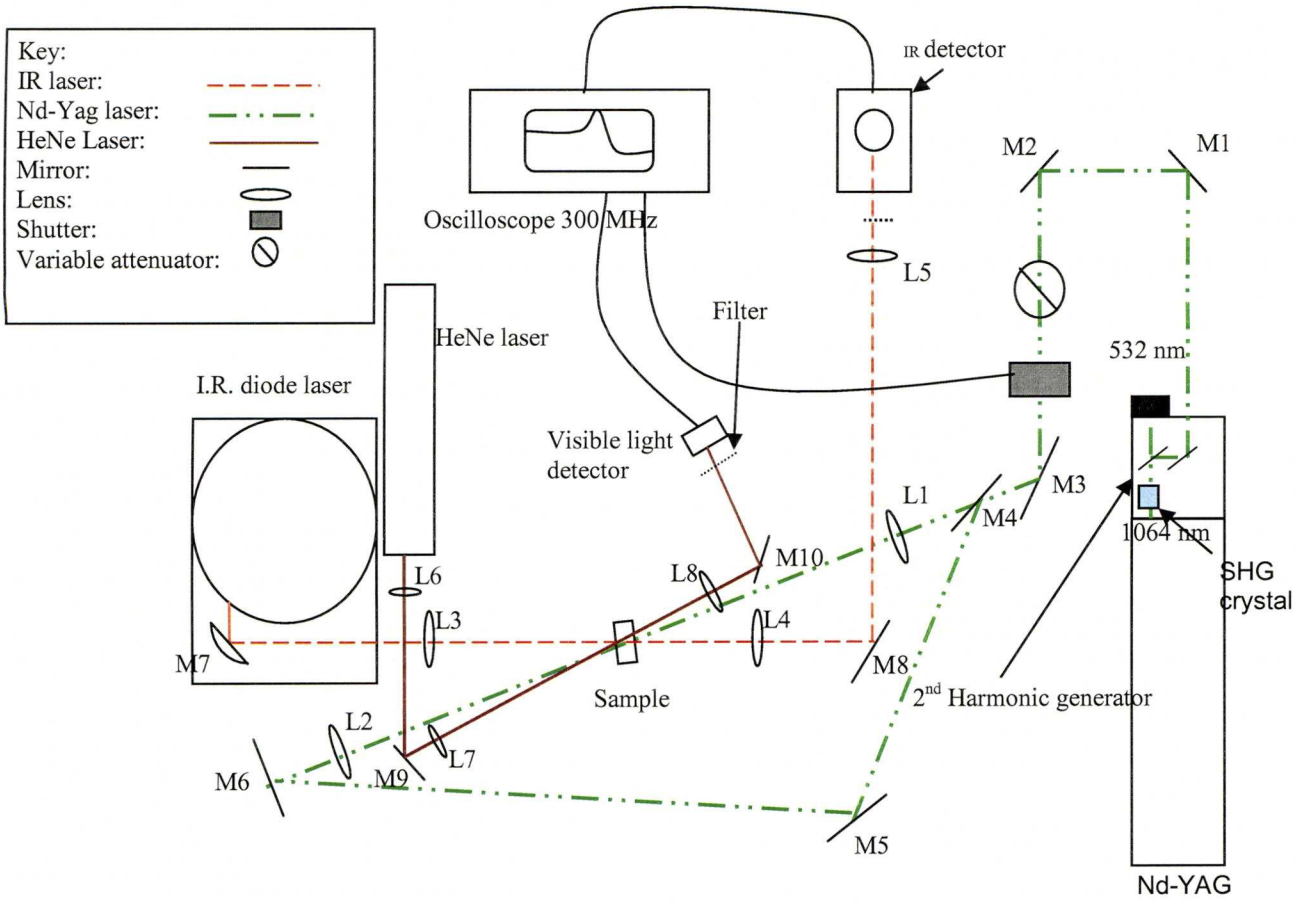

Figure 2.18: Optics modifications for HeNe setup.

Key	Material	Diameter (mm)	Focal Length (mm, lenses)
L6	Quartz	12	-50
L7	Quartz	21.2	100
L8	Quartz	24.5	100
M9	Al	24.5x23	
M10	Al	24.5x23	
Filter	550 nm bandpass filter	25.4	

Table 2.4: Additional optics for the HeNe setup

A standard HeNe laser is used with a power of 1mW. It emits at 632.8 nm, outside the major absorbance bands of the heat transducer dyes.

The HeNe laser beam is directed by a separate optics system onto the same sample spot as the cw IR laser beam, giving the ability to probe the secondary structural changes and resulting aggregation effects in the same experiment. The HeNe laser beam is initially defocused by using a negative lens, L6, to expand the beam (this ultimately allows a narrower focus on the sample to be achieved, the beam is

defocused to the point where the diameter is just smaller than the diameter of L7, allowing the best focussing possible). The beam is then directed by mirror M9 and focussed onto the sample by L7. The light remaining after interaction with the sample is redirected by M10 and refocussed by lens L8 on a fast visible light detector (Thorlabs DET210, risetime=1 ns) and the oscilloscope. The cross-sectional area of the HeNe laser beam was measured by incrementally passing a razor blade in front of the beam and differentiating the resulting light distribution in the same way as the IR beam, giving a diameter of <50 μm (Figure 2.19).

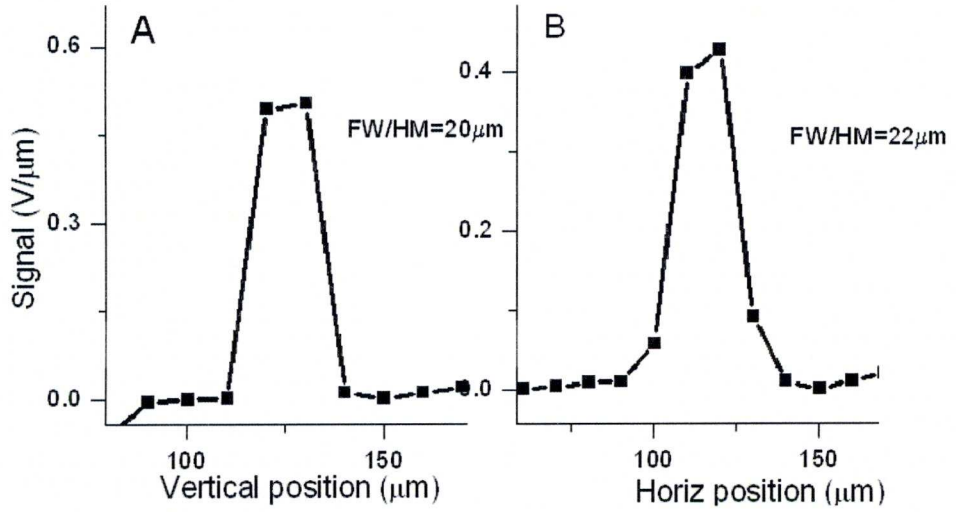

Figure 2.19: HeNe laser beam profile A)Vertical and B)Horizontal

A periodic variation in laser power is observed when using the HeNe with its standard power supply. A variac was integrated into the power supply which allowed the voltage to be turned up to give the initial high-voltage required to start the laser emitting; the voltage could then be tuned to eliminate the periodic variations, while giving the maximum possible power.

The index of refraction of D_2O changes with temperature; heating a small sample volume therefore induces a thermal lens effect on the HeNe (the influence of the thermal lens is eliminated with the IR probe by careful optimisation of the optics). This effect can be used to align the HeNe laser beam; the HeNe probe beam is collected onto a visible light detector (Thorlabs, det210) and the beam is purposefully defocused to increase the effect of the thermal lens. By adjusting the focus of the beam so the thermal lens distortion is maximised, the beam can be aligned to the centre of the pump volume. Subsequent careful focussing of the probe beam onto the detector

then eliminates the artefact, and allows us to obtain better quality measurements. (Figure 2.20)

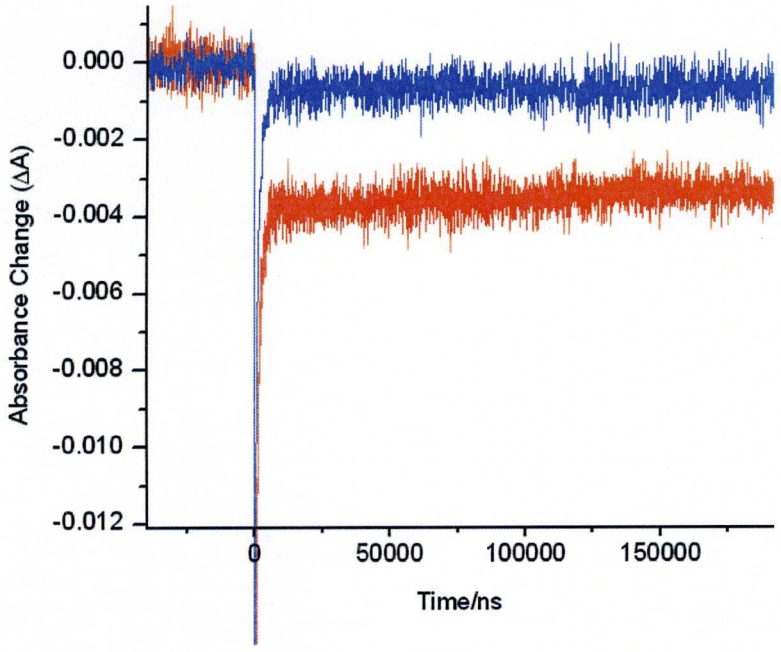

Figure 2.20: A 6 K temperature jump from 32-38°C on a neat D_2O sample probed with the HeNe beam. Comparison of the effect of the thermal lens on a focussed (blue) and defocused HeNe beam. Note the large instantaneous apparent "bleach" caused by scattered light from the Nd-YAG beam.

The thermal lens acts in a non-reproducable way, depending on the precise overlap of the two beams and the exact alignment of the probe beam onto sample and detector, sometimes acting as a positive or negative lens.

2.4.3 Measurement Procedure

A 150 μm pathlength cell was used, with AgCl windows to provide the maximum accessible time window. The IR laser beam, tuned to 1583 cm^{-1}, is initially used to adjust the temperature jump. Once the Tjump is correct, the HeNe laser beam is aligned as per the above procedure. As discussed, heat is effectively trapped by the AgCl windows and longer pathlength, so the repetition rate of laser excitation is reduced to 0.4 Hz by using the mechanical shutter to block the beam in between measurements, allowing the sample to fully cool before the next Tjump. The effectiveness of this was determined by comparing the BG and TJ measurements

before t=0 (i.e. the point in time when the laser is triggered). If the sample is retaining heat, then a disparity is clearly visible between the BG and TJ prejump intensities of a cycle of 128 measurements, indicating a higher average start temperature in the TJ set.

The signal change relating to polymer aggregation was separated from the thermal lens by performing temperature jumps of the same magnitude at a temperature outside the pNIPAM phase transition. By subtracting these curves any absorbance change related to scattering by the formation of globules can be extracted.

2.5 Temperature Jumps on the >100 ms Time Scale

To probe the dynamics of pNIPAM on longer timescales than 100 ms, a shift in pumping strategy is required. Above 100 ms, pulsed heating becomes impractical as the pathlength required to slow the cooling of the sample becomes prohibitively long; at pathlengths above 200 μm the sample will absorb the IR probe light to the extent that none can be detected. Conversely, longer timescales give the opportunity to use a cw-laser for heating, which is based on the idea that the sample will rapidly reach a quasi-steady state with the same amount of heat flowing out of the sample volume as laser energy being absorbed. On the other hand, extreme timescales on the order of minutes to hours require no complicated heat delivery mechanism at all; it is sufficient to "jump" the temperature by changing the setting on the temperature controller (water bath) and allowing the temperature to equilibrate.

2.5.1 Ar Laser Induced Temperature Jumps

The laser used to produce continuous heating on the 100 ms timescale is a Coherent Innova 300C Ar-Ion laser, from the laser loan pool at the CCLRC Central Laser Facility. This is an argon laser that produces a multiline beam at wavelengths between 530 and 454 nm with a power of 5W by electrically exciting Ar^+ ions. A wavelength selecting prism is inserted into the cavity to suppress wavelengths other than 514.5 nm, allowing efficient heat generation when combined with gold nanoparticles which absorb almost as strongly at this wavelength as at 530 nm due to the broad plasmon band. The electric shutter is used to block the beam before a measurement and the opening of the shutter acts as trigger for the oscilloscope to begin recording the measurement (the shutter takes about 500 μs to open and is controlled by a modified version of the Tjump program). For a sample with a 0.25

absorbance, a laser power of 300 mW produces an 8-12 K Tjump with the laser power-tracking mode ensuring a stable beam power. The optics setup for this system is shown below (figure 2.21):

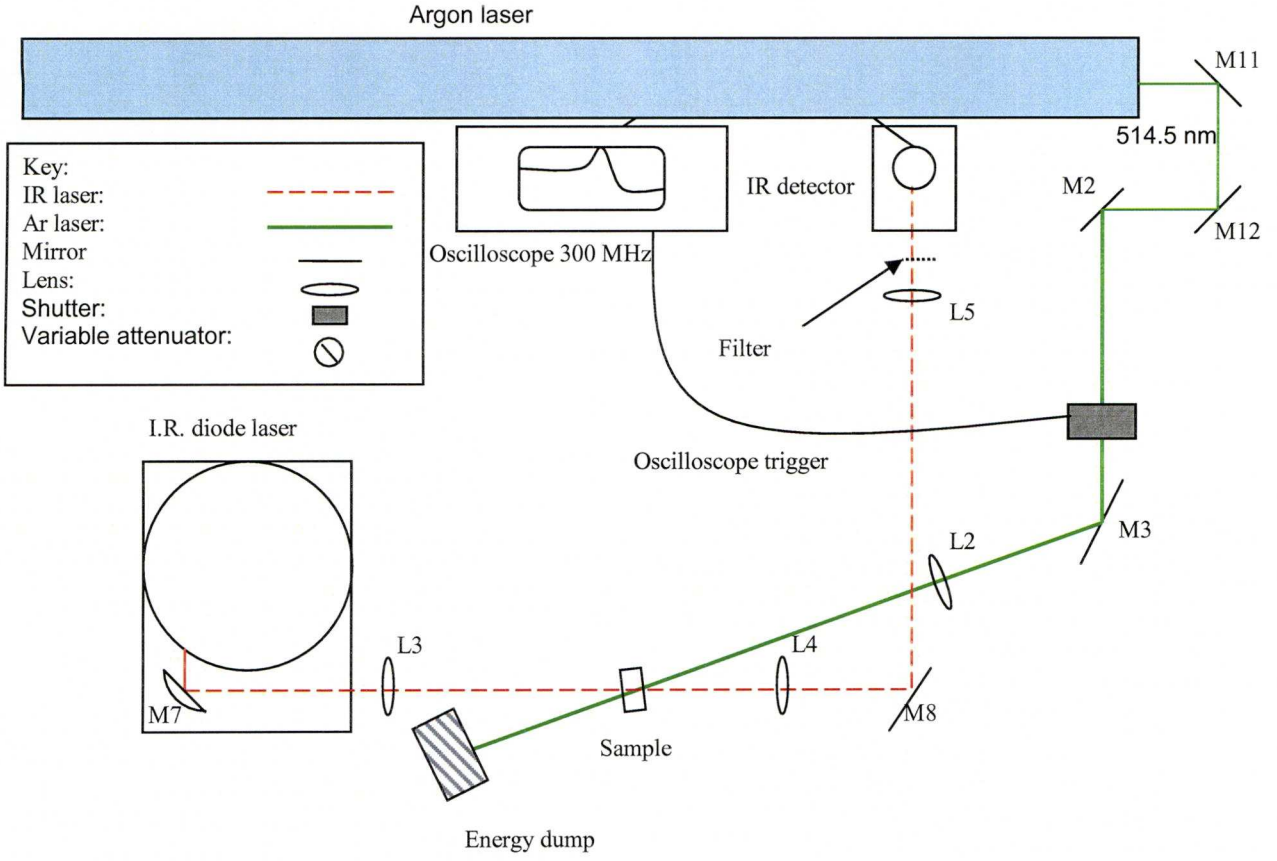

Figure 2.21: Argon laser optics setup.

Key	Material	size (mm)	Focal Length (mm, lenses)
M11	Al	50x50	
M12	Al	50x50	

Table 2.5: Additional optics for the Ar laser setup

The 514.5 nm beam exits the Argon laser above the plane of the existing beam system, and is vertically redirected onto the Nd-YAG optics level using mirrors M10 and M11 in an inverted periscope arrangement, which is placed in between mirrors M1 and M2 causing minimal disruption to the fast temperature jump setup and so allowing ease of switching between the two heating systems. The external power adjustment

provides fine control over the laser output, so the variable attenuator is removed. There is also no longer a need for beamsplitting, since heat equilibration along the beam axis takes place within 2 ms. The temperature rise time for Ar-laser heating is shown below (figure 2.22), showing that the major part of the temperature increase takes place within 15 ms.

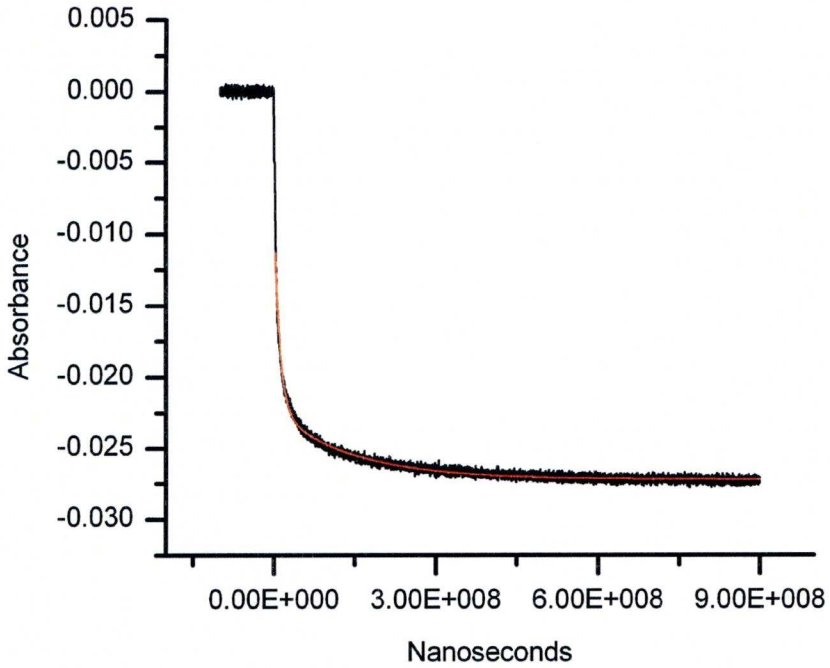

Figure 2.22: The temperature increase for a 10 mg/ml sample of pNIPAM MCL 1, measured with the cw IR beam at 1583 cm^{-1} with a final temperature increase of 12K from 32°C (Black curve). Red curve is a fit with a biexponential rise. Average of 4 measurements.

The rise time has been fitted with a biexponential rise, with time constants of 10.6 and 143 ms although exact values vary with the size of the temperature jump. Shortening the pathlength, varying the concentration of AuNPs and fitting additional CaF_2 windows to the cell were all attempted in an effort to shorten the rise time by increasing the rate of equilibration, but none of these yielded an improvement on the results seen with standard conditions.

The slow increase in temperature after the fast phase means that care must be taken regarding the size of the temperature jump. Following standard measurement protocol and jumping to equilibrium at just over the LCST (to 38°C) in order to maintain continuity with earlier pulsed laser jumps would result in a loss of time resolution. Instead, with the Ar-laser measurements measurements on the <1 s timescale the protocol was to reach a temperature of 38°C mark is hit at the end of the

fast risetime (14 ms). Measurements on the 100 s timescale were performed with 38°C as the final equilibrium temperature.

The Ar laser heating method in principle gives access to an infinite timescale, though in practice this is not the case. After 10 seconds there are irreproducible absorbance changes detected, which correspond to the visible formation of bubbles, which disrupts the measurement.

2.5.2 Water Bath Temperature Jumps

As stated previously, on timescales on which we can observe the entire aggregation process (several hours), it is sufficient to perform a Tjump by simply increasing the temperature setting on the water bath and allowing the sample to equilibrate. This is the primary method of increasing the temperature in previous long timescale studies of pNIPAM by NMR[18,106]. Using the water bath has the obvious advantage of eliminating the complexity and technical problems associated with laser excitation. An additional bonus is that the cell is heated throughout the entire sample, and homogeneously. The method also can be used for cooling the sample, although ice is added to the water bath to increase the speed of cooling. The resulting IR absorbance changes for neat D_2O are shown in figure 2.23

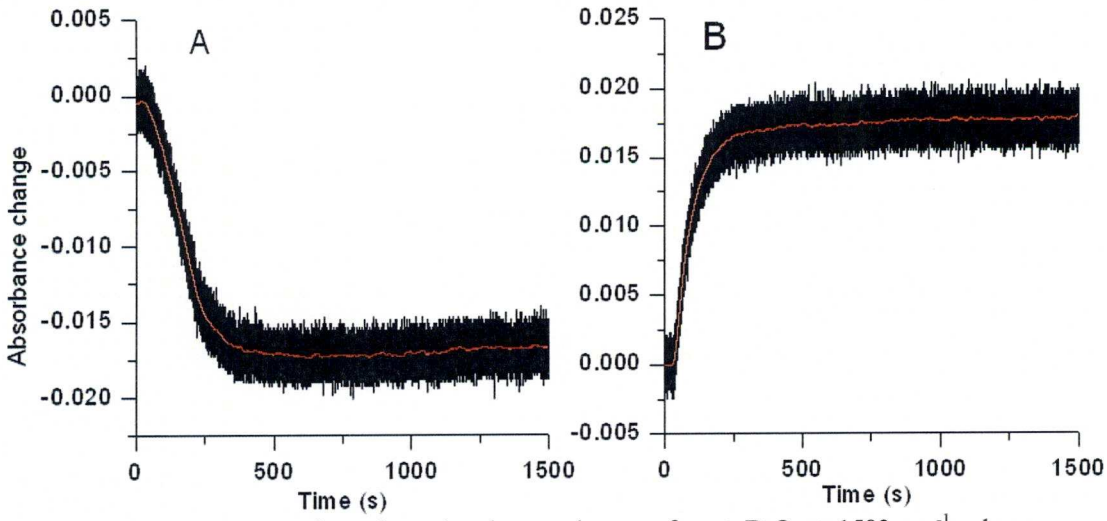

Figure 2.23: Temperature dependent absorbance change of neat D_2O at 1583 cm^{-1} when heating (A) and cooling (B) with the temperature controller from 30-38 degrees. The red line shows smoothed of the data by 500pt adjacent averaging.

The observed heating/cooling is complete within under 400 s which gives us our time resolution for measuring the full aggregation process.

2.6 Steady-State Spectroscopy

2.6.1 FTIR-Spectroscopy

pNIPAM polymers were studied using FTIR and UV-vis spectroscopy to provide detailed information about the coil-globule transition prior to temperature jump measurements. Detailed analysis of the amide I' band of pNIPAM provides an excellent source of information about the structural changes during the pNIPAM phase transition, or indeed any structural transition involving a peptide bond. Typically, infrared spectra are measured using a Fourier-transform infrared spectrometer containing a Michelson interferometer. The interferometer works as follows; light from a broadband infrared source (typically a hot filament or glow bar) is collected and passed through a 50% beamsplitter, aligned so that 50% of the light is reflected onto a fixed mirror and from there directly back to the beam splitter. The remaining light passes through the beamsplitter unchanged, and onto a mirror that is translated along the beampath periodically. Both beams meet at the beamsplitter and after a further 50% reflection loss occurs in both beams (resulting in 50% loss overall after combination), the combined beams interfere either constructively or destructively depending on the wavelength and the distance of the translatable mirror from the beam splitter. The resulting beam is passed through the sample and its intensity recorded in dependence of the mirror position, the resulting interference pattern (which contains absorbance information for all wavelengths) is deconvoluted by Fourier transformation into the FTIR absorbance spectrum. The amount of light absorbed is then calculated by comparing the amount of light transmitted through the sample against a reference (background) measurement.

Here, a BIO-RAD FTS-40 spectrometer was used. At each temperature the sample was given enough time to equilibrate fully (10 mins) before a spectrum was taken. All samples were at 10 mg/ml concentration, unless otherwise stated. The sample was held between two CaF_2 windows separated by a 50 μm Teflon spacer in a custom made copper cell with the temperature controlled by circulating water inside the cell body (temperature controller from Grant Instruments Limited).

The spectrometer is linked to a computer that uses Win-IR software. The detector is a liquid nitrogen cooled Mercury-Cadmium-Telluride (MCT) photodiode. All FTIR measurements on this machine were taken with 1 cm^{-1} resolution and were averaged over 500 single scans. Dry air is pumped through the FTIR machine and sample chamber which removes water vapour, preventing unwanted absorption peaks. Some water vapour remains in the spectrometer sample chamber and is observable in spectra (if the sample is left for longer periods of time under dry air before taking a spectrum then the water vapour peaks diminish further.) A water vapour spectrum measured when the sample stage is empty and flooded with moist air is scaled and subtracted from sample spectra to remove $H_2O_{(vap)}$ from the spectrum.

The area of interest for our study is the amide I' band, which absorbs in the same region as the temperature dependent D_2O association band, so a large fraction (~95-98%) of a neat D_2O spectrum taken at the same temperature as the sample is subtracted from the pNIPAM spectrum. For all temperature jump samples, FTIR spectra were taken before and after the experiment was performed. These measurements are used to verify that no significant structural changes have occurred during the course of the experiment and to compare relative concentrations of different samples of the same polymer. On comparing the spectra from before and after the Tjump no difference in the amide I' band is seen, indicating that the polymer is undamaged by the temperature jump measurement. An example is given in figure 2.24, showing the amide I' band of a sample which was subjected to 2 successive high signal-to-noise nanosecond measurements over 2 days. No change was seen in the amide I' which is a testament to the resilience of the polymer (figure 2.24).

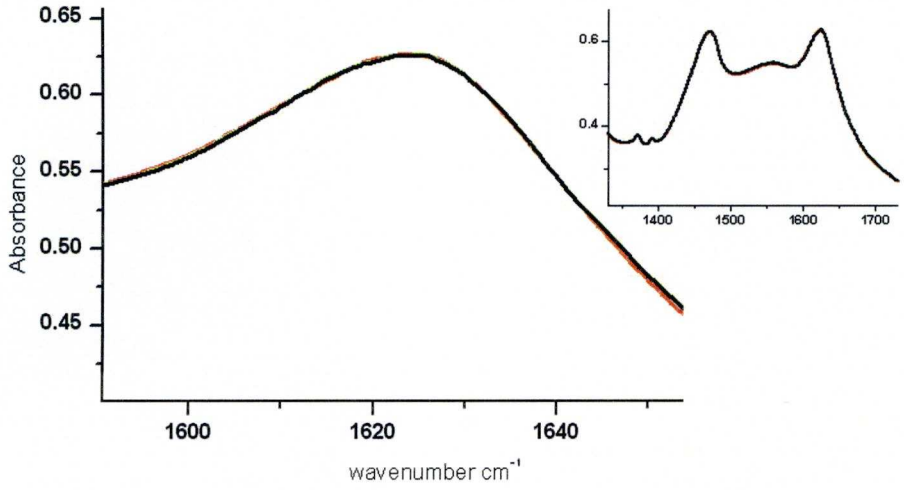

Figure 2.24: An overlay of the amide I' band from 3 FTIR spectra of a 10 mg/ml sample of NanopNIPAM with AuNP heat transducers (10^{-6} mM), one taken before and two after Tjump measurements, each taken after a successive full measurement involving around 35'000 temperature jumps (to obtain high S-N measurements of the 1622 and 1583 cm^{-1} absorbance change). (INSET) a zoomed out view of the amide I' and II' region of the same 3 spectra

2.6.2 IR band Analysis

pNIPAM FTIR spectra were taken at incremental temperatures around the LCST and corrected to remove the D_2O background and $H_2O_{(vap)}$ absorbances.

Bandwidths of the sub-bands in the amide I' band are wider than the separation of the band centres, resulting in significant overlap, so the band deconvolution requires sophisticated fitting methods. After correction for solvent and water vapour, the pNIPAM amide I' bands were fitted with the smallest possible number of pseudo-Voigt bands required to satisfactorily simulate the amide I' band. A pseudo-Voigt band is an approximation of a true Voigt band, which describes the solvent interaction induced Gaussian broadening of a Lorentzian vibrational absorption band. The pseudo-Voigt band does this by assigning the band a fractional Gaussian/Lorentzian character. (These are simpler to compute than a true Voigt fit and so require less computing time when fitting) The pseudo-Voigt function is shown below:

$$y(x)=\left(\rho\frac{A}{\pi/2}*\frac{w}{4(x-xc)^2+w^2}\right)+\left((1-\rho)*\frac{A*\sqrt{\frac{4\ln 2}{\pi}}}{w}*\exp\left(-4\ln 2*\frac{(x-xc)^2}{w^2}\right)\right) \quad 2.5$$

y(x) is the absorbance at a given wavenumber x. The first part of the function describes the Lorentzian lineshape contribution, the second the Gaussian line shape. The fractional contribution of the Lorentzian lineshape is given by ρ (which can be $0<\rho<1$). w is the width of the band (full-width, half maximum), xc is the central position of the band and A is the area. A least-squares Levenberg-Marquardt fitting routine in Origin data analysis software was used to fit the amide I' band with a combination of pseudo-Voigt peaks, and the quality of the fit was analysed by examining the residuals by eye, and numerically by the sum of the square of the residuals χ^2, provided by the fitting software after every fitting iteration.

To study the qualitative trends in band populations in a single polymer sample over the phase transition, the corrected IR spectra for a range of incremental temperatures around the LCST were fitted with a modified "global" fitting algorithm. Band areas (related to carbonyl bond populations) were allowed to vary freely, and xc, w and ρ variables were assumed to follow a linear temperature dependence. Along with the areas, these parameters were also freed to find the best possible solution to describe the global amide I' band variations. Good quality fits were achieved with this method (see chapter 3), indicating that the linear temperature dependence was an appropriate assumption given the narrow range of temperatures. The sub-band areas were converted into a fraction of the total area of the amide I' band, thus normalising band populations and allowing the band shifts of a range of polymers with varying size, copolymers and crosslinking types to be compared quantitatively.

2.6.3 UV-Vis Spectroscopy

For UV-VIS measurements a Hewlet-Packard Diode Array spectrometer and a Perkin-Elmer Lambda 25 were used. Polymer LCSTs were confirmed by measuring temperature dependent light scattering by the polymer solution at 500 nm. Temperature was increased incrementally, with the sample at each temperature allowed to equilibrate for 10 minutes before the next measurement was taken (Measuring the sample temperature with a resistor revealed that temperature equilibration was achieved after a maximum of 6 minutes, also see figure 2.25). The LCST was defined as the temperature at which the largest increase in light scattering takes place. The sample was held between two CaF_2 windows separated by a Teflon spacer (typically 1 mm to increase the amount of scatter, making the transition more easily visible) in a custom made copper cell with the temperature controlled by

circulating water inside the cell body (temperature controller from Grant Instruments Limited). Samples were generally at a concentration of 10 mg/ml, but increased concentrations had no effect on the LCST. UV-vis spectra where also taken of the sample in a 50 μm cell prior to Tjump measurements, obtaining a value for the absorbance of the heat transducer at 532 nm in order to ensure that the absorbance was sufficient for the size of the Tjump required but below the threshold set by the need for a homogenous Tjump (section 2.3.4.2).

CHAPTER 3: THE PHASE TRANSITION OF PNIPAM, STUDIED BY FTIR SPECTROSCOPY

3.1 Introduction

The major driving force behind the coil-globule transition of pNIPAM is the dehydration of the pendant side chains. It is the alkyl groups which provide the main impetus for dehydration when heated over the LCST, as the smaller amount of enthalpic stability provided when water molecules form a clathrate cage surrounding the hydrophobic groups is offset by the entropic gain from returning the bound water to the bulk solvent. The carbonyl bonds are also involved in these structural changes due to their propensity to form hydrogen bonding networks. Changes in the carbonyl hydrogen bonding state affect its vibrational frequency, therefore observing vibrational changes of the carbonyl bonds provides an effective tool for observing changes in hydration state, specifically via the Amide I' vibration, which is dominated by carbonyl stretching, thus extremely sensitive to changes in the hydrogen bonding state. Changes in the hydrogen bonding state result in a shift of this band by up to 40 cm^{-1}, resulting in sub-bands whose relative population gives an insight into the number of carbonyls in that particular hydrogen bonding state. These shifts are not large enough to resolve the individual bands, due to broadening of the sub-bands, resulting in overlapping amide I' sub-bands that shape the overall amide I' band envelope. Approximating the sub-bands with pseudo-Voigt curves and fitting using a least-squares Levenberg-Marquardt routine allows these bands to be extracted, Their relative populations can be used to probe the hydration state changes of pNIPAM.

IR spectroscopy has been used widely to study pNIPAM[3,19,24-26,28,31,34-40,71,79,107-113]. Attempts to resolve the hydration states via FTIR band fitting have already been reported by a number of groups[3,19,25,26,31,37,40,79,112], with somewhat controversial assignment of the results; Maeda *et al*[3,26] fitted the FTIR spectrum of pNIPAM and other polyalkylacrylamides above and below the LCST; they resolve the amide I' band into two bands at ~1625 and ~1650 cm^{-1}, with the 1650 cm^{-1} band growing in at the expense of the 1625 cm^{-1} band at temperatures above the LCST. They interpret the 1625 cm^{-1} band as carbonyls hydrated by the water solvent and the

1650 cm^{-1} band as inter/intramolecularly hydrogen[a] bonded carbonyls (i.e. those bonded to an amino group) respectively, with the increase in inter/intramolecular hydrogen bonding due to the polymer collapse and dehydration after the phase transition. Katsumoto *et al*[79] use band fitting to analyse the FTIR spectrum in water and simple DFT models to interpret their FTIR data. They interpret the 1625 cm^{-1} band as both hydrated and intermolecularly bonded carbonyls, and the 1650 cm^{-1} band as non-bonded carbonyls. However, the fact that they use water as a solvent rather than D_2O, means solvent subtraction is difficult, and the simple solvent model they use for their calculations (the Onsaga model for the solvent pocket with a NIPAM dimer) limits the validity of their theoretical results, particularly as the solution behaviour of the monomeric NIPAM differs from the polymer[110,114]. Thus, we see Maeda's interpretation of the 1650 cm^{-1} bond as the most likely. In later publications concerning the effect of different solvents on the band structure of pNIPAM, Katsumoto et al. report the additional observation of a band at ~1610 cm^{-1}, and assign the 1610, 1625 and 1650 cm^{-1} bands to double, single and non-hydrogen bonded carbonyls, respectively[79,113].

In this chapter, we attempt to resolve the amide I' band of pNIPAM in temperature dependent FTIR spectra. Different varieties of single chain pNIPAM and related polymers are studied, in order to judge the changes of hydration state in response to temperature and to variations in the polymer primary structure. As will be shown, the better experimental results presented here, together with more refined fitting techniques resolve an additional band to those seen by Maeda[3,26], suggesting that the two band interpretation is too simplistic. Fitting results provide additional information, which suggest that a reinterpretation of Katsumoto's band assignments[79,110,113] is required. In this chapter, we present a new interpretation of the three band system that is consistent with the experimental results in this chapter, and other published results (band assignments are shown in table 4.1.). We also study how the variations in primary structure affect the temperature at which the phase transition occurs.

[a] We will use "hydrogen bonding" throughout the text, however, strictly speaking solvation in D_2O is due to "deuterium bonding".

3.2 Experimental

3.2.1 FTIR Measurements

Details of how the FTIR measurements were taken and the fitting routines used to analyse the spectra are discussed in chapter 2.6. Briefly, for each pNIPAM sample, FTIR spectra were taken at incremental temperatures around the midpoint of the transition (found by measuring the turbidity of the solution at different temperatures with UV-vis spectroscopy) using a Biorad FTS-40 spectrometer, with identical temperature controlling methods as in the UV-vis measurements. The spectra had to be corrected for D_2O absorption by subtracting the D_2O absorption spectra at each temperature, as D_2O shows a characteristic change in absorbance with increasing temperature. An atmospheric H_2O vapour absorption spectrum was subtracted, appropriately scaled, to correct for water vapour absorbance. 500 scans were averaged for each spectrum, with 10 mg/ml samples and a 50 μm spacer in most cases, except where otherwise stated.

Additionally, a time-course measurement was performed to study the behaviour of pNIPAM when left in the collapsed state for a period of a week, to see if any further changes were apparent due to slower structural changes of the globules. In this experiment, the temperature is increased from 30°C to 44°C, with FTIR spectra taken at equilibrium at 30°C, after the temperature is increased to 44°C (and allowed to equilibrate for 8 minutes), then every hour for 3 hours, then approximately every 20 hours for 120 hours.

3.2.2 Pseudo-Voigt Fits

The amide I' band (' refering to deuterated amide groups) of each corrected spectrum was fitted with 3 pseudo-Voigt bands. Initially each amide I' band was fitted separately and it was found that shifts in the component band centre frequency, width and Gaussian/Lorentzian contribution could be approximated with a linear temperature dependence. The spectra were then fitted globally, with linearly temperature dependent parameters (i.e. band wavenumber, width and band-shape) and freely varying component band populations. A custom made global fitting function in Origin 6.0 fitting was used to perform the fits. For measurements comparing different concentrations of the same sample, the same linear parameters

were used for both samples (found by fitting both samples separately, then taking an average of the parameters found with the fitting routine. These average parameters were then used to fit both spectra). Interestingly, an attempt to use the same linear temperature dependence of the variables for fitting all samples failed to produce good fits for samples with a large difference in LCST, suggesting that although a linear temperature dependence may be effective over short temperature ranges, at longer ranges the dependence is more complicated.

3.2.3 UV-vis Measurements

UV-vis measurements were performed as described in chapter 2.6.3. Polymer LCSTs were confirmed by measuring temperature dependent light scattering by the polymer solution at 600 nm. Temperature was increased incrementally, with the sample at each temperature allowed to equilibrate for 10 minutes before the next measurement was taken (measuring the sample temperature with a resistor revealed that temperature equilibration was achieved after a maximum of 6 minutes; also confirmed by results in figure 2.26). The LCST was defined as the temperature at which the onset of light scattering at 600 nm occurs. The sample was held between two CaF_2 windows separated by a Teflon spacer (typically 1 mm) in a custom made copper cell with the temperature controlled by circulating water inside the cell body (temperature controller from Grant Instruments Limited). Samples (unless otherwise stated) were at a concentration of 10 mg/ml. Increased concentrations or chain length in our limited range have no effect on the LCST for pNIPAM.[43]

3.3 UV-vis Measurements: Results and Interpretation

Measuring turbidity changes is the most common method of determining the LCST of a new polymer, (see chapter 1.4.1). The turbidity of a solution of pNIPAM is dependent on its state of collapse, as aggregates formed from globules scatter light; an increased size or concentration of colloidal pNIPAM aggregates leads to a higher turbidity. Typically, the turbidity is measured by observing the light scattering at 600 nm[44]. The LCST is defined in most cases as the temperature at which a discontinuous change in solution properties is observed. Therefore, the LCST when measured with UV-vis spectroscopy is given by the onset of turbidity at 600 nm. In our experiments, the LCST of all samples was measured in agreement with the established protocol[44], in order to determine the LCST of some of the more unusual pNIPAM derived polymers studied.

However, we are not interested only in the onset of the transition. For pump-probe measurements, the mid-point of the transition is especially interesting, as this is the temperature at which the highest change in the sample state is observed (figure 3.1). In our pump-probe experiments, therefore, the midpoint of the transition gives the largest change in infrared absorbance, and enables measurements that are more sensitive. The midpoint is defined as halfway between the onset and the end of the transition as observed in UV-vis experiments (figure 3.2).

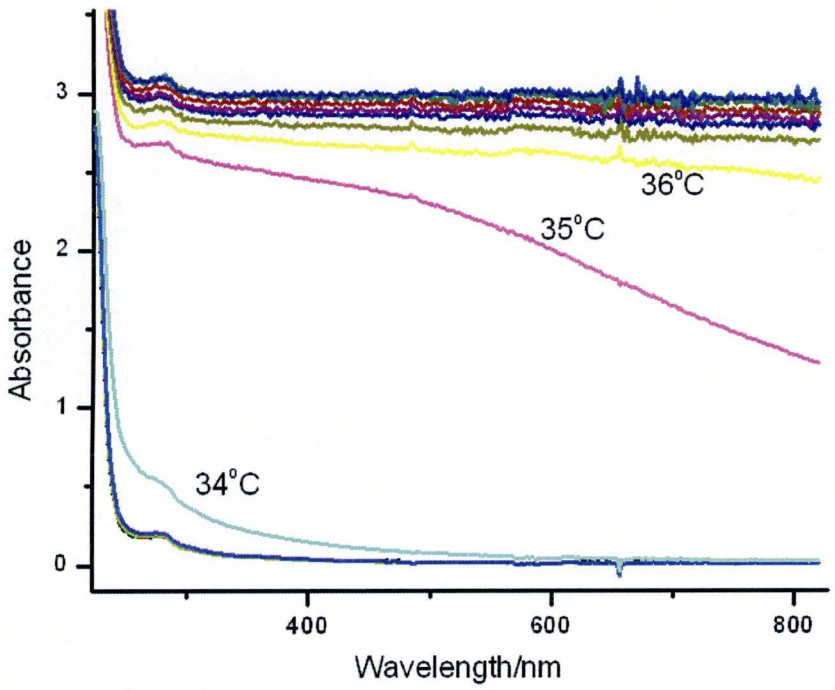

Figure 3.1 UV-vis spectra of a 10 mg/ml sample of pNIPAM-MCL-1 in D_2O, with a 3 mm spacer. Spectra were taken at incremental temperatures around the LCST.

Figure 3.1 shows the UV-vis absorbance spectra of a medium chain length sample of pNIPAM (MCL-1) at temperatures around the LCST. At the LCST (34°C), there is a clear change in the turbidity of the solution, which remains constant below this temperature.

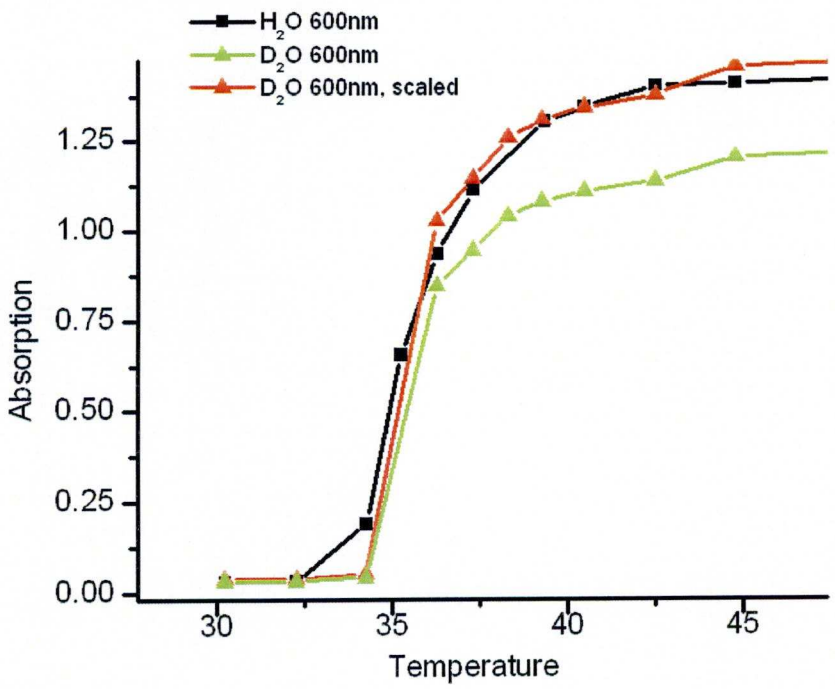

Figure 3.2 Comparison of the absorbance/scatter at 600 nm, by pNIPAM-MCL1 in H_2O and D_2O with a 1 mm spacer. The green line is the D_2O measurement scaled so the final absorbance is the same for better comparability.

Figure 3.2 shows the absorbance/light scattering by identical samples of pNIPAM MCL-1 in H_2O and D_2O at 600 nm. The (scaled) curves overlap, indicating that with our samples, deuteration causes little difference in the LCST.

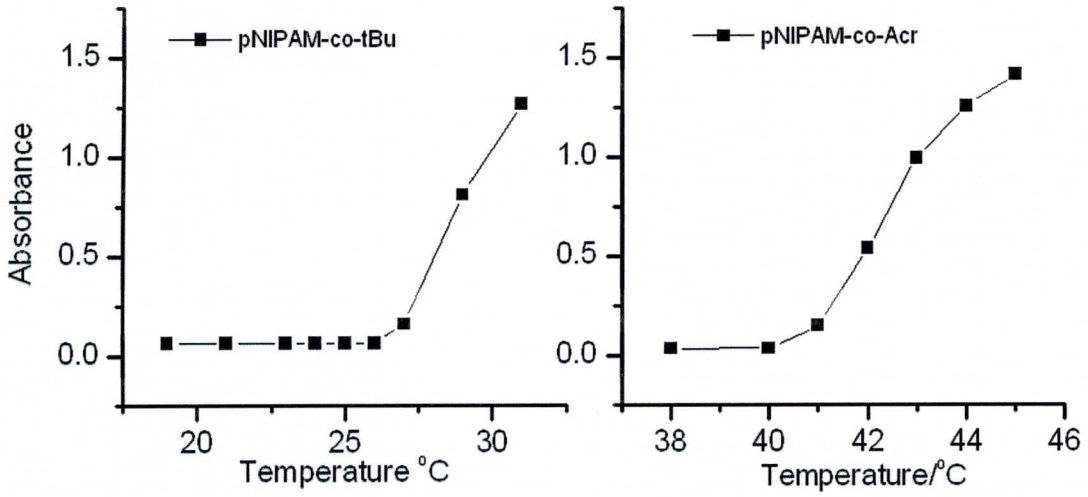

Figure 3.3 UV-vis absorbance at 600 nm around the LCST for pNIPAM-co-tBu and pNIPAM-co-Acr (see table 2.1 for sample details). Samples are in D_2O, at 10 mg/ml concentration and 1 mm pathlength.

Figure 3.3 shows the UV-vis absorbance around the LCST for two copolymers, in which a small proportion of the pNIPAM chains are replaced with either tert-butyl acrylamide (15% of side-chains), or acrylamide (with no alkyl groups, 10% of side chains). Even such a small modification of the polymer constitution causes a large change in the LCST. The effect is due to the distorting effect of the copolymer's hydrophobic substituent; t-butyl has a larger hydrophobic surface which is presented to the solvent. A larger clathrate cage therefore forms around the hydrophobic group, which decreases the entropy of the system for a small gain in enthalpy of solvation. For pNIPAM-co-acrylamide, the effect is opposite; the acrylamide copolymers have no hydrophobic component (other than the backbone), thus having a much smaller impact on the solvent cage other then the amide hydrogen bonds, which are favourable for solution.

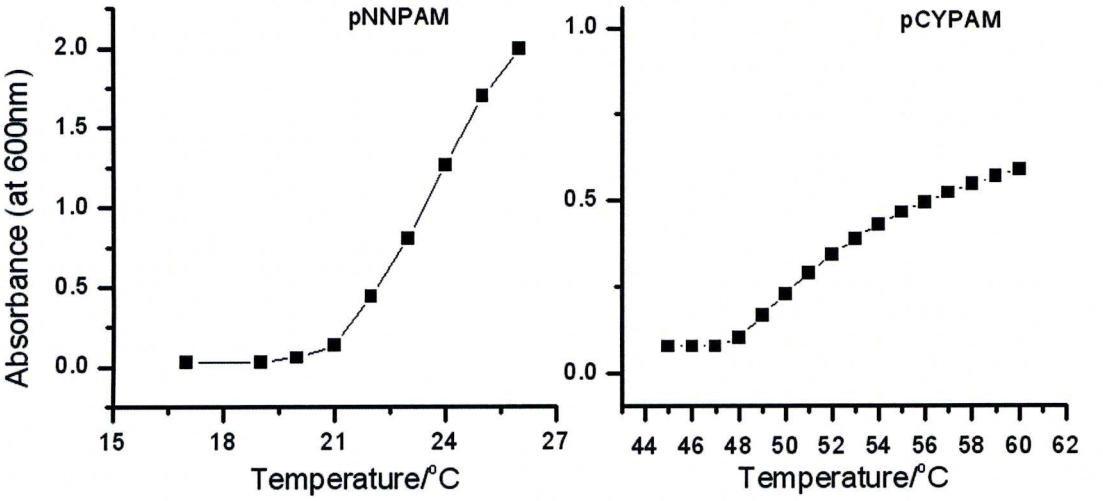

Figure 3.4 UV-vis absorbance at 600 nm around the LCST for pNNPAM HCL and pCYPAM HCL (see table 2.1 for sample details). Samples are in D_2O, at 10 mg/ml concentration and 1 mm pathlength.

Figure 3.4 shows the UV-vis absorbance for pNNPAM (poly(N-n-propylacrylamide) and pCYPAM poly(cyclopropylacrylamide), alkylacrylamide based homopolymers with alternative alkyl chains to pNIPAM synthesised in the course of this project. The LCSTs in both cases are in agreement with those observed by Maeda for the same polymers[26]. Again, we see that the polymer with the largest alkyl substituent (pNNPAM, with an n-propyl chain) has a lower LCST due to the larger clathrate cage required to solvate the alkyl group. pCYPAM has a higher LCST compared to pNIPAM due to the smaller solvent accessible area of the alkyl group, and the strained angles of the cyclopropyl chain, which reduces the overlap of the electron clouds and makes the cyclopropyl group more electrophilic (therefore soluble) when compared to an isopropyl group. The increase in turbidity for pCYPAM is more gradual than observed for other polymers. Compared with the pNNPAM absorbance, pCYPAM scatters less light above the LCST. This corresponds to a weaker temperature dependence of the amide I' band in the FTIR of pCYPAM seen during the transition when compared with other polymers (data not shown).

3.4 FTIR Measurements: Results and Interpretation

3.4.1 Fitting Procedure

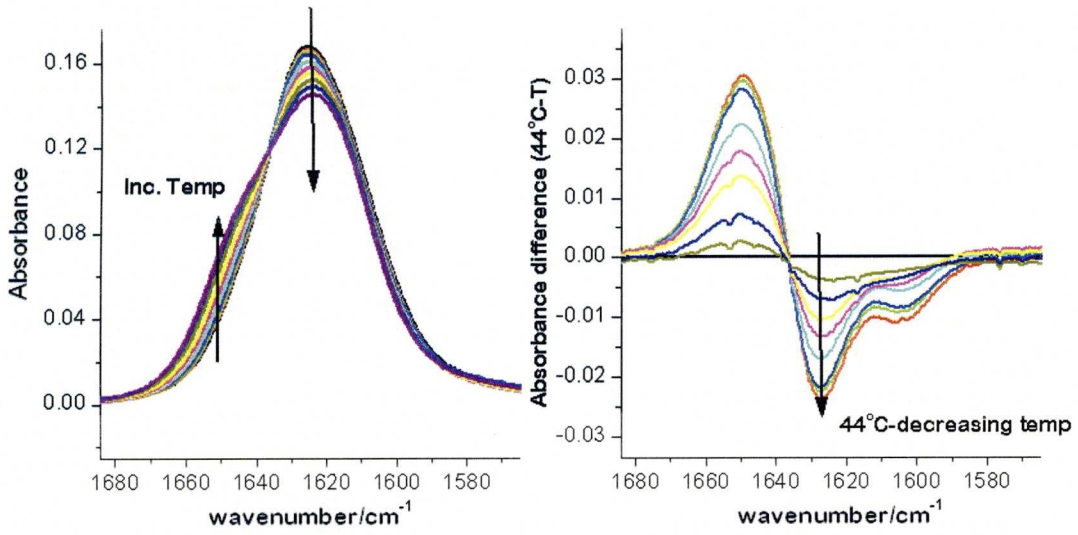

Figure 3.5 FTIR spectra of pNIPAM-MCL 1 (Table 2.1 for details), (Left) Amide I' spectra at temperatures around the coil-globule transition, corrected for D_2O background and water vapour (30-44°C, arrows show direction of temperature increase) (Right) Difference spectra of pNIPAM-MCL 1, showing the FTIR spectra at different temperatures subtracted from the FTIR spectrum at 44°C-other temperatures (arrow shows direction of temperature decrease).

Figure 3.5 shows the temperature dependent FTIR spectra of the amide I' band, corrected for the absorbance of D_2O and residual water vapour. From the visible changes in the amide I' band, one can easily observe that as temperature is increased, the 1625 cm^{-1} band is replaced by one that grows in at 1650 cm^{-1}. This agrees with the results presented previously[3,19,24-26,28,31,36,37,71,79,110]. Maeda only uses 2 bands to fit his spectra[3,19,26,71,73]. Our results show that a minimum of *three* bands are required, with the extra band located at ~1600-1610cm^{-1}: Difference spectra show a more complex behaviour than a transition between two bands; the isosbestic point at ~1637 cm^{-1} shows that there is a definite exchange in population between bands either side i.e. the 1650 cm^{-1} and 1625 cm^{-1} bands. The behaviour from 1600-1635 cm^{-1} is impossible to explain with a single band, however, and an additional band is required.

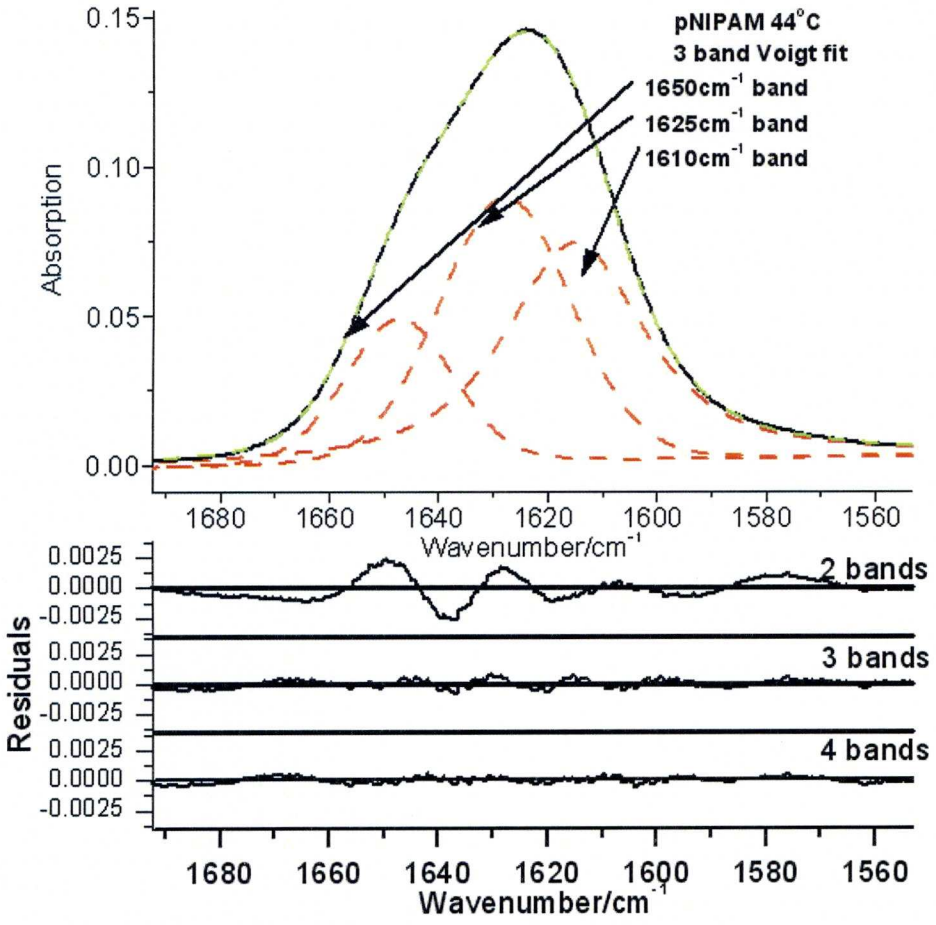

Figure 3.6 (Top) Amide I' band of a 10 mg/ml sample of pNIPAM-MCL 1 at 44°C in a cell with a 50 μm spacer, corrected for D_2O background, residual water vapour and linear background. The green dashed line is the fit result from the global 3 band fitting routine (fitting all spectra in the region 30-44°C). The red dashed lines represent the individual component bands at 44°C. (Bottom) The residuals for the 44°C spectrum for the different fit functions: From top to bottom; 2 band , 3 band global and 4 band global fitting routines for the 44°C spectrum.

Attempts to fit the amide I' band provide further proof of a more complex band picture and indicate a third band at 1610 cm^{-1}; our attempts at fitting with 2 bands gave universally poor fits which were unable to replicate the IR data, with three band fitting providing a better fit with much improved residuals (see figure 3.6). Note that careful inspection of Maeda's fits show that they do not replicate the data very well. Attempts to extract more detail with a 4 band fit gave χ^2 results that were only marginally smaller than those for the 3 band fit (see figure 3.6). However, unrealistic band-behavioural parameters were produced, even when various constraints were applied to induce the expected behaviour. Further evidence of an additional band at 1610 cm^{-1} is presented in literature; Katsumoto *et al* detect this band when fitting poly(N,N-dialkylacrylamides), and assign it to carbonyls hydrogen bonded to *two* water

molecules[79]. Meersman *et al* see this band explicitly in a pressure induced pNIPAM phase transition[37] (see section 3.5.3 for a discussion of these data).

Initially, the spectrum for each temperature was fitted with the minimum number of pseudo-Voigt bands with the best possible parameters chosen using a fitting algorithm with the band populations, centre wavelengths, line widths and Gaussian/Lorentzian contribution allowed to vary freely. To further explore the band behaviour around the LCST, we attempted a more complex fit; a "global" analysis that fits a large number of spectra simultaneously at incrementally changing temperatures around the LCST (section 2.6.2 describes this fitting routine in detail). Typically, we use 3 pseudo-Voigt bands for fitting the spectrum at each temperature. A linear temperature dependence of the spectral parameters allows the slight shifts of band positions, band widths, and Gaussian/Lorentzian character with temperature to be taken into account; the parameters describing these linear dependences are also optimised during global fitting. The resulting fits describe the amide I' curve accurately, and enable an in-depth examination of the different hydrogen bonded states at different temperatures.

The temperature gradient of the band widths was set to be positive, as this is what one would expect; increasing temperature means an increase in the mobility of both the carbonyl bonds and the species they are hydrogen bonded to. Consequently, there is an increase in the number of conformations, which widens the band. Other parameters are allowed to vary freely within the constraint of the linear temperature dependence. The areas of the sub-bands with these parameters are allowed to vary freely; the relative areas of the sub-bands are extracted, and by comparing these areas (assuming identical extinction coefficients) the solvation behaviour of the amide carbonyl bonds at temperatures around the LCST can be determined. The assumption of identical extinction coefficients is acceptable, since in fitting the spectra for pNIPAM presented in this chapter, the overall area of the amide I' band changes only by a few %, despite large changes in the band structure. Additionally, there is no general trend in whether the change is positive or negative, indicating that this effect is noise. Note that Maeda concludes on a large change in extinction coefficient between the 1625 cm^{-1} and 1650 cm^{-1} band for pNIPAM, but a small difference for poly(n-propylacrylamide)[26]. This difference for similar samples is problematic, and on analysis derives from similar small changes of the total amide I' band areas as observed here, which most likely are due to fitting inaccuracies.

The linearly temperature dependent parameters for all the fits are presented in appendix A. The temperature dependent parameters provide some interesting, if tentative, insights into the properties of the amide bond in different environments. All fits involving pNIPAM have similar temperature dependent band frequencies. Other alkylacrylamides have slightly different frequencies, however. The poly(*N*-n-propylacrylamide) (pNNPAM) homopolymers have higher band frequencies, as expected, due to the additional methylene-H, which means more electron donation into the amide bond, strengthening the carbonyl bond. t-butyl-comonomers (pNIPAM-co-tBu) contains an additional methyl group, which again, has an electron inducting effect, increasing the frequency of the bands. Most of the bands shift to higher frequency with temperature, as expected[115]. The major exception is the 1650 cm^{-1} band, which shifts towards lower frequency. This suggests a change in the band character, possibly a shift between two bands that are so close together they are difficult to resolve with our fits. This is an interesting observation, and will be discussed in more detail when examining the band assignments (Section 3.5.3).

The band widths increase marginally with temperature, and this is to be expected, as increasing temperature raises the mobility of the molecules and results in a widening of the band. Most bands have a mixture of Lorentzian and Gaussian character, however, the 1610 cm^{-1} band on average has a higher Lorentzian contribution to the band shape on average. This may indicate that the 1610 cm^{-1} band relates to a carbonyl that is a better defined binding site, which may be another indication for the suggested 1610 cm^{-1} band assignment.

Figure 3.6 gives an example of how the amide I' envelope is split into sub bands. These fits demonstrated that the spectra required a minimum of three bands, and that the parameters governing the bandshape could be approximated with a linear temperature dependence.

3.4.2 Assignment of Sub-Bands

It must be noted that due to the strong overlap of the sub-bands, the fits are not expected to provide an exact and accurate numerical value for the population of each state; however, the fits provide qualitative/semiquantitative information on changing populations, and the trends seen are good indications of the behaviour of the carbonyls and therefore provide a good insight into changes in hydration during the transition.

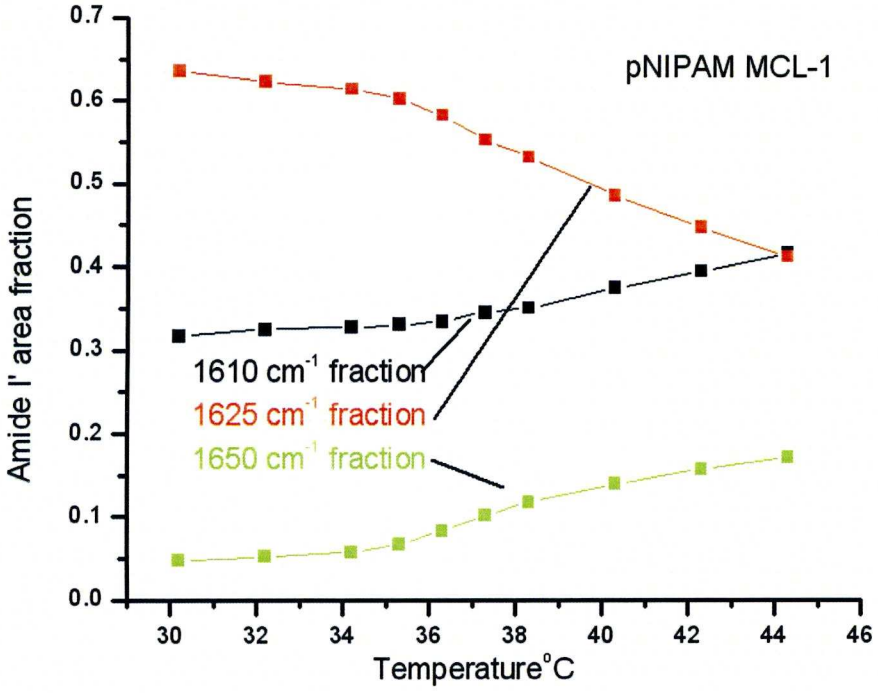

Figure 3.7 Fractional areas of the component-bands that make up the amide I' envelope. The sample is pNIPAM-MCL 1 (see table 2.1 for sample details) with 10 mg/ml concentration.

In Fig. 3.7, each component band area is displayed as a fraction of total band, reflecting the relative population of the resolved hydration states that exists at each temperature. We initially assigned the bands based on a survey of the current literature. However, the band populations in experiments presented in this chapter show behavior that is inconsistent with current band assignments by Maeda[3,19,26,30,31,69,71,74-77] and Katsumoto[25,28,79,110,116]. We have therefore devised our own interpretation that is consistent with both our results and those in the literature. The 1625 cm^{-1} band is assigned to "normally hydrated" carbonyls, in which the carbonyl bond is hydrogen bonded to two water groups. The 1650 cm^{-1} band is assigned to carbonyls bonded with a single hydrogen bond to either water or another amino group. Essentially, this carbonyl is "partially dehydrated", as normally, if possible, carbonyls will form two hydrogen bonds[117]. The 1610 cm^{-1} band represents a special case, in which the double hydrogen bonded carbonyl has further reduced frequency, due to bonding with "trapped" water molecules which have reduced motion due to the constraining effect of polymer cavities (detailed justifications and explanations for the bands and a comparison with other interpretations are given in section 3.5).

When the temperature is below the LCST, the polymer exists in an extended random coil conformation and the majority of carbonyls will be fully hydrated. This is reflected by the high area fraction of the 1625 cm^{-1} band. However, when the temperature is increased over the LCST, a discontinuous change in the temperature dependence of all bands is observed as the polymer undergoes a phase transition. The 1625 cm^{-1} band fraction is decreased, exchanging population with both the 1610 cm^{-1} and 1650 cm^{-1} band, reflecting the changing of the solvation state as the polymer undergoes the coil-globule transition.

The collapse into a globule results in an ejection of water from the core chains, and the band populations reflect this, with the increase in the 1650 cm^{-1} band relating to a decrease in the number of water molecules available for hydration, and an increase in the number of amide-amide carbonyls formed in response to the closer proximity of the chains after collapse. The 1650 cm^{-1} band has a frequency temperature dependence that is contrary to the other bands (observed in the temperature dependent parameters when fitting, see above). This may indicate that the 1650 cm^{-1} band represents two bands which are too close to resolve, suggesting that there is a slight frequency separation between carbonyls hydrogen bonded to one water molecule and those hydrogen bonded to other amino groups. The temperature dependence indicates that, as temperature is increased, the major contributor to this band changes. This can be interpreted as follows; below the LCST the chain is fully solvated, which means a majority of the side chains are fully hydrated (carbonyls are H-bonded to two water molecules); however, a small proportion will be single hydrogen bonded at any time due to fluctuations of the hydrogen bonding network, reflected by the small area fraction of the 1650 cm^{-1} (single H-bonded carbonyl) band. An increase in the number of amide-amide hydrogen bonds occurs during the phase transition, as the chains dehydrate and collapse into globules. This causes an increase in the 1650 cm^{-1} band at the expense of the fully solvated carbonyl population fraction (1625 cm^{-1}), and a small shift in the frequency of the band as amide-amide bonds are favoured.

The number of hydrogen bonds to "trapped" water molecules also increases above the LCST, as can be seen from the increase in the 1610 cm^{-1} band, which shows that the collapse results in the formation of a number of pockets in which water molecules that remain hydrogen bonded after the collapse are separated from the bulk solvent. Interestingly, there is a linear temperature dependence of the band fractions

even below the LCST. As the temperature is increased, the 1625 cm^{-1} band population exchanges with the 1610 cm^{-1} band (with very little change in the 1650 cm^{-1} band). This suggests that there are constraining cavities in the polymer chain even below the LCST in which hydrogen bonded water molecules are trapped. This agrees with the pearl-necklace model[118], which states that, below the LCST, small segments of the chain are locally collapsed (see chapter 3.5.4 for a discussion of this model and how it relates to our results).

3.4.3 Chain length, Concentration and Side Chain Effects

The Effect of Sample Concentration

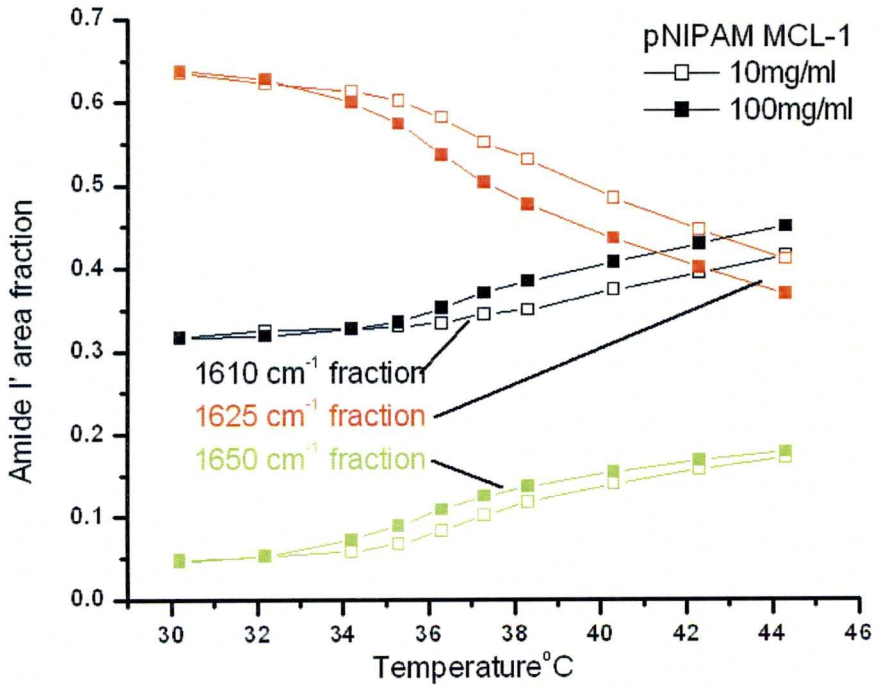

Figure 3.8 Comparison of the band composition of the Amide I' band in temperature dependent FTIR spectra for 10 mg/ml and 100 mg/ml samples of pNIPAM-MCL 1 (see table 2.1 for sample details). Note that unlike other FTIR spectra, spectra of high concentration pNIPAM-MCL were taken with an approximately 9μm spacing.

Concentration also has an effect on the hydration state, as can be observed in figure 3.8. Although band area fractions are the same below the LCST, a noticeable difference occurs at temperatures above the LCST. At higher concentration, both the 1610 and 1650 cm^{-1} bands show a larger increase during the collapse, and correspondingly more 1625 cm^{-1} bleaching is observed. Again, this can be rationalised if one considers that at higher concentrations, there will be more opportunity for intermolecular bonding and trapping of water molecules during aggregation of

separate chains. Note that the final band-area fraction seen for the 1650 cm^{-1} band (0.13) is very similar to that seen by Maeda for his two band fits.[3]

The Effect of Chain Length

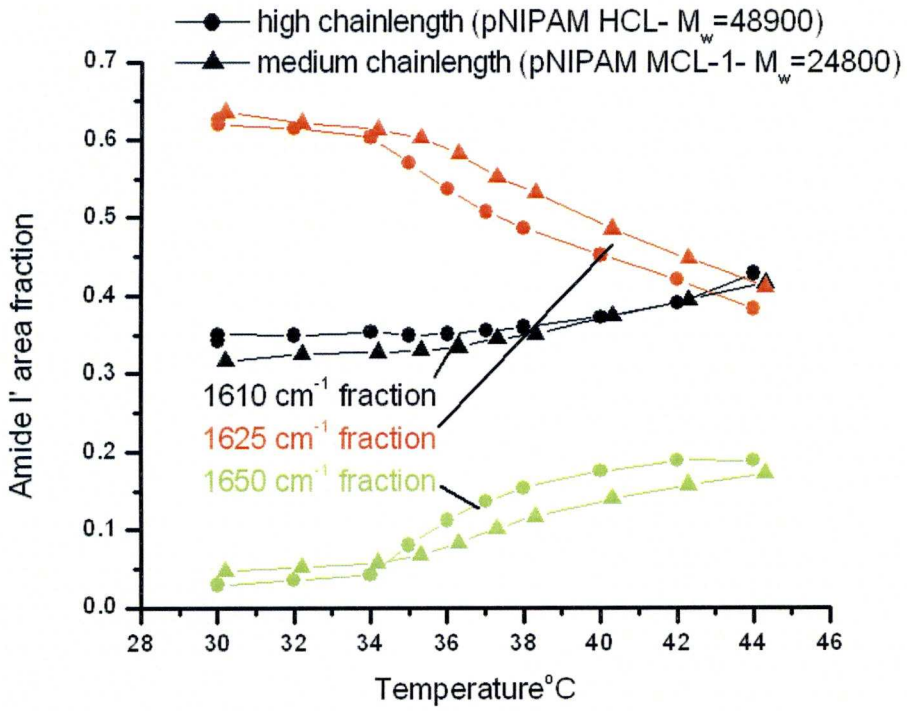

Figure 3.9 Comparison of the band composition of the Amide I' band in temperature dependent FTIR spectra for 10 mg/ml samples of pNIPAM-MCL-1 (medium chain length) and pNIPAM-HCL (high chain length, see table 2.1 for sample details).

Chain length has been shown to have little effect on the LCST[43], and the results presented in figure 3.9 agree with this, as the coil-globule transition occurs at a similar temperature regardless of chainlength. However, comparing the fractional amide I' areas of the component bands of pNIPAM with differing chainlengths reveals that the population distribution of the bands differ (figure 3.9). A comparison of the fractional areas of a longer and shorter chain length polymer reveals that both polymers react in a similar fashion to the chain collapse, with the normally solvated (1625 cm^{-1}) carbonyl population being lost to inter/intrachain (1650 cm^{-1}) and constrained solvent molecule hydrogen bonded carbonyls (1610 cm^{-1}) as the transition progresses. The smaller chain pNIPAM-MCL 1 has a similar distribution of area bands as the high chainlength sample at temperatures below the LCST (HCL has a slightly larger 1610 cm^{-1} fraction). However, the bands, most notably the 1650 cm^{-1} and 1625 cm^{-1} bands, diverge at higher temperatures, which suggests more inter/intramolecular hydrogen bonding and less fully solvated carbonyls for the long chain length polymer. In collapsed

globules, it is the carbonyls on the surface which present the largest proportion of the 1625 cm^{-1} fraction, as these have the easiest access to the solvent with less opportunity for inter/intrachain bonding. Since the volume-to-surface area ratio is increased for globules formed by longer chains, this explains the results observed here.

The Effect of Changing the Pendant Alkyl Group

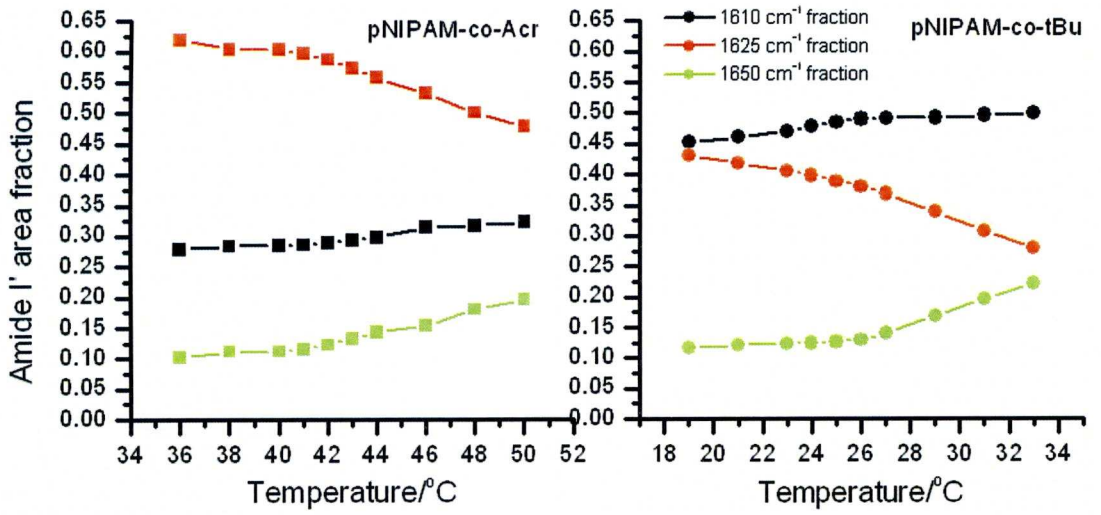

Figure 3.10 Comparison of band composition of the Amide I' band in temperature dependent FTIR spectra for 10 mg/ml samples of pNIPAM-co-Acr and pNIPAM-co-tBu (see table 2.1 for sample details).

The LCST is strongly influenced by exchanging 10% -15% of the monomers for other alkyl derivatives. pNIPAM with t-Butylacrylamide and non alkylated acrylamide co-polymers were studied, and the LCST was found to shift to 25°C and 45°C, respectively (see chapter 3.3). The change in transition temperature gives further evidence for the hypothesis that it is the hydrophobicity of the alkyl groups that drives the transition. The FTIR spectra of the two copolymers were fitted in a similar manner as pNIPAM spectra and satisfactory fits were achieved again using 3 bands (Figure 3.10). Interestingly, the fits yielded somewhat different spectral parameters, which indicates different intrinsic C=O frequency of the co-polymers (due to different electron conjugation). For pNIPAM-co-Acr, there is an additional complication caused by the carbonyl group being amide bonded to a primary amine in the acrylamide copolymers, rather than secondary (as is the case for pNIPAM and t-Bu-acrylamide), which will affect the amide I' band.

Nevertheless, the fits yield some intriguing observations. At all temperatures, the fraction of carbonyls H-bonded to constrained solvent molecules (1610 cm^{-1}) is

greater for chains with bulky t-Bu side groups and smaller for non-alkylated acrylamide copolymers than for pNIPAM homopolymer samples (figure 3.10). This change largely corresponds to a contrary population shift in the fully solvated carbonyls band (1625 cm^{-1}) rather than the inter/intramolecular bonds (1650 cm^{-1}) and thus reflects a change in the number of constrained water molecules. One would expect this, since bulkier side chains provide steric hindrance limiting the mobility of the carbonyl bound water molecules. Acrylamide, on the other hand, contains no alkyl group, which reduces steric hindrance around the peptide group.

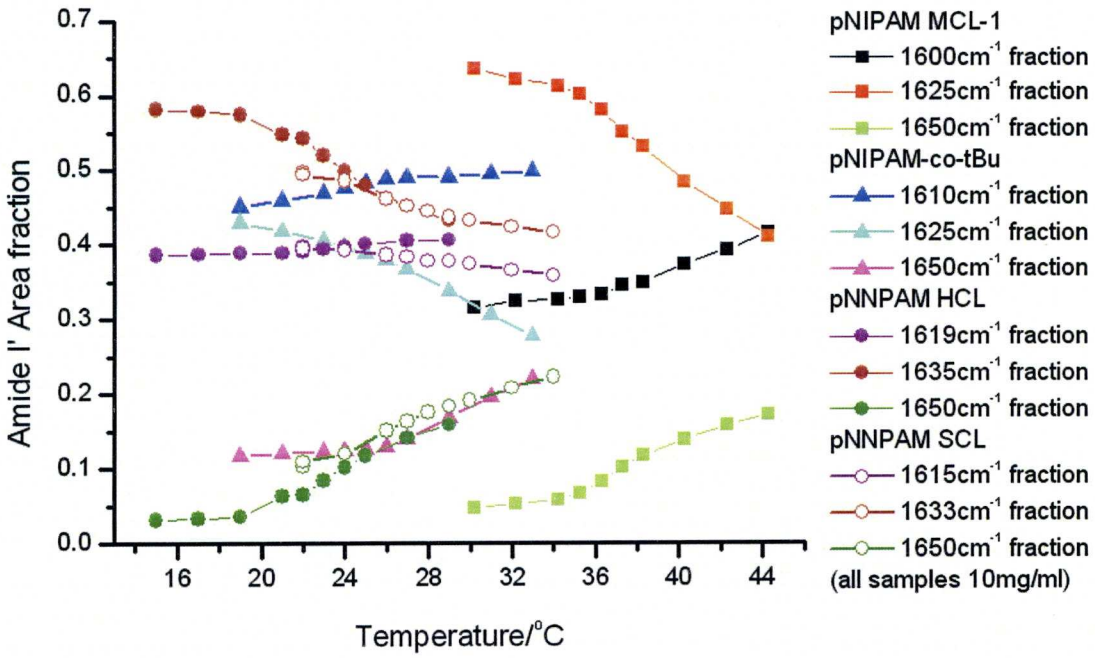

Figure 3.11 A comparison of the temperature dependence of the band fractions for the lower - LCST polymers; pNIPAM, pNIPAM-co-tBu, pNNPAM SCL and pNNPAM HCL (see table 2.1 for sample details).

A comparison of the low-LCST polymers (pNNPAM and pNIPAM-co-tBu) with standard pNIPAM is shown in figure 3.11. Below the LCST, pNNPAM has more fully hydrated carbonyls (1625/1635 cm^{-1}) and more carbonyls bonded to trapped water (1610/1619 cm^{-1}) than pNIPAM-co-tBu. Intramolecular bonding (1650 cm^{-1}) remains similar. This is an indication that the flexible pNNPAM side chain traps less water than the bulky t-Bu groups in pNIPAM-co-tBu, even in the solvated coil conformation.

3.4.4 Aggregation on the Long Timescale

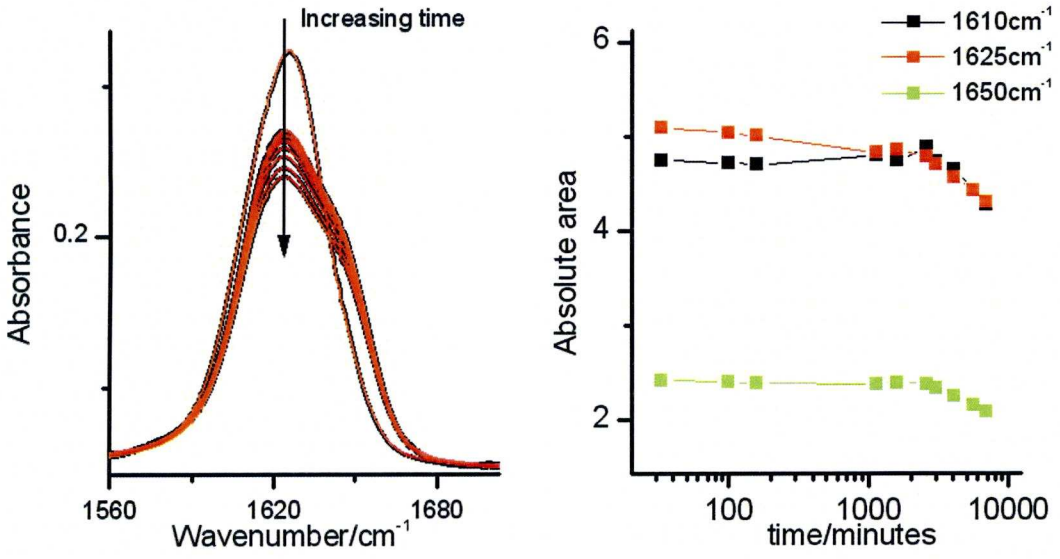

Figure 3.12 The effect of time on a 10 mg/ml sample of pNIPAM-HCL (High chain length). A spectrum was taken at 30°C, then the temperature increased to 40°C. A spectrum was taken after 8 minutes equilibration at 40°C, then every hour for three hours, then approximately every 20 hours for 120 hours.

Figure 3.12 shows the effect of time on the amide I' band composition after the coil to globule transition. The amide I' band components of pNIPAM-HCL (chosen due to the large size of the amide I' band changes) continue to show slight changes over time, long after the temperature has equilibrated. The 1650 cm^{-1} band stays fairly constant, indicating the secondary structural change is complete. However, on the 10 hour time scale the number of carbonyl-bonded trapped water molecules (1610 cm^{-1}) continues to increase slightly at the expense of the freely solvated carbonyls (1625 cm^{-1}) which implies that aggregates continue to increase in size over this time. This is akin to the effect we see with increasing concentration (figure 3.8). At around 2500 minutes (40 hours), the amide I' overall band area begins to decrease, which is a strong indication that the stability of the aggregates in solution is limited by their size. After this time, the aggregates begin to precipitate, or at least are heavy enough to sink to the bottom of the cell, out of the IR beam path. This is similar to the sedimentation observed in ATR-FTIR when a pNIPAM sample is held above the LCST[112].

3.5 Discussion

The coil-to-globule transition is an extremely complex process, so any one investigative approach is unlikely to elucidate the problem entirely. The results presented give an intriguing window into the internal processes that take place, but only at the carbonyl bonds. Other experiments give a wider picture of the transition, and allow us to understand the results presented in this chapter in context.

3.5.1 The Amide I' Band

Traditionally, the hydrogen bonding of the amide group is considered to stabilise the [$^{-}$O-C=NH^{+}] resonance structure in preference to the [O=C-NH] structure, thus lengthening and weakening the carbonyl bond. Hydrogen bonding on the C=O site increases the C=O bond length by 0.008 Å, while C-N and N-H bond lengths decrease by 0.013 Å and 0.001 Å, respectively.[119] The H-bond results in an increase in electron density at the carbonyl oxygen with a decrease in the rest of the molecule. Hydrogen bonding at the N-H site elongates the N-H and C=O bond lengths by 0.006 Å and 0.003 Å respectively while the C-N bond length decreases by 0.005 Å. These values are consistent with the resonance model. The analysis also shows that water hydrogen bonding to the C=O site downshifts the amide I band by 23 cm^{-1}. Asher *et al*[119] performed DFT calculations on NMA (*N*-methylacetamide) to confirm that the resonance model is consistent with experimental observations[120], and that carbonyl hydrogen bonding has a smaller effect on the amide II vibration than previously calculated, thus the amide II band primarily gives an indication of H-bonding to the N-H group. Therefore, the fact that both the amide I and II bands of pNIPAM change with temperature indicates that the H-bonding environment is modified at both potential points of contact as the hydration state changes.

NMA is the simplest possible case, and pNIPAM is more complicated due to the presence and effect of the hydrophobic groups so closely positioned to the amide bond, and the consequent steric effects, which place the hydrogen bonding network under additional conformational strains and complicate the assignment of bands. Additionally, the hydrophobic phase transition and subsequent close proximity to other bonds convolutes the situation further. Nevertheless, the interpretation of amide I band shifts can be based on the general principles described above.

3.5.2 The Hydrophobic Effect and the Hydration of pNIPAM

As the hydration and dehydration of isopropyl groups at higher temperatures is a key driving force behind the coil-to-globule transition, the structure of the water molecules in the hydration sphere surrounding them is of importance. The hydrophobic interaction of methyl groups has the same range as Van Der Waal's dispersion forces, but is about an order of magnitude stronger, and is considered to be a result of the tendency of the surrounding water molecules to minimise the polymer-water interface[40]. Inomata *et al*[121] describe the solvation structure as a water "cage" around the isopropyl groups (also referred to as "clathrate cages"). Such water cages have been described as "iceberg-like", due to their slower dynamics and the amount of energy required to rearrange water molecules in the cage. The cause of the formation of solvent cages is to maximise the hydrogen bonding interaction of the water molecules. The effect of such cages on the C-H bonds in the isopropyl region is an intriguing increase in the frequency of the bond vibration, indicating that the C-H bond becomes shorter in response to these interactions[3,122].

^{1}H-NMR T_1 relaxation times of methyl groups in pNIPAM increase when increasing the temperature below the LCST[18], consistent with a decreasing amount of solvation already before the collapse. Above the LCST, the T_1 relaxation time remains constant, indicating no further change in the methyl group solvation, which therefore have little or no access to the bulk solvent and are confined to hydrophobic pockets. Spěvàcěk et al[106] studied the hydration of pNIPMAM (poly(*N*-isopropylmethylacrylamide), which has an additional methyl substituent on the backbone) using NMR and were able to resolve the types of water molecules in the collapsed globule system. Particularly of interest was their discovery that trapped water molecules inside the globule are resolvable from those on the "surface" of the meso-globules by their shorter T_2 spin relaxation time. The fact that these molecules show a shorter T_2 indicates that these molecules are located in environments that are cut off from the bulk solvent ("trapped"). However, these molecules have a fairly rapid exchange rate with the bulk solvent (exchange~1 ms) which suggests that these pockets are not permanent, rather that the globule remains fluid and permeable to water molecules. H/D exchange experiments on collapsed nanogels show an exchange rate of <5 minutes, which also indicates this[56].

Dynamic light scattering measurements by Wang *et al*[123] show the radius of gyration and hydrodynamic radius for highly dilute pNIPAM chains. Beginning at ~5°C below the LCST, one can observe a sharp drop in the radii as the LCST is approached. This suggests that already below the phase transition, the average size of the random chain and water hydration layer decreases sharply, which is in agreement with both the results presented in this chapter and Kojima's theoretical pearl necklace model[118], as described in section 3.5.4.

The amount of water molecules attached to each monomer unit is a key difference between the fully hydrated and dehydrated globule conformations of the polymer. The number of water molecules bound to each unit was determined to be 7.5 at 20°C and 3 at 40°C by ultrasonic velocity measurements performed by Kogure and coworkers[124]. These values are similar to the number of bound water molecules seen by Ono *et al*[114] using dielectric relaxation methods. Ono reports 11 associated water molecules per monomer in the hydrated state and the number drops sharply below 4 above the LCST. Both studies indicate that a number of water molecules form extended H-bonded bridges in between side chains in the hydrated random coil conformation. Even in the collapsed globule state, there are associated water molecules, but the small number indicates a lack of extended H-bonded water bridges. The quantity of water molecules in the globules means that some are likely to form bridges of a single water molecule between amide groups, which may contribute to the trapping of water molecules and therefore add to the observed 1610 cm^{-1} band population observed in our spectra (see below).

3.5.3 Justification for Band Assignments

The complexity of the amide I band and the coil-globule transition has meant previous attempts to investigate the phase transition using the amide I band are contradictory, and a number of different band assignments have been proposed, with which our interpretation is in conflict. Table 3.1 shows interpretations for the amide I(') band suggested in previous studies.

Previous studies of the Amide I band

			Band frequency/cm^{-1}			
			1600-1610	1625	1650	1680-1700
Model	Refs	Spectroscopy method/polymer	Number of H-bonds/assignment			
Percot	24	Temperature dependent FTIR /pNIPAS (in water)	-	solvated	intramolecular	Non-bonded
Maeda	3,19,26,30,31,69,71,74-77	Temperature dependent FTIR/pNIPAM and modifications	-	solvated	intramolecular	Non-bonded
Ahmed	56	Temperature dependent UVRR/ pNIPAM nanogel	-	Double H-bond/Solvated	Single H-bond/Solvated (not intermolecular)	-
Katsumoto	25,110,116	FTIR of solvent effect/ pNIPAM	Double H-bond/ solvated	Single H-bond/solvated	Non-bonded	-
Katsumoto	28,79,110,116	Temperature dependent FTIR/pNIPAM (in water)	Double H-bond/ solvated	Single H-bond/solvated	Non-bonded	-
Meersman	37	Pressure dependent FTIR/pNIPAM	Double H-bond/ solvated	Single H-bond/solvated	Non-bonded	-

Table 3.1 Previous vibrational spectroscopic studies and the amide I band assignments suggested. pNIPAS=pNIPAM copolymerised with *N*-hydroxysuccinimide.

Maeda's two band analysis with hydrated carbonyls (1625 cm^{-1}) becoming intra/intermolecularly hydrogen bonded (1650 cm^{-1}) at higher temperatures, as mentioned, is limited by a simplistic fit using a small data set[26]. There is evidence presented in their difference spectra[3] which indicates additional temperature dependent spectral changes in the 1600-1610 cm^{-1} region; however, Maeda's fits do not resolve this band. Previously, the type of H-bonding involved in hydrating the carbonyl bonds (1625 cm^{-1}) was unspecified[3,19,26,30,31,69,71,74-77]. In his latest

investigation, Maeda states that the 1625 cm^{-1} band is due to hydration with two water molecules[76].

Both Percot[24] and Katsumoto[25] use water as a solvent in temperature dependent FTIR studies. This throws their interpretations into question by the difficulties posed by subtraction of the solvent background spectrum, due to the large water association band that obscures the amide I. Katsumoto *et al* suggest the assignment of the 1650 cm^{-1} band as carbonyls which have no hydrogen bonding. This is questionable, due to the number of water molecules still present in the desolvated globule[114] (see above argument), and the fact that even fully collapsed crosslinked gels are fully permeable to water, as shown by NMR[106] and H/D exchange measuments[56]. Later measurements studying the effect of different solvents on the amide I' band[28,79,110,111,116] resolve a band at 1610 cm^{-1}, which is assigned to carbonyls hydrogen bonded to two water molecules.

Meersman *et al*[37] study the solvation of pNIPAM with pressure dependent FTIR spectroscopy. Intriguingly, increasing the pressure causes a distinctive increase in the 1610 cm^{-1} band which corresponds to an increase in turbidity (indicating a phase transition into globules/aggregates), which provides clear evidence that this band is not simply a fitting artefact in our fits. However, this change is not accompanied by a corresponding increase in the 1650 cm^{-1} band (intermolecularly H-bonded carbonyl), as seen in the temperature-induced phase transition. This suggests that pressure induces a phase transition, but results in globules with a different hydration structure. Meersman assigns this band to carbonyls double hydrogen bonded to solvent[125], with reference to Katsumoto[79].

Ahmed *et al*[56] study the temperature dependence of the phase transition of pNIPAM gel nanoparticles using UVRR spectroscopy. They assign the 1650 cm^{-1} and 1625 cm^{-1} bands to carbonyls bonded to one and two water molecules, respectively, and exclude the possibility of inter/intramolecular bonding altogether. Ahmed *et al* do not see the 1610 cm^{-1} band, which is likely due to the large signal in the amide II band compared to the amide I in UVRR spectra; the amide II band is ~3 times larger than the amide I band, and is not shifted by H/D-exchange, since UVRR can be measured in H_2O, so that the two bands overlap at 1610 cm^{-1} which would make resolution of the 1610 cm^{-1} band extremely difficult. Measuring the UVRR spectrum of dried nanoparticles resolves bands at 1650 cm^{-1} and 1700 cm^{-1}, which is assigned to non-hydrogen bonding carbonyls (Maeda sees a similar band in FTIR measurements of

dry single chain pNIPAM). The enhancement of the 1650 cm^{-1} band in dry samples indicates that the 1650 cm^{-1} band has a large contribution from inter/intrachain hydrogen bonding, which disagrees with Ahmed *et al*'s interpretation.

Interpretation of the Amide I' Band Structure Proposed here

Our alternative interpretation of the amide I band structure is presented in table 3.2.

Band frequency (cm^{-1})	1600-1610	1625	1650	1680-1700
Description	"Trapped" water	Normal solvation	Inter/intra-molecular Hydrogen bonding/ normal solvation	Non-hydrogen bonding
Number of H-bonds	2	2	1	0
H-bonds donors	1"trapped" water, 1 amide or 2 "trapped" water molecules	2 water molecules or 1 water, 1 amide	Amide or water	None

Table 3.2 Amide I band assignments in our interpretation of the pNIPAM hydration structure.

The vibrational frequency of a carbonyl bond decreases with the number of hydrogen bonds it forms[119]. As temperature increases, the fraction of carbonyls in each state changes in response. Figure 3.6 shows that the temperature has a strong effect on the hydration state of the polymers, which has a corresponding effect on the frequency of the carbonyl bond. Generally, the stronger the hydrogen bonding effect, the weaker the carbonyl bond, which then vibrates at a lower frequency[119]. As the carbonyl has two possible bonding sites, each additional hydrogen bond formed results in an additional decrease in frequency[119] by ~25 cm^{-1}. Following this logic, if the non-bonded carbonyl vibration occurs[56] at 1670 cm^{-1}, then the 1650 cm^{-1} and 1625 cm^{-1} bond must be due to single and double hydrogen bonded carbonyl vibrations, respectively. We have interpreted the 1650 cm^{-1} band as single hydrogen-bonded (seen primarily in the collapsed state due to dehydration) and the 1625 cm^{-1} band as

double hydrogen-bonded carbonyls (seen primarily in the hydrated state). In our results, these bands follow the behaviour previously reported[3,19,24-26,28,31,36,37,71,73,79,110]

It is generally accepted that carbonyls form two hydrogen bonds wherever possible (for example, in MD simulations, Gnanakaran *et al*[117] show that 50-70% of carbonyls in folded solvated α-helices will hydrogen bond to water, in addition to forming the intramolecular hydrogen bonds that maintain the secondary structure; most of the others are prevented from forming a second hydrogen bond due steric hindrance by the side chains). It is therefore likely that the 1625 cm^{-1} band is due to double hydrogen bonded carbonyls, as this band is the most populous below the LCST when the chain is in a state of maximized hydration.

Both water and amides can act as hydrogen bond donors, and hydrogen bonds formed by both have approximately the same strength[126-128], however it is unlikely that a carbonyl will bond to two other amide groups simultaneously due to steric hindrance caused by the isopropyl groups. Therefore, this band can be caused by either hydrogen bonding to water or to amino groups.

When the temperature is increased above the LCST, a phase transition occurs in which the 1625 cm^{-1} band population is lost to the 1650 cm^{-1} band, reflecting the desolvation and subsequent inter/intramolecular bonding of these carbonyls during chain collapse. The 1650 cm^{-1} band represents carbonyls that are *singly* hydrogen bonded to water or amide groups, and we expect the population of both these states to increase above the LCST due to the dehydration and subsequent collapse. The sub-bands for carbonyls that are single H-bonded to either the water or amino hydrogen are so close in frequency as to be unresolvable, however, the anomalous shift in the 1650 cm^{-1} band frequency compared to other bands indicates the main contributor to this band changes as the polymer collapses and the band population increases, which implies that below the LCST the 1650 cm^{-1} band refers to carbonyls singly hydrogen bonded to water and above the LCST the major contribution is made by inter/intermolecular hydrogen bonding.

The 1610 cm^{-1} band is located at lower frequencies than normally solvated carbonyls (1625 cm^{-1}). Since there are no H-bonding locations left on the double H-bonded carbonyl (1625 cm^{-1}), another factor must strengthen the hydrogen bonding above the LCST. The 1610 cm^{-1} band therefore represents carbonyls that are more *strongly* hydrogen bonded to water. We suggest that this lower frequency band

represents carbonyls hydrogen bonded to an amide and a solvent molecule (or two solvent molecules) in pockets where the water molecules have limited interaction with the bulk solvent, essentially trapped by steric hindrance inside hydrophobic pockets created by the collapse of the polymer. Compared to "normal" solvation, where the solvent molecules are relatively free and hydrogen bonds are not permanent, a constrained solvent molecule undergoes less thermal motion and therefore can form a stronger hydrogen bond, which has a longer lifetime. Thus the already decreased vibrational frequency of the carbonyl due to double hydrogen bonding is further reduced. The slight increase of the fraction of this band with increasing temperature below the LCST indicates the random coil is tightening and an increased fraction of water molecules hydrogen-bonded to carbonyls are becoming constrained. This agrees with light scattering experiments in which a decrease in the radius of gyration even below the LCST is observed[123] and also theoretical predictions of the pearl-necklace model of polymer collapse[118] *(see section 3.5.5)*. Above the LCST, the temperature dependence of the 1610 cm^{-1} band changes by increasing more rapidly. This is as expected, since the hydrated coil collapses into a globule, thus increasing the propensity for water molecules not lost in the transition to become "trapped" in constraining cavities. The subsequent aggregation of adjacent globules would cause solvent molecules bound to the "surface" of globules to become constrained, therefore post-LCST increases in temperature result in an even larger population of the 1610 cm^{-1} band.

Evidence for Our Interpretation

If Katsumoto's assignment of the 1625 cm^{-1} band as singly hydrogen bonded carbonyls is taken, carbonyls hydrogen bonded to two water molecules would also be expected to have lower amide I' frequencies, (at around 1610 cm^{-1}), and other investigations have suggested this as a possible assignment of different amide I' sub-bands[37,79]; The temperature-dependent behaviour of the ~1610/1625 cm^{-1} band areas (figure 3.7) discounts this possibility, however, as the area of the 1610 cm^{-1} band increases with temperature, whereas that of the 1625 cm^{-1} band decreases, both below and above the LCST. Considering that the phase transition behaviour is a result of the dehydration of the pNIPAM chains, it is highly unlikely that double hydration would increase with temperature. A further argument for this is when the alkylacrylamide polymer contains bulky alkyl side chains, (such as pNIPAM-co-tBu, figure 3.10). In

this case, the 1610 cm^{-1} band is larger, although the bulky side chain should rather prevent some double hydration due to steric hindrance. However, if we consider the 1610 cm^{-1} band to be due to trapped water molecules, this observation makes sense.

Meersman *et al*[37] studied the effects of pressure on the FTIR spectrum of pNIPAM around the phase transition. Meersman[37] sees quite clearly the growth of a band at ~1610 cm^{-1} in response to an increase in pressure at 25°C, at the expense of the 1625 cm^{-1} band, with no change in the 1650 cm^{-1} band. The 1610 cm^{-1} band in this case[37,79] is assigned to double hydration. Again, the assignment of the band to doubly hydrogen bonded carbonyls indicates that as pressure is increased the hydration of the amide group increases, which is counterintuitive considering increasing pressure causes an increase in turbidity which is a strong indication that the polymer has collapsed into a globule. However, if we consider the 1610 cm^{-1} band to arise from trapped water molecules, the behaviour seen by Meersman *et al* is understandable. The molecules form globules and trap water molecules, although with different internal structures (less amide-amide bonds, more constrained water molecules).

Other results lend further weight to the assignment of the 1650 cm^{-1} band to singly hydrogen bonded carbonyls (and by extension to the assignments of the other bands); Maeda analysed the position of the amide I' band for the monomer analogues of NIPAM, NNPAM and CYPAM in solution and in neat samples. Measurements of alkyl acrylamide monomers in solution show a single band located at ~1610 cm^{-1}, with a shift towards higher wavenumbers as concentration is increased from 1-10wt% (note that as the monomer carbonyls connect to a double bonded carbon and those of the polymers connect to single bonded carbon, the C=O vibration frequencies in poly(alkylacrylamides) are higher than in the corresponding monomer analogues). Monomers in dilute solution can be expected to be fully solvated, (2 H-bonds to water). The amide I in the neat analogue solution (in which the monomers could only H-bond with each other) was centered at ~1640 cm^{-1}, giving further evidence that the 1650 cm^{-1} band in pNIPAM is primarily due to inter/intramolecular bonding[26].

NMA (*N*-methylacetamide), a peptide monomer analogue, shows an amide I' frequency of 1718 cm^{-1} in the gas phase (i.e. no hydrogen bonds), 1653 cm^{-1} in the neat liquid, where the analogue would form an intermolecular bonding network, and 1630 cm^{-1} in solution, where hydrogen bonds with water are formed, showing the hydrogen bond can be varied by almost 90 cm^{-1} depending on the strength of the H-bonding network.[3] A possible cause of the difference in frequency between neat

analogue samples and dilute solutions in water is the relative size of the monomer to water. Water is comparatively small, and the bonding network flexible enough to arrange around a monomer, so two water molecules are hydrogen bonded to every one carbonyl. Monomers of the same species are of an identical size, therefore forming such a network would prove difficult.

Analysis of the amide I' of poly(*N*-isopropyl methacrylamide)in conjunction with the amide II' band shifts in water (which reports primarily on the hydrogen bonding state of the N-D in the pendant side chain of the polymer), shows that for this polymer, approximately 40% of both the N-D and C=O related bands are shifted upon globule formation, indicating amide-amide hydrogen bond formation. This is further evidence that the major contribution to the 1650 cm^{-1} sub-band is inter/intramolecular hydrogen bonding[71].

Our results and those presented above disagree with the assignment for the 1650 cm^{-1} bands proposed by Katsumoto *et al*[25,28,79,110,111,116] who suggests its presence is due to non-bonded carbonyls. Others place the nonbonding carbonyl band at a much higher vibration; Asher sees a band at 1700 cm^{-1} for dried pNIPAM gels, and Maeda sees a band at 1673 cm^{-1} for dry poly(N-2-(ethoxyethyl)acrylamide)[74] which neither see in solution.

For pNIPAM in alcohol solution, even in the coil state, there is a significantly larger 1650 cm^{-1} band fraction[74,116]. Again, this agrees well with our interpretation, since alcohols are larger, thus carbonyls may be prevented from forming two hydrogen bonds due to steric hindrance. It is very unlikely that this could be attributed to non-bonded carbonyls in the fully hydrated coil.

In summary, our results in general agree with the Maeda/Ahmed interpretation of the 1625-1650 cm^{-1} bands[3,19,26,30-32,56,69-71,74,76,77] (with the exception that, unlike in Ahmed's model[56], the proposed interpretation does not rule out inter/intermolecular hydrogen bonding). However, we see an additional band at 1610 cm^{-1} that changes with temperature, which these studies fail to resolve. Unlike Katsumoto[79], we assign this band to arise from "trapped" water molecules which will be discussed in more detail in the next chapter (section 3.5.4).

3.5.4 "Constrained" Water Molecules

NMR measurements by Spěváček show constrained water molecules to be distinct from bulk solvent molecules[106]. This "trapped" state is not permanent,

however (as shown by the exchange rate between the two states in NMR[106] and the H/D exchange rate[56]), and is a transient state created by the dynamically fluctuating polymer. The comparatively large population of the 1610 cm^{-1} below the LCST is predicted by the pearl necklace model (see below), which suggests that the polymer has a number of locally collapsed sections throughout the random coil. The number/size of these collapsed sections increases as the temperature approaches the LCST, which will result in more carbonyl-solvating water molecules (1610 cm^{-1}) being "trapped". As mentioned above, the 1625 cm^{-1} band is likely due to carbonyls bound to two water molecules (chapter 3.5.3). The 1610 cm^{-1} band frequency is further lowered by ~15 cm^{-1}, a good indication that the carbonyl bonds referred to must *also* be double hydrogen bonded, since the effect of optimising the hydrogen bond due to trapping the solvent molecule would not be strong enough to shift the frequency to 1610 cm^{-1} for a singularly H-bonded carbonyl (1650 cm^{-1}). However, considering the 1610 cm^{-1} band refers to carbonyls in "dehydrated" sections (the "locally collapsed" sections below the LCST, or the globule above), it is likely that the amide N-H of other side-chains are a higher proportion of the hydrogen bond donors than in the random coil.

The 1610 cm^{-1} band must represent a stronger hydrogen bonding system, in which the [$^{-}$O-C=NH^{+}] resonance form is even more favoured. One possible explanation is that the carbonyl hydrogen bonded water is "trapped" due to the collapse of surrounding dehydrated regions (i.e. in a hydrophobic cavity formed by the dehydrated isopropyl groups,) and H-bonding to amide groups only. A water molecule thus separated from the bulk water will behave very differently, due to the lack of influence from water molecules in the bulk. A water molecule trapped in a cavity has a much slower frequency of hydrogen bond breaking than in bulk water, even when such cavities are made up of small molecules (acetone), with which water forms only weaker H-bonds[129]. Carbonyls bonded to trapped water molecules will therefore be more stabilised towards the extended resonance form [$^{-}$O-C=NH^{+}], which means a comparatively larger shift of the vibration frequency. Molecular motions are also slower in cavities[129], and one can imagine that without the influence of other water molecules on the bonded water's orientation, the water molecule will orientate with respect to the carbonyl to optimise the H-bond, again strengthening the bond. In addition to this, the cooperative effect induced by charge transfer during hydrogen bonding means each additional hydrogen bond to a water molecule results in the

strength of the entire hydrogen bonding chain increasing[130]. In liquid water, H_2O also has multiple H-bonds, giving the same effect, although with a mixture of strong (short/straight) and weak (long/bent) H-bonds. A normal solvation water molecule with links to the bulk solvent will have less H-bond strength due to this cooperative effect. Constrained water, however, may very well be optimised to maximise H-bond strength. Therefore, multiple amide hydrogen bonds to a single water molecule will result in even greater gains in the stability of the hydrogen bonds, which, as well as locking the water molecule in place, result in an increase in the strength of the hydrogen bonding and a more pronounced adoption of the [$^-$O-C=NH$^+$] resonance form (figure 3.13).

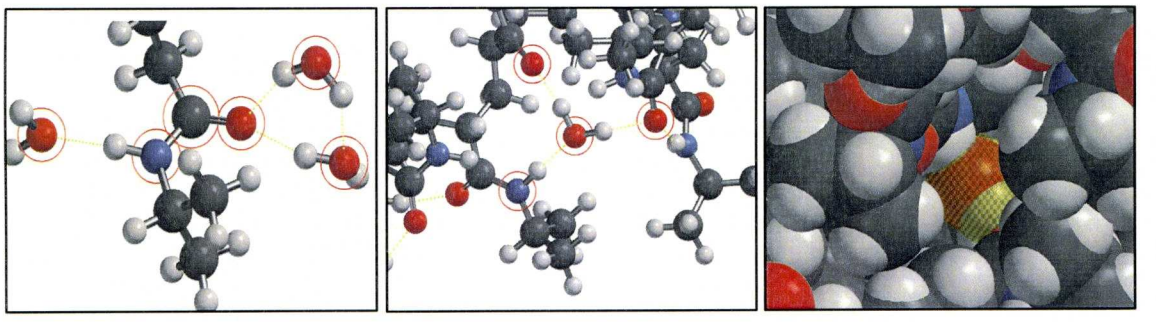

Figure 3.13 Cartoon of the suggested carbonyl environments. Key: White=hydrogen, Grey=carbon, red=oxygen, Blue=nitrogen. (Left) Hydrogen bonding of a fully extended pNIPAM chain, in which the amide group is hydrogen-bonded to two water molecules at the carbonyl and one at the amine (hydrogen-bonding molecules highlighted with a red circle). (Middle) hydrogen-bonding of a trapped water molecule system, in which the water is separated from the bulk solution and bonded to multiple carbonyls (note that in the 1610 cm^{-1} band, these carbonyls will be bonded to an additional H-bond donor). (Right) Space filling diagram of the trapped water molecule, showing how the water molecule is cut off via the isopropyl groups (water molecule is coloured orange).

From these arguments, it is clear that the 1610 cm^{-1} band can represent a number of states as long as one of the hydrogen bond donors is a trapped water molecule. For example, the C=O can be hydrogen bonded to; a constrained and a free water molecule, two constrained water molecules, a constrained water and an intrapeptide bond. In all likelihood, there is a continuum of bonding environments that takes into account a broad range of hydrogen bonding states from 1625 cm^{-1} to 1610 cm^{-1}. However, due to the overlapping nature of the amide I' component bands, our fits can extract this information as only two bands, separating them into states that decrease in population (1625 cm^{-1}, normally solvated carbonyls) and those that increase (1610 cm^{-1}, carbonyls with "constrained" hydrogen bond donors). The

comparatively large width of the 1610 cm^{-1} band is an indication of the multiple different hydration states which this band represents. It must noted that our fits can not resolve these various bonding situations from one another.

The Pearl-Necklace Model of the Collapsing Chain

From the results of the fits one can see that even below the LCST, there are carbonyls bonded to trapped water molecules (1610 cm^{-1} band). There is a change in the relative polulation of this band that indicates a tightening of the random coils in solution, as every polymer has a relative increase in the 1600-1610 cm^{-1} band when increasing temperature below the LCST. This is at odds with the typical picture of a hydrated random coil in which the entire polymer is in a fully extended and solvated state. It would instead suggest that below the LCST there are contracted pockets of the polymer which have formed (temporarily), or that small sections of the polymer collapse into globules even below the LCST. Kojima *et al* describe just such a theoretical model for the coil-globule transition[118], in which chains in a pNIPAM hydrogel produce a "pearl-necklace" type configuration, in which lengths of hydrated chain are interspersed with collapsed nodes of dehydrated polymer sections. Increasing temperature increases the number/size of the collapsed sections. Our results fit with this model, and confirm that as temperature increases, the proportion of polymer in the collapsed sections rises at the expense of the fully hydrated sections. This model is also in agreement with the observed decrease of the radius of gyration with increasing temperature below the LCST[123], which is probably due to an increase in the number of locally collapsed sections, or the growth of these collapsed sections along the chain, reducing the hydrated portion, which reduces the overall length of the polymer. The model is described in figure 3.14.

3.5.5 Effect of Concentration, Chain Length and Side-Chains on Solvation

Comparing the temperature dependence of the band fractions in samples of different concentration (figure 3.8) shows that below the LCST, solvation of the carbonyls is unaffected by concentration. The LCST marks a discontinuous change in the areas of all bands and a sudden increase in the 1610 cm^{-1} and 1650 cm^{-1} bands. At concentrations above 40 mg/ml, pNIPAM-MCL 1 is estimated to have overlapping radii of gyration (calculated using the M_w dependence observed by Kubota *et al*[16]) in

the coil state (the M_w of pNIPAM MCL-1 is 24800; the R_g for this polymer in the random coil is 5.2 nm which is close to the calculated average distance between individual chains of 5.6 nm at 40 mg/ml[131]). However, even at 100 mg/ml the majority of the gyration volume (90%) will be filled with solvent. The chains are still capable of being fully hydrated thus the effect of concentration on the pre-transition hydration behaviour is limited. It is only at temperatures above the LCST where this overlap has an effect. We interpret this as the polymer collapsing around "anchor" points in which overlapping chains are in close proximity, or where a temporary local collapse involves

two chains that are, by chance, in contact (a greater chance in a more concentrated

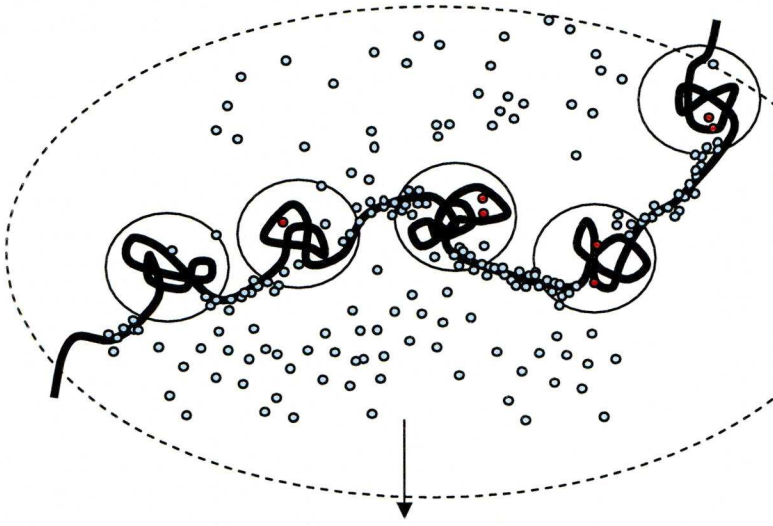

Hydrated coil: locally collapsed globules are separated by extended fully hydrated portions.

Globules provide locations for intramolecular bonding and trapping of water molecules, by separating the water molecules from the bulk solvent, or by the water molecule acting as an amide-amide hydrogen bond bridge.

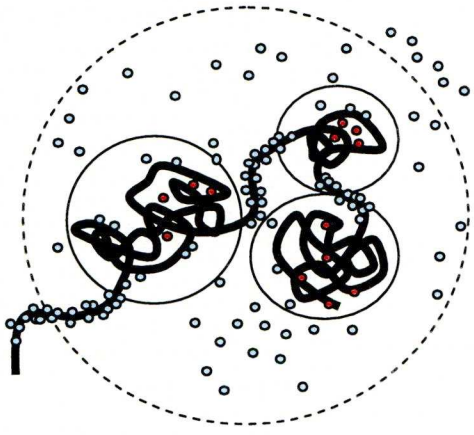

Just below LCST→Partially collapsed coil: Locally collapsed globules are larger and are more frequent, further reducing hydrated chain portions. Radius of gyration decreases correspondingly. 1610cm^{-1} band grows at the expense of the 1625cm^{-1} band due to an increased proportion of trapped water molecules.

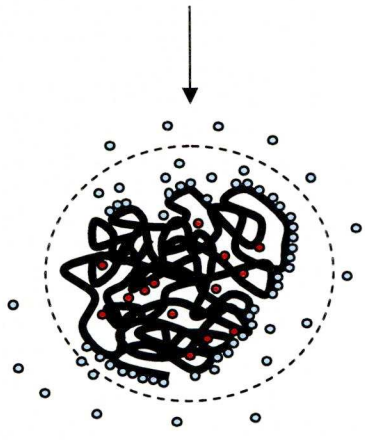

Above LCST→Globule: Above the LCST, the entire chain enters the collapsed state. Radius of gyration drops sharply and the majority of water molecules are ejected due to the hydrophobic effect. Most water remaining in the globule is trapped and effectively cut off from the solvent. Surface is hydrated normally, however, aggregation soon follows in which surface-water contact is minimised by surface-surface binding of globules.

Figure 3.14: Cartoon showing the "pearl necklace" model of the pNIPAM random coil in relation to insights from the 3 band FTIR fits presented in this chapter. Thick solid line= polymer backbone. Black circles= locally collapsed sections Blue dots= Free water molecules. Red dots= Trapped water molecules. Large dashed circles= Radius of gyration.

solution). Thus, at higher concentrations an initially collapsed globule will contain more chains, and therefore have a higher volume-to-surface ratio, thus having more chances for inter/intramolecular hydrogen bonding and a higher proportion of carbonyls bonded to trapped water molecules in cavities.

Chain length has a modest effect on the carbonyl H-bonding at temperatures below the LCST, but a major effect on the hydration state above the LCST (figure 3.9). At the low concentration (both for the pNIPAM-MCL and HCL polymers) the single polymers do not overlap (see table 3.3).

Figure	Polymer	Mw	Concentration	Distance between polymers	Radius of Gyration
3.8, 3.9	pNIPAM MCL-1	24800	10 mg/ml	8.9 nm	5.2 nm
3.8	pNIPAM MCL-1	24800	100 mg/ml	4.1 nm	5.2 nm
3.9	pNIPAM HCL	48900	10 mg/ml	11.1 nm	7.5 nm

Table 3.3 Distance between polymers, and radius of gyration for samples in figures 3.8 and 3.9.

The low concentration samples therefore collapse individually into relatively compact individual globules (on average, though there will be some cases of chains overlapping before collapse resulting in globules containing multiple chains). In the high concentration pNIPAM-MCL sample, the 1610 cm^{-1} (carbonyls hydrogen bonded to trapped water molecules) is enhanced whereas in the low concentration pNIPAM-HCL sample, the 1650 cm^{-1} (intramolecular H-bonding) band fraction is increased. Both of these changes indicate larger globule/aggregate sizes; however, the different relative band population suggest a different internal structure. The concentration comparison measurements (figure 3.8) and the time course measurements (figure 3.12) suggest that the 1610 cm^{-1} band fraction is increased more than the 1650 cm^{-1} during the aggregation processes. The larger 1650 cm^{-1} band in collapsed pNIPAM-HCL chains (figure 3.9) may, therefore, be due to larger, denser globules which are formed (prior to aggregation). A possible (tentative) interpretation of this result is as follows; with low concentration, the phase transition initially results in a "suspension" of individual globules, which eventually will aggregate, (the

aggregates continue to develop over a long period of time according to time-course measurements, figure 3.12) At high concentration below the LCST (only investigated for pNIPAM-MCL), the coil chains overlap, and thus are entangled. The collapsing chains may collapse in tandem, however, they can only do so "locally", since their ends effectively bind to each other during collapse, They are held together during the phase transition process, thus forming a looser, essentially continuous "mesh" of locally collapsed polymer chains. The low concentration larger chain-length samples, on the other hand, form comparatively larger globules. However, these globules are isolated so can collapse fully, resulting in spherical globules with more dehydrated cores.

The ratio of 1610 cm^{-1} to 1625 cm^{-1} band fractions in pNIPAM-co-Acr and pNIPAM-co-tBu (Figure 3.10) below the LCST shows the effect these copolymers have on the "pearl-necklace" conformation. The surprising inversion of the 1610:1625 cm^{-1} band fraction ratio in pNIPAM-co-tBu suggests that the relatively small number of (presumably) randomly dispersed t-butyl groups act as nuclei for these locally collapsed chain sections, since, as compared to the rest of the chain, the hydrophobic effect is greater. Alternatively, the tBu groups may provide more trapping of water molecules due to steric affects. The acrylamide groups seem to have the opposite effects, limiting the proportion of collapsed pockets, and thus decreasing the ratio of 1610:1625 cm^{-1} bands.

Hydration Changes over Time

Hydration changes slightly over time, even after the temperature has equilibrated (figure 3.12). One sees that, when the globule is left for a substantial amount of time, the band at 1650 cm^{-1} (single bonded, inter/intramolecular hydrogen bonds) changes no further. However, a small exchange between the 1625 cm^{-1} (fully solvated carbonyl) and 1610 cm^{-1} (trapped water bound carbonyl) bands is seen, with more carbonyls showing hydrogen bonding to trapped/constrained water molecules as time goes on. This indicates that, up to a point, the aggregates increase in size, or that interior motions cause the polymer to gradually find more favourable conformations, in which there is less free water inside the globules.

Time-course measurements in a similar manner were performed by Starovoytova and Spěváček[132], in which the effect of the phase transition on trapped water molecules was investigated by NMR. Time-dependence of the T_2 spin-spin

relaxation times for HDO was studied for D_2O solutions of pNIPAM. The T_2 relaxation time was measured at incremental times after the coil globule transition takes place. T_2 gives an indication of magnetic field inhomogeneity. At its simplest level, a change in T_2 represents a change in local environment. In an environment with a fluctuating magnetic field (i.e. for a HDO molecules in water solvent) the T_2 relaxation time is increased, as the rapidly changing B_0 (directional magnetic force) averages out, causing the XY spin precession to dephase more slowly. In an environment where the HDO molecule is "trapped" and thus experiences less rapidly varying magnetic field, the inhomogeneity of the environments causes faster T_2 dephasing of the spin. Thus, the T_2 of HDO in pNIPAM reports directly on the local environment experienced by the water molecules. Figure 2 of the reference[132] shows an initially large decrease in T_2 (1 order of magnitude) when initially heated over the LCST. In our time-course measurements (figure 3.12), the total IR absorbance of the amide I' band drops on the order of 50 hours, which suggests the precipitation of the sample. Spěváček *et al* also see a return of T_2 to the pre-LCST value on a similar timescale. Although they interpret this as the globules gradually contracting further to squeeze out water, our FTIR results show that it is most likely due to a decrease of the pNIPAM concentration due to precipitation in the NMR tube, leaving only neat water in the coil volume. Thus, their method (which observes water, not polymer activity) is less sensitive to the details of hydration.

3.6 Conclusions

The coil-globule transtition has been studied extensively using temperature-dependent FTIR spectroscopy. The FTIR measurements and subsequent analysis have given further insight into the complexities of the transition, with particular emphasis on the state of solvation of the polymer. 3 component bands have been identified (~1650 cm^{-1} = single H-bonded carbonyls, ~1625 cm^{-1} = normally solvated carbonyls ~1610 cm^{-1} = carbonyls H-bonded to "constrained" water molecules.)

The temperature dependence of the bands have been observed, and interpreted as an increase in the number of trapped water molecules and inter/intramolecular hydrogen bonds caused by collapsing sections of the polymer.

For the first time, comparisons of chain length and concentration reveal that variations in these factors have a noticable effect on the population densities of the

component bands; polymers with shorter chainlengths have a higher density random coil which results in a higher proportion of constrained H-bonded water molecules, and increasing concentration results in a higher number of intermolecular bonds and constrained hydrogen bonded solvent molecules. Co-polymerising pNIPAM with even a small amount of tert-butyl acrylamide or acrylamide has a drastic effect on both the LCST and the population distribution of the component bands. Our results, as well as other, agree with the pearl-necklace model in which local collapse of portions of the chain into globules occurs already below the LCST. We have expanded on the model in order to take into account the increased propensity of the chain to trap water molecules and bond intermolecularly as temperature increases below the LCST.

CHAPTER 4: PNIPAM SINGLE CHAIN DYNAMICS

4.1 Introduction

Although the equilibrium structure and solvation of pNIPAM has been investigated extensively with a large variety of different techniques (see chapters 1 and 3), the dynamics of the coil-globule transition have been probed very rarely. In particular, the phase transition dynamics of the single, uncrosslinked chain has been overlooked, no doubt due to the relative usefulness of the crosslinked gel for delayed drug release systems[11]. However, there are numerous proposed biomedical devices that utilise the single chain polymer, such as in switchable gene expression in nucleotide biopolymer conjugates for gene therapy[133,134], and switchable enzymes[134]. Measurements of the dynamics of the single chain transition undertaken so far include NMR[18] and pump-probe visible light scattering and fluorescence time-course measurements[91,92], which will be discussed in more detail in chapter 4.4.

In this chapter, we aim to further investigate the dynamics of the phase transition process by means of temperature jump measurements probed with infra-red spectroscopy. We use a number of techniques to view the transition at a variety of time scales, observing two distinct phases of the transition separated in time by several orders of magnitude.

4.2 Experimental

4.2.1 FTIR Measurements

FTIR spectra for pNIPAM samples were taken at ambient temperatures before and after all pump-probe measurements, to confirm the concentration of the sample and to confirm that no significant permanent changes take place during the dynamic measurements that would indicate that the sample was damaged by taking the measurement or that the transition is not reversible. Approximate concentrations are listed in table 4.1.

4.2.2 Samples and Experiments

The polymers used are described and characterised in chapter 2.2.1, and detailed in table 2.1. A number of different techniques have been used to observe the transition. Table 4.1 shows all measurements presented in this chapter, along with sample details. Above each measurement set, the technique and chapter describing it is listed.

4.2.3 Measurement Procedure

Procedure for High Signal-to-Noise measurements on the 20 ns-1 ms timescale (Meas 1, 2 - Experimental details 2.3)

After preparing a sample and analysing the FTIR and UV-vis spectra, the sample was mounted in the temperature jump apparatus and allowed to equilibrate for 10 minutes at the required start temperature. The IR laser was first tuned to 1583 cm^{-1}, and the energy of the Nd-YAG pump laser was adjusted for the desired Tjump, measured by observing the change in absorbance at 1583 cm^{-1} (see chapter 2.2.6). The high signal-to-noise measurements were the average of 77x128 (Meas 1) and 130x128 (Meas 2) measurements at 1622 cm^{-1} to measure the polymer kinetics, and the sample was moved after every 5x128 measurements. Between the sets of measurements at 1622 cm^{-1}, sets of 10x128 measurements at 1583 cm^{-1} were taken to give a background measurement with which to compare the polymer signal, and to readjust the size of the temperature jump to correct for slight variation in pump energy/ heat transducer absorbance. Separate Tjump experiments in time-windows of 2 μs (Meas 1) and 10 ms (Meas 2) were recorded for pNIPAM SCL samples. Data were transferred from the oscilloscope to a computer using a custom made program that converts the signal data into absorbance changes as the experiment progressed so that anomalous measurements could be discarded and repeated. To obtain the high signal-to-noise curves shown in this chapter, all individual curves for different wavelengths were averaged. By a time of 400 μs after the Tjump, cooling reduces the temperature by approximately 20% of the initial Tjump, so data after this point were not considered for analysis.

Table 4.1

Name	Sample/ conc^{n} (mg/ml)	Fig.	Start temp (°C)	Final temp (°C)	Size of jump (°C)	Wavenumber /cm^{-1}	Average of Number of meas (each wavelength).	Timescale	pathlength μm / Heat transducer (conc^{n} mM)
20ns-1ms measurements (chapter 2.3)									
Meas 1	SCL/ 22	4.1	32	37	5	1622	9856	0-2 μs	50 μm / BR (~0.5)
						1583	6400		
Meas 2	SCL/ 7	4.1	32	37	5	1622	16640	0-10 ms	50 μm / BR (~0.5)
						1583	11008		
Meas 3	SCL/ 10	4.4	32	37	5	All wavelengths	5120	0-1 ms	50 μm / BR (~0.5)
1 ms-40 ms measurements (chapter 2.4)									
Meas 4	MCL-1/ 10	4.6	32	38	6	1622	25600	0-40 ms	150 μm / AuNP (~10^{-6})
						1583	10752		
Meas 5	MCL-1/ 10	4.7	32	37.3	5.3	633 nm	8448	0-40 ms	200 μm / AuNP (~10^{-6})
						1583	1280		
>100 ms argon laser induced Tjumps measurements (chapter 2.5.1)									
Meas 6	MCL-1/ 10	4.8	32	40	8	1583,1622,1641	12	100 ms-5 s	50 μm / AuNP (~10^{-6})
Meas 7	MCL-1/ 30	4.8	32	40	8	1583,1622,1641	12	100 ms-5 s	50 μm / AuNP (~10^{-6})
Meas 8	MCL-1/ 40	4.8	32	40	8	1583,1622,1641	12	100 ms-5 s	50 μm / AuNP (~10^{-6})
Meas 9	MCL-1/ 50	4.8	32	40	8	1583,1622,1641	12	100 ms-5 s	50 μm / AuNP (~10^{-6})
Meas 10	MCL-1/ 60	4.8	32	40	8	1583,1622,1641	12	100 ms-5 s	50 μm / AuNP (~10^{-6})
Meas 11	MCL-1/ 80	4.8	32	40	8	1583,1622,1641	12	100 ms-5 s	50 μm / AuNP (~10^{-6})
Meas 12	SCL/ 10	4.9	32	40	8	1583,1622,1641	12	100 ms-5 s	50 μm / AuNP (~10^{-6})
Meas 13	SCL/ 50	4.9	32	40	8	1583,1622,1641	12	100 ms-5 s	50 μm / AuNP (~10^{-6})
Meas 14	HCL/ 10	4.9	32	40	8	1583,1622,1641	12	100 ms-5 s	50 μm / AuNP (~10^{-6})
Meas 15	HCL/ 50	4.9	32	40	8	1583,1622,1641	12	100 ms-5 s	50 μm / AuNP (~10^{-6})
>100 s water bath Tjump measurements (chapter 2.5.2)									
Meas 16	SCL/ 50	4.10/ 4.11	32	40	8	1583, 1622	1	100-14000 s	50 μm / -
Meas 17	MCL-1/ 50	4.12	32	40	8	1583, 1622	1	100-4000 s	50 μm / -

Table 4.1 Measurements presented in this chapter. The temperature jump technique used for obtaining the measurement is stated above each Tjump set. All measurements utilise a temperature controlled cell with CaF_2 windows, except for Meas 4 and 5, which use AgCl window material. All sample concentrations were checked by the relative absorbance of the Amide I' band. The sample codes refer to pNIPAM SCL (M_n/M_w~3000), MCL-1 (M_n=8620, M_w=24800), HCL (M_n=28500, M_w=48900), which are described in table 2.1.

Variable Wavelength Measurements procedure (Meas 3, experimental details chapter 2.3)

The same procedure for characterising the sample and obtaining the correct Tjump as for high-signal-to-noise measurements was followed. Once the correct Tjump had been obtained, a set of 10x512 individual measurements with a 1 ms time-window was recorded at 1583 cm^{-1}. The probe laser was then adjusted to a higher wavenumber within the amide I' envelope and 10x512 measurements were then recorded, and the sample was moved after every 2x512 measurements. The IR laser was then retuned to 1583 cm^{-1} and the pump laser power readjusted to compensate for any loss in Tjump size. The above procedure was repeated at every good IR mode available in the Amide I' band (in a randomised order to eliminate any slow drift).

Longer timescale (40 ms) Nd-YAG laser-pumped /IR-probed measurements (Meas 4, experimental details chapter 2.4)

The measurement procedure for high-signal-to-noise measurements was repeated for Meas 4, with various adjustments to extend the timescale. Meas 4 utilised 150 μm pathlength and AgCl windows to delay the cooling significantly, resulting in a much longer time window. To allow the sample to cool between laser pulses, the laser repetition rate was reduced to 0.4 Hz, resulting in measurements that took several days to complete. Temperature jumps for pNIPAM SCL and MCL-1 (meas4), were obtained on this timescale, however, only MCL was measured with good signal-to-noise. The SCL measurement was halted when it became apparent that no dynamics were present and is not shown here.

Longer Timescale (40ms) Nd-YAG laser- pumped/ HeNe laser-probed measurements (Meas 5, experimental details chapter 2.4)

The measurement procedure described above for the longer timescale Nd-YAG laser measurements was again repeated with a 200 μs pathlength and AgCl windows to further extend the time window. However, the pathlength was such that no 1622 cm^{-1} light reached the detector with a 10 mg/ml sample. The dynamics were probed using a HeNe laser to observe the transition, with the intent to detect aggregation by observing increased light scattering. The cooling was delayed to the point where the temperature did not drop to 20% of the initial Tjump until ~ 9 ms after the Tjump.

Ar laser- pumped/IR-probed measurements (Meas 6-15, experimental details chapter 2.5.1)

For Meas 6-15, the size of the temperature jump was initially calibrated by observing the absorbance change at 1583 cm^{-1}, immediately after the rise on the 0-0.1 s timescale (measured on the 0-1 s timescale). The time window was then changed to 0-100s, and a set of 3x4 measurements was then recorded for the 1583 cm^{-1}, 1622 cm^{-1} and 1641 cm^{-1} IR laser modes. After these were complete, a cyclic measurement at each of the wavelengths was then recorded to ensure that the measurements were reproducible. In all measurements after 10 s, bubble formation obscured the true absorbance changes (irreproducible absorbance changes after this time were linked to the formation of a bubble which was observable by eye after continued irradiation). Consequently, only results from 0-5 s are presented.

Water bath induced "Tjump" measurements (Meas 16, 17 - experimental details chapter 2.5.2)

Meas 16 and 17 used the procedure described in section 2.5.2, which allows us to observe the changes of pNIPAM on extremely long timescales. The procedure involves switching the water bath from 32 to 40°C (after recording the absorbance at 32°C for an initial 10 second window). The oscilloscope then records the infrared signal for every 100 s in a continuous loop. The recorded time-windows are transferred automatically to a computer and assembled manually into a continuous record of the IR signal. After the measurement is completed, this recording is converted into absorbance changes. The absorbance changes are measured for 1583 cm^{-1} and 1622 cm^{-1} to examine the response of D_2O and the polymer, respectively. Although in principle this allows us access to an infinite timescale, in practise the time window is limited by the cooling requirements of the IR detector. Thus, measurements are started once the detector has fully stabilised (~3 hours), and maintained at most until the gradual loss of coolant results in a disruption in signal (after an additional ~5 hours).

4.3 Results

4.3.1 Measurements on the Sub-ms Time Scale

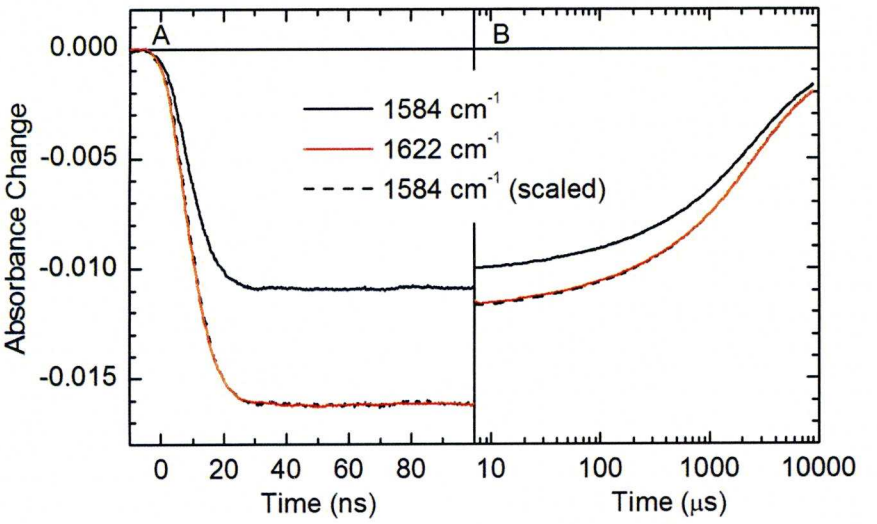

Figure 4.1 Time-dependent absorbance changes after a 5K Tjump from 32°C (50 μm pathlength). A) (Meas 1) measured on the 0-2 μs timescale for a 22 mg/ml pNIPAM SCL sample. B) (Meas 2) 0-10 ms, 7 mg/ml pNIPAM SCL. Black line: 1583 cm^{-1} absorbance changes (background); Red line: 1622 cm^{-1} absorbance changes (polymer signal). Dashed black line: 1583 cm^{-1} absorbance curve scaled to overlap the 1622 cm^{-1} polymer signal. The data are not cooling corrected.

We performed laser-induced temperature jump experiments to analyse the coil-globule transition dynamics of pNIPAM in D_2O (figure 4.1) at timescales of up to 10 ms. By measuring how long a pNIPAM sample takes to relax to its equilibrium absorbance when rapidly heated over the LCST, we should be able to measure the coil-globule dynamics if they occur on this timescale. The polymer used here is pNIPAM SCL, our shortest chain-length polymer. This was chosen for the initial Tjump experiments, since the trend in Tsuboi's visible light scattering dynamics measurements[92] is towards faster dynamics for shorter polymers.

1583 cm^{-1} is outside the amide I' band, therefore the 1583 cm^{-1} absorbance change is from the temperature dependant absorbance of D_2O only with no contribution from the polymer. The 1583 cm^{-1} absorbance shows an instantaneous decrease within our time resolution, and the absorbance then remains essentially constant until the sample begins to cool on the ms timescale (chapter 2.3.6.1). The absorbance change at 1583 cm^{-1} (10.8 mOD) shows that the temperature jump is 5 K.

When starting from 32°C, this jump easily crosses both the LCST and the midpoint of the transition.

1622 cm^{-1} is the wavelength at which the largest temperature dependent absorbance change takes place in the pNIPAM amide I' band (See figure 4.3). The 1622 cm^{-1} absorbance change contains a contribution from D_2O which is almost the same as the 1583 cm^{-1} absorbance change and a contribution from the polymer. Figure 4.1(A) shows that there is a large absorbance decrease at 1622 cm^{-1} which is faster than our time resolution, *in addition* to the expected D_2O absorbance change. This indicates that there is some change in polymer absorbance which occurs very rapidly with respect to later dynamics.

The rise of this "instantaneous" absorbance change at 1622 cm^{-1} is identical to that of the absorbance change at 1583 cm^{-1} (see the scaled curve in figure 4.1 (A), dashed black line). Thus, the rise time is limited by the time resolution of the setup. Simulations in which the observed initial absorbance change immediately after the Tjump was modelled using a convolution of a fast absorbance change with the instrumental response function (~15 ns) were performed to investigate how fast the initial polymer absorbance change would have to be in order to appear "instantaneous" within our time resolution. The simulations showed that for the initial change to follow the same time dependence as the background, the time constant for this rapid absorbance change has to be faster than 2 ns.

Temperature dependent FTIR spectra (Chapter 3) allow the prediction of the total expected absorbance changes for a given sample concentration and Tjump (i.e. the changes expected after full equilibrium has been reached at the new temperature). For the conditions of Meas 1, an absorbance change of ~12 mOD is expected at 1622 cm^{-1}. If we subtract the D_2O absorbance contribution from ΔA in Meas 1, this leaves a polymer contribution of ~6 mOD, which indicates that the transition is not completed in this instantaneous component. Up to 2 μs (Meas 1), no further absorbance change is observed (figure 4.1(A) only shows data up to 100 ns to emphasise the instantaneous dynamics). Meas 2 (figure 4.1(B)) was performed on a different sample (with a much smaller concentration), with absorbance changes measured on a longer timescale (starting essentially at 5μs). Again, polymer absorbance changes on this time scale are ~50% of those expected for the full transition. The scaled 1583 cm^{-1} curve (dashed black line in figure 4.1(B)) shows that both curves display an identical absorbance recovery due to cooling. Other than this absorbance recovery, there are no additional

absorbance changes. The polymer signal decay follows the same time dependence as the background almost exactly, even after the sample has cooled below the LCST (figure 4.1(B)). This confirms that, apart from the instantaneous component, there are no visible polymer dynamics within this time window.

4.3.2 Variable Wavelength Measurements

To further explore the early transition, the T- jump absorbance changes at incremental wavenumbers in the amide I' band from 1583-1640 cm^{-1} were measured.

1622 cm^{-1} is the most important wavelength for observing pNIPAM dynamics, as the largest change in absorbance in response to increasing the temperature occurs at this wavelength. Thus, high signal-to-noise measurements using this wavelength are the most sensitive to changes in secondary structure. The 1622 cm^{-1} absorbance changes do not provide the whole picture of the secondary structure changes, however. The amide I' band is complicated, as evidenced by the band composition and deconvolution described in chapter 3. Sub-bands shift, change width and Gaussian/Lorentzian character, and the population of the corresponding carbonyl states change with temperature. Thus, observing the transition using only one wavelength gives an incomplete picture of the changes that occur during the transition.

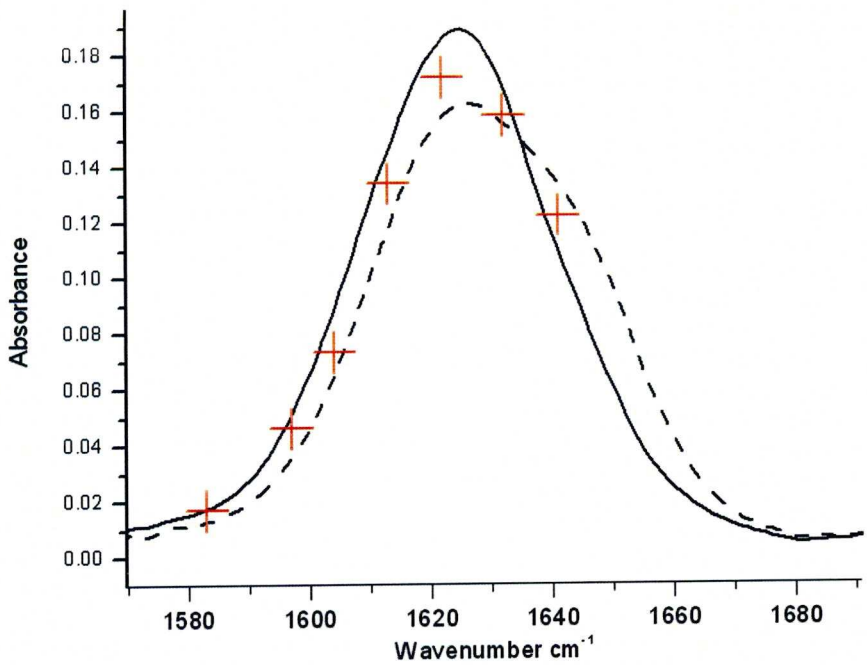

Figure 4.2 The available good IR modes of the probe laser. Red crosses indicate the location of a good laser mode. The black solid and dashed lines show the amide I' band of a 10 mg/ml sample of NANOpNIPAM (50 μm pathlength) at 30 and 42°C, respectively.

To observe the changes in the whole amide I' band with our setup, the infrared probe laser has to be tuned to as many wavelengths as possible on the amide I' band during a single experiment and absorbance changes at each wavelength have to be measured individually after a Tjump by the same temperature. The number of observable wavelengths is limited by the number of good laser modes (single wavelength, good signal to noise, figure 4.2) which the infrared laser can work at. To reduce possible variations in dynamics and sample absorbance caused by changes in sample concentration, the measurement has to be performed on a single sample, in one session. The signal-to-noise is therefore reduced, compared to the previous measurements shown in this chapter, as the time available to record the dynamics at each wavelength is limited by BR bleaching during the course of the measurement. The number of measurements used here is 10 x 512 individual measurements for each wavelength. To ensure that fluctuations in the temperature jump, caused for example, by a drop in BR transducer concentration or variations in the Nd-YAG power as the measurement progresses, the 1583 cm^{-1} absorbance change is checked in between polymer sets and readjusted to the original value. Although this keeps the temperature jump approximately constant, we still see small (<10%) variations throughout the measurement, so the final Tjump for each wavelength set is calculated from an average of the absorbance at 1583 cm^{-1} before and after each set.

The temperature dependent absorbance changes for the variable wavelength measurement Meas 3 at each wavelength are shown in figure 4.4. The absorbance change due to the polymer at each wavelength was isolated by subtracting the D_2O background signal from the overall absorbance change. The D_2O absorbance change was measured at 1583 cm^{-1}, but the absorbance change of D_2O is wavelength dependent, so this background signal was scaled by a factor determined from the temperature dependent FTIR spectra of neat D_2O. The measured absorbance changes were also scaled to account for small variations in the temperature jump in the course of the measurement (<10% change from the original). The resulting polymer absorbance change spectra (figure 4.5) give a picture of the changes in the amide I' band character after the temperature jump.

For comparison, difference spectra can be constructed from the fit parameters obtained from the temperature-dependent FTIR spectra. This allows one to predict the spectra expected at various stages in the transition. The simulations are calculated using the parameters obtained from the fits of actual FTIR spectra, see chapter 3.4.1.

The parameters can be split into linearly temperature dependent variables; lineshape, band centre point, and band width, which must be considered separately from the band areas. The relative areas of the bands represent the number of carbonyls in each state of hydrogen bonding (described in detail in chapter 3). Exchanges in the relative band area represent a change in solvation, which involves breaking of hydrogen bonds, diffusion and hydrogen bond reformation, potentially taking time. Thus, the band area shifts can be seen as a measure of secondary structural change progression. We can simulate the spectra for the polymer at 3 stages of the dynamic process:

- Before the temperature jump, the sample's IR spectrum equals the steady state FTIR spectrum measured at the start temperature.
- Shifts in the temperature dependent spectral variables are expected to occur almost instantaneously after a Tjump since these are affected by changes in the properties of carbonyl hydrogen bonds to D_2O, and require no diffusion or rearrangement of bonds, thus should react immediately to a change in temperature. There is also a linear temperature dependence of the relative band areas below the LCST (figure 3.7), likely due to local collapse and a shrinking of the radius of gyration, see chapter 3.5.4. This behaviour can be extrapolated to temperatures above the LCST, and gives an indication of the initial, potentially rapid, contraction of the polymer immediately after a Tjump. The amide I spectrum at this stage can be simulated by using the spectral parameters at the higher temperature and band areas linearly extrapolated from the behaviour below the LCST to the higher temperature.
- When the transition is complete, i.e. equilibrium has been reached at the new temperature, the IR spectrum will correspond to the observed FTIR spectrum at the higher temperature.

Figure 4.3 shows simulated spectra. The expected absorbance change spectra for each stage in the transition can be calculated by subtracting the simulated spectrum expected at the start temperature (32°C) from the spectrum reached at the different stages of the transition. As can be seen from figure 4.3(B), the difference between the spectrum calculated with the linear area shifts and that calculated for the completed transition is significant.

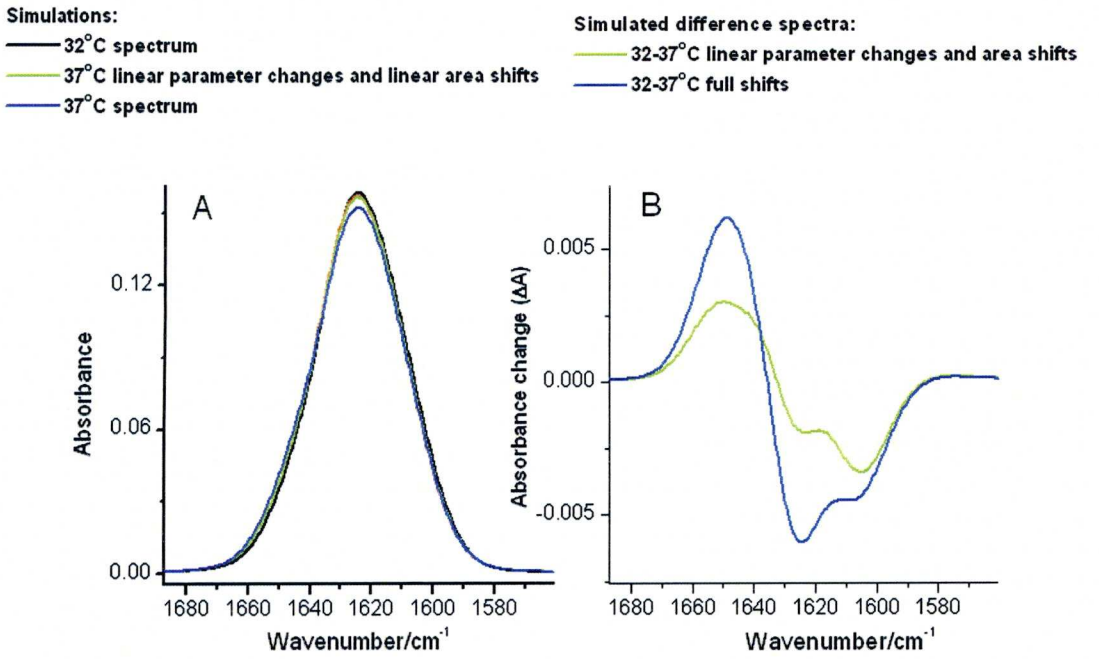

Figure 4.3 (A) Simulated amide I' FTIR spectra of pNIPAM SCL at 32°C and 37°C, compared with expected amide I band shape for the polymer at an intermediate state of the transition, where only the "linear" population changes have taken place. Simulations are calculated from the parameter shifts obtained from the fits of the FTIR spectra. The simulations are explained in the text. (B) Difference spectra calculated from the simulated spectra, providing expected absorbance changes for a 32-37°C Tjump at the intermediate and final stage of the transition.

By comparing the dynamic polymer signal at different wavelengths measured in the Tjump experiments to those expected from the difference spectrum (figure 4.5), one can conclude on the progress of the transition. After equilibrium has been attained at the higher temperature, the absorbance changes should mirror the FTIR difference spectrum of the amide I' band for 37°C when the spectrum at 32°C is subtracted (figure 4.5, black line); the experimental absorbance change spectra at 10-400 μs are quite different. This further confirms that the coil-globule transition has not yet fully taken place at this time.

The observed absorbance changes are only half of the values expected for the full transition, and decrease due to cooling rather than gradually approaching the final expected absorbance as the measurement progresses. On the other hand, a good agreement between the experimental and simulated difference spectra is obtained for the simulations using only spectral shifts and a population shift from the 1622 cm^{-1} band to the 1610 cm^{-1} band based on the linear temperature dependent population shift

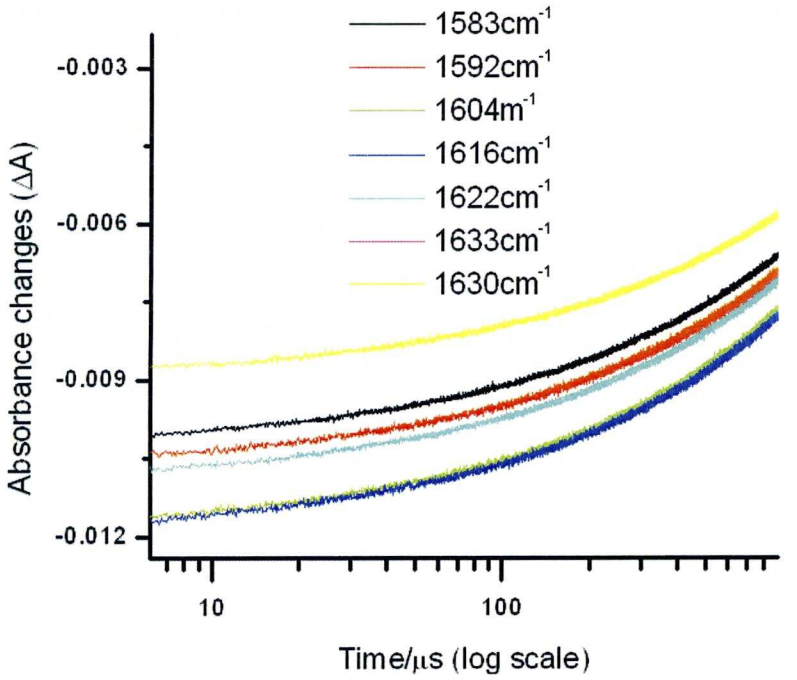

Figure 4.4 Time-dependent absorbance changes after a 5 K Tjump from 32°C (50 μm pathlength) measured on the 0-1 ms time scale for a 10 mg/ml pNIPAM SCL sample (Meas 3). See table 4.1 for details. (not cooling corrected)

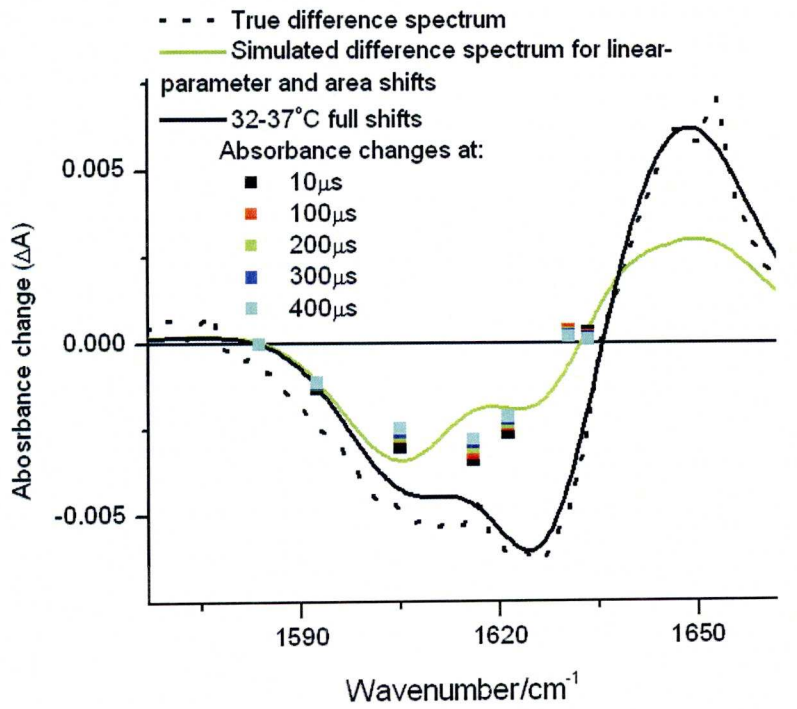

Figure 4.5 Polymer absorbance changes for pNIPAM SCL after a 5 K Tjump from 32°C (Meas 3, scaled for sample concentration and a slight TJ drift during the measurement) and different times, compared with simulated difference spectra expected for different stages in the transition (see text): green line: only "linear" area changes, extrapolated from behaviour below the LCST; black line: full transition. Note that the experimental data were not cooling corrected, so that the absorbance changes decrease with time due to cooling.

seen below the LCST, extrapolated to 37°C (figure 4.5, green line). This yields a simple picture of the early stages of the transition; in response to a temperature increase over the LCST, the coils almost instantly (i.e. within 2 ns) tighten locally (by increasing the fraction of backbone in locally collapsed globules, see chapter 3.5.4), with more hydrogen bonded solvent molecules being trapped as a consequence. The larger-scale transition to the fully globular equilibrium state, on the other hand, only occurs on the timescale of a few ms or slower (see section 4.4.1 for discussion).

4.3.3 Measurements on the 1-50 ms Timescale

In the setup used for the previous experiments, after 400 μs, the temperature has dropped by approximately 20% of the initial Tjump, which will have the effect of slowing any transition. From the above measurements it is therefore impossible to say with any certainty that there are no polymer dynamics after this time. To investigate the later parts of the transition, various adjustments were made to extend the time-window. To perform measurements on the 1-50 ms timescale, adjustments were made to the cell in order to reduce the speed at which heat can dissipate from the cell (described in detail in section 2.4.1). Changes to the path length of the cell and the window material extended the useful time window to 50 ms.

Using AgCl windows and a 150 μm pathlength, heat flow out of the cell is reduced dramatically, to the point where the 10 Hz repetition rate of the Nd-YAG laser is not sufficient for the heat to fully dissipate before the next pulse, resulting in a rapidly building temperature unless the pulse rate is limited (from 10 to 0.4 Hz).

This effect can be seen in the IR measurements at 1583cm^{-1}, which show a far slower absorbance recovery (20% at 10 ms) when compared to measurements shown in figure 4.1. Despite this, when scaling the 1583 cm^{-1} curve to match the 1622 cm^{-1} polymer signal, no difference is seen before cooling becomes a significant factor (or afterwards). Thus, no dynamics are seen, at least up to 10 ms after which cooling becomes too large to allow reliable conclusions. Even on this timescale, only 50% of the expected polymer absorbance change is seen. The same lack of dynamics on this time scale is seen in measurements on pNIPAM SCL.

Further increasing the pathlength (to) further slows the cooling up to ~18 ms (cooling by 20%) and opens up a longer time window, but rules out using IR to probe the transition, as the absorbance at 1622 cm^{-1} becomes so strong that no IR light

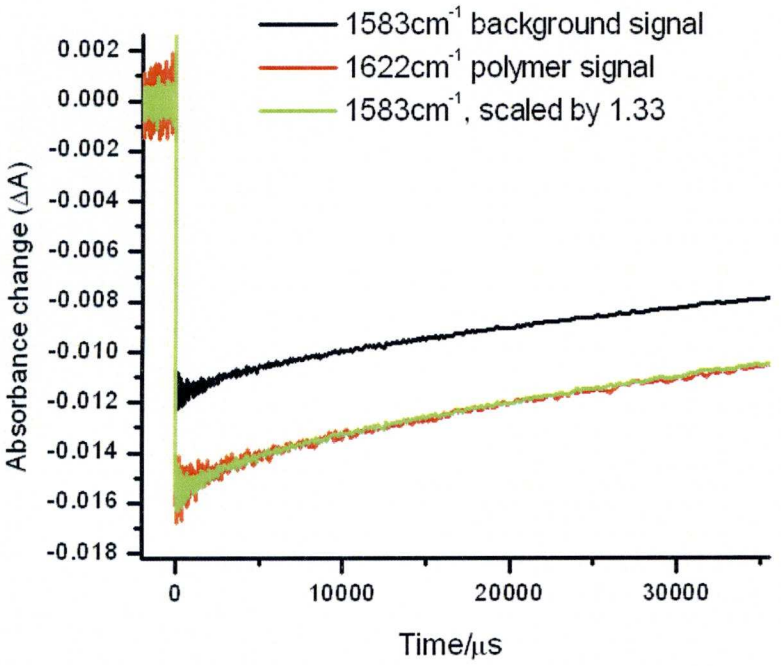

Figure 4.6 Time dependent absorbance changes of a 10 mg/ml sample of pNIPAM MCL-1 after a 6 K Tjump from 32°C (Table 4.1, Meas 4). The green line is the 1583 cm^{-1} absorbance scaled to the curve at 1622 cm^{-1}. 150 μm path length and AgCl windows were used to slow cooling.

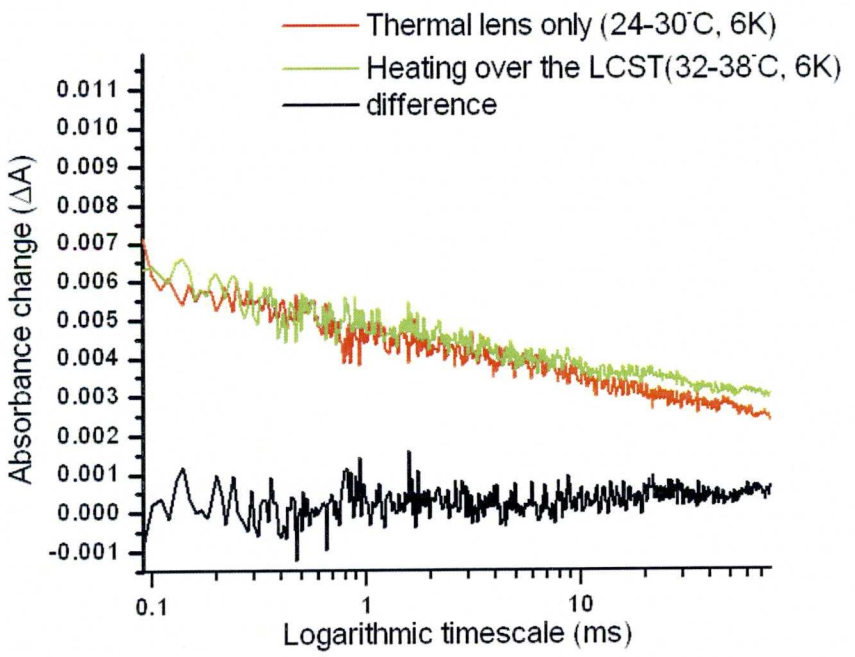

Figure 4.7 Time-dependent absorbance changes at 633 nm of a 10 mg/ml sample of pNIPAM MCL-1 (Meas 5(HeNe) in table 4.1), with a 200 μm pathlength and AgCl windows, further extending the accessible time-scale. Red line: absorbance changes for the sample heated by 6 K over a temperature range below the LCST, therefore showing no changes due to polymer interaction. Green line: 6 K Tjump from 32°C Black line: subtracted absorbance, showing the (only very small) difference between the thermal lens and transition measurements.

reaches the detector. However, implementation of a HeNe laser (described in section 2.4.2) allows the monitoring of the transition using visible light, in a similar manner to measurements reported by Tsuboi *et al*[92]. The HeNe laser system probes the transition by detecting losses in transmission due to scattering by aggregates, when the particles are sufficiently large enough to interfere with 633 nm light. Figure 4.7 shows the 633 nm "absorbance change" detected for a sample jumped over the LCST, compared with the same sample jumped by the same magnitude temperature jump, but through a temperature range outside the transition region (which measures the thermal lens effect in the absence of any loss due to additional polymer scattering).

Again, even on this timescale, we see very little difference between the "background" measurement and the results obtained for a Tjump across the transition region. There appears to be a slight divergence at later timescales (>10 ms), but this is so small that it could easily be an experimental artefact (slightly different behaviour of the thermal lens in different experiments, for example). Thus, there is no indication of fast polymer aggregation on this timescale.

4.3.4 Measurements on the >100 ms Timescale

Observations in the above sections prove that for our experimental conditions there are no other dynamic processes in the first 0-10 ms after the instantaneous shift. However, using a continuous laser for inducing Tjumps further expands our time-window.

Figure 4.8 shows measurements on the 0.01-5 second timescale, measured using the Ar laser for inducing Tjumps (described in section 2.5.1), probed with the cw infrared laser.

Interestingly, here we see the first evidence of dynamics in single chain-pNIPAM dynamics measurements. Owing to the slower temperature jump induction by the Ar-laser, the rise time of the initial temperature jump (seen at 1583 cm^{-1}) is slower than for the experiments using the Nd-YAG laser. The temperature jump is completed within 50-100 ms, with the majority of the temperature jump induced by 10ms. In Meas 6 and 7 (figure 4.8 A) 10mg/ml and B) 30 mg/ml, respectively), the absorbance changes after the temperature rise time resemble those seen on the ns-timescale (i.e., the ratio of the absorbance changes at 1622 and 1583 cm^{-1} is similar). The 1622 cm^{-1} and 1639 cm^{-1} absorbance changes in these measurements mirror those

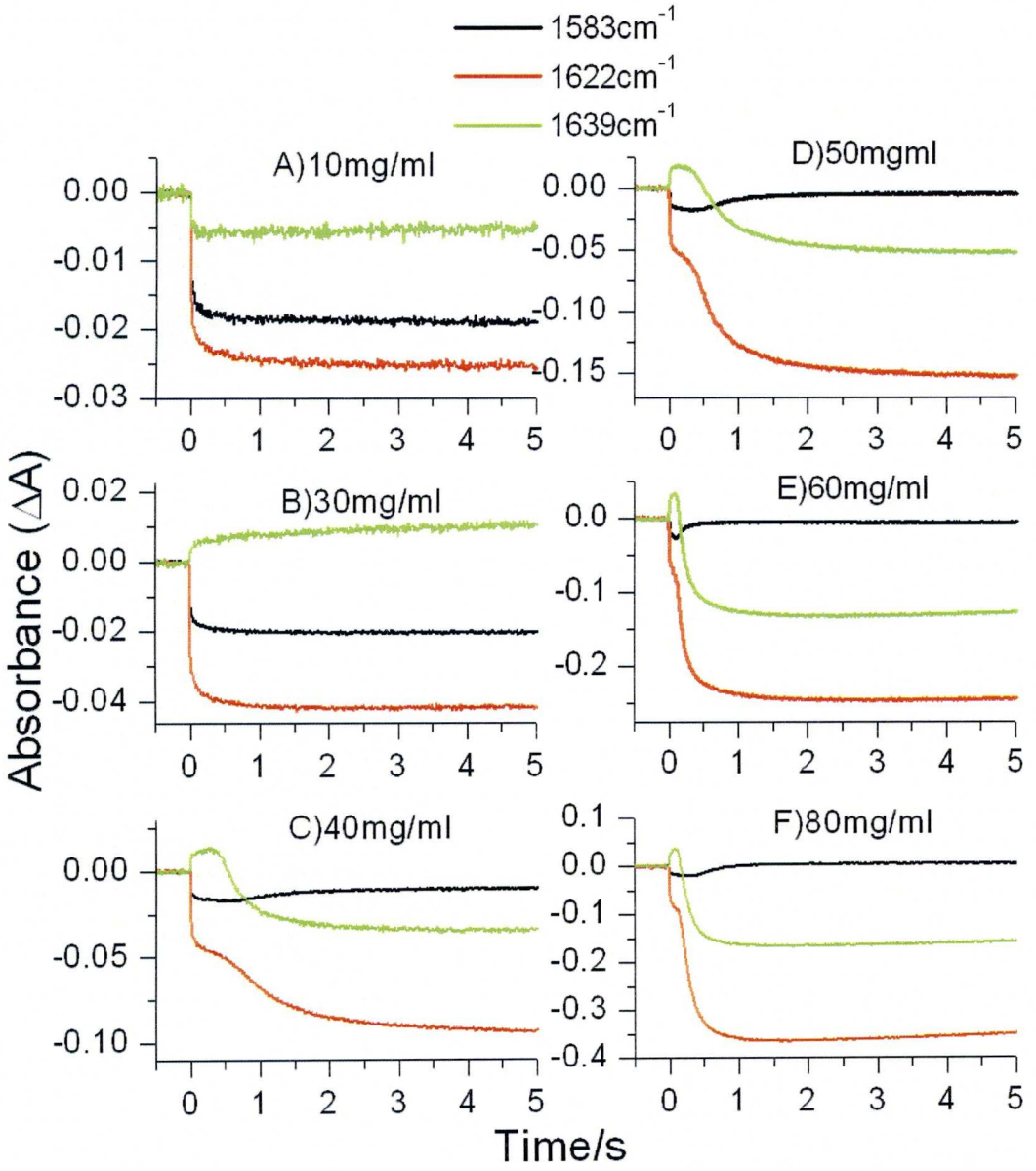

Figure 4.8 Time dependent absorbance changes after an 8 K jump from 32°C on pNIPAM-MCL1 at different concentrations. A-G: Meas 6-11 in table 4.1.

at 1583cm^{-1} (i.e. if scaled they are identical, thus all changes in this time window are due to changing temperature). No polymer absorbance change component is seen other than the initial change associated with the local collapse as already seen in figure 4.1.

However, increasing the concentration above 40 mg/ml changes the behaviour entirely. Prior to 400 ms, the absorbance changes at the polymer sensitive wavelengths reflect the low concentration measurements. The polymer signals are comparatively larger due to the increased concentration in these samples (hence the positive ΔA for the 1639 cm^{-1} measurements). However, after an induction period of 400 ms, the absorbance decreases sharply at 1622 and 1639 cm^{-1}, with a corresponding increase at

1583 cm^{-1}. These absorbance changes above 40 mg/ml after 400ms are not consistent with either the expected phase transition or aggregation. For aggregation, one expects to see an increase in "absorbance" at all wavelengths, which derives from the scattering effect of the aggregates being largely wavelength independent in the spectral region measured with the IR probe. For the phase transition, one would expect the absorbance change to follow the pattern predicted in the difference spectra; the 1622 cm^{-1} absorbance decrease should be matched by a corresponding increase of the 1639 cm^{-1} absorbance (see figure 4.5), with no effect on the 1583 cm^{-1} absorbance (due to a constant temperature). Instead, we see a large *decrease* in the absorbance at both wavelengths associated with the polymer and an *increase* in the 1583 cm^{-1} D_2O absorbance after an event that occurs at ~ 400 ms.

This suggests a loss of polymer sample in the probe volume, with the lost sample (indicated by a decrease of absorbance at the 1622 and 1639 cm^{-1}) being replaced with solvent (increase in absorbance at 1583 cm^{-1}). The fact that the 1583 cm^{-1} absorbance increases rules out the formation of a bubble as the cause of this behaviour (which would result in all three bands decreasing by a proportion relative to the initial size of the absorbance). This event is notably absent in the low concentration measurements, which suggests that the process is highly dependent on concentration.

The higher concentration measurements experience this loss of sample slightly earlier and to a larger extent, which again indicates that the process is concentration dependent.

Analogous experiments on other pNIPAM samples with different chain length sizes at similar concentrations (figure 4.9) show that this process is also strongly dependent on chainlength. pNIPAM-SCL, with an M_w of ~3000, shows no "sample withdrawal" effect even at higher concentrations of 50 mg/ml. pNIPAM-HCL, however, shows a strong sample withdrawal effect beginning at ~200 ms for 50 mg/ml samples, although significantly slower.

For pNIPAM-MCL1, the lowest concentration at which this process occurs is 40 mg/ml (figure 4.8). The chainlength dependence of the radius of gyration (R_g) of pNIPAM[16] is:

$$R_g = 0.022 \times M_w^{0.54} \qquad 4.2$$

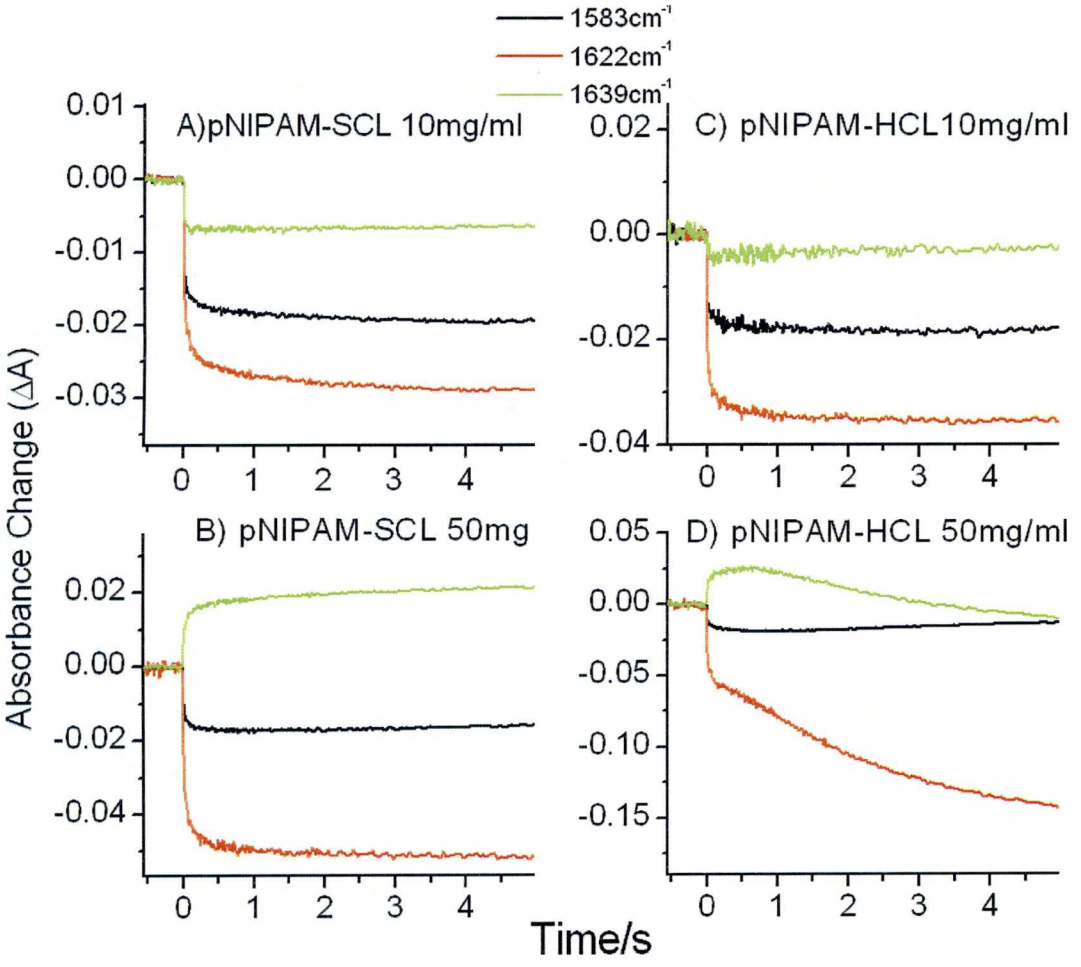

Figure 4.9 Time dependent absorbance changes after an 8 K jump from 32°C on pNIPAM-SCL and pNIPAM-HCL at different concentrations. A-D: Meas 12-15 in table 4.1.

This corresponds to an R_g of 5.2 nm for pNIPAM-MCL-1, which is comparable to the average polymer separation of 5.6 nm at 40 mg/ml (based on a calculation of solute separation by Phillips *et al*[131]), suggesting that the individual polymers are just beginning to overlap at this concentration. It seems, therefore that this phenomenon is closely linked with the overlap concentration. A possible interpretation for this will be discussed later (section 4.4). Note that in the pNIPAM-SCL measurement at 50 mg/ml there is no polymer loss, which indicates that the SCL polymers do not overlap at this concentration.

4.3.5 Measurements on the >100 s Timescale

The results of the long timescale measurements described in chapter 2.5.2 are shown in figure 4.10. Measurements on this timescale were performed by equilibrating the temperature of the sample at 32°C using a water bath. After

recording the absorbance at this temperature with the IR probe laser for 10 seconds, the temperature on the waterbath was increased to 40°C, while the absorbance changes were observed over time.

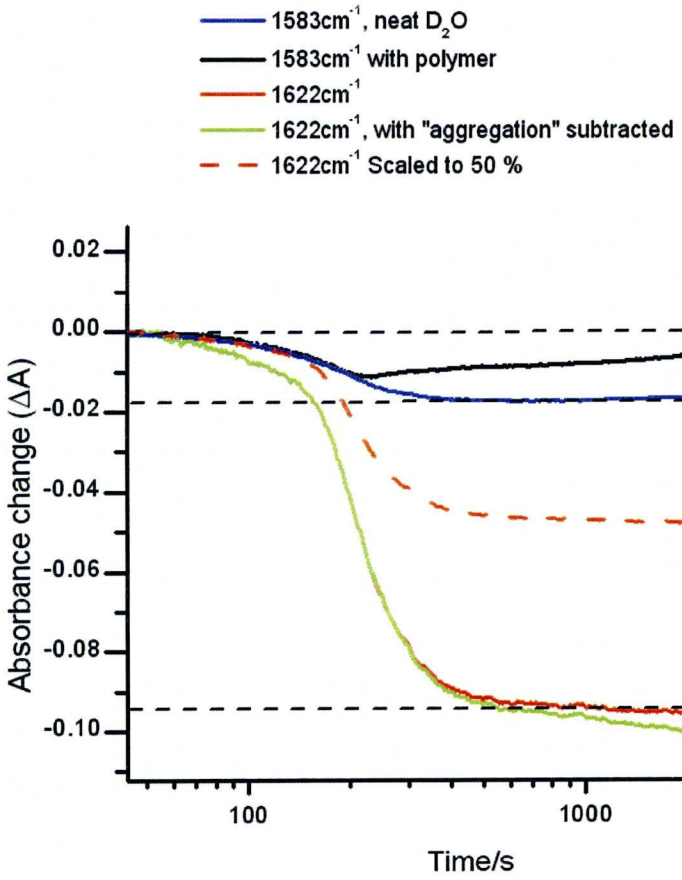

Figure 4.10 Time dependent absorbance changes on the 100-5000 s timescale for a 50 mg/ml sample of pNIPAM SCL (Meas 16, table 4.1) after an 8 K Tjump from 32°C: Black line: 1583 cm^{-1}; red line: 1622 cm^{-1}; green line: 1622 cm^{-1} with the "aggregation function" subtracted (see text); red dashed line: 1622 cm^{-1}, scaled by 0.5 (note overlap of initial phase); blue line: 1583 cm^{-1} measurement on neat D_2O after an 8 K Tjump from 32°C.

Figure 4.10 shows water bath "Tjumps" performed on a 50 mg/ml sample of pNIPAM-SCL (Meas 16), compared with a Tjump measurement performed on neat D_2O. Figure 4.9 shows that this sample is below the overlap concentration and thus was free of any overlap effects. The temperature change of the sample over time can be followed by observing the 1583 cm^{-1} absorbance, which shows noticeable initiation of sample heating at ~40 s and levels off at ~400 s in neat D_2O (blue line); the absorbance change levels off at 17 mOD, which is consistent with an 8 K temperature jump. The 1583 cm^{-1} absorbance change in the 50 mg/ml pNIPAM SCL sample (black line) initially follows the absorbance change in neat D_2O almost exactly. However, at ~210 seconds (when the sample has reached ~37°C) one observes a

remarkable divergence in the time dependence. In the polymer sample, there is an anomalous increase in apparent absorbance that cannot arise from polymer changes due to the probe frequency being outside of the amide I' band, but must be ascribed to aggregation, see below.

The 1622 cm^{-1} absorbance change of the polymer (70 mOD after D_2O absorbance is subtracted) is much larger than the absorbance change seen at 1583 cm^{-1} due to the high concentration of the polymer. Comparing this measurement to Meas 13, figure 4.9B (for the same sample, concentration and Tjump), one sees that on the 100 ms-5 s time scale, the 1622 cm^{-1} polymer absorbance change is only ~35 mOD, half of what is expected for the complete transition and half that observed in the water bath measurement Meas 16, figure 4.10. The absorbance change in the water bath measurement is what is expected for the *complete transition* from steady state FTIR difference spectra for similar conditions. This is an important observation, since it indicates that the phase transition is completed at the end of the water bath "Tjump" rise time.

Scaling the 1622 cm^{-1} absorbance change by 50% (figure 4.11, red dashed line) shows that there is an initial component that coincides with the D_2O absorbance/ temperature changes. This component is essentially "instantaneous", as there is no time lag between temperature increases (seen 1583 cm^{-1} ΔA in neat D_2O) and the polymer absorbance changes. The component can be assigned to the D_2O absorbance change at 1622 cm^{-1} due to heating and the instantaneous absorbance change of the polymer seen on shorter time scales. The rest of the polymer absorbance change is slower, indicating slower dynamics.

Scaling the 1622 cm^{-1} absorbance change to coincide with those at 1583 cm^{-1} in neat D_2O (figure 4.11, main, red and blue lines) provides more insight into the phenomenon; the 1622 cm^{-1} absorbance change lags noticeably behind what is expected for a simple temperature increase. The lag is approximately 60 s, which is a strong indication that the polymer phase transition is complete within 100 s. Meas 13 (figure 4.9B) precludes the phase transition occurring before 5s, therefore, we can state that the polymer transition is happening on the 10-100 s time-scale. As this sample is below the overlap concentration, what we see is the initial coil-globule process in single polymer chains without the interference of overlap effects.

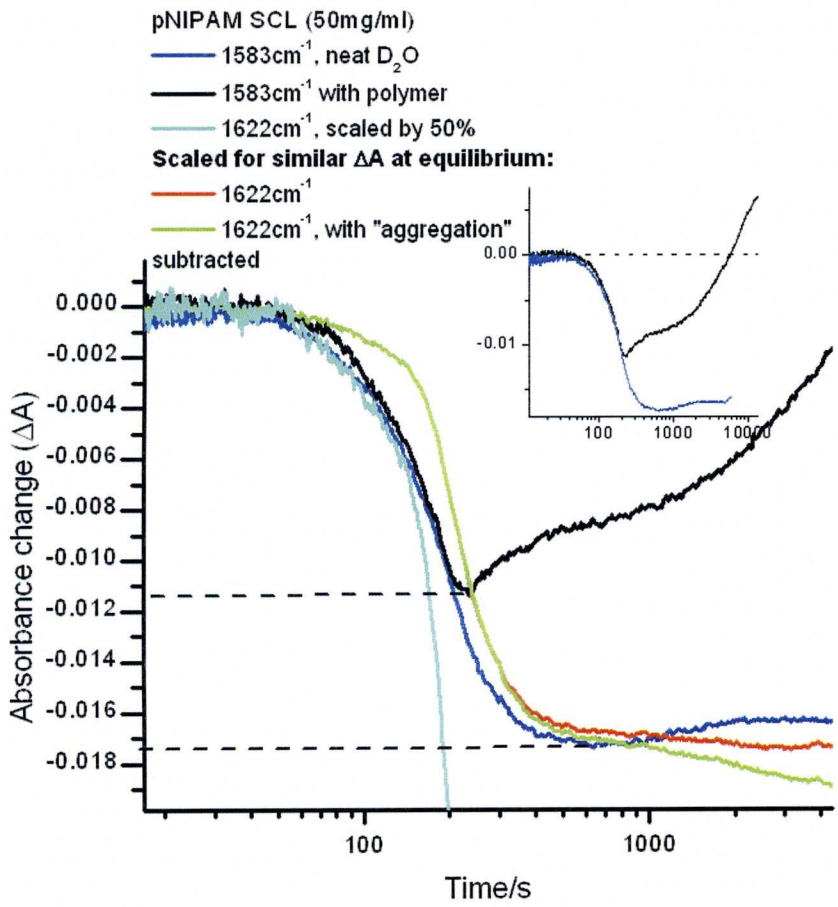

Figure 4.11 A comparison of 1583 cm^{-1} and scaled 1622 cm^{-1} absorbance changes in a water bath Tjump measurement at long timescales (Meas 16, table 4.1). **Main**: Dark blue line shows the 1583 cm^{-1} ΔA in neat D_2O, all other lines are from Meas 16, on a 50 mg/ml pNIPAM–SCL sample. The 1622 cm^{-1} curves were scaled to allow an easy comparison of ΔA at a polymer sensitive wavelength (1622 cm^{-1}) with the 1583 cm^{-1} ΔA of D_2O in the sample (black line) and neat D_2O (blue line). Red line: ΔA at 1622 cm^{-1}, scaled to allow easy comparison with ΔA at 1583 cm^{-1}; green line: ΔA at 1622 cm^{-1}, scaled and corrected for apparent increase in absorbance seen in the sample 1583 cm^{-1} measurement; cyan line: ΔA at 1622 cm^{-1}, scaled by 50%. **Inset**: same results on the 100-14000 s timescale, showing increased light scatter in polymer sample when compared with measurement on neat D_2O. Dashed lines are drawn to guide the eye.

Figure 4.11 (inset) shows the 1583 cm^{-1} absorbance change in the pNIPAM SCL sample compared with that of neat D_2O. Initially, both measurements follow almost identical time dependence due to the slow equilibration of temperature of the cell with the water bath. However, after 200 s (~5 K temperature increase), there is a sharp increase in apparent absorbance at 1583 cm^{-1} in the sample which is not seen in neat D_2O, which can be assigned to aggregation (FTIR time-course experiments show that precipitation only occurs on the order of 20 hours, see figure 3.12). Although aggregation is first seen in this experiment at 37°C, this is not in conflict with steady-state UV-vis results (chapter 3) showing that light scattering due to aggregation is induced at 33-34°C, but indicates from the delayed formation of aggregates. It takes

~100 s to form the first aggregates large enough to induce scattering at IR wavelengths. After 450 s, (7.5 minutes) the 8 K temperature increase is completed. The initial "fast" increase in apparent absorbance change seems to level off at this point. However, aggregation continues, as evidenced by the continuing increase in light scatter seen after the temperature equilibrates. This process is very slow, and continues after the measurement was stopped at 4500 s due to the loss of infrared detector coolant.

The 1622 cm^{-1} absorbance shows less apparent change than the 1583 cm^{-1} absorbance after the rise time (figures 4.10 and 4.11, red line). It is unlikely that the two wavelengths should experience different amounts of scattering. It is therefore likely that the increased scattering is counteracted by a continuing decrease in absorbance at 1622 cm^{-1}, which indicates the hydration structure continues to change. To give some idea of the 1622 cm^{-1} absorbance change without the influence of scatter, the scattering behaviour in the 1583 cm^{-1} trace was subtracted from the 1622 cm^{-1} absorbance (green line, figures 4.10 and 4.11). The apparent absorbance changes observed at 1583 cm^{-1} occur on a similar timescale to the slow absorbance changes in FTIR time course measurements (figure 3.12), in which a slow exchange between the 1625 cm^{-1} and 1610 cm^{-1} bands is observed, which we have assigned to a slow increase in aggregate sizes. These apparent absorbance changes are therefore consistent with the slow aggregation stage in the phase transition.

Figure 4.12 shows a water bath temperature "Tjump" measurement on another sample (pNIPAM MCL-1) for the same temperature jump. This sample is at 10 mg/ml, which again excludes overlap effects and allows the transition of single chains into globules to be observed. The total absorbance change at 1622 cm^{-1} in this measurement is 30.2 mOD after the temperature rise, while the absorbance change at 1583 cm^{-1} is only 20.7 mOD. In comparison, measurements on the 0.1-5 s time scale on the same sample, at the same concentration and temperature jump (figure 4.8A) show absorbance changes of 25 mOD at 1622 cm^{-1} and 19 at 1583 cm^{-1}. Thus, on the 100 ms- timescale, one sees almost twice the polymer signal, and indeed the observed absorbance change is the value expected for completion of the phase transition dynamics. Again, after scaling one sees that the 1622 cm^{-1} ΔA rise is shifted by ~30 s when compared to the 1583 cm^{-1} ΔA. This is a significant result that again indicates that the 1622 cm^{-1} ΔA (and therefore phase transition dynamics) is complete on the 10-100 s timescale.

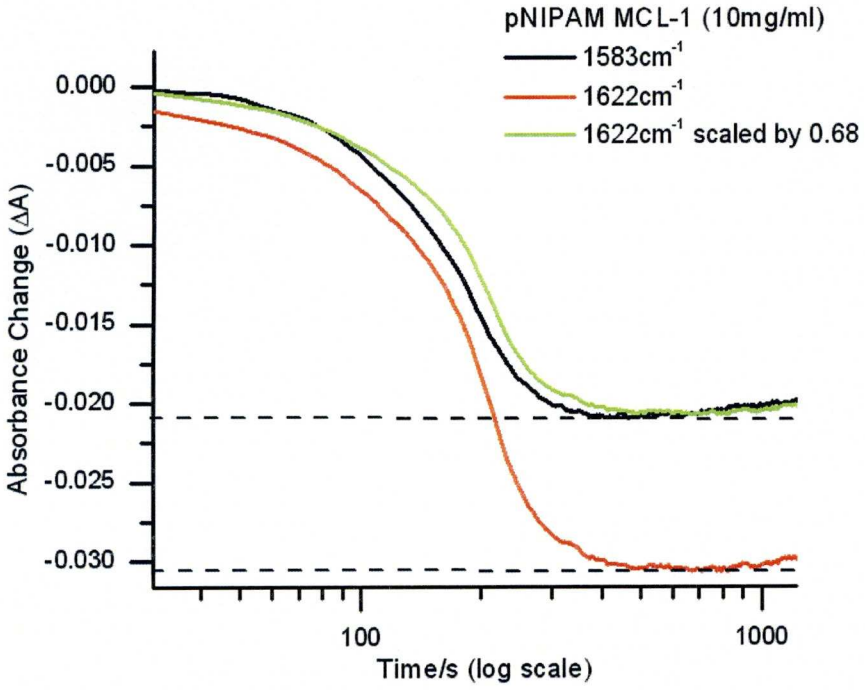

Figure 4.12 Time dependent absorbance changes on the 100-2000 s timescale for a 10 mg/ml sample of pNIPAM MCL-1 (Meas 17, table 4.1) after an 8 K Tjump from 32°C. Black line: 1583 cm^{-1}; red line: 1622 cm^{-1}; green line: 1622 cm^{-1} scaled to the 1583 cm^{-1} ΔA.

After 500 s, a small increase in absorbance at both wavelengths becomes apparent. This effect is similar to the increase in apparent 1583 cm^{-1} absorbance in pNIPAM SCL measurements (figure 4.11 inset), however, it is much less prominent and increases more slowly, which indicates that the size of aggregates is dependent on concentration, as one would expect. A more concentrated solution (like that of pNIPAM SCL in figure 4.11) has more chains in closer proximity. Therefore aggregates can form more quickly due to the smaller distances the globules must travel, and the increased number of globules available for aggregation.

4.4 Discussion

4.4.1 Discussion of Results

Local Collapse of the Polymer Backbone

The temperature jump measurements above show evidence for the fact that single chain pNIPAM polymers show a two stage dynamic process.

Figure 4.5 shows that the initial change of absorbance (within ns of increasing the temperature) can be explained by the temperature dependent shifts of the spectral parameters, *and* the linear shift in the relative area of the 1625 cm^{-1} and 1610 cm^{-1} amide I' sub-bands (fig 3.7). It can be inferred that the initial absorbance change is due to the same phenomenon that causes the pre-LCST band population shift. Steady state temperature dependent IR measurements in chapter 3, and the decreasing radius of gyration below the LCST seen by Wang *et al*[123] give a good indication that this process is due to the contraction of the coil, by an increase in the number and/or size of locally collapsed polymer sections, also see Fig. 3.14. This process changes the hydration structure by trapping water molecules that are already bound to the polymer chain. Since this is a local structural change, which also does not seem to involve a major change in hydrogen bonding, it is not suprising that it is so fast.

Single Globule Collapse

The rest of the coil-globule transition takes many orders of magnitude longer to occur (figures. 4.6 onwards) than this initial collapse, and any sign of the slower transition is notably absent in measurements on lower concentration samples (figure 4.8) until after at least 5 seconds have elapsed. The remaining 50% of the absorbance change at 1622 cm^{-1} finally occurs on the 10-100 s timescale as seen in water bath "Tjump" measurements (figures 4.10-12). This time separation between the fast and slow phenomena suggests that they are completely different molecular processes. Since the slower absorbance change is equal to what we expect from steady state FTIR measurements for the remaining transition, we can conclude that here, we see the full pNIPAM phase transition.

The slower 1622 cm^{-1} absorbance changes and aggregation both occur on similar time scales. Therefore, at least initially it is difficult to distinguish between the coil-to-globule collapse and aggregation processes. Although there is no conclusive time separation between the coil-globule transition and initial aggregation, there is certainly an observable difference in the processes at the molecular level between the polymer dynamics seen at 1622 cm^{-1} and long timescale aggregation. This can be seen by the large change in 1622 cm^{-1} absorbance initially, which corresponds to a radical change in the hydration state. This occurs when both the coil-globule transition and initial aggregation processes are present. Later, aggregation is seen separately, however. Such aggregation has only a very minor impact on the hydration state, as

evidenced by a lack of significant further changes in the 1622 cm^{-1} absorbance. Thus, the "main transition" is seen on the initial 10-100 ms timescale. We therefore can resolve three distinct phases in the phase transition dynamics of single chains. First, a change that involves an increased number of locally collapsed sections of the polymer, in line with the "pearl necklace" model, on the <10 ns timescale, but not involving major hydrogen bond changes. The major coil-globule transition (collapsed of individual chains) then occurs on the 10-100 s timescale, which is followed by a slow gradual increase in the size of aggregates over time.

To observe the coil-globule transition, in more detail, one would need to induce a temperature jump rapidly (<100 ms) and then maintain stable conditions for >100 s, a time-window that falls between those offered by the Argon laser and water bath induced Tjump systems. The measurements using Argon laser-induced Tjumps are obscured by bubble formation after 5 seconds. It is intriguing that the onset of collapse and bubble formation coincide. Possibly, aggregates act as nuclei for the formation of such bubbles?

Aggregation of Globules

Figures 4.10-12 show the later stages of the collapse, namely the process of aggregation. The general behaviour trend, agrees well with long timescale observations of the FTIR spectrum in figure 3.12, in which the 1625 cm^{-1} band contribution decreases and the 1610 cm^{-1} band increases in a process that takes approximately 20hours. In both measurements, we see the majority of the transition occur in the first minutes, followed by a slow aggregation process that changes the hydration structure only slightly. This, combined with the increase in scatter, strengthens our earlier argument that the move towards "trapped" water molecules is largely because of an increase in the aggregate size, which results in carbonyl bonds on the surface of globules becoming buried in larger globules during the aggregation process. The increase observed in the 1583 cm^{-1} absorbance change in Meas 16 (figure 4.11, inset) is rather large when compared to the FTIR measurement (figure 3.12) since the concentration of the sample in Meas 16 is much higher than that of the sample used for the FTIR measurement. Meas 17 (10 mg/ml pNIPAM-MCL, figure 4.12) shows a much more gentle increase in light scatter, which is consistent with the FTIR timecourse measurement as concentrations are similar.

Collapse of Entangled Polymer Networks

Figure 4.8 shows that above a concentration threshold, an additional process occurs in our laser Tjump experiments, which involves a loss of sample from the probe volume that is fairly rapid compared to the single chain coil-globule transition (100 ms vs. 10 s timescales). The "odd" absorbance behaviour shown in argon laser pumped experiments for high concentration samples has, to our knowledge, never been observed before. The changes in absorbance (decreasing sharply at 1622 cm^{-1} and 1641 cm^{-1}, while increasing at 1583 cm^{-1}) can only be explained with a loss of polymer sample in the probe volume due to the polymer moving outwards from the centre as discussed in chapter 4.3.4. Heating the sample over the LCST essentially turns the solvent from a "good" solvent to a "poor" one. One interpretation is that the polymers are simply diffusing along the solvent "quality" gradient created by the Gaussian heat distribution of the laser pulse. However, the fact that this process is seen only above overlap concentrations (see chapter 4.3.4, figure 4.8) throws this interpretation into doubt. Higher sample concentrations result in an increased viscosity, thus increasing concentration would probably have the opposite effect if that was the main reason for the sample loss.

The overlap concentration, at which the radius of gyration of the coiled polymer exceeds the distance between polymer chains, is the key to this process. FTIR measurements at different concentrations (figure 3.8) show that pNIPAM MCL-1 at a higher concentration has different hydration properties above the LCST to the same polymer at low concentration. This phenomenon has been interpreted in terms of "anchor points", which are nodes of polymer intersection which act to bind multiple chains together during the collapse. We tentatively suggest that the same mechanism is at play in the dynamic results shown here. What one sees is the beginning of the phase transition, resulting in the collapse of the chains. However, as the chains are "anchored" by overlapping outside the small probe volume, these chains are pulled towards the periphery of the probe volume. The fact that the polymer absorbance *decreases* is probably a result of a net movement of chains outwards from the probe volume compared with those being pulled in by collapsing chains. This may be caused by the solvent "quality" gradient; pulling chains inwards would force them into an

environment where they are decreasingly soluble. Figure 4.11 shows a cartoon to illustrate this model.

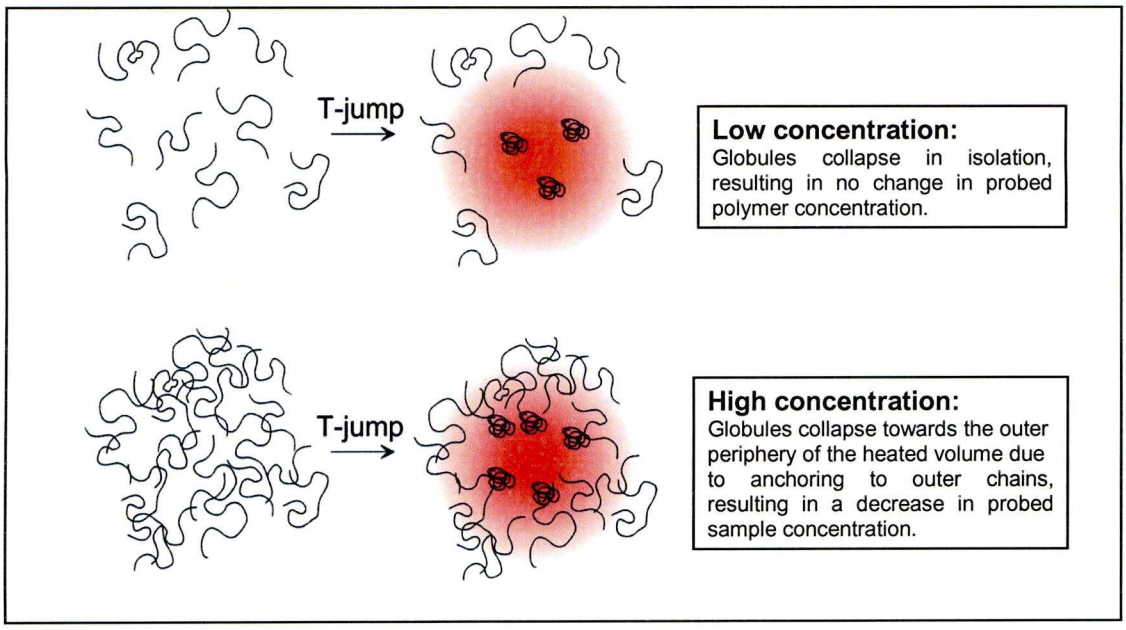

Figure 4.13 Cartoon showing a model for the interpretation of results seen in Argon laser pumped measurements (Meas 6-15 in table 4.1, figures 4.8-4.9) at high concentration.

4.4.2 Other Studies on Single Chain Transition Dynamics

There are few previous studies on the dynamics of the single chain pNIPAM phase transition with which to compare/contrast these results.[18,91,92]

NMR measurements by Yushmanov *et al*[18] probe the collapse by measuring the decrease in intensity of methyl group signals after heating the polymer. The methyl groups on the isopropyl side-chain in a "liquid-like" environment are resolvable from those in a more permanent immobile state (i.e. those on the inside of a collapsed globule). Therefore, the height of the methyl peak normalised to the pre-LCST signal gives a measure of the number of chains that are "trapped" inside the globule.

These measurements are too slow to resolve the actual dynamics, due to the heating process taking >1 s. Hence, no data is shown for the first 2-3 s. With standard pulse measurements, no further change is seen in the 0.1 wt% ~35'000 M_w pNIPAM samples with for 30 to 42°C Tjumps; however, 1% concentrations have a greater proportion of trapped methyl groups, which suggests a larger proportion of chains are held immobile inside globules at higher concentration, which therefore must be larger.

Further, although the majority of the transition is hidden due to the limited time resolution, the tail of the process is seen on the 4-5 s timescale; both observations point to additional processes in more concentrated solutions.

These NMR measurements[18] agree with our measurements. The dependence of the number of trapped methyl chains on concentration agrees with the concentration-dependent FTIR spectra, which show a higher proportion of carbonyls bonded to trapped water molecules above the LCST at higher concentrations, which would suggest larger aggregates (figure 3.8). The results also agree with the observation in the water bath Tjumped measurements of increased light scatter at high concentration (Meas 16; 50 mg pNIPAM SCL) compared with lower concentration (Meas 17; 10mg/ml pNIPAM MCL-1), figures 4.10-4.12.

The NMR results show de-wetting of the isopropyl groups to occur in different phases, partly too fast to be resolved (<3 s), partly on the timescale of a few seconds. These results are largely in agreement with our dynamic results (in which we see part of the transition to occur faster than 2 ns, with the remainder occurring on the time scale of 10 s), especially when considering that the two techniques are sensitive to changes in the solvation of different parts of the molecule. The two techniques therefore probe different aspects of the collapse. Any further discrepancy can be explained by the larger Tjump (30-42°C) in the NMR experiment and the inclusion of 0.1 M NaCl in their sample solutions, when solutions of 150 mM are known to alter the phase transition process by aiding the solvent reorganisation necessary to form hydrophobic bonds between neighbouring isopropyl groups, and depressing the LCST.

Tsuboi *et al*[91,92] have performed pump-probe Tjump experiments on single chain pNIPAM. In one of the experiments, attempts are made to probe the transition by examining the extinction of the fluorescence of an attached fluorescent group during the phase transition.[91] However, the attached group is extremely large, resulting in a complete change in the observed LCST and temperature dependence of the coil-globule transition; any conclusions drawn therefore are inapplicable to our system.

In other experiments, Tsuboi *et al* probe the coil-globule transition dynamics of pNIPAM with a 633 nm HeNe laser, in experiments similar to those shown in figure 4.7. They attempt to do so with temperature jumps utilising direct and indirect heating (the latter using heat transducers) by pulsed laser systems. The heat transducing experiments are replete with errors that cast serious doubt on the validity of the

experiment[92]. However, the results for the direct heating measurements appear reliable.

The temperature jump used is ~1-2 K followed by a recovery on the >200 ms timescale due to cooling (the use of a 1 mm pathlength, i.e. 20 times longer than that used in most of our experiments, will slow cooling by a factor of 400 compared to the ~1 ms cooling time observed in our results; the use of glass as a window material will slow cooling further). An instantaneous transmittance change is observed initially, which is ascribed to the formation of a thermal lens (we detect this in our HeNe measurements, see section 2.4.2). This is followed by a decrease in transmission on the 10 ms time scale, which is assigned to the formation of globules/aggregates, followed by a recovery on the 0.20-2 s timescale. It should be noted that the results presented[92] are at high concentrations (20-100 mg/ml), a longer pathlength (1 mm) and polymers with a much higher M_w than in our experiments

After the Tjump[92], the transmittance drops only to ~80% of the value after formation of the thermal lens before recovery sets in. UV-vis measurements in chapter 3.3 for 10 mg/ml samples and a 1 mm pathlength show that the transmittance expected after a Tjump by 2 K over the LCST (35°C) is ~15%. Scaling this by the concentration of Tsuboi's samples (20 mg/ml) shows that a transmittance of at most 8% is expected when the transition has gone to completion in their experiment. The measurements presented[92] therefore show only at most a tenth of the expected transmittance change, so the transition is far from complete before the sample begins to recover due to cooling. Thus, these results are heavily distorted by cooling, and the reported time constants do not reflect the time it takes for the transition to occur.

Comparison of these results with the measurements on the 0-5 s timescale using Ar-laser induced Tjumps (figure 4.8-4.9) also suggests that the recovery in transmittance may even result from the same "sample withdrawal" effect in higher concentration samples, since both effects occur on the same timescale[92]. Tsuboi presents measurements on samples with considerably larger chain lengths (the smallest had a M_w of 2'500'000, calculated from R_H = 46 nm, figure 3 of the reference[92], using the same $R_H(M_w)$ dependence they refer to[16], although the paper states that the largest polymer had a M_w of 10^6). At 20 mg/ml the polymers are separated by ~30 nm, indicating there is considerable overlap, thus indeed predicting a "sample loss" effect. As there is no characterisation of the temperature jump in Tsuboi's *et al*'s paper[92], there is no way to conclude which of these effects is occurring, or whether it is a

combination of both. In any case, we conclude that since Tsuboi *et al* only see a very small portion of the transition before cooling occurs, their results are unreliable.

We tentatively suggest from these observations that, in systems where chain overlapping/entanglement is present, there is no distinction between the formation of globules and aggregates. Instead one sees a single extended process. Additionally, the observation that with small chains, the "sample pulling" effect increases with concentration indicates that a greater overlap results in a faster collapse. Extrapolating this to Tsuboi *et al*'s results in which overlap is far more significant may explain why they see light scattering somewhat sooner.

pNIPAM solutions in which overlapping is prevalent therefore show different behaviour from isolated chain systems. Concentrating the sample results in greater deviation from single chain behaviour and results in a faster collapse. This supports the idea of the transition being altered by an overlap effect, where entanglement leads to a faster transition. In effect, the sample begins to take on the characteristics of a gel. A possible interpretation is that a high local concentration allows a more rapid collapse, as isolated chains have to fold back on themselves before collapse into a globule is possible. By this logic, gels, in which an extremely high local concentration is enforced by crosslinking, should have a much more rapid transition. We will see in the next chapter that this is the case.

4.5 Conclusions

We have observed absorbance changes in the amide I' region of pNIPAM following fast Tjumps on a variety of timescales from 50 ns-14000 s. We conclude that there are three distinct responses to a temperature jump over the LCST; 1) an instantaneous shift (<2 ns) consistent with a change in hydration due to an increase of the number and/or size of locally collapsed polymer sections; 2) the coil-globule transition of a single chain on the 10-100 s timescale; and 3) a slow aggregation process. This single chain collapse is only present in samples where chains do not overlap. The formation of larger globules is several orders of magnitude slower, and from extrapolating our results, would seem to conclude on the order of 20 hours which concurs with time course FTIR experiments (chapter 3). If overlapping is present, heating over the LCST results in a rapid cooperative collapse of the entangled polymer network.

CHAPTER 5: INVESTIGATION OF PNIPAM NANOPARTICLES

5.1 Introduction

Cross-linked pNIPAM gel provides a unique substrate that transforms the microscopic changes in hydration into a macroscopic change of volume in response to temperature or pH. Functionality is provided by the coil-globule phase transition, which causes a large decrease in volume and an ejection of water molecules and solutes from the core of the gel[11]. Thus, most applications to date have involved gels as either a matrix in which to load therapeutic agents and eject them later in response to an external stimuli or as a gateway in a device that allows controlled expulsion of such therapeutic agents[11]. Large macroscopic gels on the mm/cm scale often have collapse times on the order of seconds to hours[135]; however, gels used *in vivo* are more likely to be on the micro/nanometerscale[10,136].

Steady state measurements by Ahmed *et al*[56] offer some intriguing insights into the phase transition of such gels on the nm scale (NANOpNIPAM). Figure 5.1 shows the dramatic decrease in volume seen for these nanoparticles in response to a temperature increase, measured by dynamic light scattering methods (calculated from nanoparticle diameter results in Ahmed et al[56], figure 1).

The decrease in volume in response to temperature has the highest gradient around the LCST. The volume change levels off sharply at 40-45°C, indicating a limit has been reached in the ability of the nanoparticle to contract, due to the proximity of the monomer units being maximised and all unbound water being ejected (see section 5.3.1).

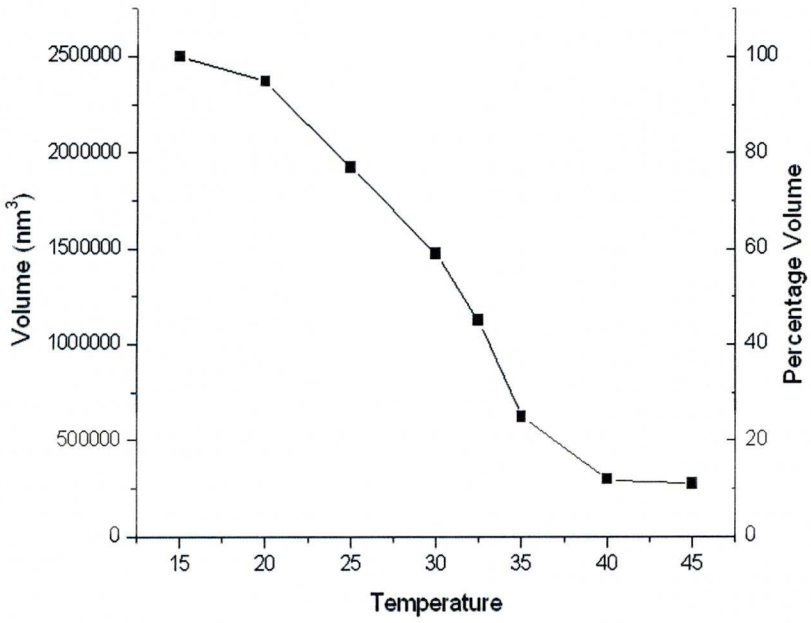

Figure 5.1 Result of the dynamic light scattering measurements of Nanoparticle diameter performed by Ahmed *et al*[56] ,converted into volume (left axis) and the percentage volume (right axis, compared to "fully expanded" nanoparticles at 15 °C). (temperature in °C)

Microgel collapse dynamics are expected to differ significantly from the single chain counterpart, due to the relatively high local concentration of pNIPAM chains and crosslinking found in a nanogel. Ahmed *et al*[56] measured the kinetics of pNIPAM nanogel collapse using UV resonance Raman pump-probe techniques and saw single exponential dynamics with a time constant of 360±90 ns for the phase transition after a 15 K Tjump encompassing the phase transition. Wang *et al*[5] performed similar experiments on microgels, probed with a HeNe laser at 632 nm after a 10 K Tjump, reporting an increase in light scatter, which they assign to a change in the index of refraction of the microgels upon collapse, and seeing a single exponential growth in light scattering with a time constant of of τ ~390 ns, after a 600 ns induction period. Reese *et al*[137] utilised similar kinetic turbidity measurements with nanogels and show apparent single exponential dynamics with a time constant of τ~120 ns. In this chapter we utilise our IR probed temperature jump setup and FTIR analysis techniques to examine the phase transition of nanogels identical to those studied by Ahmed *et al*[56] in order to further elucidate the mechanics of the transition of nanogels.

5.2 Experimental

5.2.1 Sample

NANOpNIPAM gels were kindly provided to us by Professer Asher, University of Pittsurgh, and had been synthesised in accordance with the procedures used by Ahmed *et al*[56]. Briefly, the nanoparticles were synthesised by dispersion polymerisation with copolymers with weight fractions of 86.8% of NIPAM (Aldrich, used after recrystallization), 1.5% of 2-acrylamido-2-methyl-1-propanesulfonic acid (ionic co-monomer, Aldrich), 4% of *N,N'*- methylenebisacrylamide (cross-linker, Fluka), 2.2% of sodium dodecyl sulfate (surfactant, Aldrich), and 5.5% g of ammonium persulfate (initiator, Sigma-Aldrich) See section 2.2.2 for details. The resulting nanoparticles are 145.5 nanometers in diameter (determined using by Brookhaven Instruments light scattering software).

Samples were provided in water and were transferred into D_2O by repeated dialysis. Concentrations of approximately 10 mg/ml were confirmed by comparison of FTIR spectra with those of single chain pNIPAM samples of similar concentrations. In all NANOpNIPAM Tjump experiments, AuNPs were used as heat transducers (with an approximate concentration of $1x10^{-6}$, 0.2-0.3 absorbance, depending on the requirements of the experiment). A UV-vis spectrum was taken before each measurement to check that the absorbance of the heat-transducing dyes (λ_{max} ~530 nm) is within reasonable limits (below 0.3) to give a homogeneous Tjump.

FTIR spectra of NANOpNIPAM samples were taken at ambient temperatures before and after all Tjump measurements, to confirm the concentration of the sample was ~10 mg/ml and to confirm that no significant permanent changes take place during the measurement which would indicate that the sample was damaged by taking the measurement or that the transition is not reversible.

5.2.2 Temperature Jump Measurements

Extensive dynamic measurements were performed on NANOpNIPAM using the Nd-YAG laser setup (See chapter 2, section 3 for details). Two major types of measurements were performed for the 200 ns-1 ms time window. The dynamics of the

					component measurements (Number of individual measurements)				
Name	Start temp (°C)	Final temp (°C)	Size of jump (°C)	Wavenumber /cm^{-1}	2 μs	40 μs	100 μs	2 ms	Sample conc (mg/ml)
High-signal-to-noise measurements									
meas 1	32	36.3	4.3	1622				20480	5.5
				1583				15360	
meas 2	32	35.1	3.1	1622		16762			9.2
				1583		11008			
meas 3	34	35.6	1.6	1622	25344	24704		16896	10.9
				1583	20480	17536		10240	
meas 4	34	37	3	1622	24576	19072			7/9.5
				1583	20480	14592			
meas 5	36	37.9	1.9	1622	24960	25600	24064		11.4
				1583	17792	18432	20480		
Variable wavelength measurements									
VWmeas 1	32	35	3	all wavelengths	5120	5120		5120	10.7
VWmeas 2	34	36.7	2.7	all wavelengths	5120	5120		5120	10.3

Table 5.1 Temperature jump measurements presented in this chapter. The final temperature jump is calculated as discussed in the text. All measurements are obtained in a temperature controlled cell with a 50 μm pathlength and CaF_2 windows. All samples are approximately 10 mg/ml (checked by the relative absorbance of the Amide I' band).

transition was studied with extremely high signal-to-noise by observing changes of the absorbance at 1622 cm^{-1}, where the highest absorbance change is observed (Figure 5.4). This was compared to the absorbance change at 1583 cm^{-1} to give a background measurement, since the polymer absorbance is minimal here. The dynamics of the individual component bands were studied by performing measurements in which the wavelength of the probe beam was varied incrementally throughout the amide I' band in order to obtain a picture of the how the amide I' sub-bands change dynamically in response to a temperature increase. Tjump experiments were performed with a variety of Tjump sizes and initial temperatures to further explore the mechanism of the transition. These measurements, combined with the steady state FTIR measurements, give new insight into the secondary structural changes of pNIPAM gels.

Due to the more gradual nature of the NANOpNIPAM transition (figure 5.1) compared to that seen in single chain pNIPAM, the problem of cavitation after larger temperature jumps made it impossible to cover the entire temperature region of the transition temperature in a single Tjump. Instead, the polymer kinetic response to

smaller jumps of 1-4 °C was measured, with different start temperatures , allowing the majority of the transition to be observed. Table 5.1 shows the temperature jumps performed on NANOpNIPAM that were of sufficiently good quality to be considered for analysis.

The time window of the measurements is limited by the cooling of the sample after the Tjump. A temperature drop by about 20% of the Tjump is observed after 400 μs, after which measurements are considered to be questionable due to the temperature dropping too far from the maximum reached in the Tjump (see chapter 2.3.1.6).

A large fraction of the dynamic changes occur rapidly, but the full transition takes place over many orders of magnitude in time. The limited number of time points observable in a single measurement (10000) therefore obscures earlier dynamics if viewing the entire available time window, making it necessary to view the transition on several different timescales for each temperature jump. We found that repeating a specific temperature jump experiment in time windows of 2 μs, 400 μs and 2 ms, each with approximately 25'000 individual measurements at 1622 and 1583 cm^{-1}, gave a complete picture with consistently excellent signal-to-noise.

Figure 5.2 shows how the individual measurements are combined to make the final curve. All measurements are averaged logarithmically to improve signal-to-noise (Chapter 2.3.5.3). Initially, measurements are shifted so at time zero the rapid bleach associated with the instantaneous absorbance change is half-way completed, thus correcting for the shifting of the trigger time due to variations in the amount of scattered light picked up by the triggering detector. As most of the reproducible artefacts associated with the temperature jump setup occur in the first two microseconds, only the shortest time window measurement is corrected for pressure relief and electronic overshoot (chapter 2.3.6). All measurements are individually corrected for cooling, as described in chapter 2.3.6.1, then combined by scaling adjacent time window curves so they overlap and discarding short time scale data points for the long time scale measurements. Scaling factors were in the range of 0.9-1.1, any Tjumps further than 10% from the target temperature were discarded.

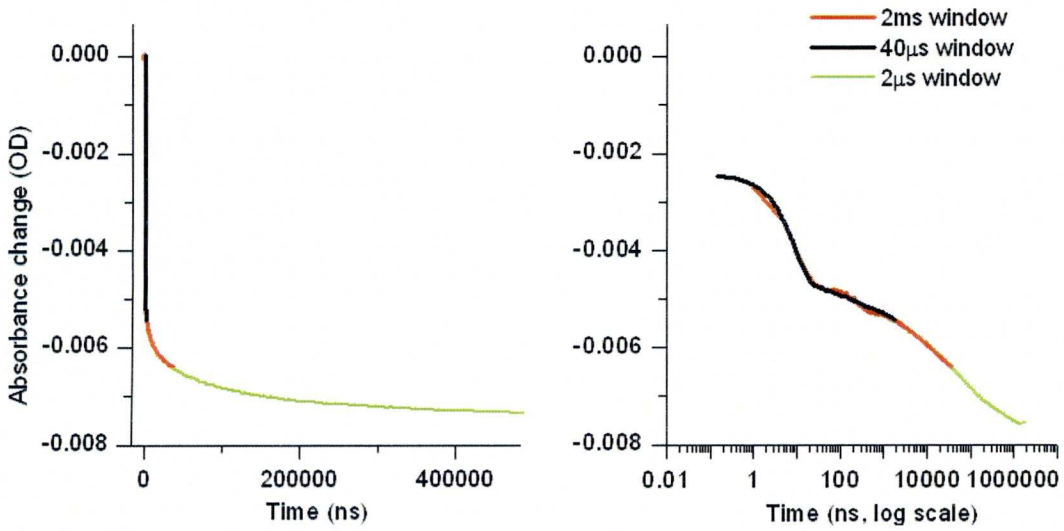

Figure 5.2 The components of Tjump measurement "meas 3", Tjumps on NANOpNIPAM from 34 to 35.6°C, (see table 5.1 for details). Note only the 2μs data have been pressure and overshoot corrected (See chapter 2.3.6), as these artefacts were completed before 2 μs and the other curves contributed only at later times to the combined curve. All component curves are cooling corrected with the relevant cooling correction for the specific time window.

5.2.3 Determination of Temperature Jump Size

Figure 5.3 shows a typical temperature jump measurement. The absorbance change are made up of three components:

1. D_2O absorbance change. This is highly reproducible, instantaneous within our time resolution and relates directly to the temperature jump.
2. Instantaneous polymer component. This extremely fast absorbance change also occurs within our time resolution and is not directly related to a change in secondary structure, but is instead attributed to temperature dependent shifts in the sub-band positions (chapter 5.3), and widths. This effect is largely due to a change in the vibrational behaviour of carbonyls which are hydrogen bonded to D_2O. The nature of the hydrogen bond changes with temperature, which affects the strength of the carbonyl bond, thus shifting its vibrational frequency. Such fast absorbance changes of the amide I' band following a Tjump have previously been reported for peptides and proteins[84,138].
3. Slow (resolved) polymer component. This directly relates information about the dynamic secondary structural changes.

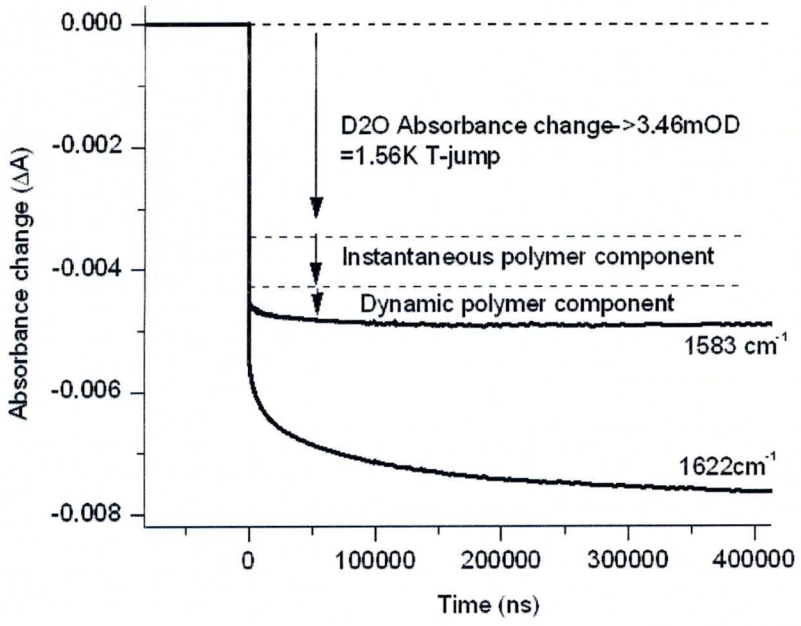

Figure 5.3 Time dependant absorbance changes in temperature jump measurement "meas 3" on NANOpNIPAM after a 1.6 K jump from 34°C. Dashed lines show the approximate individual contributions to the total absorbance change at 1583 cm^{-1}.

The size of the Tjump is measured at 1583 cm^{-1}, (chapter 2.2.6), which is located in the tail of the amide I' band (figure 5.4). Unlike single chain pNIPAM variants, NANOpNIPAM samples show a small absorbance change at 1583 cm^{-1} with a change in temperature. This can also be seen by the visible dynamics in figure 5.3 This reduces the validity of this measurement as a gauge for the size of the temperature jump. To take this into account, the temperature-induced absorbance changes at 1583 cm^{-1} at equilibrium were determined from steady state FTIR spectra, figure 5.4.

These equilibrium absorbance changes correspond to the maximum absorbance change of the polymer after a Tjump (i.e. both the instantaneous and slow components). The D_2O absorbance changes per degree ($\Delta A_{D_2O}/^{\circ}C$) have been thoroughly characterised (Chapter 2.3.5.3) for this wavelength. Unlike $\Delta A_{D_2O}/^{\circ}C$ at 1583 cm^{-1}, the polymer absorbance change with temperature ($\Delta A_{polymer}/^{\circ}C$) is not linear. However, the size of the Tjump compared to the size of the transition region is small enough to allow an estimate of the polymer absorbance change per degree from the local gradient (e.g. for Tjumps from 34°C to 35°C, the absorbance change is 1.35 mOD per °C). The total absorbance change at 1583 cm^{-1} after a Tjump is measured from ΔA at long time scales. This is then divided by the sum of $\Delta A_{D_2O}/^{\circ}C$ and the estimated $\Delta A_{polymer}/^{\circ}C$ to give the size of the temperature jump.

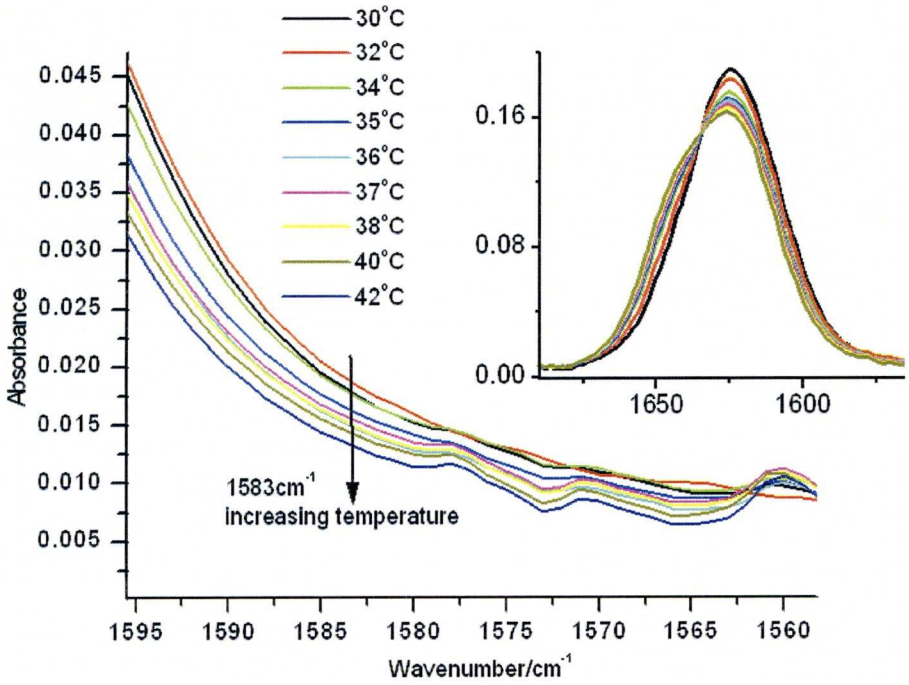

Figure 5.4 (Main): Temperature dependent absorbance of a 10 mg/ml sample of NANOpNIPAM, (50 μm pathlength), in the 1583 cm^{-1} region at temperatures from 30-42°C (Inset): The entire amide I' band for comparative purposes. The largest change in absorbance is found between 34 and 35°C.

5.2.4 Measurement Procedure

High Signal-to-Noise Measurements Procedure

After preparing a sample and taking the FTIR and UV-vis spectra, the sample was mounted in the temperature jump apparatus and allowed to equilibrate for 10 minutes at the required start temperature. The IR laser was first tuned to 1583 cm^{-1}, and the energy of the Nd-YAG laser was adjusted for the desired Tjump, measured by observing the change in absorbance at 1583 cm^{-1} (see chapter 2.2.6). Each high signal-to-noise measurement was the average of 10 sets of 20x128 measurements at 1622 cm^{-1} to measure the polymer kinetics, and the sample was moved after every 5x128 measurements. Between the sets taken at 1622 cm^{-1}, a set of 10x128 measurements at 1583 cm^{-1} was taken to give a background measurement with which to compare the polymer signal, and to readjust the size of the temperature jump to correct for slight variation in pump energy/ heat transducer absorbance. Separate Tjump experiments in time-windows of 2 μs, 40/100 μs and 2 ms were recorded. Data were transferred from the oscilloscope to a computer using a custom made computer program that converts

the signal data into absorbance changes as the experiment progressed so that anomalous measurements could be discarded and repeated. To obtain the high signal to noise curves shown in this chapter, all individual curves were averaged.

Variable Wavelength Measurements Procedure

The same procedure for characterising the sample and obtaining the correct Tjump as for high-signal-to-noise measurements was followed. Once the correct Tjump has been obtained, a set of 10x512 individual measurements in each time-window (2 μs, 40 μs and 2 ms) was recorded at 1583 cm^{-1}. The probe laser was then adjusted to a higher wavenumber within the amide I' envelope and 10x512 sets of measurements were recorded; the sample was moved after every 2x512 measurements. The IR laser was then retuned to 1583 cm^{-1} and the pump laser power readjusted to compensate for any variation in pump/energy/heat transducer absorbance. The above procedure was repeated for all time-windows at every good IR mode available in the Amide I' band (in a randomised order to eliminate any slow drift).

5.2.5 Dynamic Measurement Analysis

The absorbance changes at 1622 cm^{-1} were chosen to analyse the polymer dynamics in detail, as this is the portion of the amide I' band at which the largest absorbance changes take place, thus it is most sensitive to changes in secondary structure. By fitting this signal, one can analyse the dynamics of the transition. Attempts to fit the transition with a standard exponential decay function for any of the temperature jumps measured resulted in very poor fits, indicating that the transition is not a simple two-state process. A stretched exponential decay was used instead, which obtained good fits. The stretched exponential decay uses the following equation:

$$f(t) = A \times e^{-(kt)^{\beta}} + offset \qquad 5.1$$

β measures deviations from ideal exponential behaviour, and the value of β is an indication of how stretched the dynamic relaxation behaviour is. From β and k, it is possible to calculate the average time (<τ>) of the relaxation with the following equation:

$$< \tau >= \frac{\Gamma(1/\beta)}{k\beta} \qquad 5.2$$

5.3 Steady State FTIR Measurements

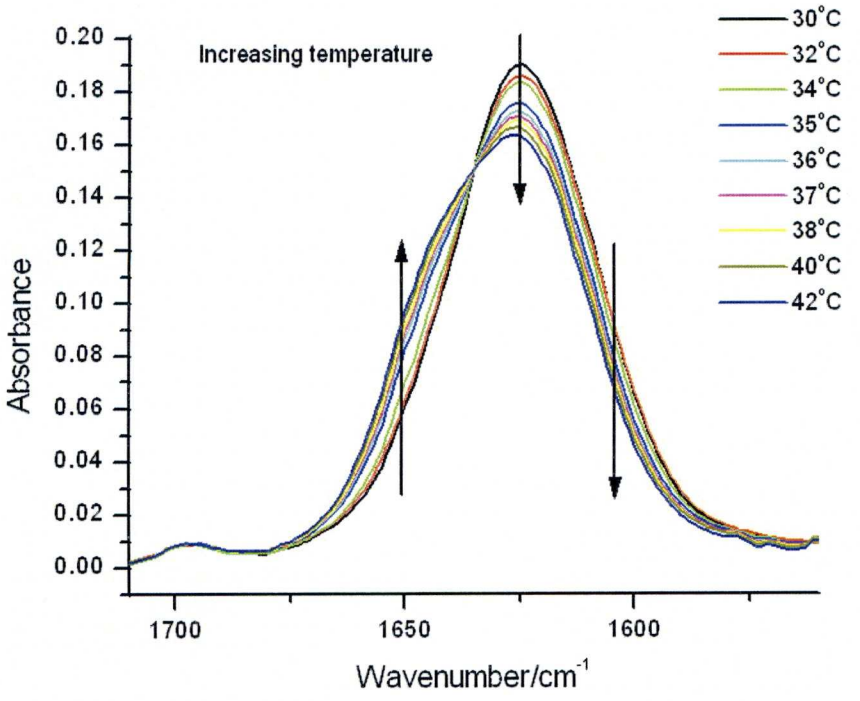

Figure 5.5 Amide I' absorbance spectra of NANOpNIPAM nanoparticles (10 mg/ml in D_2O, 50 μm pathlength) at temperatures around the LCST. Each spectrum is corrected for D_2O background and atmospheric water vapour absorptions, and smoothed by adjacent averaging..

To elucidate the changes in the NANOpNIPAM nanoparticle solvation, we used the same approach as for single chain pNIPAM (see chapter 3.4), by observing changes in the amide I' band using temperature dependent FTIR spectroscopy. Figure 5.5 displays the amide I' band for the cross-linked gel polymer. The same decrease in absorbance at 1625 cm^{-1} upon heating with an increase at 1650 cm^{-1} is seen, in the NANOpNIPAM gel as can be observed in the single chain systems, see figure 3.5. However, a significant difference to the single chain amide I' behaviour is seen at 1610 cm^{-1}, where a large decrease in absorbance is seen for NANOpNIPAM, compared to an almost constant absorbance for single chain pNIPAM.

Further details can be extracted by analysing the substructure of the amide I' band with curve fitting methods (chapter 3.4.1). Figure 5.6 shows the best fit achieved using 3 pseudo-Voigt curves in the amide I' region, with band centre wavenumbers, widths and Gaussian/Lorentzian character linearly dependent on temperature. An additional band at 1695 cm^{-1} is assigned to the comonomer 2-acrylamido-2-methyl-1-

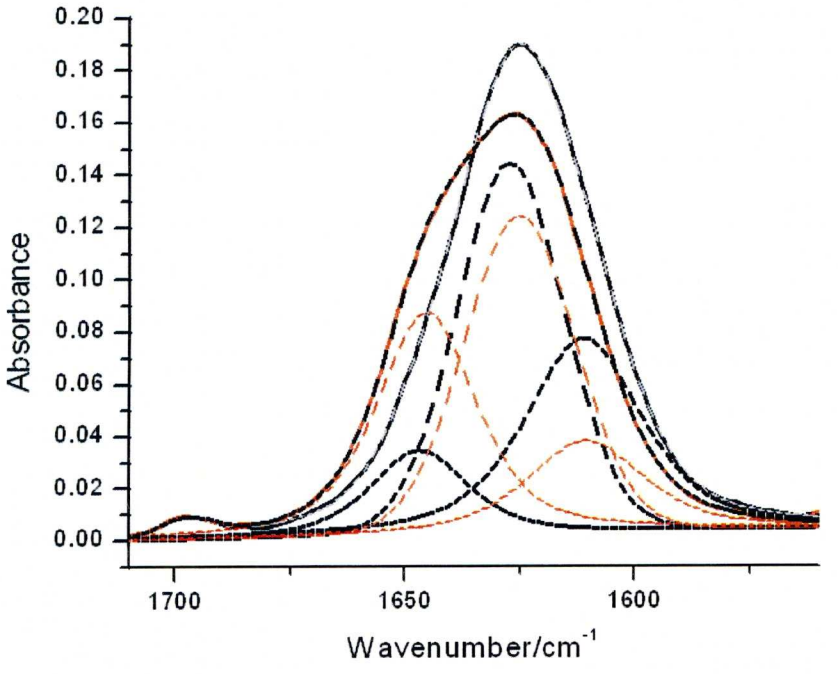

Figure 5.6. The amide I' envelope of NANOpNIPAM (see figure 5.5 for sample details), below (black lines, 30°C) and above (red lines, 42°C) the LCST. The dashed grey and black lines superimposed on the spectra show the fits. The smaller dashed black and dashed red lines show the component bands for the 30 and 42°C spectra, respectively.

propane sulfonic acid, but this peak is largely unaffected by temperature and is situated outside the amide I' envelope. It contributes less than 1% to the overall band area and is ignored in the analysis. Component-band areas are normalised by calculating the fraction of the *total* amide I' band area that each component band occupies, thus allowing for a comparison with the single chain pNIPAM polymers. Comparing these band areas with those of the "standard" single chain pNIPAM shows some remarkable differences that provide some insight into the gel phase transition, although due to the overlap of the component bands, the resulting relative areas are not expected to exactly reflect the population of the corresponding species in the sample. (Figure 5.7). The linear response to temperature of the individual bands below and above the LCST, the relative band areas and transition behaviour all differ dramatically in the NANOpNIPAM gel from any of the single chain samples.

By examining the component band behaviour, extracted by deconvoluting the amide I' envelope, and comparing to those seen in the single chain samples, one can begin to build up a picture of the secondary structure of the gels in water, and the changes that occur in response to heating.

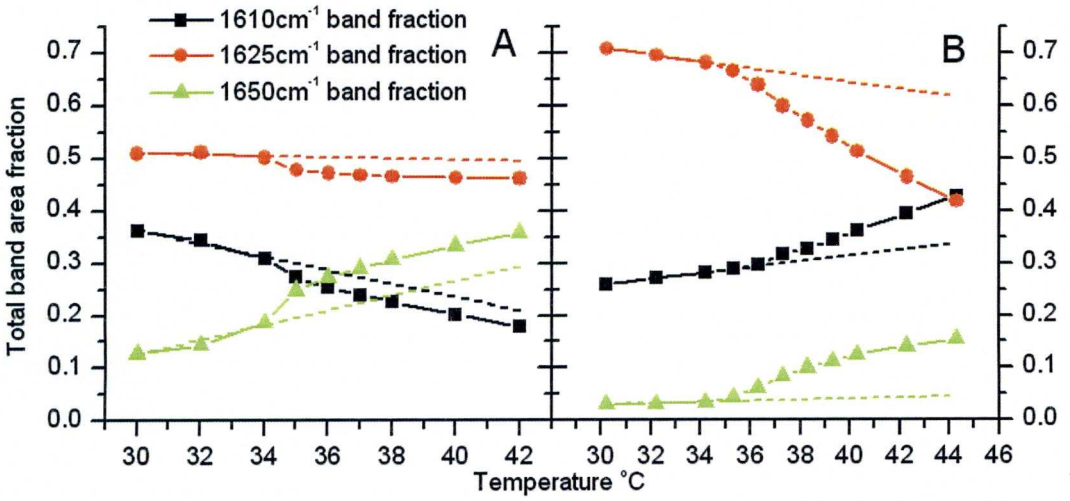

Figure 5.7: Comparison of the component areas of (A) NANOpNIPAM gels and (B) single chain pNIPAM MCL-1 (figure 3.7), both at 10 mg/ml concentration. The markers show the area fraction of each sub-band and the dashed lines show the linear behaviour of the areas below the LCST, extrapolated to higher temperatures.

Unlike the single chains, the gel polymer is anchored via a crosslinking comonomer (on average one for 12 NIPAM monomer units). This inevitably hinders the polymer's movement in solution and its freedom to find its optimum configuration based purely on the solution properties. Even in a good solvent (i.e. water below the LCST), the polymer is constrained from moving freely as a random coil. The backbone is forced into far closer proximity with other parts of the backbone due to anchoring at copolymer crosslinkers and the interweaving of chains which one would expect in a randomly formed cross-linked gel. This is reflected in the balance of component band areas that are seen below the LCST:

As discussed in detail in chapter 3, the 1650 cm^{-1} band area fraction is related to the number of amino-carbonyl hydrogen bonds, which can only occur when neighbouring chains are close enough to interact, or when a single chain folds back on itself. In a free chain in a good solvent, such interactions will be rare due to the backbone being diffusely spread out in solution (random coil), and such intramolecular bonds will be transient in nature. This is reflected in the low fractional area of the 1650 cm^{-1} amide I' component observed below the LCST for single chain pNIPAM. In contrast, the 1650 cm^{-1} band fraction in NANOpNIPAM is comparatively high, even at low temperatures. This indicates the increased amount of amide groups in close proximity, held in position by the anchoring effect of the comonomers. The amount of intramolecular hydrogen bonds increases even below the LCST in the nanoparticles, which is due to the decreasing volume (figure 5.1)[56] which increases the probability

that a favourable amide-amide hydrogen bond is formed. Complete H/D exchange of the amide N-H occurs in fully collapsed nanoparticles within 5 minutes, which indicates that these bonds are not highly stable[56].

The 1610 cm^{-1} and 1625 cm^{-1} band fractions represent carbonyl groups hydrogen bonded to water in a constrained environment (i.e. a water molecule separated from the bulk solvent and/or with its free rotation sterically hindered, or forming a bridge between adjacent chains) and free environment, respectively (see chapter 3). These band areas show a completely different temperature dependence in the two samples.

Firstly, the ratio of 1610 cm^{-1}:1625 cm^{-1} band is strongly altered on gelation. In single chain pNIPAM below the LCST, the ratio of carbonyls H-bonded with free water molecules to carbonyls H-bonded with constrained is 0.73:0.25 respectively, a larger value than in NANOpNIPAM gel (0.51:0.36). This gives some insight into the hydration of the two pNIPAM types. The presence of multiple carbonyl states in both types indicates that at all temperatures there are pockets of collapsed polymer present at temperatures below the LCST.

The single chain sample below the LCST exists as a random coil, and consequently hydration will to a large extent be maximised. Any trapping of water molecules will be transient and found in temporary locally collapsed polymer globules in the coil (in a pearl necklace type chain conformation[118], see chapter 3), and the majority of the 1610 cm^{-1} band below the LCST is likely to be due to single water molecules bridging two proximal amides or from two water molecules binding to the same carbonyl[79], which provides a stronger weakening effect on the carbonyl bond (discussed in detail in chapter 3).

The increase in 1610 cm^{-1} band area with temperature below the LCST was interpreted as a corresponding increase in the fraction of carbonyls hydrogen bonded to water molecules that are constrained, resulting from a gradual worsening of the solvent properties as a response to temperature. This causes an increase in the number and/or size of locally collapsed globules, and a gradual shrinking of the random coil's radius of gyration in response to the increasingly bad solvent. The fact this band does not change population as the nanoparticles collapse further confirms that carbonyls represented by this band are on the surface of the molecule.

The gel, on the other hand, is held in a loose lattice, with adjacent chains held in closer proximity, thus providing an environment where pockets of water molecules can

easily be cut off from the bulk solvent, or bridge easily to adjacent chains. Carbonyls H-bonded to constrained water molecules are found inside the nanoparticle. Carbonyls on the surface of the nanoparticle, on the other hand, will largely be bonded to water molecules in contact with the bulk solvent, so that the 1610:1625 cm^{-1} ratio of the fractional band areas for NANOpNIPAM particles should reflect the ratio of the numbers of carbonyls located internally (buried in the nanoparticle), and externally (i.e. on the surface, directed towards the solvent).

From the size of NANOpNIPAM particles (measured with dynamic light scattering[56]), figure 5.1, one can estimate the proportion of amide bonds on the surface, assuming a surface area of approximately 0.25 nm^2 for a single monomer. The number of monomers per nanoparticle ($2.40x10^6$)[56], and the approximate surface area of an extended nanoparticle (90000nm^2 if the nanoparticle is taken as a perfect sphere), suggest that only 15% of the monomers are on the surface. This disagrees with the relative population of the 1625 cm^{-1} band (figure 5.7), which implies that approximately 45% of the carbonyls are bonded to "free" or unconstrained water. The disparity between the two estimates suggests that the surface of the nanoparticle is far from perfectly spherical, and instead has a highly corrugated surface which increases the surface area. This is highly likely due to the random nature of the polymerisation/crosslinking process. One can also imagine that chains with a low degree of crosslinking on the surface will extend into solution below the LCST, further increasing the effective surface area (NMR measurements show that there is a decreased density of cross linking on the surface, with an increasing density as the core is approached [139]. As the gel nanoparticles collapse, the internal amides exchange population from the 1610 cm^{-1} (carbonyls double bonded to trapped water molecules) to the 1650 cm^{-1} band (intermolecular carbonyl bonding), which directly reflects the expulsion of D_2O.

When the temperature is increased over the LCST, a sudden step in the relative population of the carbonyl states is seen. This change does not follow the linear population behaviour observed below the LCST, indicating that something other than the simple decrease in volume (figure 5.1) is occurring. Instead, a change in hydration structure occurs, which takes place for the same reasons as the single chain pNIPAM phase transition, i.e. the entropic penalty for maintaining the ordered hydration sphere around the alkyl groups exceeds the enthalpy gained from forming hydrogen bonds between the amide groups and D_2O. The polymer reorientates to minimise contact of

the alkyl groups with water, which is ejected from the nanoparticle. This forms a largely dehydrated domain inside the nanoparticle, while the size of the nanoparticle decreases further.

From Ahmed *et al*'s[56] values, following an 88% reduction in the number of water molecules remaining inside the nanoparticle core after the phase transition occurs, $1.2x10^7$ water molecules remain. Compared to $2.4x10^6$ amide, there are only 5 H_2O molecules per monomer. Thus, there are still some water molecules present inside the nanoparticle, which is also evidenced by the number of carbonyls hydrogen bonded to constrained water molecules (1610 cm^{-1}). H/D exchange occurs within 5 minutes, which indicates that intrapolymer hydrogen bonding is not permanent and that the nanoparticle is still (fully) permeable to water.[56]

Upon phase transition, there is a noticeable increase in the 1650 cm^{-1} band, assigned to intramolecular amide-amide hydrogen bonds. This happens at the expense of both the 1610 cm^{-1} (carbonyls hydrogen bonded to trapped water molecules) and 1625 cm^{-1} bands (carbonyls bonded to unconstrained or bulk solvent), this indicates that both the surface and core pNIPAM environments undergo a phase transition, in which the secondary structure rearranges to limit alkyl-water interaction. The previous amide I' band behaviour indicates that this will involve an expulsion of water from the core chains of the nanoparticle. Possible interpretations for the decrease in the 1625 cm^{-1} band population are the local rearrangement of surface monomers to decrease water access to the alkyl groups. An additional contribution may be that single uncrosslinked "strands" protruding from the surface may undergo a phase transition similar to that seen in single chain polymer dynamics (see chapter 4)

Ahmed *et al* study the steady state behaviour of NANOpNIPAM with UV-resonance Raman spectroscopy[56] and see a similar increase in the absorbance of the 1650 cm^{-1} band, although they claim that the 1625 cm^{-1} and 1650 cm^{-1} are two different kinds of water bonded carbonyl (i.e., carbonyls bonded to two and one water molecules, respectively, an assignment which ignores the possibility of intramolecular H-bonding). This disagrees with our findings of 3 bands, and others who have studied the amide I' for single chain polymers[26], in which the band at 1650 cm^{-1} is assigned to the formation of intramolecular amide-amide hydrogen bonds. A likely reason for the disagreement is seen in the UVRR spectrum; the amide I band is situated on the shoulder of the amide II band, which in UVRR much more prominent than in IR (having at least 3 times higher absorbance and being located 100 cm^{-1} closer to the

amide I band due to the increased frequency of the N-H bend compared to the N-D bend), and the amide I and II overlap at ~1600 cm^{-1}. In deconvoluting the bands in the spectra presented[56], it would be extremely difficult to extract the 1600/1610 cm^{-1} band with the obstruction presented by the amide II band. Also, the use of water as a solvent affects the frequency of the amide I band; carbonyls H-bonded to water rather than D_2O should be shifted 5-10 cm^{-1} to higher wavenumbers. This is indeed the case for their ~1650 cm^{-1} band, which occurs at 1654 cm^{-1} compared to ours at 1647 cm^{-1}. The 1625 cm^{-1} bands are at similar frequency, which indicates their 1625 cm^{-1} band is actually a composite of the two bands. Further indication that our assignment is correct is presented in Ahmed's own results[56]. Figure 7 of this reference[56] compares the UVRR spectrum of both a dry nanoparticle sample and one at a temperature above the LCST in solution, and it is notable that a large absorbance is seen in the dry nanoparticle at ~1650 cm^{-1}, which can only be attributed to intermolecular amide-amide bonds or unbonded, isolated carbonyls. The same peak is seen at approximately the same wavenumber in the solvated nanoparticle. It is argued that for the solvated nanoparticle, intramolecular hydrogen bonding between adjacent monomers is rendered impossible due to steric hindrance, however, the presence of this band suggests that amide-amide bonding occurs between adjacent chains.

5.4 Dynamic Measurements

5.4.1 Temperature Jump Comparisons

Effect of Initial Temperature

Here, the effect of starting an Nd-YAG induced Tjump at different temperatures around the LCST while maintaining the size of the Tjump is analysed. The absorbance changes at 1622 cm^{-1} and 1583 cm^{-1} are measured after a Tjump is induced. For both wavelengths, the initial change in absorbance is due to D_2O, and at 1583 cm^{-1}, only minor absorbance changes occur later due to the tail of the amide I' band (see chapter 5.2.3). At 1622 cm^{-1}, a much larger decrease of absorbance is observed at later times, reflecting changes in hydration upon structural changes. The absorbance changes seen do not follow monoexponential behaviour, but extend over many orders of magnitude in time. We therefore use a stretched exponential fit to

analyse the dynamics; however, the fits are not so well defined, since the transition has not gone to completion in the available time-window. The fit values generated are therefore unreliable, but serve as a useful means of comparison.

Figures 5.8 and 5.9 show the comparison of two 1.6-1.9 K Tjumps starting at temperatures of 34 and 36°C, respectively. The Tjump from 34°C (meas 3) starts below the centre point of the phase-transition in D_2O at 34.5°C (see figure 5.7), and consequently the sample before the Tjump will contain NANOpNIPAM particles in a more hydrated and less collapsed state. For the Tjump from 36°C, the sample prior to heating contains particles which are mostly collapsed, as 36°C lies on the upper edge of the transition. Looking at the variations in volume associated with temperature

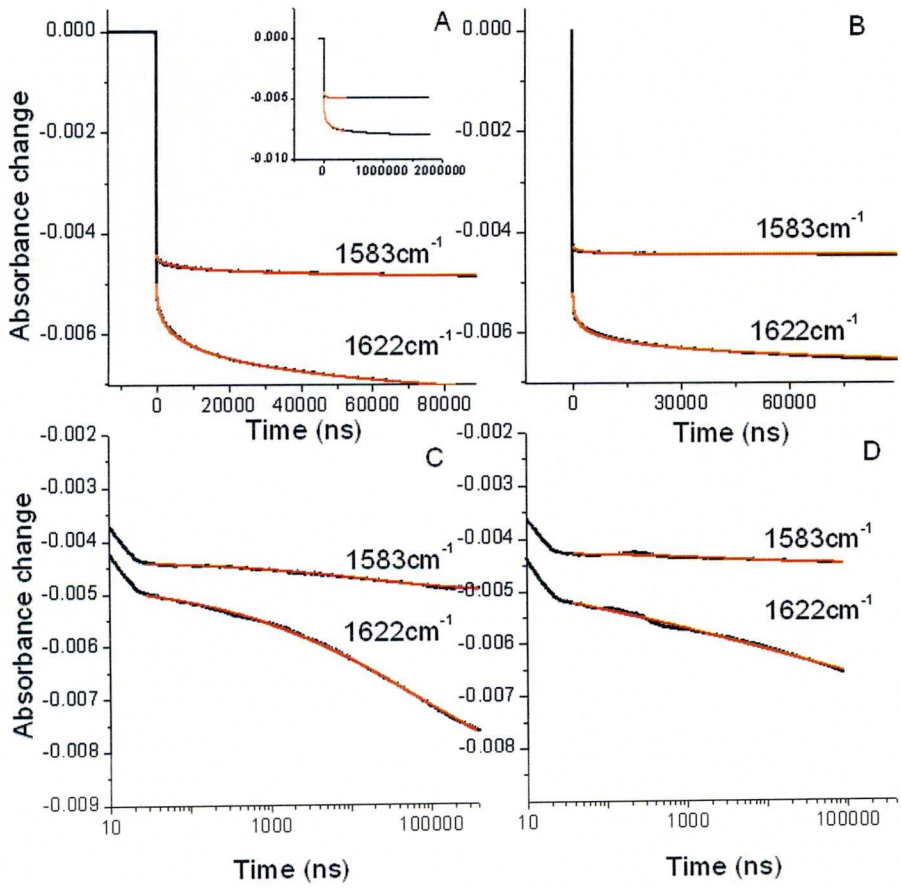

Figure 5.8 Absorbance changes of NANOpNIPAM (~10 mg/ml) after Tjumps of ~2 K at different start temperatures. Graphs A and C show "meas 3", using a Tjump from 34 to 35.6°C, graphs B and D show "meas 5", using a Tjump from 36 to 37.9°C (Table 5.1). Black lines are the measured signal, red lines show the stretched exponential fit with the parameters shown in table 5.2. A) (main) and B): linear timescale up to 100000 ns; A) (inset) linear timescale showing entire time range of 2 ms; C) and D): logarithmic timescale.

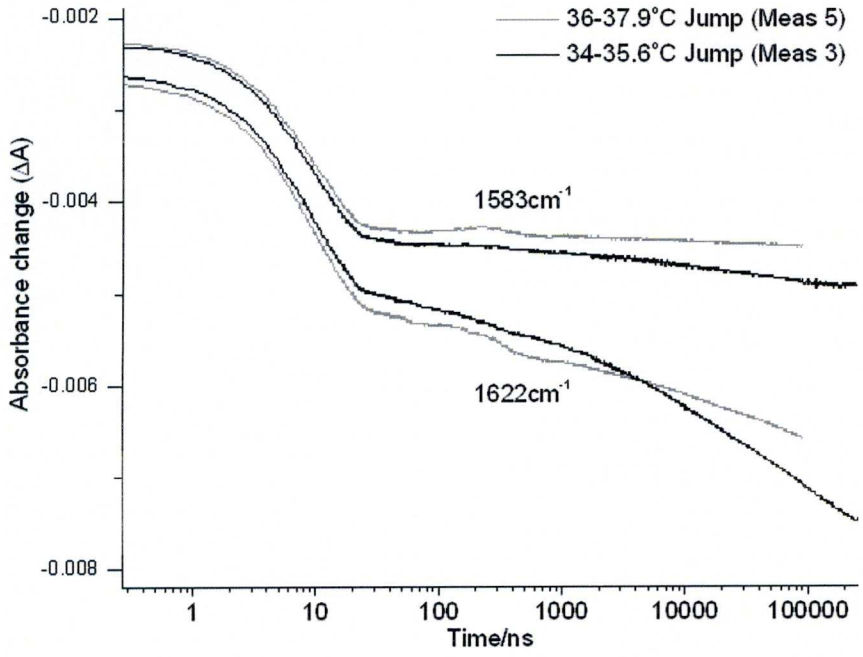

Figure 5.9 Direct comparison of the absorbance changes shown in figure 5.8 for NANOpNIPAM samples (~10mg/ml) after Tjumps of ~2 K at different start temperatures. Black lines: "meas 3", after a Tjump from 34 to 35.6°C; grey lines: "meas 5" after a Tjump from 36 to 37.9°C. See table 5.1 for sample/Tjump details.

changes (figure 5.1), one can see that between 32.5 and 35 °C the polymer volume is most sensitive to temperature, whereas above 35°C the volume change with temperature slows considerably as it reaches the point where the polymer cannot collapse any further (figure 5.1[56]). The two temperature jumps, therefore, span two phases of polymer collapse, and the differing dynamics seen reflect this.

At the higher temperature (meas 5), significantly less absorbance change is seen than at the lower temperature (meas 3), which is consistent with the total absorbance changes expected from the temperature-dependent FTIR spectra, (-0.011 for meas 3, -0.004 for meas 5; both values take into account sample concentration and size of the temperature jump; both values are in addition to the D_2O absorbance change of approx. -0.004). This is also intuitive, since at 36°C, the nanoparticle is already partly collapsed. Both measurements show large deviations from monoexponential behaviour (see table 5.2 for the fitting parameters obtained). It has to be noted that the amplitudes of the non-instantaneous dynamic component show the opposite behaviour to what is expected (A_{meas5} is larger than A_{meas3}, see table 5.2); this is a fit artefact, due to the stretched nature of the fitting and the fact that only the initial stages of the absorbance

changes are within the time window. The fit of meas 5 in particular is highly problematic, because the data are only available to 80 μs, some residual pressure relief occurs on the same time scale and the relaxation is clearly not finished. The amplitudes provided by the fits are therefore not to be trusted.

The β values provide an indication of the stretched nature of the fits and are more informative. The Tjump from 34°C (meas 3) has a β value of 0.29, whereas the Tjump from 36°C (meas 5) has a β value of 0.096, which indicates extremely stretched nonexponential dynamics.* Figure 5.9 also seems to indicate that the dynamics at higher temperature (meas 5) are slower than those at lower temperature (meas 3). If one considers that the amount of thermal energy available is greater at 36°C, one would expect a higher start temperature to speed up the transition. Instead the opposite seems to occur (see below for more results supporting this observation), so this effect must be linked to structural considerations (see chapter 5.5).

Figure 5.10 shows similar results for Tjumps by ~3 K, starting at 32 and 34°C, which give an even clearer indication of the effects observed. In this case, all measurements start below the LCST and jump to a temperature above it. Here, the greater deviation from monoexponential behaviour at higher start temperature is very obvious, already from a visual inspection from the data, and confirmed by the fit results. The curves also confirm that samples show slower absorbance changes when Tjumps begin at higher temperatures. Results obtained for the same starting temperature are remarkably consistent when concentration and slight deviations in the Tjump are accounted for, so the effect is reproducible for different samples.

For the Tjumps starting at 32°C, we expect a ΔA of -0.0139, and for the Tjumps starting at 34°C, a ΔA of -0.0141 (in addition to D_2O absorbance changes of ~0.006). The absorbance changes expected upon completion of the transition are therefore almost the same (this is to be expected, as both jumps cross the LCST); in contrast, the absorbance changes observed within the time window are smaller when starting at 34°C than when starting at 32°C. This indicates that measurements starting at 34°C show slower dynamics, which is also confirmed by visual inspection of the results (figure 5.10) and the fits (table 5.2).

* It has to be noted that fitting meas 5 with a fixed value of β=0.2 gives virtually the same fit quality, but a more reasonable smaller value for A (0.0025), which indicates that the fit parameters in table 5.2 for meas 5 are highly suspicious. On the other hand, fitting meas 5 with β=0.25 results in a bad fit. This suggests that meas 5 is indeed more stretched than meas 3 (β=0.29).

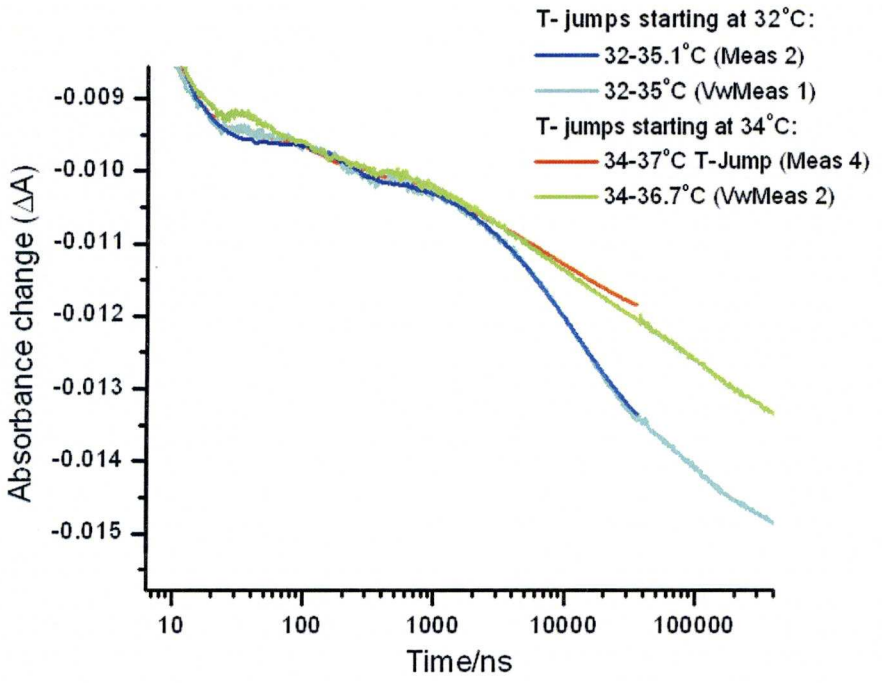

Figure 5.10 Absorbance changes of NANOpNIPAM (~10 mg/ml) at 1622 cm^{-1} for ~3K Tjumps. Blue line: "meas 2", after a Tjump from 32 to 35.1°C; red line: "meas 4" after a Tjump from 34 to 37°C; cyan line: "Vwmeas1" after a Tjump from 32 to 35°C; green line: "Vwmeas 2" after a Tjump from 34-36.7°C. Absorbance changes are scaled to match experimental conditions (concentration and Tjump) for meas 4. See table 5.1 for details.

Thus, starting the Tjump at a temperature where the nanoparticle is already in a relative state of collapse (34 vs. 32°C or 36 vs. 34°C) results in slower dynamics. It can therefore be argued that if allowed to find equilibrium at a temperature at which it is partially collapsed, the nanoparticle impedes the further transition in some way. Possible interpretations for this are provided in the discussion, chapter 5.5.

Effect of the Size of the Temperature Jump

Figure 5.11 shows a comparison of three temperature jump measurements that start at the same temperature; since the amplitude of the absorbance changes for a larger Tjump is correspondingly higher, the results were scaled for the size of the Tjump (and slight variations in concentration), so that the initial amplitude changes agree almost perfectly.

Comparing the stretched exponential fits of the measurements is inconclusive, as without observing the end of the transition in the fitting window (i.e., the tailing off of the non-exponential decay), $<\tau>$ values will be highly inaccurate. However, all observed dynamics have considerable non-exponential behaviour, shown by low β

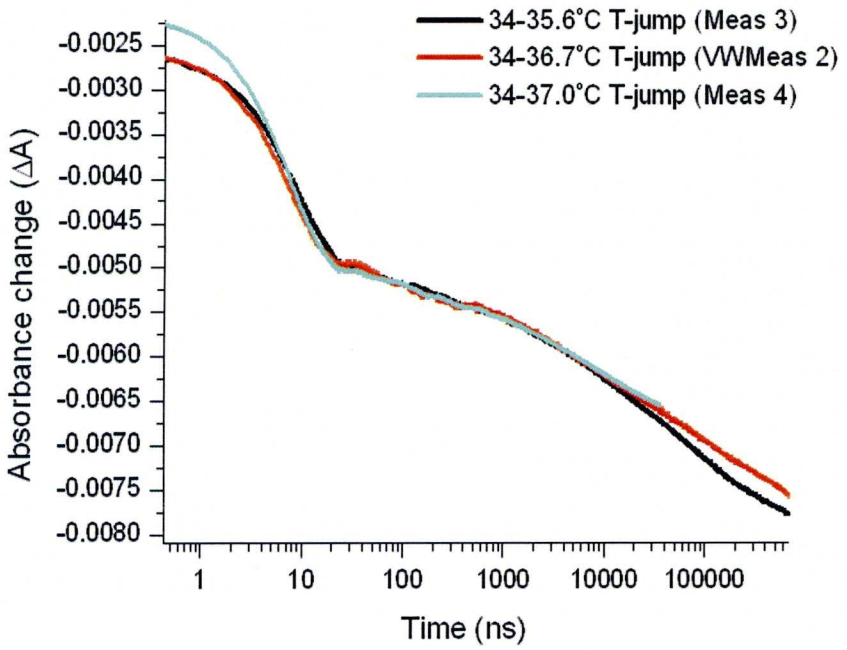

Figure 5.11 Absorbance changes of NANOpNIPAM (~10 mg/ml) at 1622 cm^{-1}, after Tjumps beginning at 34°C (scaled by the comparative size of the Tjump and concentration). Black line: "meas 3", a 1.6 K Tjump; red line: "VWmeas 2", a 2.7K Tjump; cyan line: "meas 4"; a 3 K Tjump (see table 5.1).

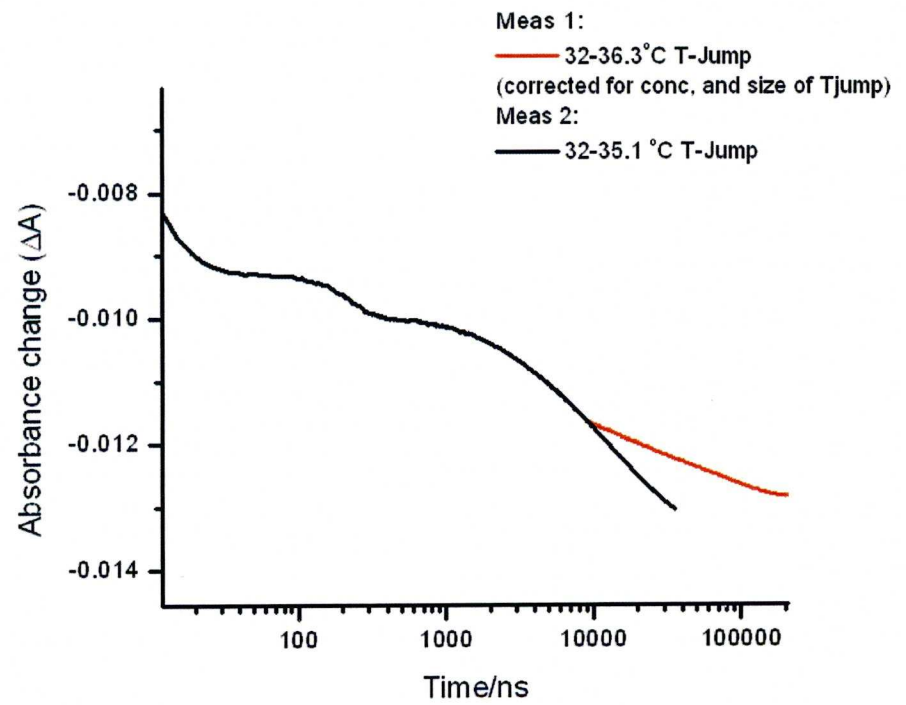

Figure 5.12 Absorbance changes of NANOpNIPAM (~10 mg/ml) at 1622 cm^{-1}, for Tjumps beginning at 32°C (scaled by the comparative size of the Tjump and concentration). Red line: "meas 1", a 4.3 K Tjump; black line: "meas 2", a 3.1 K Tjump (see table 5.1).

values, which are similar for all results after Tjumps starting at 34°C, meaning that the dynamics are similar. On scaling the absorbance changes (figure 5.11), we see an intriguing overlap of the initial dynamics of the absorbance changes. After approximately 10 μs, the dynamics begin to diverge. This interesting result shows that initially the dynamics are heavily influenced by the start temperature. However, later in the transition, the temperature reached begins to have an effect, with a larger Tjump giving slightly slower dynamics later in the transitions.

Comparing absorbance changes after Tjumps at lower temperatures highlights this effect. Figure 5.12 shows absorbance changes after Tjumps starting from 32°C. In the later part of the dynamics, meas 1, using 4.3 K Tjumps, shows much slower dynamics than meas 2, using 3.1K Tjumps. Although cavitation obscures the signal <10 μs in meas 1, making comparisons between fits problematic, we can see that jumping to a higher temperature above the LCST causes significantly slower dynamics, at least for the later phase, which confirms the results in figure 5.11.

The high signal-to-noise combination measurements and fit results are shown in table 5.2

				1622 cm^{-1} fit parameters				
Description	Start temp (°C)	Final temp (°C)	Size of jump (°C)	A	k	B	y0	$\langle\tau\rangle$=
Meas 1	32	36.3	4.3	0.00157	3×10^{-5}	0.692	-0.0158	42μs
Meas 2	32	35.1	3.1	0.00456	6×10^{-5}	0.654	-0.0139	22μs
Meas 3	34	35.6	1.6	0.00371	1×10^{-5}	0.294	-0.00838	10μs
Meas 4	34	37	3.0	0.00756	2.5×10^{-6}	0.218	-0.0161	23ms
Meas 5	36	37.9	1.9	0.00574	6.5×10^{-7}	0.0963	-0.0092	1.39×10^{4}s

Table 5.2: Parameters of fits of the high S/N TJump measurements at 1622 cm^{-1}. A= amplitude, k= rate constant, β= stretching coefficient, y0= offset (maximum absorbance change when decay is complete), $\langle\tau\rangle$= average time constant, see equations 5.1 and 5.2. Grey shading indicates that fits are problematic, either due to cavitation (meas 1), a limited fitting window (meas 1, 4 and 5) or extremely stretched dynamics (meas 5)

5.4.2 Variable Wavelength Measurements

The 1622 cm^{-1} absorbance changes do not provide the whole picture of the salvation changes. The amide I' band is complicated, as evidenced by the band deconvolution described in chapter 5.3. Sub-bands shift, change width and Gaussian/Lorentzian character, and the population of the corresponding carbonyl states change with temperature. Thus, observing the transition using only one wavelength gives an incomplete picture of the changes that occur during the transition.

To observe the changes in the whole amide I' band with our setup, the infrared probe laser has to be tuned to multiple wavelengths in the amide I' band during a single experiment and absorbance changes at each wavelength have to be measured individually, while jumping the temperature by the same temperature (see Chapter 4.3.2 and figure 4.2 for details). To reduce possible variations in dynamics and sample absorbance caused by changes in sample or the pump laser, the measurement has to be performed on a single sample, in one session. The signal-to-noise is therefore reduced, compared to the previous measurements shown in this chapter, as the time available to record the dynamics at each wavelength is limited by AuNP bleaching during the course of the measurement. The maximum number of measurements used here is 10 x 512 individual measurements for each wavelength, for each of the three time windows used previously (2 μs, 40 μs and 2 ms). To correct for fluctuations in the size of the temperature jump, caused, by a drop in AuNP transducer concentration or variations in the Nd-YAG power as the measurement progresses, the 1583 cm^{-1} absorbance change where polymer absorbance is minimal is checked between measurements at other wavelengths and readjusted to the original value. Although this keeps the temperature jump approximately constant, we still see small (<10%) variations throughout the 30 measurements of each set, so the final Tjump for each wavelength set is calculated from an average of the absorbance change at 1583 cm^{-1} before and after each set.

Variable wavelength measurements were taken for Tjumps from 32 to 35°C and 34 to 36.7°C. The corrected absorbance changes are shown in figure 5.13.

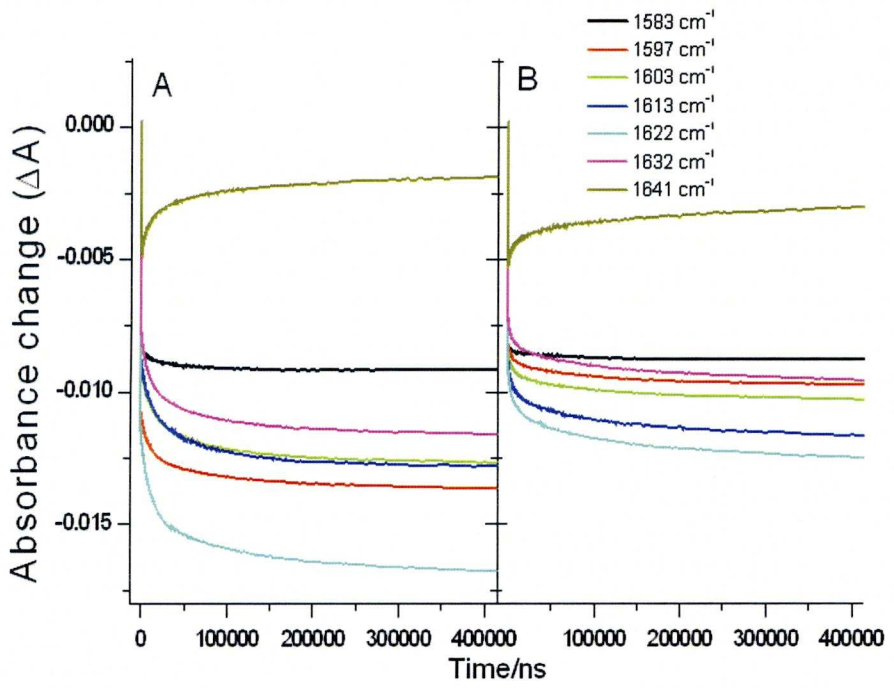

Figure 5.13 Variable wavelength temperature jump measurements on NANOpNIPAM, (~10 mg/ml concentration). A) "VWmeas 1", Tjumps from 32 to 35°C; B) "VWmeas 2" Tjumps from 34 to 36.7°C (see table 5.1 for sample/Tjump details). The probe wavenumber is denoted by the colour for each trace (see legend for details).

The size and sign of the absorbance changes at each wavelength reflect the change seen in the steady state data. The absorbance changes are a combination of instantaneous D_2O and polymer shifts, and a slow shift due to changes in the polymer hydration structure, and this can be most clearly seen in the 1639 cm^{-1} measurement, the only wavenumber to show a positive change in NANOpNIPAM absorbance with increasing temperature, see figure 5.5. The Tjumps at higher temperature show a more stretched exponential character (representation of data on a log-scale, figure 5.14, shows this more effectively, also see the β value in table 5.3).

The absorbance changes for the different wavelengths for each variable wavelength measurement were fitted globally, sharing k, β and $<\tau>$, but leaving amplitude and offset free to vary for each wavelength, figure 5.14. Fit parameters for the measurements are shown in table 5.3. The average time constants are unreliable as a true indication of the timescale of the dynamics, particularly at the higher temperature, due to the highly stretched nature of the dynamics. However, comparisons with the high signal-to-noise fits described in table 5.2, show that

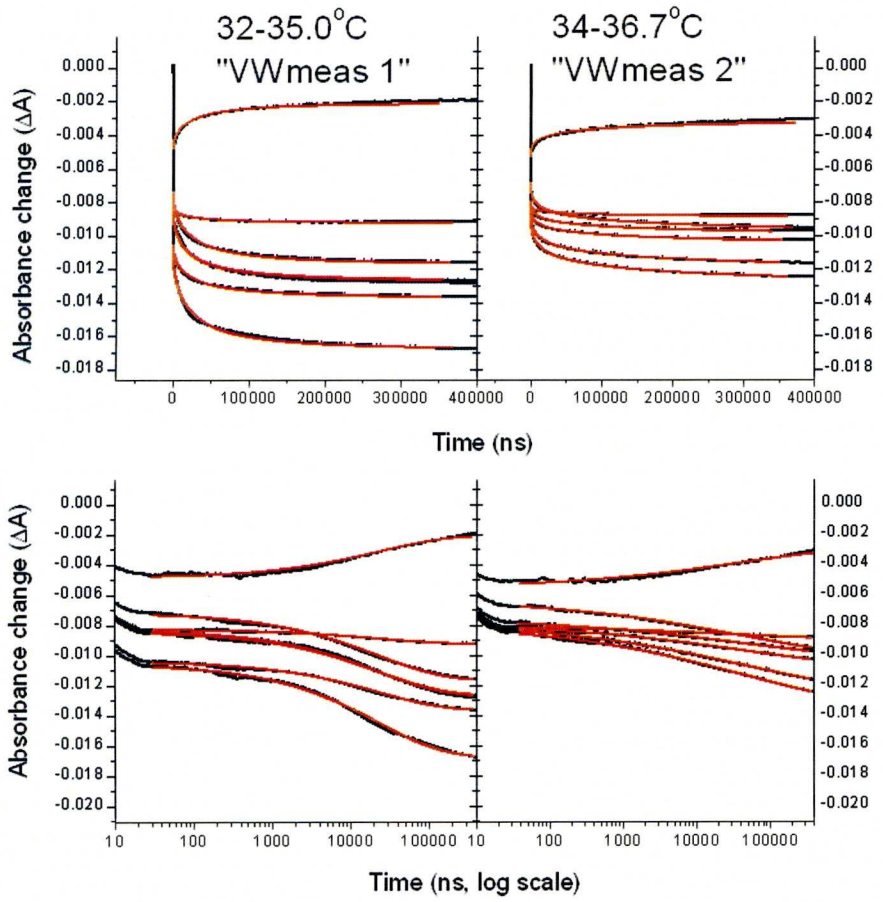

Figure 5.14 Variable wavelength measurements on NANOpNIPAM (figure 5.13) (black lines) fitted with a global stretched exponential decay (red lines).

the variable wavelength measurements yield time constants with the same order of magnitude as their closest counterparts in the high signal to-noise measurements. VWmeas 1 and meas 2 both use Tjumps from 32 to ~35°C, and have average time constants of 46 μs and 22 μs, respectively. VWmeas 2 and meas 4 use Tjumps from 34 to ~37°C and have average time constants of 692 μs and 23 ms respectively; however, these results are less reliable due to the clearly more stretched behaviour; in addition, the actual value of the meas 4 $<\tau>$ is suspect due to the small time-window.

Difference spectra can be constructed from the fit parameters obtained from the temperature-dependent FTIR spectra (chapter 5.3) to calculate the expected absorbance change spectra at different stages after a Tjump has taken place. The parameters can be split into linearly temperature dependent spectral variables; lineshape, band position, and band width, which must be considered separately from the band areas.

description		"VWmeas 1" 32-35.0°C	"VWmeas 2" 34-36.7°C
Start temp		32	34
Final temp		35.0	36.7
	k	4.0×10^{-5}	2.0×10^{-5}
	β	0.52	0.276
	$<\tau>=$	46 μs	692 μs
1583 cm^{-1}	A	9.80×10^{-4}	0.00102
	y0	-9.24×10^{-3}	-0.00902
1597 cm^{-1}	A	3.29×10^{-3}	0.00271
	y0	-0.01367	-0.0102
1603 cm^{-1}	A	4.23×10^{-3}	0.00271
	y0	-0.0127	-0.0108
1613 cm^{-1}	A	0.00446	0.00463
	y0	-0.0127	-0.0124
1622 cm^{-1}	A	6.18×10^{-3}	0.00557
	y0	-0.0168	-0.0134
1632 cm^{-1}	A	4.47×10^{-3}	0.00394
	y0	-0.0117	-0.0102
1639 cm^{-1}	A	-0.00275	-0.00286
	y0	-0.00209	-0.00278

Table 5.3: Stretched exponential fit results for the measurements shown in figure 5.14. Symbols are described in table 5.2.

As FTIR measurements were recorded at incremental temperatures of 1 degree around the LCST, area parameters for intervening temperatures were calculated from a weighted average of the fit values for spectra on either side. The relative areas of the bands represent the number of hydrogen bonded carbonyls in each state of bonding (described in detail in section 3.4.2). Exchanges in the relative band areas represent a change in solvation state, which involves breaking of H-bonds, diffusion and bond reformation, as well as major structural changes of the polymer backbone (shrinkage of nanoparticles), particularly around the LCST, which is expected to take some time. Thus, the band area shifts can be seen as a measure of structural progression. We can simulate the spectra for the polymer at 4 stages of the dynamic process:

- Before the temperature jump, the sample's IR spectrum equals the steady state FTIR spectrum measured/simulated at the start temperature.
- We would expect shifts in the temperature dependent spectral parameters to occur almost instantaneously after a temperature jump. These are affected by changes in the properties of carbonyl hydrogen bonds to D_2O, and require no diffusion or rearrangement of bonds, thus are expected to react instantaneously (on our time-scale) to a change in temperature. The

simulated spectra assume only shifts of the band parameters, but no population/area changes.

- There is a linear temperature dependence seen in the relative band areas below the LCST, likely due to local collapse and a shrinking of the radius of gyration (figure 5.7). This behaviour can be extrapolated to above the LCST, and predicts the extent of the initial rapid local contraction of the polymer immediately after a Tjump. As seen in chapter 4.3.2, this is the initial stage of linear chain pNIPAM collapse (before the large-scale phase transition takes place) and occurs rapidly, within the deadtime of our setup. Thus, spectra were simulated at the new temperature with the areas obtained from the extrapolation of the linear dependence below the LCST.
- When the temperature jump and all dynamics are complete, the absorbance spectrum will equal the absorbance spectrum observed in the polymer steady state FTIR spectrum, i.e. including the full area change.

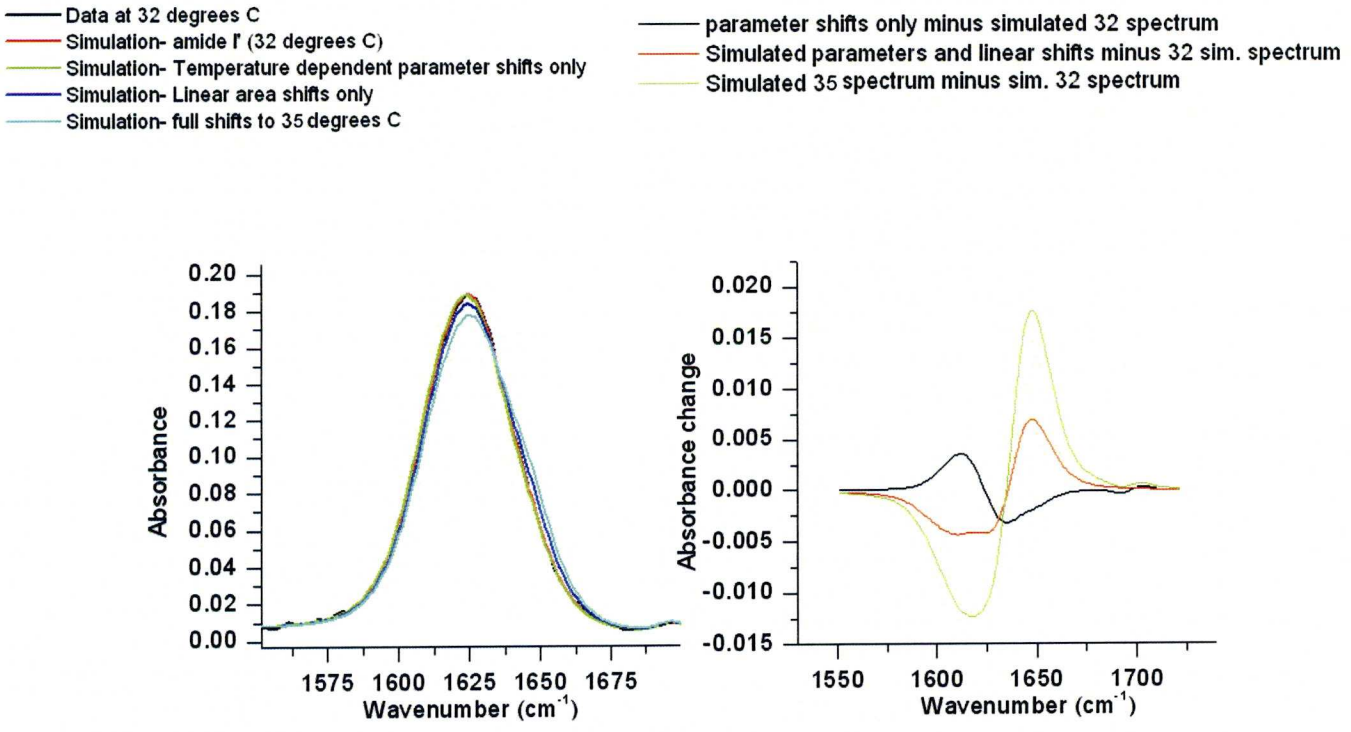

Figure 5.15 (Left) Amide I' band spectrum of NANOpNIPAM at 32°C, compared with expected band shapes for the polymer at various states of the phase transition after a Tjump at 35°C. Simulations are calculated from the parameter from the fits of the steady state FTIR spectra shown in figure 5.5. The simulations are explained in the text. (Right) Difference spectra calculated from the simulated data, providing expected absorbance change spectra for a 32 to 35°C Tjump.

The expected absorbance difference spectra, for each stage in the transition, can be calculated by subtracting the simulated spectrum expected at the start temperature from the spectrum reached at various stages of the transition. Figure 5.15 shows simulated spectra compared with an FTIR spectrum recorded at the start temperature. As can be seen from figure 5.15b, there is a dramatic difference between the difference spectra associated with temperature dependent parameter shifts only and the linear area shift difference spectra, whereas the difference between the linear area shifted spectra and the completed transition is largely one of scale for this Tjump. By comparing the dynamic polymer signal at different wavelengths measured in the Tjump experiments to those expected from the difference spectrum, one can conclude on the progress of the transition, see figure 5.16.

Figure 5.16 shows the IR-absorbance change spectra of the polymer at different times after the Tjump, taken from cooling and pressure relief corrected results (figure 5.13), compared to the simulated difference spectra at different stages of the relaxation for the two variable wavelength measurements. The experimental results at short times (40 ns after Tjump is induced) are for the most part grouped around the difference spectrum for linear area shifts. This indicates that these linear area shifts, and thus the underlying local solvation changes, are rapid, occurring within the 40 ns dead time of the measurements. After this time, the measured absorbance changes progress towards the difference spectrum calculated for the completed transition. Again, we see that the transition is slow, and in both Tjump experiments shown, the transition is not complete by the time cooling begins to disrupt the measurement.

The 1639 cm^{-1} absorbance is the only laser mode to report the changes in the 1650 cm^{-1} band, which we have characterised as being intramolecular amide-amide hydrogen bonded carbonyls. This band is interesting from the point of view that an increase in the number of amide-amide hydrogen bonds is a major indication that the transition is occurring, as exchanges between the 1625-1610 cm^{-1} bands may occur as a result of as simple contraction of the nanoparticle sphere. The progression of the 1639 cm^{-1} band is a good indication that it is the full transition that is observed.

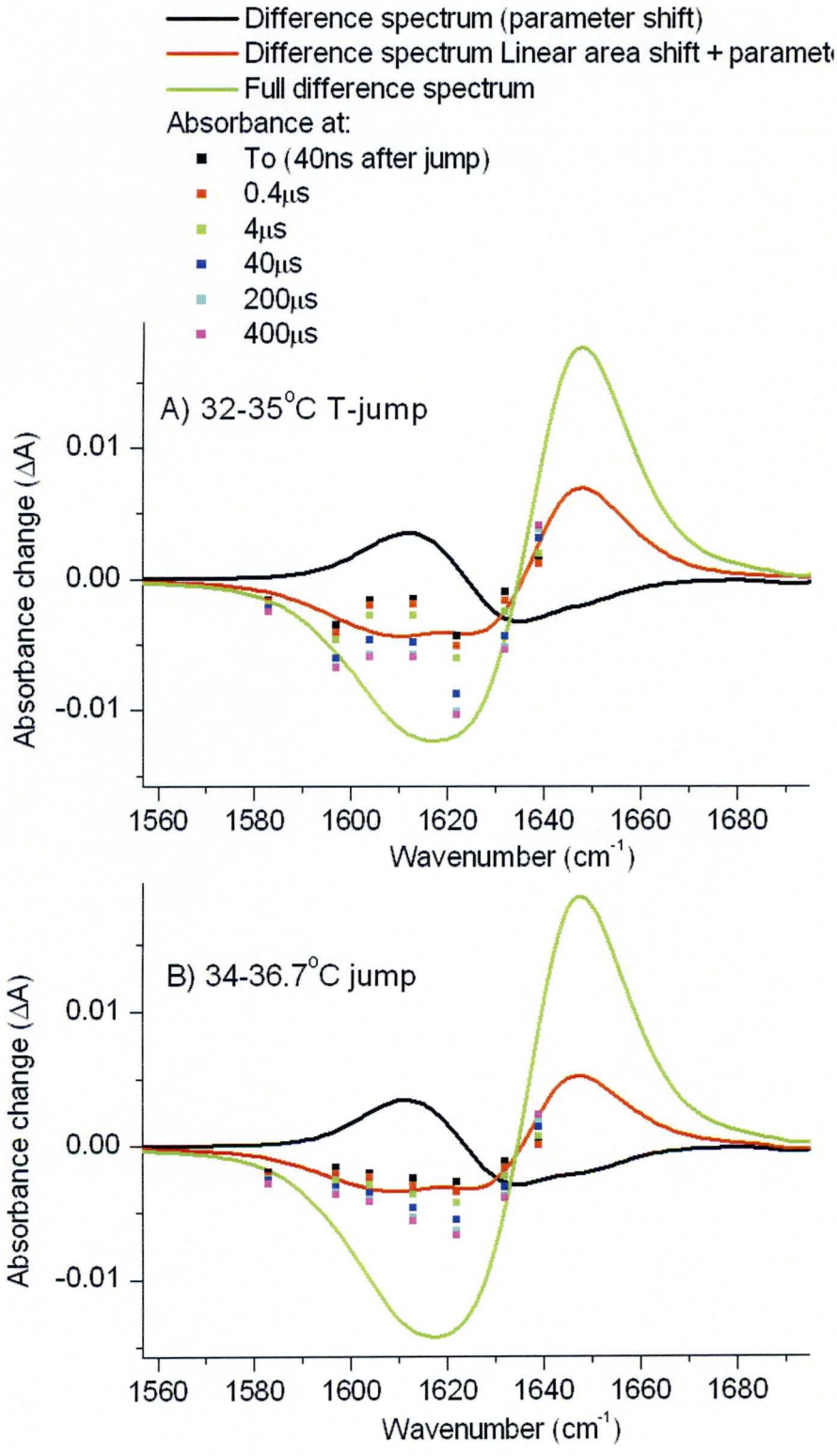

Figure 5.16 Absorbance change spectra at different delay times, constructed from the measurements in figure 5.13, compared with simulated difference spectrum at different stages during the transition following Tjumps of 32-35°C (A) and 34 to 36.7°C (B). The absorbance changes at each time point are calculated by subtracting the expected D_2O absorbance for Tjumps of this size at the specific wavelength of the IR trace, values which are calculated using appropriate neat D_2O FTIR difference spectra.

Interestingly, the absorbance progression is far slower after the 34-36.7°C Tjump than the 32-35°C Tjump, an observation which matches the high signal-to-noise kinetic experiments, and shows that starting the Tjump closer to the transition temperature and thus reaching higher final temperatures slows the transition dramatically. This is further evidence that starting temperature jumps in a more advanced state of collapse impedes the transition, which will be discussed in more detail in the following section.

5.5 Discussion

One must consider that the results shown here conflict with those previously reported (see 5.1), with the few previous dynamics studies on nano/microgels showing dynamics with time-constants less than 1μs[5,56,137]. Ahmed *et al*[56] in particular see dynamics that follow a single exponential decay (indicating a single, two state process), with a time-constant of 360±90 ns on NANOpNIPAM nanoparticles with preparation methods essentially identical to the ones investigated here. In our measurements, we see much more stretched, non-exponential and slower behaviour in the dynamics. Possible explanations for the observations shown in our dynamic measurements are as follows:

1) The slow stretched-exponential behaviour is due to aggregation of the collapsed particle

As temperature increases and side chains become increasingly insoluble, the polymer reaches a state at which no further "squeezing out" of internal water molecules is possible and the particle has reached its minimum volume. Pendant side chains can retreat no further from the poor solvent, so aggregation of nanoparticles occurs to shield the outer pNIPAM chains from solvent interaction.

Aggregation may explain observations by Wang and coworkers[5] in their time-resolved light scattering measurements on pNIPAM nanogels (see chapter 5.1). Wang et al perform 10 K temperature jump measurements on pNIPAM nanoparticles, which they probe by observing light scattered by the sample due to a change in the index of refraction of nanoparticles after phase transition. They see a delayed increase in the amount of light scattering with a time constant of 390 ns, which is similar to dynamics observed by Ahmed *et al*[56]. Interestingly, Wang *et al*[5] see a disparity between the size of the change in transmittance of steady state and dynamic measurements of the same

polymer, in which the dynamic measurements show only 3-4% of the transmittance change seen in the steady state measurements. The size of the Tjump is similar to those in measurements by Ahmed, and transient spectra in that study show that for a 15 K jump beginning at 30°C the entire transition is completed within >1 μs (the final transient spectrum is almost identical to the steady state spectrum. Ahmed's technique is sensitive to hydration changes rather than aggregation, which, as we saw in chapters 3 and 4, has only a comparatively small effect on the hydration state when compared to the main transition. Wang attributes his observations to only a small fraction of the outer shell of the nanoparticles undergoing a phase transition on the fast time scale, which is unlikely, in light of observations by Ahmed[56] that the hydration structural changes are complete within 1μs and considering the similar experimental condition. It seems more likely that the much larger light scatter found in the steady state measurements is due to aggregation, which is a slow process, as shown in chapter 3. It has to be noted that another difference between these studies is the fact that Wang *et al* use microgels that do not contain the ionic comonomer 2-acrylamido-2-methyl-1-propane-sulfonic acid contained in particles used by Ahmed and co-workers[56]. Therefore, it makes sense to suggest that the additional light scatter in Wang *et al*'s results developing on slower time scales is due to the formation of aggregates, whereas no such phase exists in particles used by Ahmed and co-workers[56], which contain ionic groups which act to repulse the nanoparticles to prevent aggregation. Aggregation would be the last stage in the transition, as it requires distant nanoparticles to diffuse through the solution to come into contact.

Aggregation is unlikely to be the cause of the major features in the dynamics we see; the NANOpNIPAM particles we use contain a small percentage of charged comonomers that act to repel the nanoparticles, like those used by Ahmed *et al*[56], and we probe with a technique that is primarily sensitive to hydration changes, and much less to aggregation. As seen with the single chain pNIPAM samples in chapter 4, aggregation is a slow process when compared with the solvation-phase transition seen in high temperature jumps that cover the entirety of the transition[5,56], and is unlikely to be detected on the time-scale on which measurements presented in this chapter are performed.

2) The reducing size of the particle begins to present a hindrance to the collapse mechanism.

If we consider figures 5.9 and the dynamics presented therein, the divergent traces of the absorbance changes at 1622 cm^{-1} show differences in dynamics that hint at what is occurring. At 34°C and 36°C, the volumes of the static nanoparticles are 82300 nm^3 and 55520 nm^3 respectively, a 33% decrease, and as the nanoparticles contain the same amount of polymer material, the extra volume is water. The minimum volume for the nanoparticles is 27400 nm^3, at which almost all free water has been ejected (the particle is essentially a dense sphere). At some point the during the collapse into a dense sphere the internal space occupied by the pNIPAM monomers will effectively block the channels used by water to escape the internal environment, or at least tighten to the point where the size of such channels is highly restrictive to the flow of water molecules.

A grossly simplifying model can be used to estimate the size of the channels in the nanoparticle, through which the ejected water would escape to the bulk solvent. The density of monomers per nm^3 is calculated by dividing the number of monomers per nanoparticle, provided by Ahmed *et al*[56], by the volume of the ellipsoid at a particular temperature. Assuming that a linear chain of oblate ellipsoids (with a volume estimated from the mass of a monomer and a density of 1.5 g/cm^3) separated by 2 carbon-carbon bonds (0.25 nm) represents a single chain of pNIPAM (figure 5.17), the channel size can be estimated by calculating the distance between oblate elipsoids in a regular lattice for that density, assuming that in one dimension, the distance between the ellipsoids is 0.25 nm (constrained by the linear chain). Below the LCST (at 30°C) when the nanoparticle is almost fully extended, channels have a size of approximately ~1.2 nm. If we compare this to the size of a water molecule, (0.2 nm in the largest dimension) we see this enables a number of water molecules to travel simultaneously through the channel. When fully collapsed (40°C), the pores are effectively closed, signifying that there is very little scope for the free movement of water molecules through the nanoparticle. At 32 and 34°C (start temperatures for meas 2 and 4, in figure 5.10) the average width of the channels are estimated to be 0.9 and 0.6 nm, respectively. Effectively, the decreased pore size would slow water ejection significantly due to friction with the walls of the channels as temperature increases. Thus, if the Tjump is from 32-35°C, solvent can escape more easily, at least initially. A

Tjump from 34-37°C, already begins in a state of partial collapse. Due to narrower channels, internal water molecules will find it much more difficult to escape the core of the nanoparticle, which results in slower dynamics. In both cases, NPs contract during the transition, making the later part of the transition slower, and thus the dynamics more stretched, although this is even more pronounced at higher temperatures, when channels essentially disappear, so that the final stage relies on polymer fluctuation to allow the release of water molecules. It must be noted that this calculation is a very rough estimate only. However, it does provide an interesting insight into the slowing of the dynamics when starting at higher temperatures. Also, this is an average pore size; channel sizes may vary throughout the polymer, particularly as the cross-linking density is not homogeneous throughout the polymer[139], and larger channels may allow the penetration of water throughout a collapsed nanoparticle.

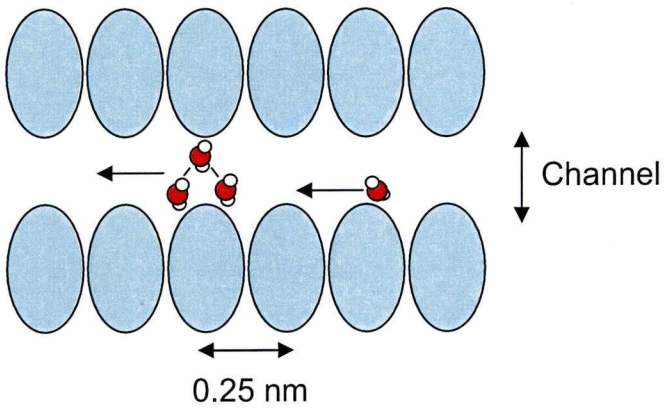

Figure 5.17 Cartoon showing the simple model with which the estimate of channel size was calculated.

In Ahmed's study[56] the permeability to water was checked by measuring the rate of the hydrogen-deuterium exchange, and it was seen that for the fully collapsed nanoparticles at 55°C, all hydrogen was exchanged within the 5 minutes it requires to take the measurement, though at this high a temperature, the polymer has already reached its minimum volume (which is reached at 40°C). The same conclusion is reached in NMR measurements by Spevácek *et al*[106] in which trapped water in collapsed pNIPAM chains is resolved from free water molecules, and the two water states are shown to exchange on the 1 ms timescale. Therefore, collapsed nanoparticles are dynamic entities, and fluctuation in the structure will allow even trapped water molecules in the

interior to be released eventually. Regardless, to affect the speed of the transition, the channel width only has to hinder the transit of water.

3) The nanogels are heterogenous in composition.

It has been reported that the crosslinking comonomer is more reactive than NIPAM[139] and consequently, in the formation of the nanoparticles, a larger proportion of the central nanogel will be crosslinker with a negative gradient in the crosslinker concentration as the edge of the particle is approached. Because of this, the peripheral pNIPAM chains of the nanoparticle may have a different LCST when compared to the core. The crosslinker, *N-N'*-methylenebis(acrylamide), is more hydrophilic due to the lack of pendant alkyl groups, thus the LCST of the core of the nanoparticle will be higher due to its increased solubility. An example of this phenomenon is in the steady state measurements for pNIPAM-co-Acr in chapter 3. (pNIPAM co-polymerised with acrylamide comonomers, which contain no alkyl side chain) The copolymer pNIPAM-co-acr, in which 10% of NIPAM monomer units are replaced with *N*-acrylamide, (which lacks a pendant alkyl group), has an increased LCST of 42°C. It is therefore logical to assume that the peripheral pNIPAM chains in the gel would have a slightly lower LCST and collapse first, possibly leading to the situation described schematically in figure 5.18.

Interpretation 2 suffices to explain our observations of temperature effects on transition dynamics. Interpretation 3 may be an additional effect which further enhances the effect of interpretation 2. If we combine these interpretations we begin to develop a consistent picture of events on the molecular level. At temperatures close to the LCST, as the temperature jump measurements presented in this chapter, the nanoparticles are in a state of partial and inhomogeneous collapse. Following this argument, at higher start temperatures, the outer chains will be in an advanced state of collapse when compared to the core chains, although the amount of this collapse depends on the exact value of the starting temperature.

Considering the decreasing channel sizes postulated above (*2*), these outer chains in an advanced state of collapse will form a partially dehydrated, hydrophobic shell around the hydrated core, forming a barrier to the expulsion of internal water molecules due to the reduced size of the channels. Our results reflect this.

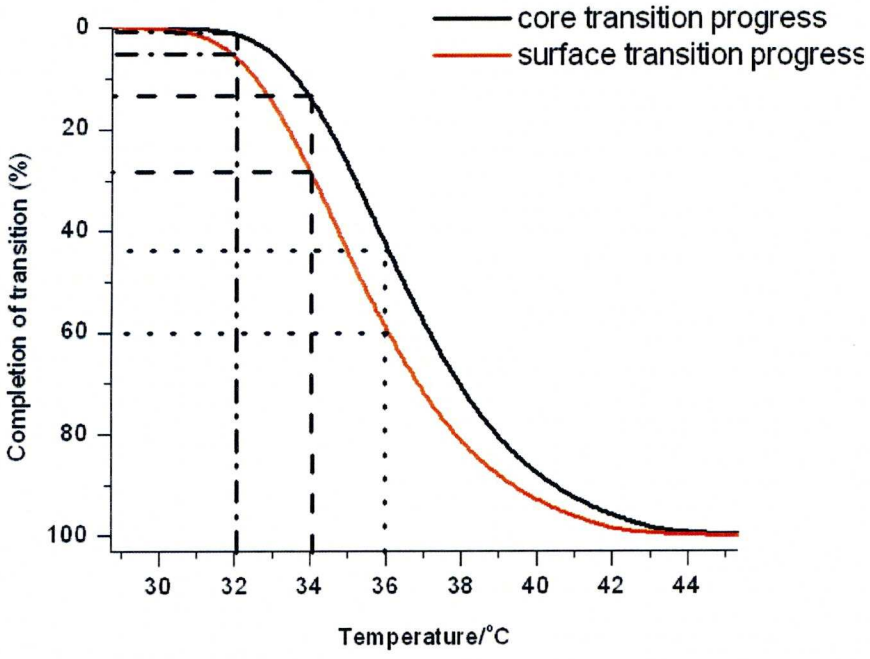

Figure 5.18 The difference between the transition of the core and outer chains of a NANOpNIPAM particle, as postulated in the text. Additional lines are added as an aid to the eye.

In measurements where the start temperatures are identical, the external chains will be in the same state of collapse before the Tjump is induced. Measurements at higher start temperatures, on the other hand, deviate considerably more from a simple exponential decay, and are much more stretched. In the higher temperature jump measurements that begin at a temperature that is over the midpoint of the transition, consequently have a collapsed outer-shell that will extend further towards the core of the nanoparticle, which is in a higher state of collapse, thus impeding the ejection of water from the core chains that are still hydrated further than for a 34°C start temperature, slowing and distorting the transition dramatically. This pattern is repeated throughout the measurements presented in this chapter.

The exponential decay observed in Ahmed's UVRR pump-probe measurements (τ=360±90 ns)[56] is very different from our stretched exponential dynamics, and indicates that the transition is essentially a two state process. In their experiment, the kinetics are measured by observing the differences in peak height of

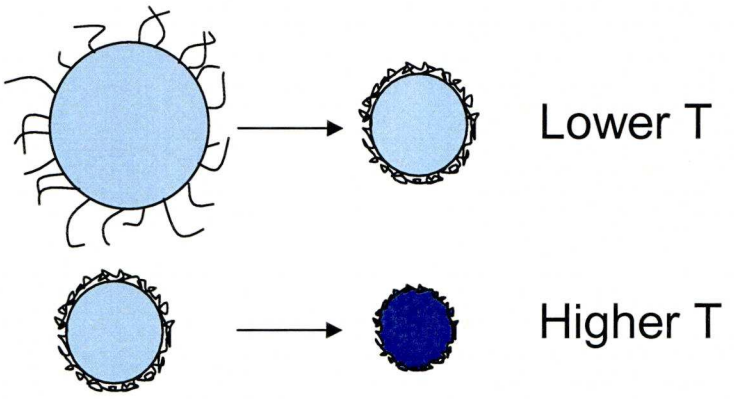

Figure 5.19. Cartoon showing a potential interpretation of the data in this chapter. The upper progression represents a Tjump from a lower temperature to one barely exceeding the transition point. In this case, there is a collapse of the chains on the periphery of the nanoparticle and a slight reduction in volume, which happens quickly as there is no external barrier to water exiting the molecule. The lower progression represents a jump from a temperature just below the LCST in this case, an outer shell of collapsed chains in formed even before the Tjump due the inhomogeneous transition temperature through the nanoparticle cross-section. This outer shell forms a barrier to water exiting the molecule, resulting in a slower transition that deviates more strongly from exponential behaviour.

the Amide I band by calculating difference spectra measured at various delay times. Although the information obtained is similar to that obtained in our measurements, the different Tjumps used in that study account for the changes in polymer kinetic behaviour seen for these experiments.[56] Ahmed uses 15°C Tjumps from 30-45°C, a jump that encompasses the entire transition.

The different dynamics observed under these conditions can be explained in terms of the changes in secondary structure experienced by the polymer. As the nanoparticle begins the Tjump induced collapse in a fully extended and hydrated state and the entire nanoparticle is heated over the transition temperature, the interior water molecules experience no difficulty in exiting the molecules as the polymer collapses as they are not impeded by a collapsed shell surrounding the molecule. The phase transition therefore occurs as a single, cooperative event. The transition is further accelerated by the effect of the higher final temperature in these measurements. Thermal motion will be increased when compared to our measurements, resulting in a faster overall transition. The exponential character reported for the transition indicates a two state process, so it can be said that Ahmed has effectively measured and fitted the empirical transition, without further complications caused by the formation of a collapsed shell which impedes the collapse.

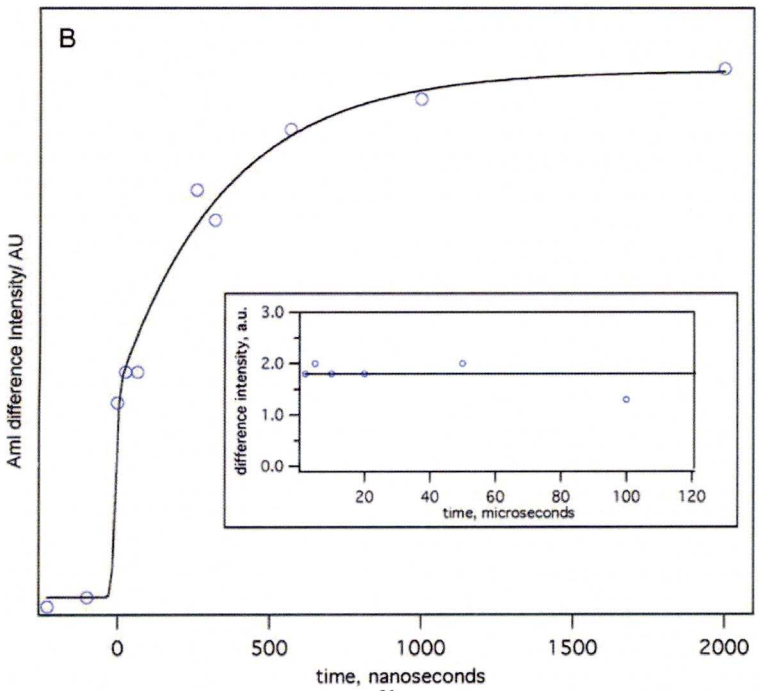

Figure 5.20 UVRR results by Ahmed *et al*[56]. (Main) the peak to peak amide I band intensity in the transient difference spectra at different delay time following a Tjump from 30 to 45°C. (Insert). The amide band intensity in the difference spectra shows a small decrease at 100 μs which indicates sample volume cooling due to thermal diffusion.

It is unclear whether an additional extended phase is present from Ahmed's results, due to a number of issues. Firstly, the signal-to-noise is quite low in Ahmed's results (figure 5.20). Furthermore data on longer time scales are limited by the onset of cooling/ the translation of the heated volume out of the probed volume due to the use of a jet as the sample medium.

In devices using pNIPAM as an on-off switch for delayed drug release etc., it is unlikely that such a large temperature jump can be induced to cause a perfect transition. Devices rely on a small increase in local temperature to nudge the polymer over the transition temperature. Further, the few devices currently undergoing testing rely on an external means of increasing the temperature[10,136]. Such devices are unlikely to use something as small as a nanogel, and instead rely on microgels as gateways, or as a matrix for loading actives for drug release[11] which due to their increased radius will have an increased disparity between the crosslinker/ single chain ratio through the cross-section of the molecule, thus causing an increased likelihood of a collapsed shell formation on the surface when heating. Our results therefore are more likely to represent the reality seen for pNIPAM gels in drug release devices controlled by temperature changes, and have implications for devices that rely on preloading the therapeutic actives into the polymer matrix prior to release, as if the shell is compact

enough to impede water diffusion, the effect will be much greater for slowing the release of a larger therapeutic active.

5.6 Conclusion

The measurements in this chapter were performed in order to study the phase transition of NANOpNIPAM particles with IR spectroscopy in terms of structural change. Steady state FTIR measurements give an insight into the changes in the carbonyl hydrogen bonding environments as a function of temperature, and therefore the solvation state at these temperatures. Pump-probe Tjump experiments give an intriguing insight into the secondary structural changes when heating a nanoparticle from a semi-collapsed state. Comparisons of Tjumps from different start temperatures and of different sizes, along with other investigations on the same nanoparticle performed by Ahmed *et al*[56] suggest that differences in dynamics are due to the formation of a dehydrated shell of collapsed chains which impede the expulsion of water from the core chains, altering the dynamics of the transition.

CHAPTER 6: CONCLUSIONS

This thesis has contributed to the knowledge of the H-bonding structural changes involved in the coil-globule phase transition of pNIPAM (and related polymers). These polymers hold great promise for use in controlled drug release due to their thermoresponsive nature.

The coil-globule transition has been studied extensively using temperature-dependent FTIR and IR spectroscopy. In particular, two major approaches were utilised:

FTIR measurements: Fourier transform infrared measurements have been used to study changes in the hydrogen bonding of the polymer at incremental *equilibrium* temperatures around the LCST. These measurements examine how the H-bonding structure changes in response to the phase transition.

Tjump Measurements: Laser induced temperature jumps probed with infrared have been used to examine the *dynamic* structural changes as the transition progresses in reaction to a temperature perturbation. These measurements study how fast the transition occurs, and explore the events that lead to the formation of globules.

In order to summarise the main findings of this thesis it is appropriate to address these two approaches separately.

1. FTIR measurements:

There have been numerous FTIR studies that follow an approach similar to 1 (see chapter 2 for a review). However there is controversy over the assignment of the amide I' sub-bands in the current literature, and therefore some confusion as to the true nature of the structural transition. Such FTIR studies examined the structural aspect of the phase transition by observing changes in the amide I' band, the vibration of which is sensitive to changes in hydrogen bonding.

The FTIR studies reported here show for the first time that variations in chain length and concentration have a noticeable effect on the population densities of the

amide I' component bands, indicating that these factors effect the structure of the polymer in solution in both the random coil and globular configuration. Chapter 3 reports how the steady state measurements and subsequent amide I' analysis in this thesis give new insight to the complexities of this transition. A key finding was that co-polymerising pNIPAM with even a small amount of tert-butyl acrylamide, or an acrylamide monomer with no alkyl side chain, has a drastic effect on both the LCST and the population distribution of the component bands, showing that the alkyl groups are the main driving forces behind the transition.

By using a global band fitting analysis on the amide I' band, 3 component bands have been identified. In general for single chain pNIPAM variants, , the number of normally solvated carbonyls (1625 cm^{-1}) decreases on heating. A corresponding increase is observed in the number of single/intramolecular (1650 cm^{-1}) H-bonds and carbonyls that are H-bonded to "trapped" water molecules (1610 cm^{-1}) as globules are formed.

The suggested interpretation is consistent with the behaviour of the amide I' shown in the varied polymer systems presented in chapter 3 and 5. Furthermore, the consistency is maintained with the results already present in the literature (see chapter 3.5.3). There has previously been a lack of satisfactory interpretation .. The 1610 cm^{-1} band highlights the existence of solvated carbonyls in constrained environments, though the band probably encompasses a large variety of states (this is suggested by the large 1610 cm^{-1} band width, despite a probable decrease in the band width of individual carbonyl H-bonding states due to separation from the solvent in cavities). FTIR can distinguish between the carbonyls in constrained (1610 cm^{-1}) and normally solvated (1625 cm^{-1}) environments due to the band population exchange, but cannot resolve further detail. A molecular modelling approach is necessary to further investigate the states that populate the 1610 cm^{-1} band, and to give a more precise picture of what is occurring on a molecular level.

The observed behaviour leads to a compelling model for the phase transition based on the pearl-necklace model; local collapse of portions of the chain into globules occurs even below the LCST, with the results pointing to a propensity for the chain to trap water molecules and form intermolecular bonds as temperature increases below the LCST, consistent with locally collapsed sections.

Comparison with the amide I' behaviour of nanogels (see chapter 5.3) shows that the H-bonding structure in gels differ. Below the LCST in gels, there is already a

large proportion of carbonyls H-bonded to trapped water molecules (1610 cm^{-1}) and other amide groups (1650 cm^{-1}), reflecting the close proximity of the crosslinked chains. Upon phase transition, it is the H-bonds to trapped water molecules that are lost in favour of intramolecular bonding. As the trapped water molecules are those found internally, these molecules are therefore ejected from the nanoparticle as it collapses.

2. Tjump measurements:

This thesis has shown that there are in fact three distinct responses to a temperature jump over the LCST; 1) an instantaneous shift (<2ns) consistent with a change in hydration due to an increase of the number and/or size of locally collapsed polymer sections; 2) the coil-globule transition of a single chain on the 10-100 s timescale; and 3) a slow aggregation process. These transition dynamics for the single chain pNIPAM were investigated in chapter 4, where it was shown that absorbance changes in the amide I' region of pNIPAM following fast Tjumps on a variety of timescales from 50 ns-14000 s.

The formation of larger globules is several orders of magnitude slower than the phase-transition, and by careful extrapolation of the results, the aggregation process seems to conclude on the order of 20 hours, which concurs with time course FTIR experiments (chapter 3.4.4). If overlapping is present, heating over the LCST results in a rapid cooperative collapse of the entangled polymer network, which suggests that increasing cross-linking speeds up the transition. These results are therefore consistent with those seen in chapter 5, in which gels show a more rapid transition. The observation of the 10-100 second transition is the first reliable observation of the structural change dynamics for the transition. Unfortunately, this process occurs within the rise time of the waterbath measurements, and is too slow to observe using the Argon laser as a Tjump inducer. To precisely characterise the single chain dynamics, it is imperative that a new method is devised to probe this time-region. Possible approaches include a new laser system which is stable for longer periods (an infrared laser capable of directly heating the D_2O solvent, which may eliminate the bubble formation seen in Ar laser measurements), or a modification of the current waterbath setup to decrease the rise-time, such as using a cell with a built in thermostat.

Finally, in chapter 5 the phase transition of crosslinked NANOpNIPAM nanoparticles was explored. Further pump-probe Tjump experiments gave an intriguing insight into the secondary structural changes observed during heating of a

pNIPAM nanoparticle from a semi-collapsed state. Comparisons of Tjumps from different start temperatures and of different sizes, along with other investigations on the same nanoparticle performed by Ahmed *et al*[56] suggest that differences in dynamics are due to the formation of a dehydrated shell of collapsed chains which surround the nanoparticle. This impedes the expulsion of water from the core chains, altering the dynamics of the transition; a discovery that may have important implications for devices that rely on preloading the therapeutic actives into the polymer matrix prior to release. If the shell is compact enough to impede water diffusion, the effect will be much greater for slowing the release of a larger therapeutic active.

REFERENCES

(1) Vogel, M. *The Journal of Physical Chemistry B* **2009**.

(2) Schild, H. G.; Tirrell, D. A. *Journal of Physical Chemistry* **1990**, *94*, 4352-4356.

(3) Maeda, Y.; Higuchi, T.; Ikeda, I. *Langmuir* **2000**, *16*, 7503-7509.

(4) Chee, C. K.; Rimmer, S.; Soutar, I.; Swanson, L. *Polymer* **2001**, *42*, 5079-5087.

(5) Wang, J.; Gan, D.; Lyon, L. A.; El-Sayed, M. A. *Journal of the American Chemical Society* **2001**, *123*, 11284-11289.

(6) Cho, E. C.; Lee, J.; Cho, K. *Macromolecules* **2003**, *36*, 9929-9934.

(7) Krusic, M. K.; Ilic, M.; Filipovic, J. *Polymer Bulletin* **2009**, *63*, 197-211.

(8) Fernandez-Barbero, A.; Suarez, I. J.; Sierra-Martin, B.; Fernandez-Nieves, A.; de las Nieves, F. J.; Marquez, M.; Rubio-Retama, J.; Lopez-Cabarcos, E. *Adv. Colloid Interface Sci.* **2009**, *147-48*, 88-108.

(9) Purushotham, S.; Chang, P. E. J.; Rumpel, H.; Kee, I. H. C.; Ng, R. T. H.; Chow, P. K. H.; Tan, C. K.; Ramanujan, R. V. *Nanotechnology* **2009**, *20*, 305101.

(10) Hoare, T.; Santamaria, J.; Goya, G. F.; Irusta, S.; Lin, D.; Lau, S.; Padera, R.; Langer, R.; Kohane, D. S. *Nano Letters* **2009**, *9*, 3651-3657.

(11) Alarcon, C. D. H.; Pennadam, S.; Alexander, C. *Chemical Society Reviews* **2005**, *34*, 276-285.

(12) Fernández-Barbero, A.; Suárez, I. J.; Sierra-Martín, B.; Fernández-Nieves, A.; de las Nieves, F. J.; Marquez, M.; Rubio-Retama, J.; López-Cabarcos, E. *Advances in Colloid and Interface Science*
Colloids, polymers and surfactants.Special Issue in honour of Brian Vincent, 147-148, 88-108.

(13) Ngai, K. L.; Plazek, D. J.; Roland, C. M. *Macromolecules* **2008**, *41*, 3925-3929.

(14) Heskins, M.; Guillet, J. E. *Journal of Macromolecular Science, Part A* **1968**, *2*, 1441 - 1455.

(15) Walter, R.; Ricka, J.; Quellet, C.; Nyffenegger, R.; Binkert, T. *Macromolecules* **1996**, *29*, 4019-4028.

(16) Kubota, K.; Fujishige, S.; Ando, I. *Polymer Journal* **1990**, *22*, 15-20 Note: The DLS measurements by Kubota are performed on much larger polymers, which will therefore be less sensitive to the "persistence length" effect, in which two neighbouring monomers cannot take a random conformation with respect to each other, and only after certain a distance separation of monomers along the chain is the "memory" of the orientation of the initial conformation lost. This will increase the radius of gyration in smaller polymers such as the ones used in this study, resulting in an even closer correlation between Rg and polymer separation.

(17) Kubota, K.; Fujishige, S.; Ando, I. *Journal of Physical Chemistry* **1990**, *94*, 5154-5158.

(18) Yushmanov, P. V.; Furo, I.; Iliopoulos, I. *Macromolecular Chemistry and Physics* **2006**, *207*, 1972-1979.

(19) Maeda, Y.; Nakamura, T.; Ikeda, I. *Macromolecules* **2002**, *35*, 10172-10177.

(20) Tokuhiro, T.; Amiya, T.; Mamada, A.; Tanaka, T. *Macromolecules* **1991**, *24*, 2936-2943.

(21) Tiktopulo, E. I.; Bychkova, V. E.; Ricka, J.; Ptitsyn, O. B. *Macromolecules* **1994**, *27*, 2879-2882.

(22) Winnik, F. M. *Macromolecules* **1990**, *23*, 233-242.

(23) Kujawa, P.; Winnik, F. M. *Macromolecules* **2001**, *34*, 4130-4135.

(24) Percot, A.; Zhu, X. X.; Lafleur, M. *Journal of Polymer Science Part B-Polymer Physics* **2000**, *38*, 907-915.

(25) Katsumoto, Y.; Tanaka, T.; Sato, H.; Ozaki, Y. *Journal of Physical Chemistry A* **2002**, *106*, 3429-3435.

(26) Maeda, Y.; Nakamura, T.; Ikeda, I. *Macromolecules* **2001**, *34*, 1391-1399.

(27) Guo, Y.; Sun, B.; Wu, P. *Langmuir* **2008**, *24*, 5521-5526.

(28) Katsumoto, Y.; Tanaka, T.; Ihara, K.; Koyama, M.; Ozaki, Y. *Journal of Physical Chemistry B* **2007**, *111*, 12730-12737.

(29) Maeda, Y.; Yamamoto, H.; Ikeda, I. *Macromolecules* **2003**, *36*, 5055-5057.

(30) Maeda, Y.; Tsubota, M.; Ikeda, I. *Colloid and Polymer Science* **2003**, *281*, 79-83.

(31) Maeda, Y.; Higuchi, T.; Ikeda, I. *Langmuir* **2001**, *17*, 7535-7539.

(32) Maeda, Y. *Langmuir* **2001**, *17*, 1737-1742.

(33) Sun, B.; Lin, Y.; Wu, P.; Siesler, H. W. *Macromolecules* **2008**, *41*, 1512-1520.

(34) Hirashima, Y.; Suzuki, A. *Journal of Colloid and Interface Science* **2007**, *312*, 14-20.

(35) Kesselman, E.; Ramon, O.; Berkovici, R.; Paz, Y. *Polymers for Advanced Technologies* **2002**, *13*, 982-991.

(36) Cheng, H.; Shen, L.; Wu, C. *Macromolecules* **2006**, *39*, 2325-2329.

(37) Meersman, F.; Wang, J.; Wu, Y. Q.; Heremans, K. *Macromolecules* **2005**, *38*, 8923-8928.

(38) Wu, Y. Q.; Meersman, F.; Heremans, K.; Ozaki, Y. *Journal of Molecular Structure* **2006**, *799*, 134-140.

(39) Wang, L. X.; Wang, D. Q.; Wu, Y. Q. *Chemical Journal of Chinese Universities-Chinese* **2005**, *26*, 2319-2322.

(40) Sun, B. J.; Lin, Y. N.; Wu, P. Y.; Siesler, H. W. *Macromolecules* **2008**, *41*, 1512-1520.

(41) Callow, M. E.; Callow, J. A.; Ista, L. K.; Coleman, S. E.; Nolasco, A. C.; Lopez, G. P. *Applied and Environmental Microbiology* **2000**, *66*, 3249-3254.

(42) Chen, G. P.; Imanishi, Y.; Ito, Y. *Journal of Biomedical Materials Research* **1998**, *42*, 38-44.

(43) Fujishige, S.; Kubota, K.; Ando, I. *Journal of Physical Chemistry* **1989**, *93*, 3311-3313.

(44) Schild, H. G. *Progress in Polymer Science* **1992**, *17*, 163-249.

(45) Schmitt, F. J.; Park, C.; Simon, J.; Ringsdorf, H.; Israelachvili, J. *Langmuir* **1998**, *14*, 2838-2845.

(46) Yamato, M.; Utsumi, M.; Kushida, A.; Konno, C.; Kikuchi, A.; Okano, T. *Tissue Engineering* **2001**, *7*, 473-480.

(47) Yang, W. Y.; Prince, R. B.; Sabelko, J.; Moore, J. S.; Gruebele, M. *Journal of the American Chemical Society* **2000**, *122*, 3248-3249.

(48) Cole, C. A.; Schreiner, S. M.; Monji, N. *Abstracts of Papers of the American Chemical Society* **1986**, *191*, 205-POLY.

(49) Chee, C. K.; Rimmer, S.; Soutar, I.; Swanson, L. *Polymer International* **2006**, *55*, 740-748.

(50) Jarkova, E.; Johner, A.; Maresov, E. A.; Semenov, A. N. *European Physical Journal E* **2006**, *21*, 371-386.

(51) Kujawa, P.; Segui, F.; Shaban, S.; Diab, C.; Okada, Y.; Tanaka, F.; Winnik, F. M. *Macromolecules* **2006**, *39*, 341-348.

(52) Schild, H. G.; Muthukumar, M.; Tirrell, D. A. *Macromolecules* **1991**, *24*, 948-952.

(53) Chee, C. K.; Hunt, B. J.; Rimmer, S.; Rutkaite, R.; Soutar, I.; Swanson, L. *Soft Matter* **2009**, *5*, 3701-3712.

(54) Borner, H. G.; Kuhnle, H.; Hentschel, J. *Journal of Polymer Science Part a-Polymer Chemistry*, *48*, 1-14.

(55) Yoshida, R. *Current Organic Chemistry* **2005**, *9*, 1617-1641.

(56) Ahmed, Z.; Gooding, E. A.; Pimenov, K. V.; Wang, L. L.; Asher, S. A. *Journal of Physical Chemistry B* **2009**, *113*, 4248-4256.

(57) Wooten, W. C.; Blanton, R. B.; Coover, H. W. *Journal of Polymer Science* **1957**, *25*, 403-412.

(58) Shields, D. J.; Coover, H. W. *Journal of Polymer Science* **1959**, *39*, 532-533.

(59) Ricka, J.; Meewes, M.; Nyffenegger, R.; Binkert, T. *Physical Review Letters* **1990**, *65*, 657-660.

(60) Ohta, H.; Ando, I.; Fujishige, S.; Kubota, K. *Journal of Molecular Structure* **1991**, *245*, 391-397.

(61) Binkert, T.; Oberreich, J.; Meewes, M.; Nyffenegger, R.; Ricka, J. *Macromolecules* **1991**, *24*, 5806-5810.

(62) Scarpa, J. S.; Mueller, D. D.; Klotz, I. M. *Journal of the American Chemical Society* **1967**, *89*, 6024-&.

(63) Heskins, M.; Guillet, J. **1968**, *2*, 1441.

(64) Kubota, K.; Hamano, K.; Kuwahara, N.; Fujishige, S.; Ando, I. *Polymer Journal* **1990**, *22*, 1051-1057.

(65) Wang, X. H.; Wu, C. *Macromolecules* **1999**, *32*, 4299-4301.

(66) Hammes, G. G.; Roberts, P. B. *Journal of the American Chemical Society* **1969**, *91*, 1812-1816.

(67) Arrondo, J. L. R.; Goni, F. M. *Progress in Biophysics & Molecular Biology* **1999**, *72*, 367-405.

(68) Venyaminov, S. Y.; Prendergast, F. G. *Analytical Biochemistry* **1997**, *248*, 234-245.

(69) Maeda, T.; Yamamoto, K.; Aoyagi, T. *Journal of Colloid and Interface Science* **2006**, *302*, 467-474.

(70) Maeda, Y. *Sen-I Gakkaishi* **2005**, *61*, P10-P13.

(71) Maeda, Y.; Nakamura, T.; Ikeda, I. *Macromolecules* **2001**, *34*, 8246-8251.

(72) Maeda, Y.; Nakamura, T.; Ikeda, I. *Macromolecules* **2002**, *35*, 217-222.

(73) Maeda, Y.; Sakamoto, J.; Wang, S.-y.; Mizuno, Y. *J Phys Chem B* **2009**, *113*, 12456-12461.

(74) Maeda, Y.; Sakamoto, J.; Wang, S.-Y.; Mizuno, Y. *J Phys Chem B* **2009**, *113*, 12456-12461.

(75) Maeda, Y.; Taniguchi, N.; Ikeda, I. *Macromolecular Rapid Communications* **2001**, *22*, 1390-1393.

(76) Maeda, Y.; Yamabe, M. *Polymer* **2009**, *50*, 519-523.

(77) Maeda, Y.; Yamamoto, H.; Ikeda, I. *Langmuir* **2001**, *17*, 6855-6859.

(78) Maeda, Y.; Yamauchi, H.; Kubota, T. *Langmuir* **2009**, *25*, 479-482.

(79) Katsumoto, Y.; Tanaka, T.; Ozaki, Y. *Journal of Physical Chemistry B* **2005**, *109*, 20690-20696.

(80) Maeda, Y.; Sakamoto, J.; Wang, S. Y.; Mizuno, Y. *Journal of Physical Chemistry B* **2009**, *113*, 12456-12461.

(81) Ramajo, A. P.; Petty, S. A.; Volk, M. *Chemical Physics* **2006**, *323*, 11-20.

(82) Gooding, E. A.; Ramajo, A. P.; Wang, J. W.; Palmer, C.; Fouts, E.; Volk, M. *Chemical Communications* **2005**, 5985-5987.

(83) Woodruff, W. H.; Dyer, R. B.; Williams, S.; Callender, R. H.; Gilmanshin, R. *Abstracts of Papers of the American Chemical Society* **1996**, *211*, 57-INOR.

(84) Dyer, R. B.; Gai, F.; Woodruff, W. H. *Accounts of Chemical Research* **1998**, *31*, 709-716.

(85) Zimm, B. H.; Bragg, J. K. *Journal of Chemical Physics* **1959**, *31*, 526-535.

(86) Williams, S.; Causgrove, T. P.; Gilmanshin, R.; Fang, K. S.; Callender, R. H.; Woodruff, W. H.; Dyer, R. B. *Biochemistry* **1996**, *35*, 691-697.

(87) Wang, T.; Zhu, Y. J.; Getahun, Z.; Du, D. G.; Huang, C. Y.; DeGrado, W. F.; Gai, F. *Journal of Physical Chemistry B* **2004**, *108*, 15301-15310.

(88) Huang, C. Y.; Klemke, J. W.; Getahun, Z.; DeGrado, W. F.; Gai, F. *Journal of the American Chemical Society* **2001**, *123*, 9235-9238.

(89) Werner, J. H.; Dyer, R. B.; Fesinmeyer, R. M.; Andersen, N. H. *Journal of Physical Chemistry B* **2002**, *106*, 487-494.

(90) Tsuboi, Y.; Nishino, M.; Matsuo, Y.; Ijiro, K.; Kitamura, N. *Bulletin of the Chemical Society of Japan* **2007**, *80*, 1926-1931.

(91) Tsuboi, Y.; Yoshida, Y.; Kitamura, N.; Iwai, K. *Chemical Physics Letters* **2009**, *468*, 42-45.

(92) Tsuboi, Y.; Yoshida, Y.; Okada, K.; Kitamura, N. *Journal of Physical Chemistry B* **2008**, *112*, 2562-2565 Note: The temperature jumps utilising heat transducing dyes is subject to a number of errors that calls into question the validity of the results. A path length of one mm is used, which in combination with the concentration of the dye sample gives an absorbance of ~ five. Thus any light is extinguished long before reaching the end of the pathlength, resulting in a large imbalance in the heat distribution throughout the cell. Further, the use of Rhodium B as a heat transducing dye (which fluoresces) does not have a fast enough relaxation rate to provide sufficient heating. No indication of the how the size of the temperature jump was calibrated or the start temperature are given for both the direct and indirect heating methods which calls into doubt exactly how much of the transition is probed. Finally, the calculation used to calculate the time constant of the decay is incorrect (though it appears from the results that this is a typing error).

(93) Li, Z.; Wang, F.; Roy, S.; Sen, C. K.; Guan, J. J. *Biomacromolecules* **2009**, *10*, 3306-3316.

(94) Zhao, C. W.; Zhuang, X. L.; He, P.; Xiao, C. S.; He, C. L.; Sun, J. R.; Chen, X. S.; Jing, X. B. *Polymer* **2009**, *50*, 4308-4316.

(95) Lapointe, J.; Martel, S. *Conf Proc IEEE Eng Med Biol Soc* **2009**, *1*, 4246-4249.

(96) Petty, S. A.; "The stability and dynamics of alpha-helical peptides - an infrared study", PhD thesis, University of Liverpool, 2003.

(97) Ramajo, A. P.; "Fast Folding Dynamics of alpha-Helical Peptides", pHD Thesis, University of Liverpool, 2006.

(98) Whynes, R.; PhD Thesis, University of Liverpool, 2010.

(99) Mokhtari, A.; Fini, L.; Chesnoy, J. *Journal of Chemical Physics* **1987**, *87*, 3429-3435.

(100) Wray, W. O.; Aida, T.; Dyer, R. B. *Applied Physics B-Lasers and Optics* **2002**, *74*, 57-66.

(101) Levy, R.; Thanh, N. T. K.; Doty, R. C.; Hussain, I.; Nichols, R. J.; Schiffrin, D. J.; Brust, M.; Fernig, D. G. *Journal of the American Chemical Society* **2004**, *126*, 10076-10084.

(102) Hartland, G. V. *Journal of Chemical Physics* **2002**, *116*, 8048-8055.

(103) Hu, M.; Hartland, G. V. *The Journal of Physical Chemistry B* **2002**, *106*, 7029-7033.

(104) Pozo Ramajo, A.; "Fast Folding Dynamics of alpha-Helical Peptides", PhD Thesis, University of Liverpool, 2006.

(105) Gupta, R. N.; Jain, P. C.; Nanda, V. S. *The Journal of Chemical Thermodynamics* **1976**, *8*, 627-629.

(106) Spevacek, J.; Starovoytova, L.; Hanykova, L.; Kourilova, H. *Macromol. Symp.* **2008**, *273*, 17-24.

(107) Vidyasagar, A.; Smith, H. L.; Majewski, J.; Toomey, R. G. *Soft Matter* **2009**, *5*, 4733-4738.

(108) Ma, J. H.; Fan, B.; Liang, B. R.; Xu, J. *Journal of Colloid and Interface Science*, *341*, 88-93.

(109) Koga, S.; Sasaki, S.; Maeda, H. *Journal of Physical Chemistry B* **2001**, *105*, 4105-4110.

(110) Katsumoto, Y.; Tanaka, T.; Ozaki, Y. *Kobunshi Ronbunshu* **2003**, *60*, 256-268.

(111) Katsumoto, Y.; Kubosaki, N. *Macromolecules* **2008**, *41*, 5955-5956.

(112) Dybal, J.; Trchova, M.; Schmidt, P. *Vibrational Spectroscopy* **2009**, *51*, 44-51.

(113) Katsumoto, Y.; Tanaka, T.; Sato, H.; Ozaki, Y. *Journal of Physical Chemistry A* **2004**, *205*, 209-223.

(114) Ono, Y.; Shikata, T. *Journal of Physical Chemistry B* **2007**, *111*, 1511-1513.

(115) Graff, D. K.; Pastrana-Rios, B.; Venyaminov, S. Y.; Prendergast, F. G. *Journal of the American Chemical Society* **1997**, *119*, 11282-11294.

(116) Katsumoto, Y.; Tanaka, T.; Ozaki, Y. *Macromol. Symp.* **2004**, *205*, 209-223.

(117) Gnanakaran, S.; Hochstrasser, R. M.; Garcia, A. E. *Proc. Natl. Acad. Sci. U. S. A.* **2004**, *101*, 9229-9234.

(118) Kojima, H.; Tanaka, F. *Macromolecules* **2010**, *43*, 5103-5113.

(119) Myshakina, N. S.; Ahmed, Z.; Asher, S. A. *J. Phys. Chem. B* **2008**, *112*, 11873-11877.

(120) Triggs, N. E.; Valentini, J. J. *Journal of Physical Chemistry* **1992**, *96*, 6922-6931.

(121) Inomata, H.; Goto, S.; Saito, S. *Macromolecules* **1990**, *23*, 4887-4888.

(122) Gu, Y. L.; Kar, T.; Scheiner, S. *Journal of the American Chemical Society* **1999**, *121*, 9411-9422.

(123) Wang, X.; Wu, C. *Macromolecules* **1999**, *32*, 4299-4301.

(124) Kogure, H.; Nanami, S.; Masuda, Y.; Toyama, Y.; Kubota, K. *Colloid and Polymer Science* **2005**, *283*, 1163-1171.

(125) Meersman, F.; Smeller, L.; Heremans, K. *Biophysical Journal* **2002**, *82*, 2635-2644.

(126) Li, D.; McHugh, M. A.; van Zanten, J. H. *Macromolecules* **2005**, *38*, 2837-2843.

(127) Johansson, A.; Kollman, P.; Rothenberg, S.; McKelvey, J. *Journal of the American Chemical Society* **1974**, *96*, 3794-3800.

(128) Mitchell, J. B. O.; Price, S. L. *Chemical Physics Letters* **1991**, *180*, 517-523.

(129) Gilijamse, J. J.; Lock, A. J.; Bakker, H. J. *Proc. Natl. Acad. Sci. U. S. A.* **2005**, *102*, 3202-3207.

(130) Ludwig, R. *Angewandte Chemie International Edition* **2001**, *40*, 1808-1827.

(131) Phillips, C. M.; Mizutani, Y.; Hochstrasser, R. M. *Proc. Natl. Acad. Sci. U. S. A.* **1995**, *92*, 7292-7296.

(132) Starovoytova, L.; Spevacek, J. *Polymer* **2006**, *47*, 7329-7334.

(133) Murata, M.; Kaku, W.; Anada, T.; Sato, Y.; Kano, T.; Maeda, M.; Katayama, Y. *Bioorg. Med. Chem. Lett.* **2003**, *13*, 3967-3970.

(134) Hinrichs, W. L. J.; Schuurmans-Nieuwenbroek, N. M. E.; van de Wetering, P.; Hennink, W. E. *Journal of Controlled Release* **1999**, *60*, 249-259.

(135) Shibayama, M.; Nagai, K. *Macromolecules* **1999**, *32*, 7461-7468.

(136) Kim, D. H.; Rozhkova, E. A.; Rajh, T.; Bader, S. D.; Novosad, V. *Nanotech Conference & Expo 2009, Vol 2, Technical Proceedings* **2009**, 294-297.

(137) Reese, C. E.; Mikhonin, A. V.; Kamenjicki, M.; Tikhonov, A.; Asher, S. A. *Journal of the American Chemical Society* **2004**, *126*, 1493-1496.

(138) Volk, M. *European Journal of Organic Chemistry* **2001**, 2605-2621.

(139) Guillermo, A.; Addad, J. P. C.; Bazile, J. P.; Duracher, D.; Elaissari, A.; Pichot, C. *Journal of Polymer Science Part B-Polymer Physics* **2000**, *38*, 889-898.

APPENDIX A

	pNIPAM MCL1 low conc	pNIPAM MCL1 high conc	pNIPAM SCL	pNIPAM HCL	pNIPAM tBu	pNIPAM Acr	pNNPAM HCl	pNNPAM SCL	pCYPAM	Nano
xcoff1	1625.90	1625.90	1626.42	1626.33	1626.43	1624.77	1633.45	1633.17	1634.91	1632.39
xcgrad1	0.02	0.02	0.05	0.02	0.10	0.06	0.02	-0.04	-0.21	-0.18
30	1626.46	1626.46	1628.06	1627.01	1629.39	1626.66	1634.08	1631.92	1628.62	1627.06
45	1626.75	1626.75	1628.89	1627.35	1630.88	1627.61	1634.40	1631.30	1625.47	1624.39
woff1	27.28	27.28	18.88	28.15	22.72	30.73	23.38	19.61	33.82	24.74
wgrad1	0.05	0.05	0.14	0.04	0.03	0.01	0.10	0.14	0.00	0.09
30	28.66	28.66	23.23	29.41	23.59	30.97	26.34	23.73	33.82	27.49
45	29.36	29.36	25.40	30.05	24.02	31.08	27.83	25.79	33.82	28.86
nuoff1	0.17	0.17	-0.06	0.23	0.13	0.38	0.45	-0.09	0.22	0.12
nugrad1	0.00	0.00	0.01	0.00	0.00	0.00	0.00	0.00	0.00	0.00
30	0.13	0.13	0.19	0.20	0.01	0.34	0.36	0.03	0.10	0.10
45	0.12	0.12	0.31	0.18	-0.04	0.33	0.32	0.10	0.05	0.09
xcoff2	1650.06	1650.06	1642.11	1653.80	1645.88	1641.47	1648.74	1642.98	1636.55	1650.62
xcgrad2	-0.07	-0.07	0.10	-0.15	0.04	0.12	0.07	0.20	0.11	-0.13
30	1648.08	1648.08	1645.00	1649.20	1647.09	1644.97	1650.91	1648.90	1639.73	1646.78
45	1647.09	1647.09	1646.45	1646.90	1647.69	1646.72	1652.00	1651.86	1641.33	1644.86
woff2	10.84	10.84	16.58	9.77	18.04	20.86	13.90	19.08	16.44	22.68
wgrad2	0.29	0.29	0.17	0.30	0.15	0.06	0.22	0.09	0.30	0.08
30	19.61	19.61	21.62	18.82	22.60	22.65	20.60	21.66	25.44	24.97
45	24.00	24.00	24.14	23.34	24.88	23.55	23.95	22.94	29.94	26.11
nuoff2	1.07	1.07	0.89	1.09	0.42	0.54	-0.01	-0.55	0.66	0.68
nugrad2	-0.02	-0.02	-0.02	-0.02	0.00	0.00	0.00	0.02	-0.01	0.00
30	0.46	0.46	0.35	0.47	0.37	0.59	0.01	0.20	0.35	0.65
45	0.15	0.15	0.07	0.17	0.34	0.62	0.03	0.57	0.20	0.64
xcoff3	1594.19	1594.19	1606.96	1594.20	1608.85	1602.24	1616.98	1614.67	1573.43	1612.36
xcgrad3	0.46	0.46	0.21	0.49	0.24	0.25	0.11	0.10	0.29	-0.04
30	1607.86	1607.86	1613.36	1608.80	1615.95	1609.66	1620.29	1617.59	1582.03	1611.10
45	1614.70	1614.70	1616.57	1616.09	1619.51	1613.37	1621.94	1619.05	1586.33	1610.47
woff3	22.86	22.86	23.62	27.43	29.48	29.15	28.85	21.91	3.50	30.18
wgrad3	0.23	0.23	0.12	0.17	0.01	0.04	0.00	0.17	0.98	0.00
30	29.68	29.68	27.26	32.49	29.78	30.50	28.85	26.90	32.98	30.18
45	33.08	33.08	29.08	35.02	29.92	31.17	28.85	29.39	47.72	30.19
nuoff3	1.05	1.05	-0.10	1.14	0.17	1.08	-0.08	0.24	0.61	0.61
nugrad3	0.00	0.00	0.00	0.00	0.00	0.00	0.01	0.01	-0.01	0.00
30	0.96	0.96	0.02	1.00	0.06	1.01	0.16	0.41	0.29	0.68
45	0.91	0.91	0.07	0.93	0.00	0.97	0.28	0.49	0.13	0.71

Table A1 The temperature dependences of the fitting parameters for the 3 band amide I' fits presented in chapter 3, described in the text.

Each column denotes .a different polymer type with the specific polymer code (the polymer details are found in table 2.1). In each fit in chapter 3, the polymer code is referred to in the fit caption.

Rows separated by double spacing contain the details of a different fit parameter, in the format (parameter type)(gradient/offset)(band number)The parameter types are defined as follows: Xc= band frequency(cm^{-1}), w=band width(cm^{-1}), nu= Gauzzian/Lorentzian contribution.. ~Off and ~grad refer to the offset and gradient in the linear temperature dependence obtained for that parameter (generating the equation y=grad(t)+off, where t is temperature). "30" and "45" row headers refer to the values generated by the linear temperature dependence at 30 and 45°C, effectively showing the values for the parameters above and below the transition. Band 1, 2 and 3 refer to the band found at 1610cm^{-1} (C=O bonded to trapped water), 1625cm^{-1} (normally solvated C=O), and 1650cm^{-1} (inter/intramolecularly bonded C=O) See Chapter 2.6.2 for details of how the fits were implemented, and chapter 3.4 for the results.